



HAL
open science

Acidic-basic properties of catalysts for conversion of biomass

Dusan Stosic

► **To cite this version:**

Dusan Stosic. Acidic-basic properties of catalysts for conversion of biomass. Other. Université Claude Bernard - Lyon I, 2012. English. NNT : 2012LYO10284 . tel-00946707

HAL Id: tel-00946707

<https://theses.hal.science/tel-00946707>

Submitted on 14 Feb 2014

HAL is a multi-disciplinary open access archive for the deposit and dissemination of scientific research documents, whether they are published or not. The documents may come from teaching and research institutions in France or abroad, or from public or private research centers.

L'archive ouverte pluridisciplinaire **HAL**, est destinée au dépôt et à la diffusion de documents scientifiques de niveau recherche, publiés ou non, émanant des établissements d'enseignement et de recherche français ou étrangers, des laboratoires publics ou privés.

N° d'ordre 284-2012

Année 2012

THESE DE L'UNIVERSITE DE LYON

Délivrée par

L'UNIVERSITE CLAUDE BERNARD LYON 1

ECOLE DOCTORALE DE CHIMIE

Pour l'obtention du DIPLOME DE DOCTORAT

(arrêté du 7 août 2006)

Présentée et soutenue publiquement le 18 Décembre 2012

par

Dušan STOŠIĆ

TITLE : Acidic-basic properties of catalysts for conversion of biomass

TITRE : Propriétés acido-basiques de catalyseurs pour la conversion de la biomasse

Directeur de thèse : Mme Aline Auroux

JURY

Mme. A. AUROUX	Directeur de thèse
Mme. S. BENNICI	Co-encadrant
M. F. DUMEIGNIL	Rapporteur
M. A. TRAVERT	Rapporteur
M. J.-M. LANCELIN	Examineur
M. J.-L. DUBOIS	Examineur
Mme. V. RAKIC	Examineur
M. J.-L. COUTURIER	Membre invité

UNIVERSITE CLAUDE BERNARD - LYON 1

Président de l'Université

M. François-Noël GILLY

Vice-président du Conseil d'Administration

M. le Professeur Hamda BEN HADID

Vice-président du Conseil des Etudes et de la Vie Universitaire

M. le Professeur Philippe LALLE

Vice-président du Conseil Scientifique

M. le Professeur Germain GILLET

Secrétaire Général

M. Alain HELLEU

COMPOSANTES SANTE

Faculté de Médecine Lyon Est – Claude Bernard

Directeur : M. le Professeur J. ETIENNE

Faculté de Médecine et de Maïeutique Lyon Sud – Charles Mérieux

Administrateur provisoire : M. le Professeur G. KIRKORIAN

UFR d'Odontologie

Directeur : M. le Professeur D. BOURGEOIS

Institut des Sciences Pharmaceutiques et Biologiques

Directeur : Mme la Professeure C. VINCIGUERRA.

Institut des Sciences et Techniques de la Réadaptation

Directeur : M. le Professeur Y. MATILLON

Département de formation et Centre de Recherche en Biologie Humaine

Directeur : M. le Professeur P. FARGE

COMPOSANTES ET DEPARTEMENTS DE SCIENCES ET TECHNOLOGIE

Faculté des Sciences et Technologies

Directeur : M. le Professeur F. De MARCHI

Département Biologie

Directeur : M. le Professeur F. FLEURY

Département Chimie Biochimie

Directeur : Mme le Professeur H. PARROT

Département GEP

Directeur : M. N. SIAUVE

Département Informatique

Directeur : M. le Professeur S. AKKOUCHE

Département Mathématiques

Directeur : M. le Professeur A. GOLDMAN

Département Mécanique

Directeur : M. le Professeur H. BEN HADID

Département Physique

Directeur : Mme S. FLECK

Département Sciences de la Terre

Directeur : Mme la Professeure I. DANIEL

UFR Sciences et Techniques des Activités Physiques et Sportives

Directeur : M. C. COLLIGNON

Observatoire de Lyon

Directeur : M. B. GUIDERDONI

Polytech Lyon

Directeur : M. P. FOURNIER

Ecole Supérieure de Chimie Physique Electronique

Directeur : M. G. PIGNAULT

Institut Universitaire de Technologie de Lyon 1

Directeur : M. C. VITON

Institut Universitaire de Formation des Maîtres

Directeur : M. R. BERNARD

Institut de Science Financière et d'Assurances

Directeur : Mme la Professeure V. MAUME-DESCHAMPS

Acknowledgments

This work has been accomplished from November 2009 to December 2012 in the Institut de Recherches sur la Catalyse et l'Environnement de Lyon (IRCELYON).

I would like to express my very great appreciation to Madam Aline Auroux for her valuable and constructive suggestions during the planning and development of this research work. Her willingness to give her time so generously has been very much appreciated. This work could not be done without her help.

I would like to express my deep gratitude to Madam Simona Bennici for her patient guidance, enthusiastic encouragement and useful critiques of this research work. Her fast reactions to solve the problems substantially speed up my work.

Special thanks go to Madam Vesna Rakić without whom I would not come in to this research institute. From our long conversations about research, but also about music, literature and politics I have learned a lot.

I wish to thank Mr. Jean-Luc Dubois, Mr. Jean-Luc Couturier and Mr. Christophe Calais from ARKEMA Company for sharing their knowledge and results. Especially, I am grateful to Mr. Dubois, scientific advisor of Arkema, for his suggestions and corrections in publishing scientific articles. They have been of immense help to me.

I wish to thank to Mr. Franck Dumeignil for managing the Guerbetol project and welcoming me in his laboratory in Lille. I also thank Mr. Mickaël Capron for being a good host during my stay at his laboratory and Lille.

I would like to express my gratitude to Mr. Arnaud Travert and Mr. Sergey Sirotin for their contribution to my work.

Special thanks are addressed to the technical services of IRCELYON for valuable technical contributions in Raman, XRD, BET, XPS, and chemical analysis.

I had a real pleasure of working with my colleagues who were in Energy Group at IRCELYON during this period: Georgeta Postole, Gareth Whiting, Reem Kourieh, Adrien Mekki-Berrada (thanks for all the great music), Hao Yu, Emil Obeid, Otman Otman, Hongying Zhao, Jingxuan Cai, Didier Grondin, Gabrielle Scalabrino, Zouhair Salama, Emeline Potdevin, Philippe Perron, Emeline Lefebvre and Amira Jabbari-Hichri. Thank you for the help and all the fun we had together.

French National Research Agency (ANR-09-CP2D-19) is greatly acknowledged for financial support.

Finally, I would like to thank my family for their support and understanding during the last three years.

Contents

List of Publications	1
List of Communications	2
1. Background and Objectives	3
2. Experimental Description	13
3. List of Catalysts	20
4. References	25
5. Published Results	29
Publication I	31
Publication II	65
Publication III	103
Publication IV	109
Publication V	121
Publication VI	131
Publication VII	159
6. Conclusions	179
Abstract (English, French)	186

List of Publications

The results of this thesis have been published or submitted to publication in several international journals which are listed below:

- I. **Dušan Stošić** and Aline Auroux, Couplings. In: A. Auroux (ed) *Calorimetry and Thermal Methods in Catalysis* (Springer Series in Materials Science), Springer, Heidelberg, chapter III.
- II. **Dušan Stošić** and Aline Auroux, Characterization of acid-base sites in zeolites. In: A. Auroux (ed) *Calorimetry and Thermal Methods in Catalysis* (Springer Series in Materials Science), Springer, Heidelberg, chapter IX.
- III. **Dušan Stošić**, Simona Bennici, Jean-Luc Couturier, Jean-Luc Dubois and Aline Auroux, Influence of surface acid-base properties of zirconia and titania based catalysts on the product selectivity in gas phase dehydration of glycerol, *Catalysis Communications* 17 (2012) 23–28.
- IV. **Dušan Stošić**, Simona Bennici, Sergey Sirotin, Christophe Calais, Jean-Luc Couturier, Jean-Luc Dubois, Arnaud Travert and Aline Auroux, Glycerol dehydration over calcium phosphate catalysts: effect of acidic-basic features on catalytic performance, *Applied Catalysis A General* 447-448 (2012) 124-134.
- V. **Dušan Stošić**, Simona Bennici, Vesna Rakić and Aline Auroux, CeO₂-Nb₂O₅ mixed oxide catalysts: preparation, characterization and catalytic activity in fructose dehydration reaction, *Catalysis Today* 192 (2012) 160– 168.
- VI. **Dušan Stošić**, Simona Bennici, Vladimir Pavlović, Vesna Rakić and Aline Auroux, Tuning the acidity of niobia: characterization and catalytic activity of Nb₂O₅-MeO₂ (Me = Ti, Zr, Ce) mesoporous mixed oxides, *ChemCatChem*, submitted.
- VII. Vladislav Rac, Vesna Rakić, Zoran Miladinović, **Dušan Stošić** and Aline Auroux, Influence of desalination proces on the acidity of HZSM-5 zeolite, *Thermochimica Acta*, accepted.

List of Communications

- I. Conference of Yugoslav Materials Science Society (YUCOMAT), 6–10th Sep., 2010: Herceg Novi, Montenegro, Preparation and characterization of CeO₂-Nb₂O₅ mixed-oxide catalysts, **Dušan Stošić**, Vesna Rakić, Simona Bennici and Aline Auroux, *Oral presentation*.
- II. VII International Symposium on Group Five Elements, 8-11th May, 2011: Riccione, Italy, CeO₂-Nb₂O₅ mixed-oxide catalysts: preparation, characterization and catalytic activity, **Dušan Stošić**, Vesna Rakić, Simona Bennici and Aline Auroux, *Oral presentation*.
- III. EUROPACAT X Congress, 28th Aug. – 2th Sep., 2011: Glasgow, Scotland, Influence of surface acid-base properties on the product selectivity in gas phase oxidation of glycerol, **Dušan Stošić**, Simona Bennici, Jean-Luc Couturier, Jean-Luc Dubois and Aline Auroux, *Poster*.
- IV. 12th European Meeting on Environmental Chemistry (EMEC 12), 7-10th Dec., 2011: Clermont-Ferrand, France, Influence of the acid-base properties of oxide catalysts in fructose dehydration to 5-HMF, Reem Kourieh, **Dušan Stošić**, Vesna Rakić, Simona Bennici and Aline Auroux, *Poster*.
- V. 15th International Congress on Catalysis (ICC 15), 1-6th July, 2012: Munich, Germany, Reactivity of methanol over Nb₂O₅-CeO₂ multifunctional catalysts: Microcalorimetry, FT-IR, TPR and TPD-MS studies, **Dušan Stošić**, Simona Bennici, Vesna Rakić and Aline Auroux, *Poster*.
- VI. 7th International Conference on Environmental Catalysis (ICEC 2012), 2-6th Sep., 2012: Lyon, France, Tuning the acidity of niobia: characterization and catalytic activity of Nb-Me (Me = Ti, Zr, Ce) mesoporous mixed oxides, **Dušan Stošić**, Simona Bennici, Vesna Rakić and Aline Auroux, *Poster*.
- VII. Calorimetry and Thermal Effects in Catalysis (CTEC 2012), 26-29th June, 2012: Lyon, France, Synthesis and catalytic properties of Nb-Me (Me = Ti, Zr, Ce) mesoporous mixed oxides, **Dušan Stošić**, Vesna Rakić, Simona Bennici and Aline Auroux, *Poster*.
- VIII. Calorimetry and Thermal Effects in Catalysis (CTEC 2012), 26-29th June, 2012: Lyon, France, Evaluation of the acidity of solid catalysts by adsorption of 2-phenyl-ethylamine from aqueous phase, Otman Otman, **Dušan Stošić**, Simona Bennici and Aline Auroux, *Poster*.

1. Background and Objectives

1.1 Background

Biomass is the term used for all organic material that stems from living or recently living organisms [1]. The main part of it is produced by green plants converting sunlight into plant material through photosynthesis and includes all land and water based vegetation, as well as all organic wastes. From the chemistry standpoint the biomass resource can be considered as organic matter where the energy of sunlight is stored in the chemical bonds. Biomass generally constitutes of carbon, hydrogen and oxygen. However, nitrogen and small quantities of other atoms, including alkali, alkaline earth and heavy metals can also be found [2]. Chemical energy is released when the bonds between adjacent carbon, oxygen and hydrogen atoms are broken by digestion, combustion or decomposition [2]. The term biomass excludes organic materials called fossil fuels, which differ from the present day biomass in that they come from organic matter that has been converted by geological processes into substances such as petroleum, coal, or natural gas. This is because although fossil fuels have their origin in ancient biomass, they are not considered as biomass by the generally accepted definition, because they contain carbon that has been "out" of the carbon cycle for a very long time. Their combustion therefore disturbs the carbon dioxide content in the atmosphere. By contrast, biofuels give out significantly less greenhouse gas emissions than fossil fuels and can even be greenhouse gas neutral if efficient methods for production are developed [1-3].

Prior to the discovery of inexpensive fossil fuels, our society was dependent on plant biomass to meet its energy demands [4]. The discovery of crude oil, in the 19th century, created an inexpensive liquid fuel source that helped industrialize the world and improved standards of living. These non-renewable petroleum feed stocks are currently used to provide liquid hydrocarbons that serve as transportation fuels and to supply unsaturated hydrocarbons that serve as feedstock for the production of diversity of chemicals and consumer products [4, 5]. Due to the high demand and dependency of industrial progress on the chemicals derived from fossil fuels, the research in this area of catalysis over the past half century has led to development of highly optimized processes for petroleum treatment [6, 7]. However, as the worldwide supply of petroleum is diminishing, there is a growing interest in development of renewable transportation fuels and chemicals to supplement and replace those derived from petroleum [6-10]. Biomass represents a potential alternative source of liquid fuels and chemicals, because it is an abundant, renewable source of carbon containing molecules [2]. However, the processing of biomass often requires multiple reaction steps because of the high

1. Background and Objectives

oxygen content and degree of functionality of biomass-derived feed molecules [8, 11]. Due to these reasons, the production of fuels and chemicals from biomass is uneconomical at present time compared to petroleum refining [12], even though the price of biomass is lower than that of crude oil [2].

The conversion of biomass-derived feedstocks to fuels and chemicals in a manner that is cost-competitive with the refining of petroleum requires the development of new approaches that simplify the processing steps and increase the activity and selectivity of heterogeneous catalytic materials, thus reducing capital and operating costs associated with separation and purification steps by reducing the use of homogeneous catalysts and organic solvents [9]. In this respect, investigation of properties of the solid catalysts (such as acidic, basic and red-ox) and their correlation with the activity-selectivity patterns in the given chemical process is of great importance.

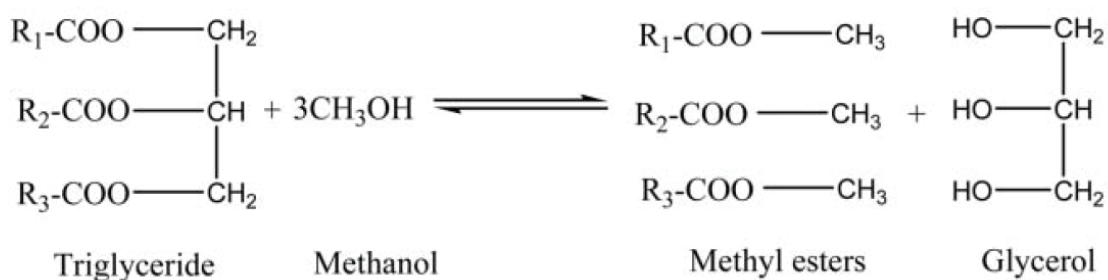
Biomass derived feedstocks for a production of biofuels and chemicals can be classified into one of three categories according to the source: cellulosic biomass, starch- and sugar-derived biomass (or edible biomass), and triglyceride-based biomass [13].

This work is restricted to glycerol dehydration in the gas phase and fructose dehydration in the aqueous phase reactions.

Glycerol from biomass

Triglycerides, or animal fats and vegetable oils, are found in the plant and animal kingdom and consists of water insoluble, hydrophobic molecules that are made up from one glycerol unit and three fatty acids. The reactions for the direct transformation of vegetable oils and animal fats into methyl esters and glycerol have been known for over a century. However, it is only recently, following more than 10 years of research and development, that the transesterification of triglycerides (using rapeseed, soybean and sunflower oils) has gained significance for its role in the manufacture of high quality biodiesel fuel (Scheme 1) [14-16]. As a result, several chemical [17] processes to produce fatty acid methyl esters from vegetable oil are now commercially available. Glycerol is normally generated at the rate of 1 mol of glycerol for every 3 mol of methyl esters synthesized; approximately 10 wt% of the total product [17].

1. Background and Objectives



with $\text{R}_1, \text{R}_2, \text{R}_3$ = hydrocarbon chain from 15 to 21 carbon atoms

Scheme 1. Overall reaction for production of biodiesel through transesterification reaction of vegetable oils (from [18]).

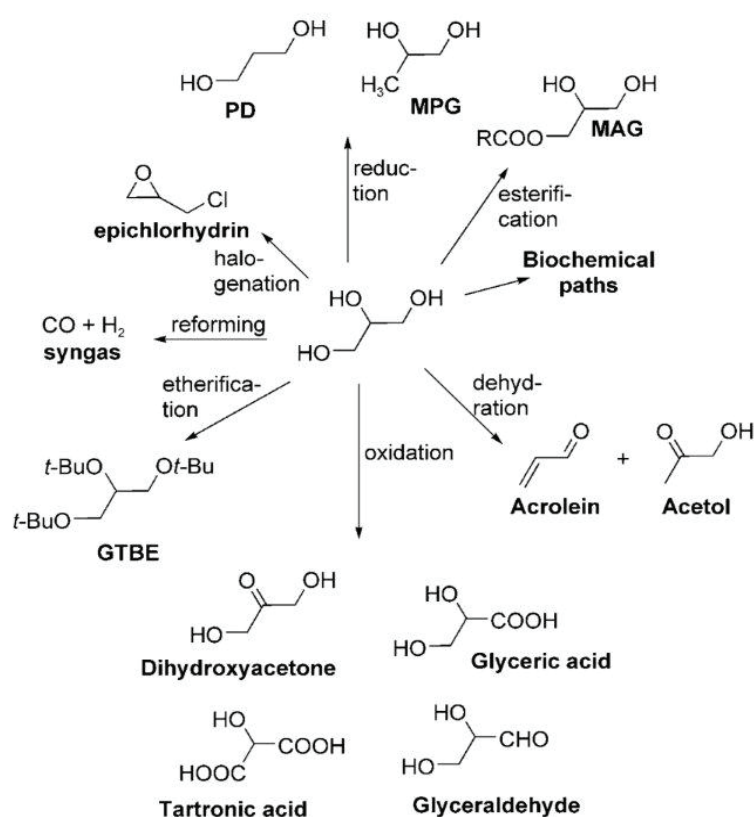
The production of biodiesel is increasing all over the world and, as a consequence, the amount of produced glycerol is also increasing. It is projected that 1.54 million tons of glycerol will be generated worldwide in 2015 [19]. Although the global production of biodiesel is still limited, the market price of glycerol has dropped rapidly and could destabilize the free market of oleochemicals. Studies have shown that the glycerol commodity market is very limited and any increase in biodiesel production will cause a sharp decline of its current value. With the increased expansion of biodiesel and the sharp decrease of glycerol prices, glycerol is expected to become a major platform chemical and has been recently identified as an important building block for future biorefineries [20]. Thus in order to make biodiesel sector sustainable and more profitable all of produced glycerol should be efficiently processed.

Glycerol dehydration in the gas phase

More than 1500 direct applications of glycerol are already known, especially in cosmetics, pharmaceuticals and food industries [21]. Glycerol is a material of choice mainly because of its physical characteristics, while some uses rely on its chemical properties [22]. Due to the presence of three hydroxyl groups, glycerol is completely soluble in water and alcohols, whereas it is completely insoluble in hydrocarbons. Further, the presence of hydroxyl groups leads to the formation of intra- and inter-molecular hydrogen networks, which explains its high boiling point (290 °C at atmospheric pressure) and high viscosity [22]. It is a very hydrophilic species, and is employed as such when the amount of water has to be controlled, namely in glue or other adhesives [22].

1. Background and Objectives

Glycerol is a molecule with a large functionalisation potential that offers numerous opportunities for chemical or biochemical conversions for producing value-added chemicals. Therefore, using glycerol for the synthesis of value-added chemicals is of great industrial importance, not only because glycerol is formed in large amounts during the biodiesel process, but also because glycerol is a nontoxic, edible, renewable and biodegradable compound [23, 24]. Selection of some of these possibilities is shown in Scheme 2. More detailed information is available in recent Review papers [14, 18, 25-28].



Scheme 2. Selection of glycerol valorization pathways (from [24]).

One of the promising routes for glycerol valorization is its catalytic dehydration to produce acrolein, which is used as starting material for the synthesis of acrylic acid and acrylates, widely used in the textile and resin industry; and hydroxyacetone (acetol). Another important product is methionine (an amino acid used as an animal feed supplement to accelerate animal growth). Acrolein is also used in some syntheses of fine chemicals [24]. Acetol is mainly used to produce products such as propylene glycol via hydrogenation reaction and acrolein through dehydration [29]. Additionally acetol is also used in food and textile industry [29]. Therefore,

1. Background and Objectives

if glycerol is used to produce acetol and/or acrolein, this technology would increase the profitability of biodiesel production plants and reduce the cost of producing biodiesel.

The acidity of the active phase is considered as a crucial factor that influences the catalytic performance in this process of acrolein production [24, 26]. Previous work on glycerol dehydration suggests that acrolein is formed on strong Brønsted acid sites [30]; protonation occurs at the central hydroxyl group of glycerol, a water molecule and a proton are eliminated from the protonated glycerol, and then 3-hydroxypropanal, which is unstable and readily dehydrated into acrolein is produced by tautomerism. The effect of acidity of active phase has been thoroughly studied and various solid acid catalysts have been tested in the dehydration of glycerol to yield acrolein, including zeolites [31-35], supported heteropolyacids [36-39] and phosphoric acid impregnated activated carbon [40] or Al_2O_3 and TiO_2 [41], niobium oxide [42, 43] and WO_3/ZrO_2 catalysts [44, 45], in a gas phase reaction.

The catalysts that have Lewis acid and basic sites on their surface showed better performance in glycerol dehydration to yield acetol. It is proposed that on Lewis acid sites, protonation proceeds at the terminal hydroxyl group of glycerol, and acetol is produced through dehydration and deprotonation accompanied by tautomerism [30]. The proposed mechanism of glycerol dehydration which happens on Lewis acid sites implies dehydration as initial step; while the reaction which goes on basic sites starts with a dehydrogenation step. The resulting 2,3-dihydroxypropanal can either further react via consecutive dehydration and hydrogenation to yield acetol, or can form – via a retro-aldol reaction – formaldehyde and hydroxyacetaldehyde, which can be subsequently hydrogenated to ethylene glycol [30]. Another possibility is that, on basic centers, reaction proceeds through dehydration, starting from a terminal hydroxyl group [46]. This leads to formation of enol intermediate, which can undergo rapid rearrangement to acetol. Among the catalysts that have showed high performance in this reaction to yield acetol are copper-chromite [47], different sodium doped metal oxide catalysts (Na/CeO_2 , $\text{Na/Al}_2\text{O}_3$, $\text{Na/Ga}_2\text{O}_3$, Na/ZrO_2) [48], ZrO_2 , Al_2O_3 [37], nanocasted $\text{SnO}_2\text{-Mn}_2\text{O}_3$, $\text{SnO}_2\text{-TiO}_2$ and $\text{NiO-CO}_2\text{O}_4$ oxides [49] and zirconium doped mesoporous silica catalysts [50].

While it is quite clear that acidity of the active phase of the catalysts (number, strength and nature of the acid sites) is the determining factor that influences selectivity in the gas phase reaction of glycerol dehydration to selectively yield acrolein, it remains a very challenging

1. Background and Objectives

topic to explain in more detailed way the selective catalytic conversion of glycerol to hydroxyacetone.

Fructose from biomass

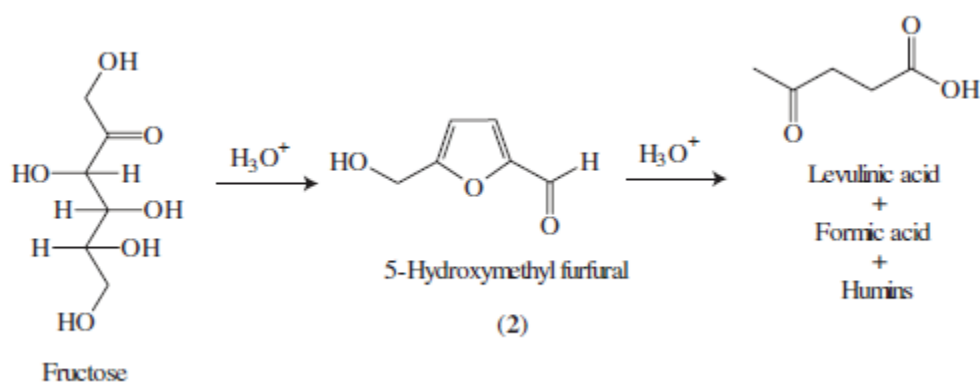
Edible biomass mostly consists of starches, which are commonly found in the vegetable kingdom. Starches are a glucose polysaccharide that have α -1,4 and α -1,6 glycoside linkages, which result in an amorphous structure of the polymer [51]. Starches can easily be broken down into water-soluble sugars. Sugars can also be extracted directly from certain types of biomass, such as sugarcane. Hexoses are the six-carboned carbohydrates and are the most abundant monosaccharides existing in nature and are readily available biomass primary compounds. Among them d-fructose is one of the most economical and suitable to be used as the chemical feedstock [5]. One of the promising routes for utilization of fructose as important biomass derived feedstock is its dehydration to 5-HMF (5-hydroxymethylfurfural). HMF and its ensuing 2,5-disubstituted furan derivatives can replace key petroleum based building blocks [52]. For example, HMF can be converted to 2,5-furandicarboxylic acid (FDCA) by selective oxidation, and Werpy and Petersen [20] and Pentz [53] have suggested that FDCA can be used as a replacement for terephthalic acid in the production of polyesters such as polyethyleneterephthalate [20] and polybutyleneterephthalate. They have also suggested that the reduction of HMF can lead to products such as 2,5-dihydroxymethylfuran and 2,5-bis(hydroxymethyl)tetrahydrofuran, which can serve as alcohol components in the production of polyesters, thereby leading to completely biomass-derived polymers when combined with FDCA. In addition, HMF can serve as a precursor in the synthesis of liquid alkanes to be used, for example, in diesel fuel [54].

Dehydration of fructose to 5-HMF

It is generally accepted that the synthesis of HMF is based on the triple dehydration of fructose (Scheme 3) [55]. The dehydration can occur in either aqueous or non-aqueous media, usually in the presence of the acid catalyst. The acid catalyzed dehydration leads, besides to HMF, to traces of various other dehydration products, such as levulinic acid, formic acid and polymeric side products called humines or humic acids [56]. Concerning the mechanism of dehydration, Haworth and Jones [57] were the first to suggest the dehydration of fructose in HMF. Later, Van Dam et al. [58], Antal et al. [59], and Kuster et al. [60] studied the dehydration of hexoses (fructose and glucose) and demonstrated that the chemistry of the

1. Background and Objectives

formation of HMF is very complex; besides dehydration, it includes a series of side reactions such as isomerization, fragmentation, and condensation which influence strongly the yield of the process. Van Dam et al. [58] and Cottier et al. [61] showed that aqueous and nonaqueous dehydration processes led to about 37 products.



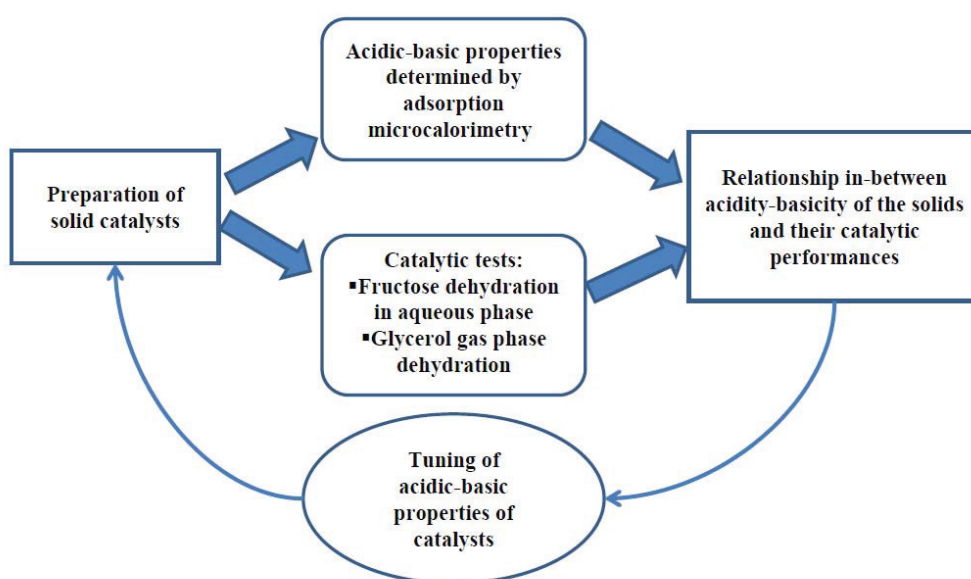
Scheme 3. Simplified reaction scheme for the dehydration of fructose (from [55]).

The dehydration of fructose is known to be catalyzed by Brønsted as well as Lewis acids. Among the solid catalysts that have shown high performance in this reaction to yield 5-HMF are niobic acid ($\text{Nb}_2\text{O}_5 \cdot n\text{H}_2\text{O}$) [62], niobium phosphate (NbOPO_4) [62, 63], TiO_2 [64], zirconium pyrophosphate and γ -titanium phosphate catalysts [65], vanadyl phosphate ($\text{VOPO}_4 \cdot 2\text{H}_2\text{O}$) [66], WO_x/ZrO_2 [67] and HY zeolite [68].

1. Background and Objectives

1.2 Objectives

The objectives of this work, which are graphically presented in Scheme 4, are to determine the relationship between the acidic-basic features of tested solids and their catalytic performances in gas phase dehydration of glycerol and fructose dehydration in aqueous phase reactions. In this way it is possible to rationalize tuning of used catalytic formulations and prepare catalysts with desired acidic-basic properties. The main technique used to reveal the acidic-basic properties of solid materials in this work is adsorption microcalorimetry.



Scheme 4. Presentation of the goals and objectives of this work.

Adsorption microcalorimetry as a tool for investigation of acidic-basic properties of solid catalysts

Heterogeneous catalysis involves specific chemical interactions between the surface of a solid and the reacting gas (or liquid phase) molecules. The catalytic cycle is generally composed of adsorption steps, surface reaction processes, and desorption steps. The energetics of these surface chemical events plays an important role in determining the catalytic properties of the surface. Among the techniques that are used for the study of these interactions, such as Fourier transform infrared spectroscopy (FTIR), X-ray photoelectron spectroscopy (XPS), temperature-programmed oxidation (TPO), temperature-programmed reduction (TPR) or temperature-programmed desorption (TPD), adsorption microcalorimetry is the only one that measures directly heat evolved when the adsorbate molecule contacts the surface of the solid.

1. Background and Objectives

This heat provides information related to the energy of the bonds formed between the adsorbed species and the adsorbent and hence to the nature of the bonds and to the chemical reactivity of the surface. When acidic (SO_2) or basic (NH_3) probe molecule is used, this method provides precise measurement of number, strength and strength distribution of basic and acidic sites on the surface of the solid catalyst, respectively. This technique and its applications are discussed in more details in Publications I and II of this manuscript.

Having this in mind the work done in this thesis can be outlined as:

(1) Two chapters included in the book entitled “Calorimetry and Thermal Analysis in Catalysis” to be published by Springer-Verlag Berlin and Heidelberg GmbH & Co, were written in order to gain a better understanding of adsorption microcalorimetry technique and its application to characterization of solid catalysts. The focus of this thesis was on investigation of surface acidic-basic properties of materials by this technique and correlation of these properties with activity/selectivity patterns in investigated reactions. (Publications I and II)

(2) A set of zirconia and titania based catalysts is prepared with intention of investigating their acidic-basic properties by adsorption calorimetry technique. The catalysts are also tested in the gas phase dehydration of glycerol. The aim of this work is to gain a better understanding of the nature of active sites for the dehydration reaction, which could help to develop more efficient solid catalysts for a sustainable use of biomass-derived glycerol by chemical industry. The aim is also the tuning of a desirable ratio of acidic to basic sites especially active for a given reaction. (Publication III)

(3) In order to expand the previous study (on the influence of acidic-basic features of solid catalysts and their performance in the glycerol dehydration on the catalysts of different nature) and to check if the same relationships can be established, a set of calcium phosphates with different Ca/P ratios are synthesized. Additionally, in order to investigate the influence of wolframate species on acidic-basic properties and catalytic activity of hydroxyapatites, HAP impregnated with tungsten oxide is also investigated. The results of detailed characterization of their textural and red-ox properties are discussed. Furthermore, data concerning acidic/basic features of these materials is also presented. Special attention is

1. Background and Objectives

devoted to the correlation between catalytic activity and surface acid–base properties. (Publication IV)

(4) Ceria-niobia mixed oxides are prepared by co-precipitation method in order to investigate how the relative amounts of two-component oxides influence the physico-chemical and catalytic properties of obtained materials. Having in mind that catalytic functions of solid materials are governed by their surface features, in order to predict their activity and selectivity in various reactions, complete characterization of the synthesized samples with respect to their structural, textural, acid–base, and red-ox properties is presented. Catalytic behavior of these materials in the reaction of fructose dehydration to 5-hydroxymethylfurfural (5-HMF) is discussed in terms of their acidic-basic properties. (Publication V)

(5) In order to tune and investigate the change in properties of niobia with the presence of another component oxide, mesoporous Nb₂O₅-MeO₂ (M = Ce, Zr, Ti) mixed metal oxides are studied. The results of their characterization and catalytic activity are presented. The focus is on the connection in-between acidic-basic features and selectivity to desired products in a given reaction. (Publication VI)

(6) The acidity of the active phase and textural properties can significantly influence the activity and selectivity of a tested catalyst in fructose dehydration in aqueous phase and glycerol dehydration in gas phase. Zeolites are important class of catalytic materials which are well known for their catalytic activity and selectivity. However, microporosity of zeolites, which plays a crucial role in their shape selectivity, can also be their biggest drawback. Therefore, the influence of the alkaline treatment on the creation of mesopores and changes in acidity of zeolite ZSM-5 (SiO₂/Al₂O₃ = 23, 50 and 80) modified by desilication is investigated in order to enlarge the accessibility to bigger reacting molecules. Results of a detailed microcalorimetric, volumetric and thermokinetic study are presented in this work. Additionally, data obtained by X-ray diffraction, low temperature adsorption of nitrogen and solid-state ²⁷Al MAS NMR are presented. (Publication VII)

2. Experimental Description

2.1 Catalysts preparation

The following chapter describes the catalysts preparation and experimental techniques used in this work.

2.1.1 Zirconia and titania based catalysts

WO₃-ZrO₂ (10 wt.% of WO₃), La₂O₃-ZrO₂ (30 wt.% of La₂O₃) and CeO₂-ZrO₂ (25 wt.% of CeO₂) were commercial samples purchased from Dai Ichi Kigenso Kabushiki Kaisha. They were calcined in air at 500 °C for 5 h before use. ZrO₂, TiO₂ anatase and TiO₂ rutile were purchased from Saint-Gobain Norpro, and were calcined in air at 500 °C for 5 h before use.

HPW/TiO₂ (10 wt.% of HPW) was prepared by incipient wetness impregnation with an aqueous solution of phosphotungstic acid on to the TiO₂ anatase. The sample was dried in air at 110 °C overnight, followed by calcination in air at 500 °C.

HPW/WO₃-ZrO₂ (4 wt.% of HPW) was prepared by incipient wetness impregnation with an aqueous solution of phosphotungstic acid on to the WO₃-ZrO₂ sample. The sample was subsequently dried in air at 110 °C overnight and calcined in air at 450 °C.

2.1.2 Calcium phosphates with different Ca/P ratios

Hydroxyapatite samples with Ca/P ratios of 1.50 (product reference: nanoXIM.TCP202) and 1.66 (nanoXIM.HAp402) were commercial samples purchased from Fluidinova S.A. They were calcined in air at 450 °C for 5 h before use.

Sample 1.66 HAP was modified by incipient wetness impregnation, at room temperature, with aqueous solutions of calcium acetate and phosphoric acid to form Ca-rich (Ca/HAP) and Ca-deficient (P/HAP) calcium phosphates respectively. Subsequently, samples were dried in air at 110 °C overnight, followed by calcination in air at 450 °C.

W/HAP sample was prepared by incipient wetness impregnation, at room temperature, with an aqueous solution of tungstic acid on 1.66 HAP. The sample was dried in air at 110 °C overnight and calcined in air at 450 °C.

2. Experimental Description

2.1.3 Ceria-niobia mixed-oxides

Ceria–niobia mixed oxides with a wide range of niobia content were prepared by co-precipitation from ammonium–niobium oxalate complex (99.99%, Aldrich) and cerium nitrate (99.9%, Strem Chemicals) aqueous solutions. The requested quantities of these precursors were dissolved in deionized water at room temperature. The solutions were mixed with continuous monitoring of pH. Ammonia solution (16 wt.%) was added gradually dropwise to the mixture of two solutions with vigorous stirring, until precipitation was completed (pH = 9). Pure ceria was obtained by precipitation from solution of cerium nitrate by ammonia in the same way. All the precipitates were then filtrated and washed with hot distilled water (0.5 L), dried overnight in an oven at 110–120 °C and calcined in air at 400 °C for 10 h. The calcination temperature has been chosen on the basis of thermogravimetric measurements. Nb₂O₅ was purchased from H.C. Starck Company and calcined at the same temperature.

2.1.4 Nb₂O₅-MeO₂ (Me = Ti, Zr, Ce) mesoporous mixed oxides

Mixed mesoporous oxides were prepared from niobium pentachloride NbCl₅ (99.99, Strem Chemicals INC.), zirconium tetrachloride ZrCl₄ (99.99, Sigma-Aldrich), cerium trichloride CeCl₃ (99.99, Sigma-Aldrich) and titanium dichloride TiCl₂ (99.99, Sigma-Aldrich). Triblock copolymer surfactant (PE 105, Sigma-Aldrich) was used as a structure directing agent. Mixed oxides were synthesized by dissolving 1 g of surfactant in 10 g of dehydrated ethanol, and by adding 7 mmol of metal chloride salts into the solution with vigorous stirring. The molar ratio of niobium to other metals was 1. Water (0.333 mol) was added to the solution with further stirring. The resulting sol was gelled in a Petri dish at 30 °C for 14 days. The aged gel samples were then calcined at 500 °C for 5 h in air for removal of the surfactant. The calcination temperature has been chosen on the basis of thermogravimetric measurements.

2.1.5 Zeolites and hierarchical zeolites

Commercial MFI type zeolites (HZSM-5) chosen for the desilication process were supplied by Zeolyst International. Samples characterized by three different silica to alumina ratios were used and denoted as Z_x, where Z and x mark ZSM-5 and silica to alumina ratio, respectively: Z23 (producer's code CBV 2314, SiO₂/Al₂O₃=23), Z50 (CBV 5524G, SiO₂/Al₂O₃=50) and Z80 (CBV 8014, SiO₂/Al₂O₃=80). Parent zeolite samples, designated as Z_xP were prepared by calcination in air at 500 °C during 5 h, in order to obtain their hydrogen forms. In a typical

2. Experimental Description

experiment, 5g of the ammonium form of a ZSM-5 sample was introduced to 150 ml of 0.2 M NaOH solution at 90 °C and stirred for the duration of 30 minutes. The sample was then filtrated, thoroughly washed with deionized water until a neutral pH was reached and dried at 120 °C overnight. Subsequently, an acid washing was performed using hydrochloric acid (0.1 M, 150 mL) for 6 h at room temperature. The samples were then filtered, washed and dried again. Following the acid treatment, the samples were converted to their ammonium forms by three-fold ion-exchange (0.1 M ammonium nitrate at 90 °C during 1 hour). The resulting zeolitic materials were filtered, washed with deionized water, dried at 120 °C and finally converted to hydrogen form by calcination in air at 500 °C for 5h. The obtained samples were coded Z x M, where x has the same meaning as in the names of the parent zeolites.

2. Experimental Description

2.2 Catalysts characterization

Different techniques were used to characterize the physico-chemical properties of the catalysts which are listed as the following:

Thermogravimetry (TG-dTG, performed on a “Labsys-TG” instrument from Setaram) was used in order to determine this lowest temperature of calcination at which no significant loss of mass occurred with further heating. The crude samples (~50 mg) were heated from 25 °C to 800 °C with a heating rate of 5 °C min⁻¹ in a flow of air, which was chosen as a soft oxidizing agent for calcination.

The surface areas and pore sizes were measured by nitrogen adsorption at -196 °C on a Micromeritics 2010 apparatus after heat pretreatment under vacuum for 3 h at a temperature 100 °C lower than the calcination temperature.

The X-ray diffraction (XRD) measurements were carried out on a Bruker D5005 powder diffractometer scanning from 3° to 80° (2θ) at a rate of 0.02 degree s⁻¹ using a Cu Kα radiation (λ=0.15418nm) source. The applied voltage and current were 50 kV and 35 mA, respectively.

Elemental analysis was performed using ICP optical emission spectroscopy (ICP–OES) with an ACTIVA spectrometer from Horiba JOBIN YVON.

The X-ray photoelectron spectra were measured on a KRATOS AXIS Ultra DLD spectrometer equipped with a hemispherical electron analyzer and an Al anode (Al Kα=1486.6 eV) powered at 150 W, a pass energy of 20 eV, and a hybrid lens mode. The detection area analyzed was 700×300 μm. Charge neutralization was required for all samples. The peaks were referenced to the C–(C, H) components of the C 1s band at 284.6 eV. Shirley background subtraction and peak fitting to theoretical Gaussian-Lorentzian functions were performed using an XPS processing program (vision 2.2.6 KRATOS). The residual pressure in the spectrometer chamber was 5×10⁻⁷ Pa during data acquisition.

Raman spectroscopy measurements were performed using a LabRAM HR (Jobin Yvon) spectrometer. The excitation was provided by the 514.5 nm line of an Ar⁺ ion laser (Spectra physics) employing a laser power of 100 μW. The laser beam was focused through microscope objective lenses (×100) down to a 1 μm spot on the sample.

2. Experimental Description

Diffuse reflectance infrared (DRIFT) spectra were collected with a Nicolet 8700 THERMO SCIENTIFIC instrument by co-addition of 100 scans at 2 cm^{-1} resolution. The instrument was equipped with a Praying Mantis accessory (Harrick) and a liquid nitrogen-cooled MCT detector. The samples were diluted in KBr, and a spectrum of KBr was used as a reference.

The morphology of samples was investigated by scanning electron microscopy (SEM, JEOL JSM-6390 LV). Prior to the analysis the samples were covered with Au using a sputter coater Baltec scd 005 accessory. Time of sputtering was 100 ms using a current of 30 mA.

Redox properties of investigated samples were revealed by TPR (temperature programmed reduction) technique using a TPD/R/O- 1100 (ThermoFisher) instrument. Prior to the TPR run, the fresh sample was treated in a O_2/He stream (0.998%, v/v, with a flow rate of 20 mL min^{-1}), ramping the temperature at $10\text{ }^\circ\text{C min}^{-1}$ from room temperature to $850\text{ }^\circ\text{C}$ and maintaining it at this temperature for 60 min. Subsequently, sample was cooled down to $40\text{ }^\circ\text{C}$. The TPR measurements were carried out using H_2/Ar (4.98%, v/v) as reducing gas mixture, with flow rate of 20 mL min^{-1} . The heating rate was $10\text{ }^\circ\text{C min}^{-1}$ from $40\text{ }^\circ\text{C}$ to $850\text{ }^\circ\text{C}$. The consumption of H_2 was detected by a thermal conductivity detector (TCD). The TPR peak areas were calibrated with given H_2/Ar (4.98%, v/v) mixture injections.

The nature of acid sites on the surface of investigated solids was determined by FTIR of adsorbed pyridine. Infrared spectra were recorded, in the $4000\text{--}400\text{ cm}^{-1}$ spectral range, with a resolution of 2 cm^{-1} , using a Bruker Vector 22 FT-IR spectrophotometer equipped with DTGS detector, collections of 100 scans were recorded. The self-supporting wafer (30–50 mg of catalyst, 18 mm diameter) was first activated in situ at $300\text{ }^\circ\text{C}$ in oxygen flow for 14 h, subsequently evacuated at the same temperature for 2 h and then exposed to pyridine (Air Liquide, 99.8%, vapor pressure 3.3 kPa) at room temperature for 5 min. The desorption was carried out by evacuation for 30 min each at room temperature, $100\text{ }^\circ\text{C}$, $200\text{ }^\circ\text{C}$ and $300\text{ }^\circ\text{C}$. The IR spectra were recorded at room temperature after desorption at each temperature.

The microcalorimetric studies of ammonia adsorption were performed at $150\text{ }^\circ\text{C}$ in a heat flow calorimeter (C80 from Setaram) linked to a conventional volumetric apparatus equipped with a Barocel capacitance manometer for pressure measurements. Ammonia used for measurements (Air Liquide, purity $> 99.9\%$) was purified by successive freeze-pump-thaw cycles. About 100 mg of sample was pretreated in a quartz cell under evacuation overnight at

2. Experimental Description

a temperature 100 °C lower than the calcination temperature. The differential heats of adsorption were measured as a function of coverage by repeatedly introducing small doses of ammonia gas onto the catalyst until an equilibrium pressure of about 66 Pa was reached. The sample was then outgassed for 30 min at the same temperature, and a second adsorption was performed at 150 °C until an equilibrium pressure of about 27 Pa was attained in order to

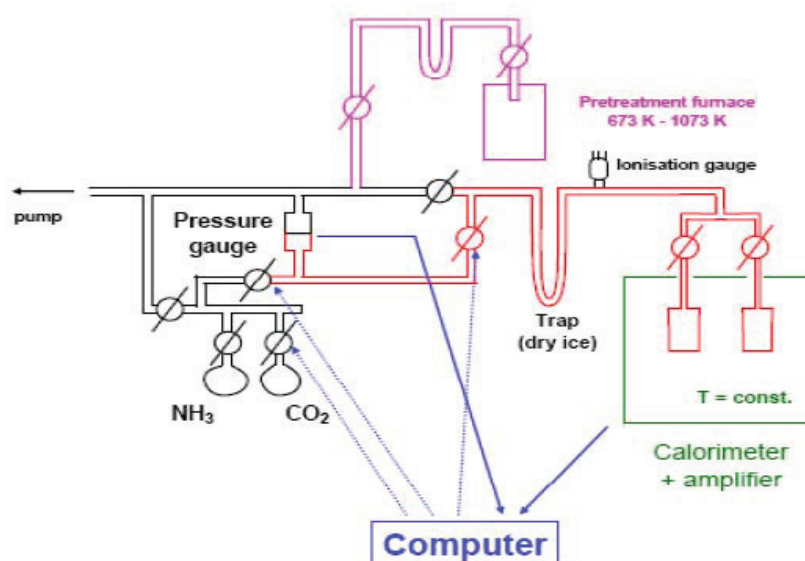


Figure 2. 1. Scheme of adsorption microcalorimetry system (IRCELYON).

calculate the irreversibly chemisorbed amount of ammonia at this pressure (see Figure 2.1).

2.3 Catalytic reactions

The gas phase dehydration reaction of glycerol was carried out at 350 °C under atmospheric pressure in a fixed-bed Pyrex reactor (420 mm length × 8 mm inside diameter). The reaction temperature was monitored by a thermocouple inserted into the middle of the catalyst bed. The catalyst was first crushed and sieved (300-500 μm), then mixed with quartz sand (50–80 mesh) and loaded in the middle of reactor with quartz wool packed in both ends. The catalysts were initially pretreated at 300 °C in a flow of nitrogen (30 mL min⁻¹) for 2 h. Glycerol solution (30 wt% in water) was introduced in the flow of nitrogen with help of syringe pump at a flow of 0.48 g h⁻¹. The composition of fed gas was N₂:H₂O: glycerol, equal to 18.7: 75: 6.3 in vol. %. The catalytic performance of the solid catalysts was evaluated at a gas hourly space velocity (GSHV) of reaction stream of 4400h⁻¹. The sampling time, after stabilization of

2. Experimental Description

temperature at 350 °C, was 90 min. Products were collected after the reactor in a cold trap. The concentrations of reactants and products obtained in the liquid phase (glycerol, acrolein, acetol) were measured by gas chromatography using a flame ionization detector (Column Alltec ECTM-1000 FFAP column 30 m × 0.53mm × 1.2 μm). Quantification was done by using the external standards. Volatile products running outside the cold trap (CO, CO₂) were analyzed online with a two columns Varian Chrompack micro-GC. The first column, silica plot, allows the CO analysis, while the second column, packed with molecular sieve, allows CO₂ analysis.

Fructose dehydration reaction was performed using batch catalytic system. Experiments were performed in a 100 mL stainless still autoclave, at 130 °C. In a typical procedure, 600 mg of fructose was dissolved in 60 mL of water and then 80 mg of solid catalyst was added. Water was chosen as a green and appropriate solvent for dehydration of fructose to 5-HMF. Starting time of the reaction was taken when the reaction mixture reached 130 °C. Time needed to reach this temperature was 30 min. Samples were withdrawn from the reaction mixture at 1 h intervals; the changes of fructose, 5-HMF, levulinic acid (LA) and formic acid (FA) concentrations with time were followed by collecting ¹H NMR spectra, using liquid NMR technique (Bruker AVANCE 250 spectrometer equipped with a multinuclear 10 mm Probe).

3. List of Catalysts

Table 1. List of titania and zirconia based catalysts investigated in this work.

Catalyst	Preparation method	Precursors	Calcination Temp. ^a (°C)	Publication
ZrO ₂	Commercial sample: Saint-Gobain Norpro	/	500	III
WO ₃ -ZrO ₂	Commercial sample: Dai Ichi Kigenso Kabushiki Kaisha	/	500	III
HPW/WO ₃ -ZrO ₂	Impregnation	H ₃ PW ₁₂ O ₄₀ , WO ₃ -ZrO ₂ (Dai Ichi Kigenso Kabushiki Kaisha)	450	III
CeO ₂ -ZrO ₂	Commercial sample: Dai Ichi Kigenso Kabushiki Kaisha	/	500	III
La ₂ O ₃ -ZrO ₂	Commercial sample: Dai Ichi Kigenso Kabushiki Kaisha	/	500	III
TiO ₂ anatase	Commercial sample: Saint-Gobain Norpro	/	500	III
TiO ₂ rutile	Commercial sample: Saint-Gobain Norpro	/	500	III
HPW/TiO ₂	Impregnation	H ₃ PW ₁₂ O ₄₀ , TiO ₂ anatase (Saint-Gobain Norpro)	500	III

^a All catalysts were calcined in air

3. List of Catalysts

Table 2. List of calcium-phosphate catalysts investigated in this work.

Catalyst	Ca/P molar ratio	W (wt.%)	Preparation method	Precursors	Calcination Temp. ^a (°C)	Publication
1.5 HAP	1.50	/	Commercial sample: Fluidinova S.A.	/	450	IV
1.66 HAP	1.66	/	Commercial sample: Fluidinova S.A.	/	450	IV
Ca/HAP	1.77	/	impregnation	1..66 HAP, (Ca(CH ₃ COO) ₂ •H ₂ O	450	IV
P/HAP	1.39	/	impregnation	1..66 HAP, H ₃ PO ₄	450	IV
W/HAP	1.50	15	impregnation	1..66 HAP, H ₂ WO ₄	450	IV

^a All catalysts were calcined in air

3. List of Catalysts

Table 3. List of niobia-ceria samples investigated in this work.

Catalyst	Preparation method	Precursors	Calcination Temp. ^a (°C)	Publication
CeO ₂	precipitation	Ce(NO ₃) ₃ •6H ₂ O	400	V
75% CeO ₂ -25%Nb ₂ O ₅	coprecipitation	Ce(NO ₃) ₃ •6H ₂ O , C ₄ H ₄ NNbO ₉ • xH ₂ O	400	V
50%CeO ₂ -50%Nb ₂ O ₅	coprecipitation	Ce(NO ₃) ₃ •6H ₂ O , C ₄ H ₄ NNbO ₉ • xH ₂ O	400	V
25%CeO ₂ -75%Nb ₂ O ₅	coprecipitation	Ce(NO ₃) ₃ •6H ₂ O , C ₄ H ₄ NNbO ₉ • xH ₂ O	400	V
Nb ₂ O ₅	precipitation	C ₄ H ₄ NNbO ₉ • xH ₂ O	400	V

^a All catalysts were calcined in air

3. List of Catalysts

Table 4. List of niobium based mesoporous mixed oxides investigated in this work..

Catalyst	Preparation method	Precursors	Calcination Temp. ^a (°C)	Publication
Nb ₂ O ₅	Evaporation induced self assembly	NbCl ₅	550	VI
Nb ₂ O ₅ - ZrO ₂	Evaporation induced self assembly	NbCl ₅ , ZrCl ₄	550	VI
Nb ₂ O ₅ - CeO ₂	Evaporation induced self assembly	NbCl ₅ , CeCl ₃	550	VI
Nb ₂ O ₅ - TiO ₂	Evaporation induced self assembly	NbCl ₅ , TiCl ₂	550	VI

^a All catalysts were calcined in air

3. List of Catalysts

Table 5. List of zeolites and hierarchical zeolites investigated in this work.

Catalyst	Preparation method	SiO ₂ /Al ₂ O ₃ Ratio	Calcination Temp. ^b (°C)	Publication
Z23P ^a	Commercial sample: Zeolyst International	23	500	VII
Z23M	Silicone extraction by alkaline treatment	Not determined	500	VII
Z50P ^a	Commercial sample: Zeolyst International	50	500	VII
Z50M	Silicone extraction by alkaline treatment	Not determined	500	VII
Z80P ^a	Commercial sample: Zeolyst International	80	500	VII
Z80M	Silicone extraction by alkaline treatment	Not determined	500	VII

^a Commercial MFI type zeolites (HZSM-5).

^b All catalysts were calcined in air

4. References

- [1] A. P. Haggerty, *Biomass Crops: Production, Energy and the Environment*, Nova Science Publishers, Inc. New York, 2011.
- [2] D. L. Klass, *Biomass for Renewable Energy, Fuels, and Chemicals*, Academic Press, San Diego, 1998.
- [3] P. McKendry, *Bioresource Technol.* 83 (2002) 37-46.
- [4] G. W. Huber, S. Iborra, A. Corma, *Chem. Rev.* 106 (2006) 4044-4098.
- [5] A. Corma, S. Iborra, A. Velty, *Chem. Rev.* 107 (2007) 2411-2502.
- [6] A. Corma, G. W. Huber, L. Sauvanaud, P. O'Connor, *J. Catal.* 247 (2007) 307-327.
- [7] G. W. Huber, P. O'Connor, A. Corma, *Appl. Catal. A-Gen.* 329 (2007) 120-129.
- [8] J. N. Chheda, G. W. Huber, J. A. Dumesic, *Angew. Chem. Int. Ed.* 46 (2007) 7164-7183.
- [9] A. J. Ragauskas, C. K. Williams, B. H. Davison, G. Britovsek, J. Cairney, C. A. Eckert, W. J. Frederick, J. P. Hallett, G. J. Leak, C. L. Liotta, J. R. Mielenz, R. Murphy, R. Templer, T. Tschaplinski, *Science* 311 (2006) 484-489.
- [10] J. Rostrup-Nielsen, *Catal. Rev.* 46 (2004) 247-270.
- [11] J. N. Chheda, J. A. Dumesic, *Catal. Today* 123 (2007) 59-70.
- [12] B. Kamm, *Angew. Chem. Int. Ed.* 46 (2007) 5056-5058.
- [13] G. W. Huber, A. Corma, *Angew. Chem. Int. Ed.* 46 (2007) 7184-7201.
- [14] J. Chowdury and K. Fouky, *Chem. Eng.* 100 (1993) 35-39.
- [15] F. Karaosmanoglu, K. B. Cigizoglu, M. Tuter, S. Ertekin, *Energy Fuels* 10 (4) (1996) 890-895.
- [16] L. C. Meher, D. Vidya Sagar, S. N. Naik, *Renewable Sustainable Energy Rev.* 10 (2006) 248-268.
- [17] M. McCoy, *Chem. Eng. News* 84 (2006) 7-8.
- [18] C-H. (Clayton) Zhou, J. N. Beltramini, Y-X. Fan, G. Q. (Max) Lu, *Chem. Soc. Rev.* 37 (2008) 527-549.
- [19] Global Industry Analysts, http://www.strategyr.com/Glycerin_Market_Report.asp.
- [20] T. Werpy, G. Petersen, *Top Value Added Chemicals from Biomass*, vol. 1, US Department of Energy (USDOE), Oak Ridge, 2004.
- [21] R. R. Soares, D. A. Simonetti and J. A. Dumesic, *Angew. Chem. Int. Ed.* 45 (2006) 3982-3985.
- [22] M. Pagliaro, M. Rossi, *The Future of Glycerol: 2nd Edition*, RSC Publishing, Cambridge, 2010.
- [23] Z. Z. J. Wang, J. Zhuge, H. Fang, B. A. Prior, *Biotechnol. Adv.* 19 (2001) 201-233.

4. References

- [24] B. Katryniok, S. Paul, V. Bellière-Baca, P. Rey, F. Dumeignil, *Green Chem.* 12 (2010) 2079-2098.
- [25] D.T. Johnson, K.A. Taconi, *AIChE J.* 26 (2007) 338-359.
- [26] B. Katryniok, S. Paul, M. Capron, F. Dumeignil, *ChemSusChem* 2 (2009) 719-730.
- [27] M. Pagliaro, R. Ciriminna, H. Kimura, M. Rossi, C. Della-Pina, *Angew. Chem. Int. Ed.* 46 (2007) 4434-4440.
- [28] Y. Zheng, X. Chen, Y. Shen, *Chem. Rev.* 108 (2008) 5253-5277.
- [29] M. H. Mohamad, R. Awang, W. M. Z. W. Yunus, *Am. J. Appl. Sci.* 8 (2011) 1135-1139.
- [30] A. Alhanash, E. F. Kozhevnikova, I. V. Kozhevnikov, *Appl. Catal. A: Gen.* 378 (2010) 11-18.
- [31] C.J. Zhou, C.J. Huang, W.G. Zhang, H.S. Zhai, H.L. Wu, Z.S. Chao, *Stud. Surf. Sci. Catal.* 165 (2007) 527-530.
- [32] E. Yoda, A. Ootawa, *Appl. Catal. A* 360 (2009) 66-70.
- [33] Y.T. Kim, K.D. Jung, E.D. Park, *Micropor. Mesopor. Mater.* 131 (2010) 28-36.
- [34] C.J. Jia, Y. Liu, W. Schmidt, A.H. Lu, F. Schüth, *J. Catal.* 269 (2010) 71-79.
- [35] A.S. de Oliveira, S.J.S. Vasconcelos, J.R. de Sousa, F.F. de Sousa, J.M. Filho, A.C. Oliveira, *Chem. Eng. J.* 168 (2011) 765-774.
- [36] S.H. Chai, H.P. Wang, Y. Liang, B.-Q. Xu, *Appl. Catal. A* 353 (2009) 213-222.
- [37] S.H. Chai, H.P. Wang, Y. Liang, B.Q. Xu, *Green Chem.* 10 (2008) 1087-1093.
- [38] E. Tsukuda, S. Sato, R. Takahashi, T. Sodesawa, *Catal. Commun.* 8 (2007) 1349-1353.
- [39] H. Atia, U. Armbruster, A. Martin, *J. Catal.* 258 (2008) 71-82.
- [40] W. Yan, G.J. Suppes, *Ind. Eng. Chem. Res.* 48 (2009) 3279-3283.
- [41] W. Suprun, M. Lutecki, T. Haber, H. Papp, *J. Mol. Catal. A* 309 (2009) 71-78.
- [42] S.H. Chai, H.P. Wang, Y. Liang, B.Q. Xu, *J. Catal.* 250 (2007) 342-349.
- [43] N.R. Shiju, D.R. Brown, K. Wilson, G. Rothenberg, *Top. Catal.* 53 (2010) 1217-1223.
- [44] A. Ulgen, W. Hoelderich, *Catal. Lett.* 131 (2009) 122-128.
- [45] A. Ulgen, W.F. Hoelderich, *Appl. Catal. A* 400 (2011) 34-38.
- [46] D. Stošić, S. Bennici, J.-L. Couturier, J.-L. Dubois, A. Auroux, *Catal. Commun.* 17 (2012) 23-28.

4. References

- [47] C-W. Chiu, A. Tekeei, W. R. Sutterlin, J. M. Ronco, G. J. Suppes, *AIChE J.* 54 (2008) 2456-2463.
- [48] A. K. Kinage, P. P. Upare, P. Kasinathan, Y. K. Hwang, J.-S. Chang, *Catal. Commun.* 11 (2010) 620-623.
- [49] C.L. Lima, S.J.S. Vasconcelos, J.M. Filho, B.C. Neto, M.G.C. Rocha, P. Bargiela, A.C. Oliveira, *Appl. Catal. A* 399 (2011) 50–62.
- [50] H. Atia, U. Armbruster, A. Martin, *Appl. Catal. A* 393 (2011) 331–339.
- [51] US Department of Energy “Feedstock Composition Gallery” US Department of Energy, 2005 (http://www.eere.energy.gov/biomass/feedstock_glossary.html).
- [52] M. Bicker, J. Hirth, H. Vogel, *Green Chem.* 5 (2003) 280-287.
- [53] K. W. Pentz, Great Britain Published Patent Application No. 2, 131, 014, 1984.
- [54] G. W. Huber, J. N. Chheda, C. J. Barrett, J. A. Dumesic, *Science* 308 (2005) 1446-1550.
- [55] O. O. James, S. Maity, L. A. Usman, K. O. Ajanaku, O. O. Ajani, T. O. Siyanbola, S. Sahu, R. Chaubey, *Energy Environ. Sci.* 3 (2010) 1833-1850.
- [56] P. E. Shaw, J. H. Tatum, R. E. Berry, *Carbohydr. Res.* 5 (1967) 266-273.
- [57] W. N. Haworth, W. G. M. Jones, *J. Chem. Soc.* (1944) 667-679.
- [58] H. E. Van Dam, A. P. G. Kieboom, H. Van Bekkum, *Starch-Starke* 28 (1986) 95-106.
- [59] M. J. Antal, W. S. L. Mok, G. N. Richards, *Carbohydr. Res.* 199 (1990) 91-102.
- [60] B. F. M. Kuster, *Starch-Starke* 42 (1990) 314-322.
- [61] L. Cottier, G. Descotes, *Trends Heterocycl. Chem* 2 (1991) 233-230
- [62]. P. Carniti, A. Gervasini, S. Biella, A. Auroux, *Catal. Today* 118 (2006) 373–378.
- [63] C. Carlini, M. Giuttari, A. M. R. Galletti, G. Sbrana, T. Armaroli, G. Busca, *Appl. Catal. A-General* 183 (1999) 295-304.
- [64] M. Watanabe, Y. Aizawa, T. Iida, R. Nishimura, H. Inomata, *Appl. Catal. A: Gen.* 295 (2005) 150–156.
- [65] F. Benvenuti, C. Carlini, P. Patrono, A. M. Raspolli Galletti, G. Sbrana, M. A. Massucci, P. Galli, *Appl. Catal. A* 193 (2000) 147-158.
- [66] C. Carlini, P. Patrono, A.M.R. Galletti, G. Sbrana, *Appl. Catal. A: Gen.* 275 (2004) 111–118.
- [67] R. Weingarten, G. A. Tompsett, W. C. Conner Jr., G. W. Huber, *J. Catal.* 279 (2011) 174-182.
- [69] C. Moreau, R. Durand, S. Razigade, J. Duhamet, P. Faugeras, P. Rivalier, P. Ros, G. Avignon, *Appl. Catal. A-Gen.* 145 (1996) 211-224.

5. Published Results

Publication I

Couplings with calorimetry

Dušan Stošić^{1*} and Aline Auroux¹

¹Institut de Recherches sur la Catalyse et l’Environnement de Lyon, UMR 5256 CNRS/Université Lyon 1, 2 avenue Albert Einstein, 69626 Villeurbanne Cedex, France

*corresponding author: dusan.stosic@ircelyon.univ-lyon1.fr

3.1 Introduction

Catalytic cycle in heterogeneous catalysis can be divided in five consecutive steps; diffusion of reactants to surface, adsorption of reactants, surface reaction processes, desorption of products and diffusion of reactants from the surface [1]. A fundamental understanding of the great diversity of chemistry occurring at the surface requires familiarity with molecule-surface interaction. The energetics of chemical events occurring on the surface play an important role in determining the catalytic properties of the surface, since different surfaces will cause a substance to react in different ways. It is known from the literature that oxidation of methanol can lead to different reaction products, and different selectivities depending on surface properties (structural and chemical) of catalyst used in this reaction [2,3]. Study of adsorption of probe and reactive gas molecules onto surface of catalysts lead to the better understanding of the nature of gas-solid interactions and give valuable information about the properties of the adsorbent surface and thus is of primary importance in catalysis.

Adsorption is an exothermic process and when a reactive molecule interacts with the surface of the solid heat is evolved. This heat is related to the energy of the bonds formed between the adsorbed species and the adsorbent and hence to the nature of the bonds and to the chemical reactivity of the surface. From a number of techniques used to study this interaction only a few provide information about the strength of chemisorption itself. The determination of the differential heats evolved, by a suitable microcalorimeter, when known amounts of gas probe molecules are adsorbed on catalytic surface is the most suitable and accurate method which allows the determination of the number, strength and energy

distribution of the adsorption sites [4-12]. The effective use of this technique in heterogeneous catalysis depends on choice of probe molecule, since the nature of the probe determines which surface property is going to be investigated.

The definition of various heats of adsorption/desorption and their relationship with thermodynamic quantities directly obtainable by calorimetry are given in Table 3.1.

Table 3.1 Definition of various heats of adsorption/desorption.

Name and symbol	Unit	Definition	Measurement method
Integral heat of adsorption: q_{int}	J	Quantity of heat evolved when n a moles are adsorbed at constant temperature on an adsorbent initially <i>in vacuo</i> , without a change in the volume of the cell: $Q_{\text{int}} = n a (U_a - U_g)$	Isotherm calorimetry
Molar integral heat $Q_{\text{int}} = \frac{q_{\text{int}}}{n^a}$	J mol ⁻¹	Integral heat per mole adsorbed	Isotherm calorimetry
Differential heat of adsorption: q_{diff}	J mol ⁻¹	Defined from integral heat by: $Q_{\text{diff}} = \left(\frac{\partial q_{\text{int}}}{\partial n^a} \right)_{T,A}$	Isotherm calorimetry
Isosteric heat: q_{st}	J mol ⁻¹	Heats of adsorption calculated from adsorption isotherms: $q_{\text{st}} = -RT^2 \left(\frac{\partial \ln P}{\partial T} \right)_{n^a}$	Adsorption isotherm

3.2 Coupled calorimetry-volumetry

Adsorption microcalorimetry is a powerful technique for the energetic characterization of solid surfaces, as well as for the thermodynamic description of solid-gas interfacial phenomena.

To access the energetic heterogeneity of surface small doses of probe gas (typically < 10 μmol g⁻¹) have to be added successively on the solid to saturate active sites progressively.

Corresponding heats range from 100 to 1000 mJ, and require few hours for being evolved. Since the development of commercial instrumentation able to measure quantitatively such low heats and adsorbed amounts, microcalorimetry has gained importance as one of the most reliable methods for the study of gas solid interactions [5,7,8].

A calorimeter that is suitable for measurement of heats of adsorption is required to have the following characteristics:

1) High sensitivity, with sufficient precision, to follow the changes of differential and integral heats with coverage, allowing the use of small doses of probe molecules.

2) High thermal stability, to have a well-stabilized base line, which is necessary to study the slow process of adsorption.

3) Large interval of utilization temperature. This is important for studying the interactions of different reactants with surface.

4) Good accessibility of the calorimeter proper allowing the connections with volumetric apparatus. Relatively large dimensions as well as suitable geometry of the calorimetric cells are also required for same purposes.

Most commonly used are heat-flow microcalorimeters of the Tian-Calvet type [5,8]. The detailed theory and operation of this calorimeter can be found elsewhere [11]. The apparatus is composed of an experimental vessel, where the studied system is located, which is placed into a calorimetric block (Fig. 3.1). The temperature of the block, which functions as heat sink, is controlled very precisely. The heat generated in the system flows to the heat sink and is accurately measured by means of detector. This is made of a large numbers of identical thermocouples (a thermopile) that surrounds the vessel and connected to the block (Fig 3.2) in such a way that vessel and block temperature are always close to each other. A signal is generated by the detector that is proportional to the heat transfer per unit time. Undesired signals due to the external temperature fluctuations in the calorimetric block are minimized by connecting in opposition two heat flow detectors from two identical vessels, one of which is used to perform the experiment, the other being used as a reference. Heat related to the introduction of the probe and other parasitic phenomena are thus compensated.

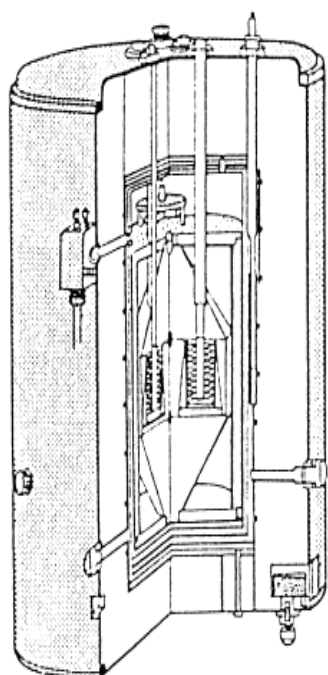


Fig. 3.1 Calvet microcalorimeter.

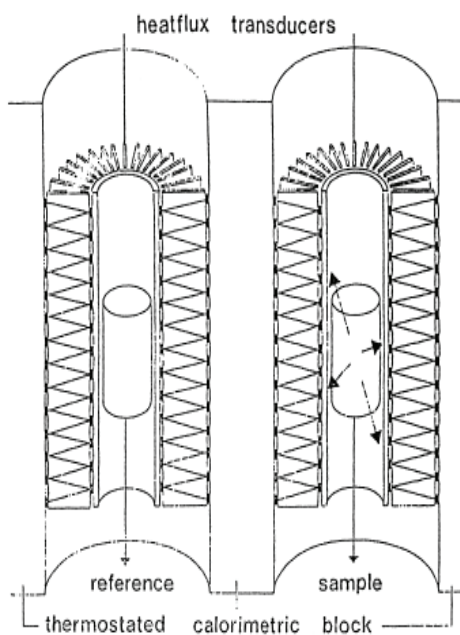


Fig. 3.2 Thermostated calorimetric block.

The heat generated by the process inside the vessel is transferred completely through the thermocouples, provided that radiation, conduction along the wall of the vessel, conduction and convection through the fluid phase are minimized by the design of the apparatus. A voltage signal, E , is generated by the thermocouples and recorded over the time of the thermal event, whose end is indicated by the returning of the thermopile output signal to the base line. The total heat evolved during the event is given by the area under the thermogram:

$$Q_{\text{exp.}} = K \int_{\text{exp.}} E dt \quad 1$$

where K is the instrument constant [11].

This highly sensitive heat flow calorimeter linked to sensitive volumetric system makes it possible to study gas-solid interactions and catalytic reactions. The apparatus used for this kind of measurement is presented in Fig. 3.3. The volumetric determination of the adsorbed amount of gas is performed in a constant volume vessel linked to a vacuum pump. The apparatus consists of two parts: the measuring element equipped with a capacitance manometer and a cell section, which includes the cells placed in the calorimeter (a sample cell in which the adsorbent solid is placed, and an empty reference cell). The volume of this vessel is determined by the expansion of a known quantity of gas, contained in the measuring

part of the assembly, into the previously evacuated cell section. This calibration must be made with the same gas and at the same temperature as the proposed study is going to be done.

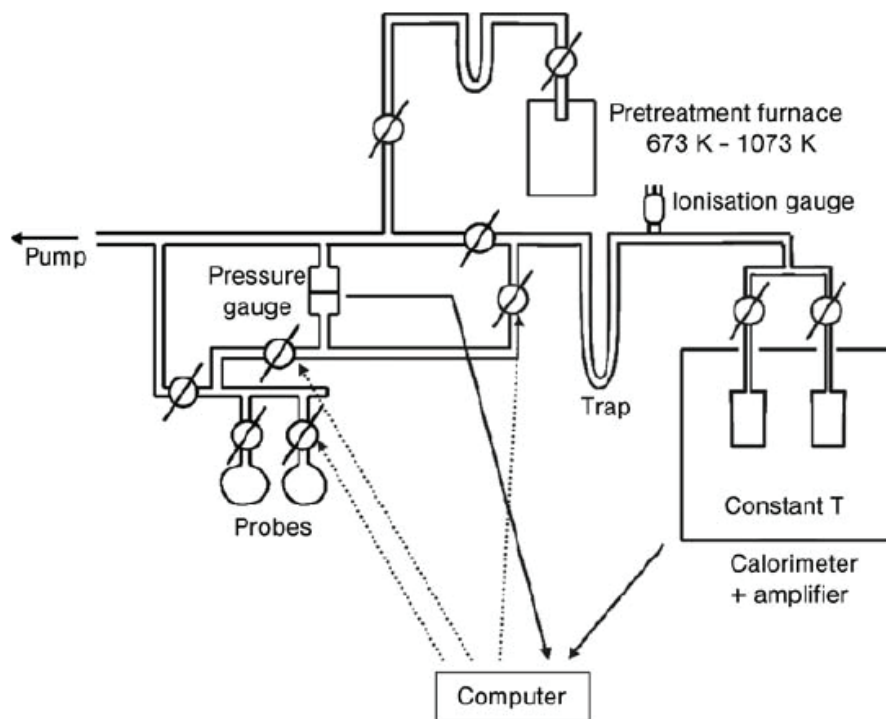


Fig. 3.3 Schematic diagram of the volumetric-calorimetric line.

In a typical experimental procedure the sample is first outgassed at the desired pretreatment temperature and under high vacuum in the calorimetric cell. After cooling to the adsorption temperature and when the thermal equilibrium of the system is reached, successive doses of gaseous probe molecules are brought into contact with catalyst sample. The heat flow signal and the corresponding pressure change are monitored and recorded until equilibrium is reached after admission of each dose. The volume of doses is minimized in order to detect any change in adsorption heats evolved with increasing the coverage of surface active sites. The adsorption is considered complete when for a significant increase in pressure there is no detectable heat evolution or gas adsorption. The adsorption temperature is maintained constant during the experiment. The irreversibly chemisorbed amount (V_{irr}) can be evaluated from the difference between the primary adsorption isotherm (adsorbed amount of gas as function of equilibrium pressure over sample) and a secondary isotherm obtained after desorption under vacuum and re-adsorption of the gaseous probe at the same temperature. By subtraction of re-adsorption

isotherm from the first adsorption isotherm amount of strong sites can be roughly estimated. The data obtained directly from adsorption calorimetry measurements are represented in Fig.3. 4, where both the calorimetric signal and the evolution of pressure are plotted as a function of time for each dose added.

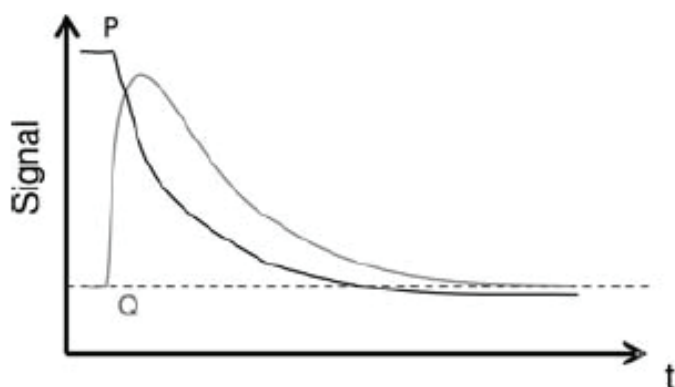


Fig. 3.4 Recorded data, pressure and heat flow signal, as a function of time for each dose of probe molecules.

From accumulation of these raw data until the full coverage is attained we can get information about the sample properties that can be summarized on various plots (Fig. 3.5):

a) The volumetric isotherms ($n_a = f(P)$) for a cycle of adsorption I, desorption by pumping at the same temperature and then re-adsorption (II). The irreversibly adsorbed volume (V_{irr}), which characterizes the strong sites of the catalyst, can then be calculated as the difference between the adsorption volume and the re-adsorption volume at a given equilibrium pressure.

b) The corresponding calorimetric isotherms ($Q_{int} = f(P)$).

c) The integral heats (Q_{int}) as a function of the adsorbed quantities (n_a). This representation leads to the detection of coverage ranges with constant heat of adsorption, those for which the evolved heat is a linear function of coverage.

d) The differential heat, $q_{diff} = Q_{int} / \partial n_a$ (molar heat of each dose of adsorbate) as a function of n_a . The ratio of the amount of heat evolved for each increment to the number of moles adsorbed in the same period is equal to the average value of the differential enthalpy of adsorption in the interval of the adsorbed quantity. The curve of differential heat as a function of surface coverage is traditionally represented as histograms. For simplification the steps of histogram are often replaced by a continuous curve connecting the centres of steps.

Differential heats of chemisorption usually decrease with increasing the surface coverage. The way in which the profile of differential heat changes with increasing surface coverage depends on nature of adsorbate and adsorbent. Sharp heat falls at low surface coverage are in general regarded to surface heterogeneity.

e) The energy distribution spectra in which $-dn_a/dq_{diff}$ is expressed as a function of q_{diff} . The area under this curve represents the number of molecules that are adsorbed with a given evolved heat. This kind of representation is not as accurate as a previous one.

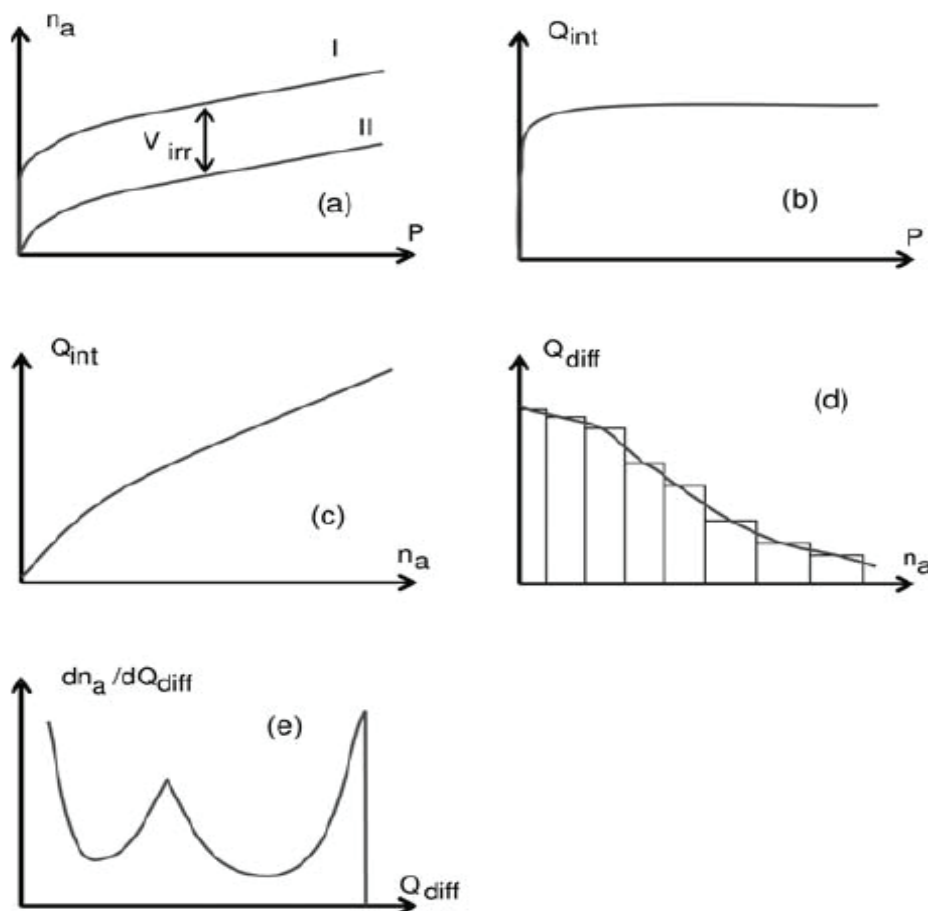


Fig. 3.5 Data obtained from volumetric-calorimetric adsorption experiments.

Although it is not possible to determine the nature of adsorbed species, or even to distinguish between different kinds of adsorbed species from the calorimetric data, the variation of the differential heats of adsorption with coverage quite clearly shows energy distribution of surface active sites with respect to a given adsorbate and their varying reactivity on given adsorbents. A general representation of differential heats of adsorption as a function of uptake of probe molecule (Fig. 3.6) presents the following features:

a) An initial region of high heats of adsorption, representing adsorption on the strongest sites, which are usually thought to be of Lewis type. After this region the curve drops abruptly.

b) One or more regions of intermediate strength sites. Regions of constant heat in this region are attributed to sets of sites of constant strength. This is taken as an indication of discrete inhomogeneity. These features, when adsorption of base molecule on the surface of zeolite is in question, are attributed to Brønsted acid sites.

c) A region where heats decrease more or less steeply depending on the heterogeneity of the sites. In this area a bump on the curve can sometimes be observed, which indicates lateral interactions between adsorbed molecules.

d) At a high coverage heat of adsorption approaches a constant value characteristic of hydrogen bonding between the molecule and the sample or physisorption of the molecules. This constant value is dependent on the nature of the probe molecule.

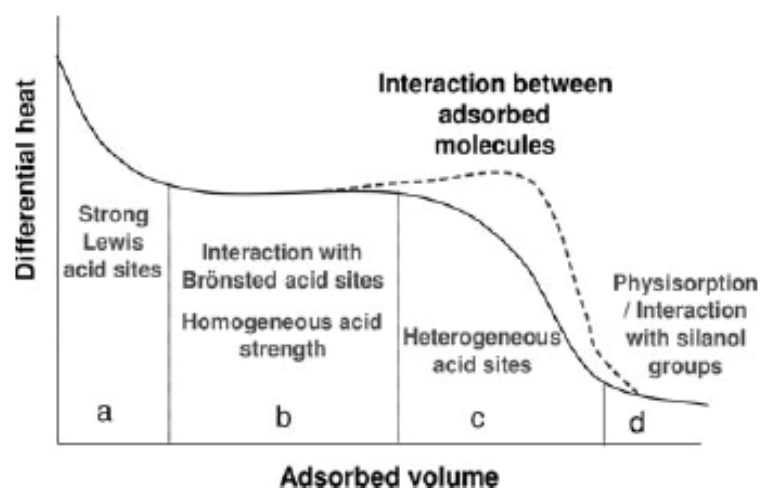


Fig. 3.6 Regions in a typical curve of differential heats of adsorption versus adsorbed amount. All regions (a, b, c, d) can be observed for zeolite samples presenting both Lewis and Brønsted acid sites, as probed by ammonia adsorption. For oxides presenting only Lewis acid sites, the regions a, c and d are observed.

This kind of representation of calorimetric data can be used to assess the uniformity-non-uniformity of the surface of the adsorbent with respect to energy, the energy of the lateral (adsorbate-adsorbate) interactions, and the structural or substructural (textural) changes that the adsorbent often undergoes as a result of interaction with the adsorbed substance [13].

Study of the thermokinetics of the heat evolution combined with volumetric and calorimetric data can provide a better insight into the adsorption mechanism and into the location of adsorbing sites on the catalyst surface [14, 15, 16]. It has been shown that interpretation of the shapes of individual thermograms facilitates identification of simultaneous processes with different kinetics as well as the variation of kinetics with coverage.

The kinetics of heat release during adsorption can be monitored by the change in thermokinetic parameter τ [14]. The calorimetric signal decreases exponentially with the time of adsorption after the maximum of each adsorption peak. This can be expressed in the form $D=D_m e^{-t/\tau}$, where D and D_m are the deviation at time t and maximum deviation of calorimetric signal, respectively. The thermokinetic parameter in this expression can be computed as the inverse of the slope of the logarithm of the evolved heat curve during the return to equilibrium. Variations of the thermokinetic parameter, determined in this way, can then be plotted versus the amount of adsorbed probe.

When ammonia or pyridine were used as a probe molecules to study the acidity of zeolites at a given temperature [14,16], the time needed to establish equilibrium after the addition of doses at first increases with increasing coverage (Fig. 3.7). This is due to the fast adsorption rate because the molecules are bonded irreversibly to the strongest acid sites. The curve then passes through a maximum as the adsorption rate decreases because the smaller number of strong sites is available and the molecules must diffuse over greater distances on the surface. This coverage should correspond to the filling of the acid sites of intermediate strength. Finally only the exchange between probe molecules among the weaker sites occurs. This is a fast process resulting in decrease of equilibrium time, which reaches a value close to the time constant of the calorimeter. In this way differentiation between strong and weak adsorption can be done.

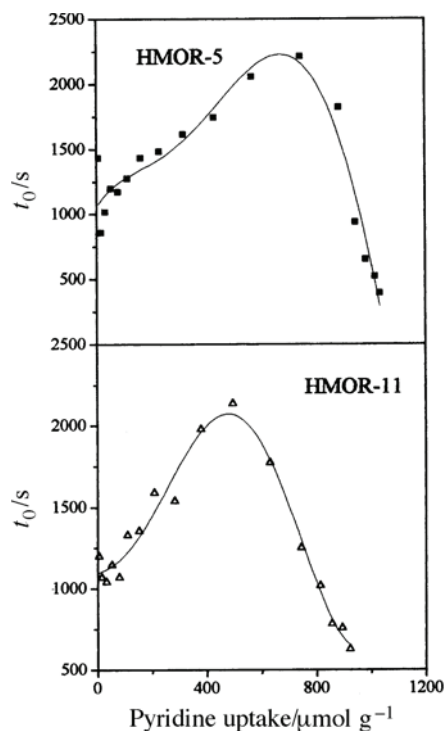


Fig. 3.7 Thermokinetic parameter as a function of pyridine uptake on mordenite samples (from [16]).

The time needed to establish the equilibrium depends on the quantity of adsorbed probe, on the temperature, number and strength of surface active sites and on the inertia of calorimeter. At lower temperatures, a slower adsorption is observed in covering the strong adsorption centres than at higher temperatures. The long time to establish the equilibrium is apparently related to redistribution of the adsorbed probe on the centres that are energetically more favourable [17]. When the time to establish thermal equilibrium is determined solely by inertia of calorimeter, one can be sure that the adsorption temperature was well chosen.

Entropy of adsorption, determined from adsorption equilibrium constants obtained from adsorption data (adsorption isotherms and differential heats of adsorption) can be also estimated.

Adsorption is an exothermic process and takes place with decrease in both free energy ($\Delta G < 0$) and entropy ($\Delta S < 0$). With respect to the adsorbate, the gas-solid interaction results in a decrease in entropy of the system. The differential molar entropies of the system can be plotted as a function of the coverage. The interest of a continuous measurement of derivative entropy of adsorption stems from the fact that any variation of its magnitude provides information on: i) a variation of the adsorbate-adsorbent interactions as a function of coverage (it allows the heterogeneities of the adsorbing surface to be detected), ii) a

collective modification of the state of the interaction of the molecules already adsorbed, iii) or a combination of both [17].

3.3 Coupled calorimetry-gravimetry

Gravimetry can be associated with adsorption calorimetry either in vacuum or in gas flow system. When vacuum system is used methodology of experiment is similar as used in calorimetry-volumetry technique. Desired amount of the sample is placed on microbalance which is surrounded by Tian-Calvet thermopile. Adsorbed amount of gas is determined by measuring the change in the sample mass. The heat flow signal and the corresponding mass change are monitored and recorded until equilibrium is reached after admission of each dose. Results obtained by this technique are comparable to that obtained when volumetric system is used to determine the amount of adsorbed gas. Volumetric measurements are to be preferred to gravimetric measurements for these determinations because it is very difficult to ensure a good and reproducible thermal contact between a sample of adsorbent, hanging from a balance beam, and the inner cell of a heat-flow calorimeter [11].

Flow adsorption calorimetry involves the use of carrier gas passing continuously through the adsorption cell. The catalyst is placed on a glass frit in a gas circulation cell in the calorimeter. Examples of gas flow cells are represented in Fig. 3.8. In order to determine the amounts of gas adsorbed flow calorimetry, in this case, is used in combination with thermogravimetry (TG). When this system is used in pulse mode it allows the measurement of heats of adsorption of a gaseous reactant on a solid or interaction heats between a gaseous reactant and pre - adsorbed species. When used as a flow reactor, it allows the kinetic study of catalytic reactions as well as the study of the activation or the aging of the catalyst. This is also a suitable system to perform calorimetric temperature programmed reduction (TPR), temperature programmed oxidation (TPO) or temperature programmed desorption (TPD) experiments. In addition to calorimetry, temperature programmed desorption (TPD) of adsorbed probe molecules can in principle also be used to estimate heats of adsorption [19].

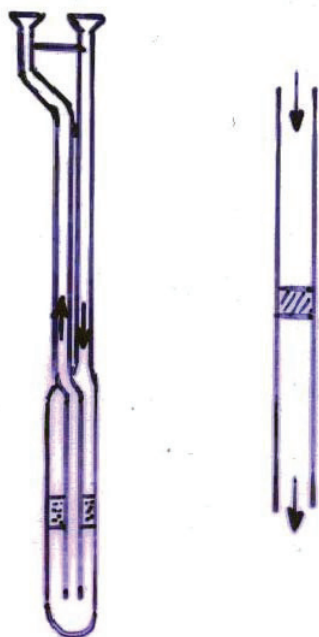


Fig. 3.8 Gas flow cells.

3.4 Temperature Programmed Desorption (TPD) Technique

The temperature programmed desorption of probe molecules is commonly used method for measuring basic or acidic properties of catalyst surfaces. In this procedure the sample is subjected to temperature programmed heating and pre-adsorbed gas is progressively desorbed. The rate of desorption increases with temperature increase, goes through a maximum, and finally goes back to zero as the surface is cleared from adsorbate. TG-DSC-MS is experimental setup (Fig. 3.9) that can be used for this kind of measurements. During this experiment endothermic heat signal, temperature of desorption and concentration of desorbed molecules is measured. Desorption energy distribution of probe molecules that is available from these data, can be related to the acid strength distribution of surface active sites by hypothesis that desorption energy is equal to the energy of acid re-protonation.

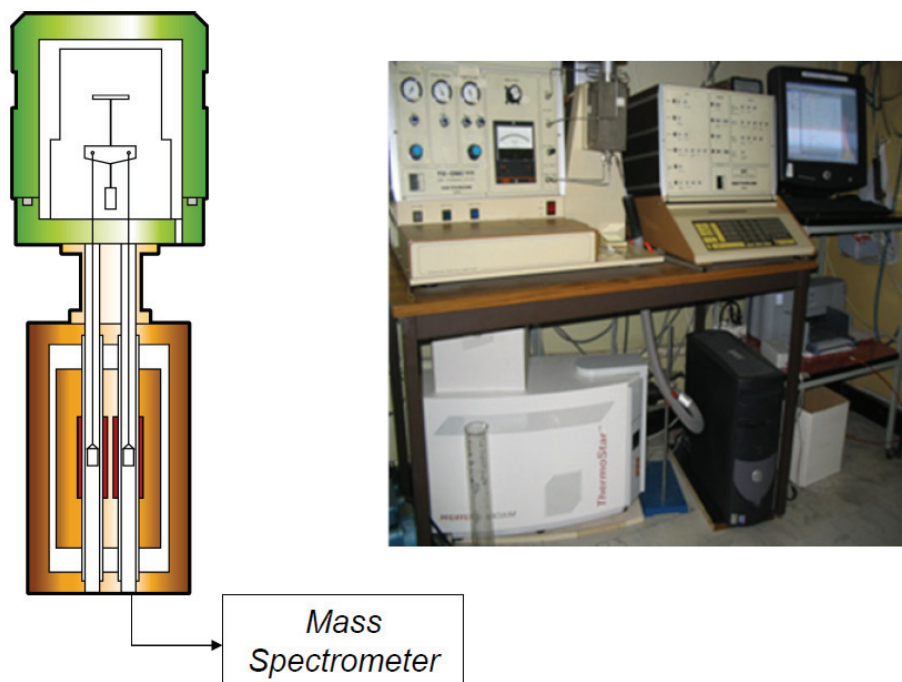


Fig. 3.9 Schematic representation and a photograph of a TG-DSC-MS apparatus.

Despite the fact that TPD is widely used because of its simplicity the main drawbacks of this technique have to be pointed out.

- TPD gives an average value of acid strength rather than a distribution.
- Results obtained by this technique are strongly affected by mass or heat transfer and diffusion.
- TPD enables only to distinguish the strength of active sites, but not their types.
- Desorption on weak sites is hindered by adsorbates on strong sites.
- During desorption, a readsorption may occur.
- Peaks overlap, so TPD can be used only to roughly distinguish the various acid site strengths.

TPD of reactive amines is a very useful technique for measuring Brønsted site densities in zeolites [20-23]. Alkylammonium ions, formed by protonation of amines at Brønsted sites react in a very narrow temperature range in TPD through a reaction similar to Hoffman elimination reaction. Fig. 3.10 shows a result for TPD-TGA-MS of isopropylamine from an H-MFI sample having a bulk Si/Al ratio of 26 [24]. The TGA results are useful since one can determine whether there are residual species on the sample after desorption and one can quantify the amounts which desorb without having to calibrate the mass spectrometer.

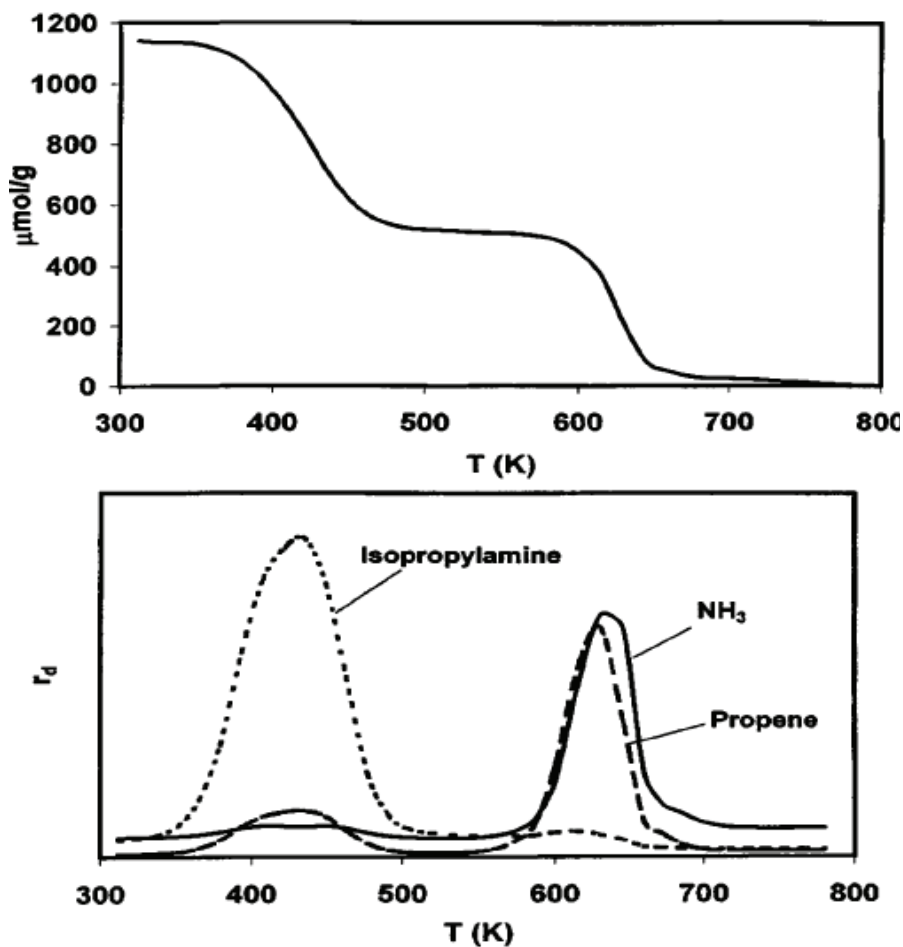


Fig. 3.10 TPD-TGA-MS results for isopropyl amine in H-MFI sample. The desorption of propylene and ammonia above 550 K corresponds to decomposition of the amine at the Brönsted acid sites (from [24]).

From MS results the nature of acid sites can be determined. Upon heating in vacuum two stages of weight loss and two stages of product evolution can be observed. The molecules associated with low-temperature desorption can probably be assigned to a number of different types of species, including molecules associated with Lewis-acid sites, molecules associated with hydroxyl defects, and molecules which are hydrogen bonded to protonated amines at the Brönsted sites. At high temperature molecules desorb as propylene and ammonia. This desorption feature can be associated with protonated molecules at Brönsted sites. Fact that the measured site density is independent of the choice of alkylamine gives further confirmation that TPD-TGA-MS results provide a true evaluation measure of the Brönsted site density [25].

3.5 Temperature Programmed Reduction (TPR)

From calorimetric TPR-TPO experiments heats of reduction and reoxidation of cationic or metal species can be determined. Data obtained from these experiments may provide kinetic data of theoretical significance as well as an insight into the mechanism of the reduction processes.

TPR profiles of copper exchanged ETS-10, obtained by differential scanning calorimetry (DSC) and carried out with a hydrogen stream in helium, are presented in Fig. 3.11 [26]. All the reduction profiles show complex structure, in which a stepwise reduction of CuO to Cu through Cu₂O intermediates occurred with overlapping of the two peaks. By analysis of this profiles authors gained useful information concerning the identification of supported species and the determination of intermediate oxidation states of metals during reduction.

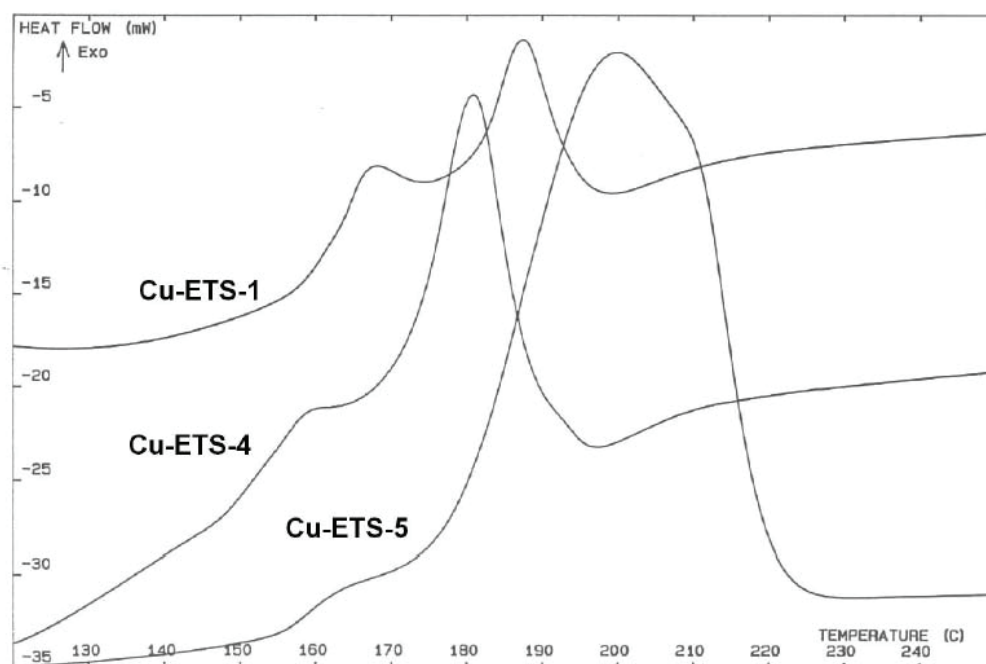


Fig. 3.11 DSC curves of reduction by hydrogen as a function of temperature for Cu-ETS samples (from [26]).

In another study in order to compare reducibility power of hydrogen, ethane, and ethylene authors performed the reduction of fresh vanadium pentoxide by each of them (diluted in helium) in a TG-DSC apparatus [27]. Fig 3.12 shows the heats of reduction which are exothermic and the derivative of the thermogravimetric curves which are negative if

associated with a weight loss occurring during the reduction. According to the weight loss, a similar reduction extent was recorded for all three cases. Heat flow measurements have shown that reducibility levels of V_2O_5 by ethane and hydrogen similar, whereas ethylene is much more active than ethane over that oxide.

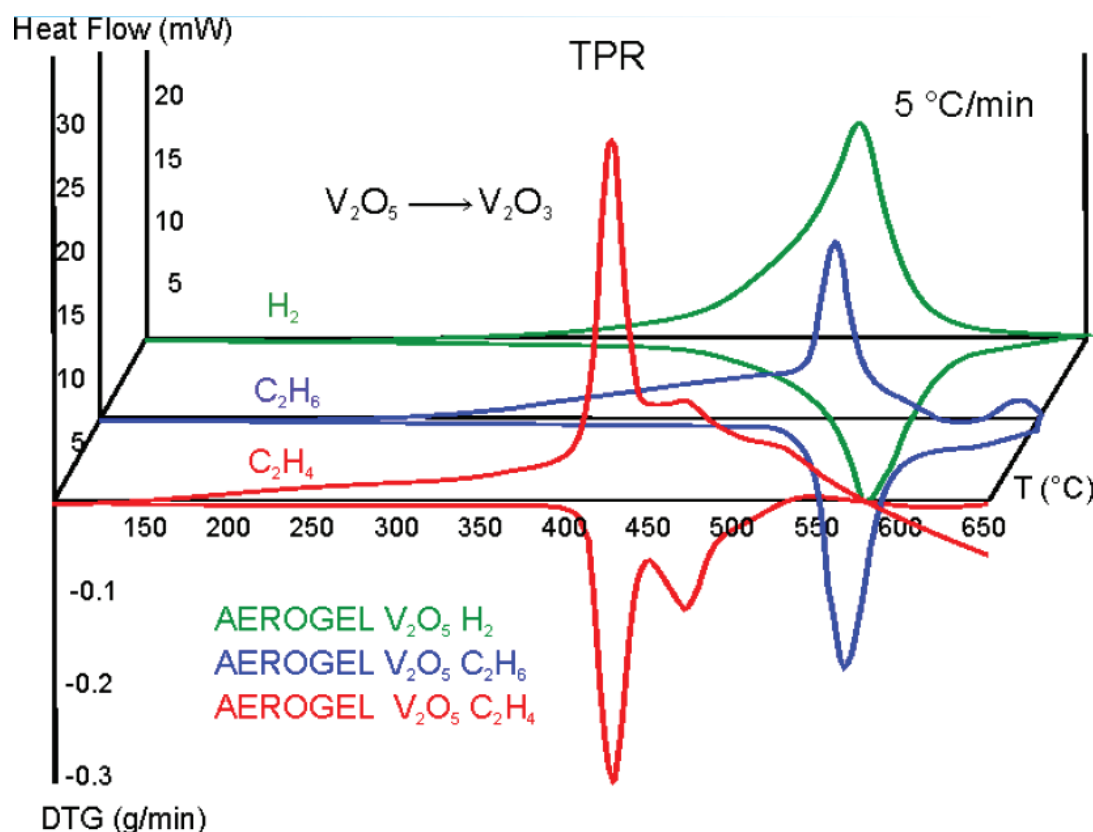


Fig. 3.12 Heats of reduction of V_2O_5 and associated derivatives of the thermogravimetric curves as a function of temperature, for various reducing agents (from [27]).

3.6 Calorimetry – gas chromatography / mass spectrometry

This coupling can be used for characterization of acidic or basic character of solid catalysts, and for study of solid-gas reactions. Systems used for these measurements are usually modified DSC instruments connected with GC/MS by a heated capillary tube [28-32]. In a typical experiment small pulses of probe gas are injected at regular intervals into the carrier gas stream from a gas sampling valve. The gas flows are regulated by mass flow controllers. The concentration of ammonia down-stream of the sample is monitored with the MS/GC and heat evolution with the calorimeter.

When gas-solid reactions are under investigation this system allows simultaneous determination of heats of reaction and identification of products. Scheme of the apparatus is shown in Fig 3.13.

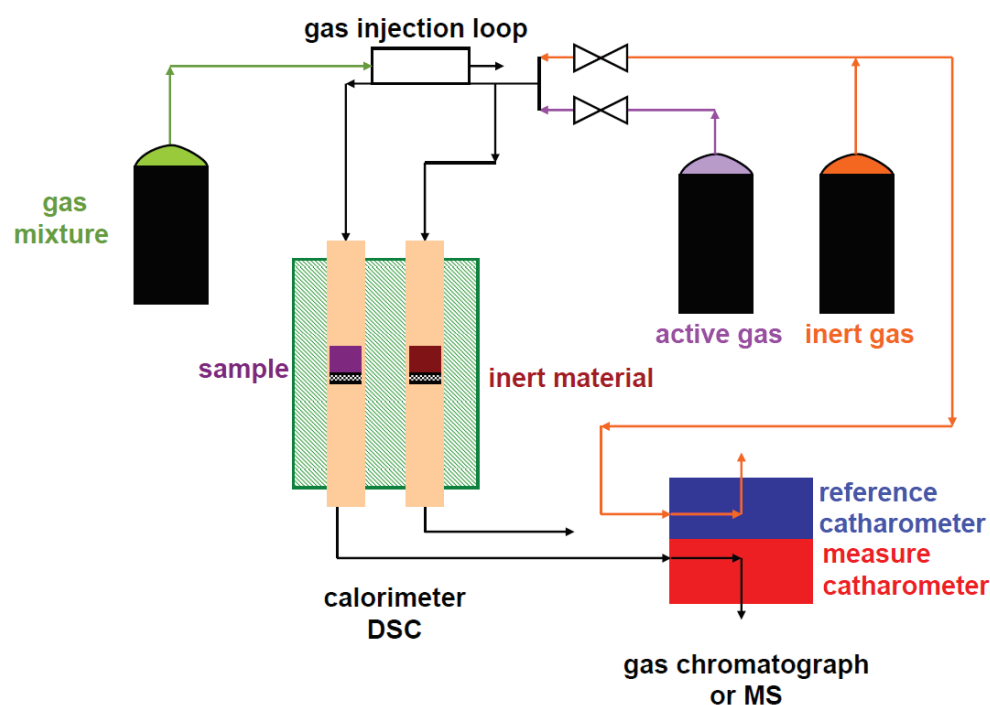


Fig. 3.13 Experimental device.

3.7 Calorimetry-syringe pump-UV-Vis fluorescence spectrometry

Isothermal titration calorimetry is a technique that can directly measure liquid-solid or liquid-liquid interactions. This method has been used for determination of acid-base properties of solid catalysts in an inert phase (n-decane), for determination of heats of reaction in liquid phase (alkylation, anisole + benzoic anhydride on H-Beta zeolite), and for determination of heats of adsorption of different pollutants on an adsorbent [33]. It is also recognized as the only technique that can directly measure the binding energies of biological processes such as protein-ligand binding and protein-protein binding [34].

Instrument that is usually employed in this technique is differential heat flow calorimeter of Tian-Calvet type equipped by a stirring system. A programmable syringe pump is linked to the calorimeter by capillary tubes. Using this syringe pump, successive pulses of known amounts of a solution of a probe molecule can be sent on the sample which is maintained on constant temperature during the experiment. UV-Vis spectrometer is connected to the calorimetric cell by an optic fiber, and it is used to monitor the changes in

concentration of the probe molecule. From equilibrium concentration after each dose of solution, adsorption isotherms can be constructed. Scheme of the instrument is presented in Fig. 3.14.

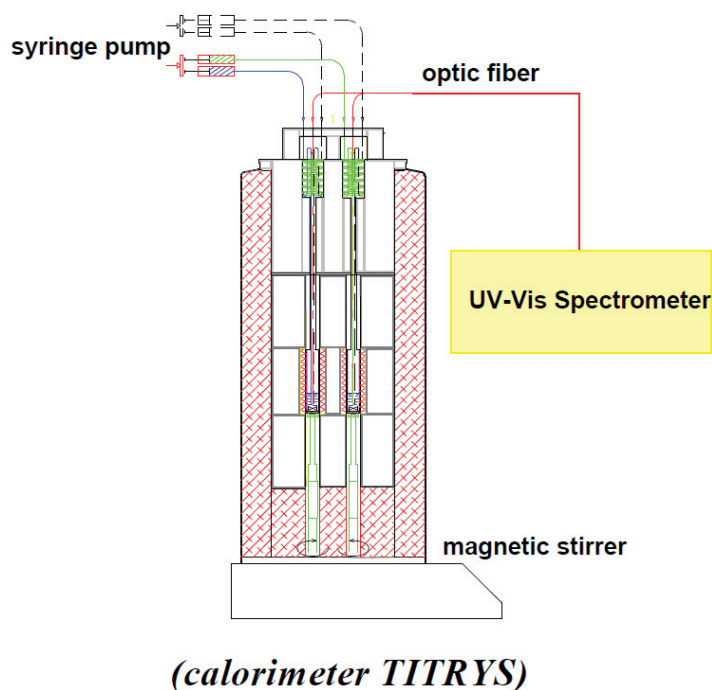


Fig. 3.14 Schematic representation of a TITRYS calorimeter connected to UV-Vis spectrometer.

This method has been used for characterization of acidity of solid catalysts, or to investigate adsorptive properties of solid materials by measuring the adsorption heats evolved upon injection of dilute solutions of chosen molecules onto the solid itself in a slurry of appropriate solvent. The output of typical microcalorimetric experiment is shown in Fig. 3.15. Each pulse injection of dosed amount of solution of probe molecule gives as a result the exothermic signal that formed a specific peak related to the heat of adsorption. This heat derives from two different contributions: the exothermic enthalpy of adsorption and the endothermic enthalpy of displacement of adsorption; while the enthalpy effects originating from dilution and mixing phenomena can be neglected due to the differential design of the calorimeter and the preheating of the probe solution. The amount of adsorptive in solution is measured simultaneously with a UV-Vis spectrometer, leading to an adsorption isotherm which is measured over the range of base addition used in calorimetric titration. Study of evolution of UV-Vis signal with time (Fig. 3.16) during adsorption of each dose added gives a better insight in to the adsorption mechanism.

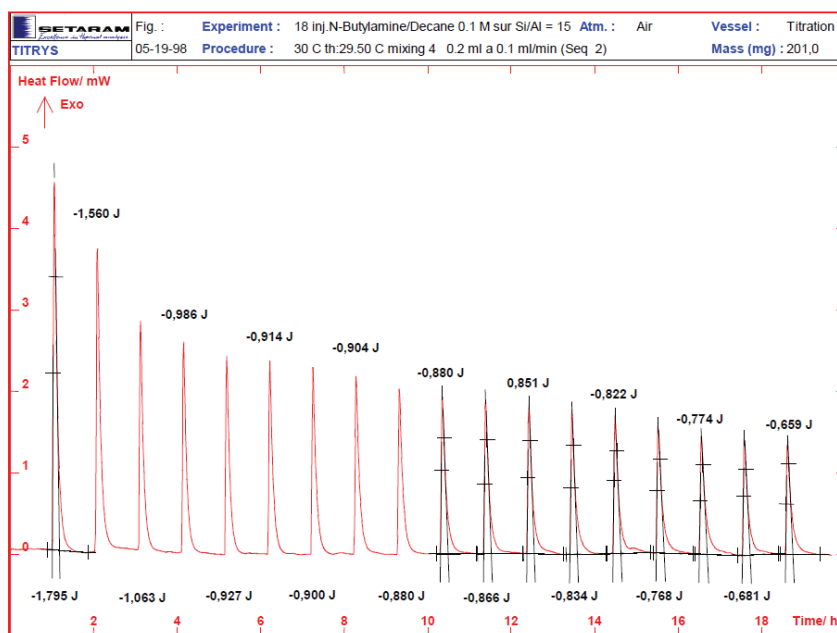


Fig. 3.15 The output of typical microcalorimetric experiment for successive doses.

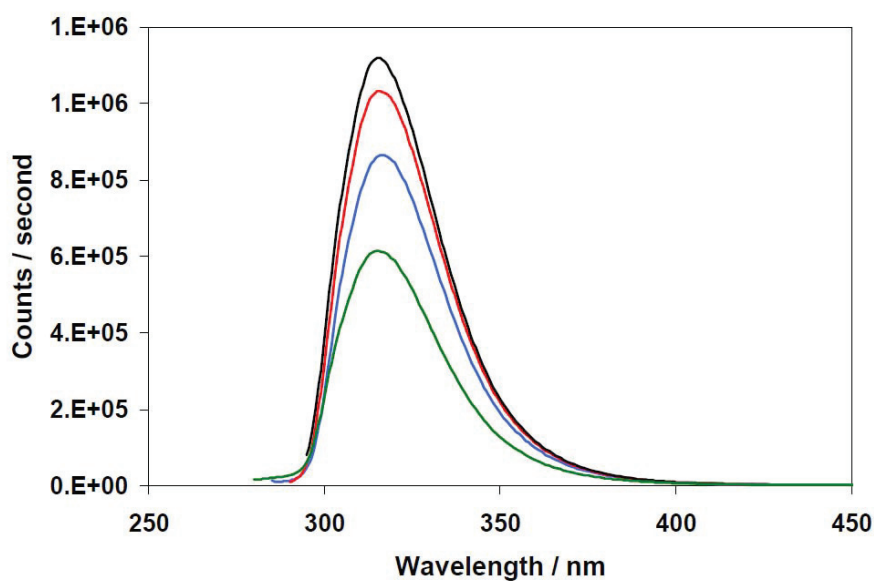


Fig. 3.16 UV-Vis signal evolution as a function of time for one injection.

Combination of data obtained from calorimetric measurements and adsorption isotherms permits a determination of the number of active sites, the equilibrium constants, and the enthalpy of a binding to each type of the site [35-39].

For microcalorimetric determination of the strength of solid acids in solution, pyridine, n-butylamine and aniline are the usual probe molecules that are used. The measurements are

done in a non-interacting hydrocarbon solvent (e.g. cyclohexane) whose molecular mass is close to that of donor in order to cancel out contribution from a dispersion component to the measured enthalpy [36]. Throughout the experiment the molar enthalpy of neutralization, $\Delta H_{\text{neut}}^\circ$, is measured. If $\Delta H_{\text{neut}}^\circ$ values are going to be used as measurements of relative acid strength, some assumptions have to be made. This is because the measured enthalpy of neutralization is made up from contributions from several sources: proton loss from the acid and proton gain by the base, changes in solvation as the acid and base are converted to the conjugate base and acid, plus any enthalpy changes associated with formation of ion pairs that form or break up during the neutralization process. In order for the differences in measured $\Delta H_{\text{neut}}^\circ$ values to reflect the differences in the acid strength of acid solids requires that all contributions to $\Delta H_{\text{neut}}^\circ$ other than the proton affinity of the acid are constant. This can be taken as reasonable assumption only when closely related solid acids are compared [36, 40-42]. Another point is that titration calorimetric measurements of this kind are usually performed at temperatures close to room temperature so the process of adsorption is more likely to be kinetically controlled. In this way adsorption could occur simultaneously on different types of active sites and average value of $\Delta H_{\text{neut}}^\circ$ is obtained for each dose of probe molecule. Because of this real strength distribution of acid sites is not always available from these measurements.

Useful feature of this method is possibility to change solvent and investigate the influence of solvent on acid strength. Niobium oxide and niobium phosphate were investigated by this technique, using aniline and 2-phenyl-ethylamine as probe molecules, in order to understand the effective acidity of these solids measured in various solvents (decane, cyclohexane, toluene, methanol, and isopropanol) of very different polarities and proticities. Using this technique it is possible to discriminate the acid site strength distribution more accurately than with conventional gas-solid phase titration with ammonia [43]. In another study acid strength of sulfonic acids supported on polystyrene and silica solids were determined in water and cyclohexane. It was shown how the relative acid strength of these very similar types of supported acid depends markedly on the nature of solvent. The relative acidities of these solid materials are reversed when going from water to cyclohexane. This leads to a conclusion that if these measurements are to be used for predicting catalytic activity, it is essential that they are made in solvents similar to those in which the catalysts are ultimately to be used [44].

3.8 Limitations of technique

Results obtained by adsorption microcalorimetry are not sufficient to determine the nature of adsorbed species, or even to distinguish between different kinds of adsorbed species. When examination of catalyst surface is done, that possess both Lewis and Brønsted acidity, by adsorption of base probe molecule such as ammonia, it is difficult to discriminate strong Lewis from strong Brønsted acid sites solely by adsorption microcalorimetry. This is due to the fact that differential heats of NH_3 interaction with strong Lewis and Brønsted acid sites are relatively close to each other. For this reason complementary informations from suitable IR, MAS NMR and XPS investigations are necessary to identify these sites [45]. However, because of the complex nature of the active site strength distribution it is not possible to make a detailed correlation between sites of different nature and their strength.

Initial values representing very small concentrations of the strongest active sites can be easily missed in the measurement if the gas doses are not small enough.

If kinetics of adsorption is determined by diffusion limitations, determined heats of adsorption may reflect an average heat of the various strong sites, rather than a specific effect. In this case adsorption on active but less-accessible sites may occur only after better-exposed but less-active sites have interacted. Differential heat profiles determined under diffusion restrictions may reflect less surface heterogeneity than actually exists on surface of the adsorbent [11]. The sample bed thickness has also to be considered because the molecular mobility in the sample bed is a limitation to rapid data collection [7].

Finding correlations of surface properties of catalyst (in the case of adsorption calorimetry: acid, basic and redox properties) with its catalytic behaviour is sometimes difficult. The lack of correlation is due to the fact that by microcalorimetry measurements the total amount of acid or basic sites is obtained and only a fraction of these active sites may actually be involved during the catalytic reaction [46]. There could be surface sites that are either too weak to activate the reactants or are too strong, leading to strongly held species which block and deactivate these sites or causing excessive fragmentation of reactant or products. It has been recognized that the catalytic properties of Brønsted acid sites (proton donors) can be different from Lewis acid sites (electron pairs acceptors). For example, it has been suggested that Brønsted acids are much more active than Lewis acids for skeletal

transformations of hydrocarbons [47], and as said before it is impossible to differentiate them solely by adsorption microcalorimetry technique.

3.9 Influence of the adsorption temperature on the acid/base determination

In order that adsorption microcalorimetry can give an accurate representation of active site strength distribution the adsorbed probe molecule must be equilibrated among all sites on the catalyst surface within the time frame of the experiment. If external or internal mass-transfer limitation exists the adsorption on surface sites is controlled by kinetics instead of thermodynamics [5]. In this case the profile of differential heats as function of coverage would not accurately represent energy spectrum of the surface active sites and the adsorbent surface would appear to be more homogeneous. For these reasons, it is important to study the effect of the adsorption temperature and verify that molecules possess sufficient thermal energy to obtain the thermodynamically stable site occupation.

When the process of adsorption was studied on various temperatures two different kinds of temperature dependence were observed [48, 49]. One type was described as a change of the profile of differential heat of adsorption with increasing coverage of pyridine on HY zeolite and silica-alumina as temperature was raised. The adsorption of pyridine was performed at 423 K and 473 K. For lower coverage, the profile of integral heats obtained for the adsorption at 473 K, lies above that obtained at 423 K. This difference is decreasing as the surface coverage is increasing, and at high coverage the situation is opposite. The difference between the differential heat curves with temperature suggests that there is difference in selectivity when adsorption is performed on higher temperatures compared to adsorption on lower temperatures. Adsorption occurred on stronger acid sites in preference to weaker sites on higher temperature, whereas random adsorption occurred simultaneously on both weak and strong sites at low temperatures. The authors [48, 49] proved this hypothesis by monitoring the change in the intensity of the hydroxyl infrared adsorption bands on a HY zeolite at different temperatures for the progressive titration of acid sites with pyridine. This behaviour proves the importance of high surface mobility of probe molecules on the catalysts surface for equilibration on active sites.

The second type of behaviour was a slight decrease in the differential heats of ammonia adsorption on HY above 473 K and NaY above 313 K with an increase of temperature. This

decrease was attributed to the fact that the temperature dependence of the heat of adsorption was thermodynamically defined by the difference in molar heat capacity between adsorbed state and gaseous state.

Unusual behaviour was observed for adsorption of ammonia on protonated ZSM zeolite at 416 K [50]. Differential heat curve passed through a maximum at relatively low coverage. This behaviour was explained by conjunction of three independent phenomena: immobile adsorption, mass-transfer limitations and preferential location of the most energetic acid sites in the internal pores of zeolite structure. The maximum was eliminated by heating of samples between doses to increase the surface mobility of the preadsorbed ammonia and allow it to migrate and adsorb on the most acidic sites. In this way most accessible sites are made available for new doses of ammonia at lower temperature. After this the heat curve showed a slightly higher value than the initial heat for the conventional method of adsorption, and it did not show any maximum.

From the discussed experimental results it is clear that results obtained by adsorption microcalorimetry technique are strongly dependent on the temperature at which the experiments are performed. For samples which possess strong sites, increasing the adsorption temperature yields a better description of the thermodynamic site strength distribution. For samples which possess weaker sites adsorption at higher temperatures produces a large decline in the adsorption capacity. In any case the choice of adsorption temperature is constrained and involves compromise between using high temperatures to reduce equilibrium times, and using lower temperatures to achieve high coverage of the active sites at reasonable pressures.

3.10 Probe molecules

The key for effective utilisation of microcalorimetry in heterogeneous catalysis is the judicious choice of gas-phase molecules for study. Although total number of surface active sites and potentially active centres can be estimated by this technique, the obtained values are strongly dependent on the nature and size of the probe molecule. As a general rule, no matter which surface property is examined (acidic, basic or redox); probe molecule should be stable with temperature and with time. Furthermore, as discussed before, the adsorbed probe should be sufficiently mobile to equilibrate on active sites on temperature of the experiment.

3.11 Probing surface acidic properties

Though it is very reliable, the calorimetric measurement of surface acidity of solid catalysts depends on the choice of the basic probe molecule used to neutralize the acid sites. Ammonia ($pK_a = 9.24$, proton affinity in gas phase = $857.7 \text{ kJ mol}^{-1}$) and pyridine ($pK_a = 5.19$, proton affinity in gas phase = $922.2 \text{ kJ mol}^{-1}$) are the favoured probe molecules to probe overall surface acidity of catalysts, because both Lewis and Brønsted acid sites retain these molecules.

Ammonia is among the smallest strongly basic molecules and its diffusion is little affected by the porous structure, if at all. Because of this, it is the most commonly used probe molecule for testing surface acid properties. It is adsorbed as an ammonium ion, and the corresponding heat of adsorption depends both on the proton mobility and on the affinity of ammonia for the proton.

Heats of adsorption of strong base molecules are related to intrinsic acidity of the site and to the interaction energy between the deprotonated surface of the sample and the protonated base [51]. From this it is a logical question how strongly do different bases interact with the Brønsted and Lewis sites, and which base interacts more strongly. A study of surface acidity by adsorption of various basic probe molecules (ammonia, pyrrole, dimethyl ether and acetonitrile) on dealuminated Y type zeolites proved that obtained acid site distribution strongly depends on the basicity of probe molecule [52]. Ammonia proved to be a reliable probe molecule when Brønsted acid sites were being investigated. It helped to unveil two site populations whose properties varied with Si/Al ratio. These two populations differ by local environment of the associated AlO_4 tetrahedra. Ammonia, however, failed to reveal inhomogeneity of one particular acid population. Dimethyl ether appeared as a too weak a base, whereas pyrrole, showing no steric hindrance in this case, appeared as a rather amphoteric probe which helped visualize the basicity difference between the parent and dealuminated materials. Acetonitrile proved to be a reliable probe to monitor quantitatively and qualitatively Lewis acidity.

In another study with various base probe molecules experiments have been performed on ferrierite sample, covering a wide range of basic strength, in the order acetonitrile > dimethyl ether > water > pyrrole > ammonia [53]. It has been shown that the strength distribution depends on the basicity of the probe molecule. Moreover the total

number of neutralized sites appeared constant irrespective of the nature of the probe, except for pyrrole, and nearly equal to the number of protons (Figure 17).

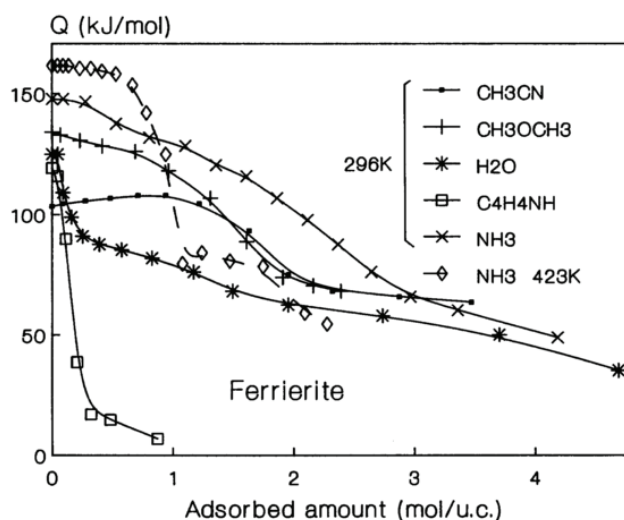


Figure 17 Differential heats of adsorption of various probe molecules on a ferrierite sample versus the probe uptake (from [53]).

Using a series of amines as probe molecules, Parrilo et al. found a good correlation between heats of adsorption and gas phase proton affinities, but not with the proton transfer energies of those bases in aqueous phase [54-56]. These results indicate that the proton transfer dominates the interaction between the adsorbate and the acid sites. However, in a theoretical study published by Teraishi the fact that the heat of ammonia adsorption depends both on the proton affinity and the ammonium ion affinity was underlined [57]. With regard to the catalytic reaction in zeolites, the activity depends not only on the proton affinity but also on the stability of the cationic intermediate in the zeolite. The heat of ammonia adsorption, which includes the later effect, is thus in disagreement with proton affinity and provides a different measure of acidity, which is better suited to evaluate the acid strength of the zeolite in relation with its catalytic activity.

3.12 Probing surface basic properties

The number of acidic probe molecules that are able to cover wide range of strength is rather small. Moreover the difficulty in evaluating surface basic properties stems from the fact that these molecules may interact simultaneously with cations (such as Na^+). The ideal probe molecule should be specific to basic sites, it should distinguish interaction with oxide ion and hydroxyls and it should not give rise to chemical reactions.

Carbon dioxide ($pK_a = 6.37$), owing to its acidic character, is commonly used to characterize the basicity of solids. A large number of species of this molecule on solid surfaces can be formed; on basic hydroxyl groups there is a formation of hydrogen carbonate species, on basic oxygen ions different kinds of carbonate species can be formed. IR evidence concerning the formation of carbonate-like species of different configurations has been reported for metal oxides, which accounts for the heterogeneity of the surface revealed by microcalorimetric measurements [58]. Localization of the carbonate species formed either on surface (in the form of unidentate, bidentate or bridged species) or in the bulk (polydentate species) is essential for the results obtained by microcalorimetry. The heat evolved from the CO_2 interaction can result not only from its adsorption on basic surface sites, but also from its reaction with the bulk. Moreover, if basic character of zeolites is investigated, CO_2 can interact with extra framework cation.

Sulphur dioxide ($pK_a = 1.89$) is another molecule commonly used to investigate basicity of solid catalysts. SO_2 adsorption on the surface of metal oxides is complex. Several types of species can be formed according to hydroxylation state and the acidity or basicity of surface [58]. Interaction of SO_2 with basic O^{2-} leads to formation of sulfite type species. The sulfite ion is pyramidal and it can coordinate to metal in a form of monodentate, bidentate or bridged. Sulfur dioxide can also interact with surface hydroxyl groups and form hydrogen sulfite species. It can also be coordinated to Lewis acid sites where it forms weakly bonded species.

The number of CO_2 adsorption sites is always much lower than that found for SO_2 suggesting that adsorption of CO_2 is more specific than that of SO_2 . The latter, having a very strong acidic character, therefore probes almost all the basic sites regardless of their strength.

3.13 Probing surface redox properties

The heats of reduction of oxide samples can be determined by studying the adsorption of hydrogen, CO and various hydrocarbons on the fully oxidized catalysts [27, 59]. The extent of reduction of the catalyst surface can be evaluated in particular using H_2 . The measurement of hydrocarbon (e.g. propene, propane, acrolein, etc.) adsorption heats is complicated by the subsequent reaction of the adsorbed species or by incomplete desorption of the products [60].

In the case of CO reduction, the catalyst – oxygen bond energy has to be calculated by subtracting the heat of formation of CO₂.

However, it is known that, in the absence of processes other than plain surface coordination, CO acts as a weak Lewis base and can interact with the strongest surface Lewis acid sites. NO can also be employed either as a probe to identify Lewis acid sites or as a reducing agent. However, NO may disproportionate into N₂O and oxygen and it is also very likely to form nitrosyl complexes in the presence of transition metal ions [60].

The heats of oxidation of the reduced oxides can be further measured using O₂ adsorption. Large variations of the re - oxidation heat can be sometimes observed when any further oxidation is limited by the diffusion of oxygen into the reduced portion of the particle [61].

References

1. Arnaut L, Formosinho S, Burrows H (2007) Chemical kinetics: from molecular structure to chemical reactivity. Elsevier, Amsterdam
2. Tatibouët JM et al (1997) Methanol oxidation as a catalytic surface probe. *Appl Catal A Gen* 148: 213-252
3. Baldani M, Wachs IE et al (2001) Methanol: a “smart” chemical probe molecule. *Catal Lett* 75: 137-149
4. Farneth WE, Gorte J et al (1995) Methods for characterizing zeolite acidity. *Chem Rev* 95: 615-635
5. Cardona-Martinez N, Dumesic JA (1992) Applications of adsorption microcalorimetry to the study of heterogeneous catalysis. In: Eley DD, Pines H, Weisz PB (ed) *Advances in catalysis*, vol 42. Academic Press, Inc. San Diego, pp 149-244
6. Andersen PJ, Kung HH (1994) Characterization of catalysts with microcalorimetry. In: Spivey J J, Agarwal SK (ed) *Catalysis*, vol 11. Royal Society of Chemistry, Cambridge, pp 441-466
7. Auroux A et al (1997) Acidity characterization by microcalorimetry and relationship with reactivity. *Top Catal* 4: 71- 89
8. Solinas V, Ferino I et al (1998) Microcalorimetric characterisation of acid-basic catalysts. *Catal Today* 41: 179-189
9. Spiewak BE, Dumesic JA et al (1996) Microcalorimetric measurements of differential heats of adsorption on reactive catalyst surfaces. *Thermochim Acta* 290: 43-53
10. Auroux A (1994) Thermal Methods: Calorimetry, differential thermal analysis, and thermogravimetry. in: Imelik B, Vedrine JC (ed) *Catalyst characterization: physical techniques for solid materials*. Plenum Press, New York, pp 611-635.
11. Gravelle PC et al (1972) Heat-Flow microcalorimetry and its application to heterogeneous catalysis. In: Eley DD, Pines H, Weisz PB (ed) *Advances in catalysis*, vol 22. Academic Press, Inc. San Diego, pp 191-263.
12. Auroux A et al (2008) Acidity and basicity: determination by adsorption microcalorimetry. In: Karge H, Weitkamp J (ed) *Molecular sieves—science and technology: acidity and basicity*. vol 6. Springer, Heidelberg, pp 45-152

13. Tarasevich YI et al (2001) Interaction of water and other polar substances with various sorbents according to calorimetric and chromatographic data. *Theor Exp Chem* 37: 197-214
14. Auroux A, Huang M, Kaliaguin S et al (1996) Decrystallization process of HNaY zeolites upon mechanical milling: a microcalorimetric and thermokinetic study. *Langmuir* 12: 4803-4807
15. Cardona-Martinez N, Dumesic JA et al (1990) Acid strength of silica-alumina and silica studied by microcalorimetric measurements of pyridine adsorption. *J Catal* 125: 427-444.
16. Ferino I, Monaci R, Rombi E, Solinas V et al (1998) Microcalorimetric investigation of mordenite and Y zeolites for 1-methylnaphthalene isomerisation. *J Chem Soc Faraday Trans* 95: 2647-2652
17. Kapustin GI, Brueva TR, Klyacho AL, Rubinshtein AM et al (1981) Analysis of distribution of adsorbate molecules within zeolite crystals by thermokinetics. *Kinet Catal* 22: 183-195
18. Gervasini A, Auroux A et al (1993) Thermodynamics of adsorbed molecules for a new acid-base topochemistry of alumina. *J Phys Chem* 97: 2628-2639
19. Damjanović Lj, Auroux A et al (2009) Determination of acid/base properties by temperature programmed desorption (TPD) and adsorption calorimetry. In Chester A, Derouane E (ed) *Zeolite chemistry and catalysis: an integrated approach and tutorial*, Springer Verlag, Berlin, p 107-167
20. Gricus Kofke TJ, Gorte RJ, Farneth WE et al (1988) Stoichiometric adsorption complexes in H-ZSM-5. *J Catal* 114: 34-45
21. Gricus Kofke TJ, Gorte RJ, Kokotailo GT, Farneth WE et al (1989) Stoichiometric adsorption complexes in H-ZSM-5, H-ZSM-12, and H-mordenite zeolites. *J Catal* 115: 265-272
22. Gricus Kofke TJ, Kokotailo GT, Gorte RJ et al (1989) Stoichiometric adsorption complexes in [B]- and [Fe]-ZSM-5 zeolites. *J Catal* 116: 252-262
23. Tittensor J, Gorte RJ, Chapman D et al (1992) Isopropylamine adsorption for the characterization of acid sites in silica-alumina catalysts. *J Catal* 138: 714-720
24. Gorte RJ et al (1999) What do we know about the acidity of solid acids? *Catal Lett* 62: 1-13

25. Pereira C, Gorte RJ et al (1992) Method for distinguishing Brønsted-acid sites in mixtures of H-ZSM-5, H-Y and silica-alumina. *Appl Catal A* 90: 145-157
26. Gervasini A, Picciau C, Auroux A et al (2000) Characterization of copper-exchanged ZSM-5 and ETS-10 catalysts with low and high degrees of exchange. *Micropor Mesopor Mater* 35–36: 457–469
27. Le Bars J, Védrine JC, Auroux A, Pommier B, Pajonk GM et al (1992) Calorimetric study of vanadium pentoxide catalysts used in the reaction of ethane oxidative dehydrogenation. *J Phys Chem* 96: 2217-2221
28. Siril PF, Davison AD, Randhava JK, Brown DR et al Calorimetric study of vanadium pentoxide catalysts used in the reaction of ethane oxidative dehydrogenation. *J Mol Catal A: Chem* 267: 72-78
29. Westmoreland PR, Inguilizian T, Rotem K et al Flammability kinetics from TGA/DSC/GCMS, microcalorimetry and computational quantum chemistry. *Thermochim Acta* 367-368: 401-405
30. Groszek AJ et al (1998) Flow adsorption microcalorimetry. *Thermochim Acta* 312: 133-143
31. Siril PF, Brown DR et al (2006) Acid site accessibility in sulfonated polystyrene acid catalysts: calorimetric study of NH₃ adsorption from flowing gas stream. *J Mol Catal A: Chem* 252: 125-131
32. Felix SP, Jowitt CS, Brown DR et al (2005) Base adsorption calorimetry for characterising surface acidity: a comparison between pulse flow and conventional “static” techniques. *Thermochim Acta* 433: 59-65
33. Rakić V, Damjanović Lj, Rac V, Stošić D, Dondur V, Auroux A et al (2010) The adsorption of nicotine from aqueous solutions on different zeolite structures. *Water Res* 44: 2047-2057
34. Thomson JA, Ladbury JE (2004) Isothermal titration calorimetry. In Ladbury JE, Doyle ML (ed) *Biocalorimetry 2 Applications of calorimetry in the biological sciences*, Wiley-VCH, Weinheim. p 35-58
35. Lim YY, Drago RS, Babich MW, Wong N, Doan PE et al (1987) Thermodynamic studies of donor binding to heterogeneous catalysts. *J Am Chem Soc* 109: 169-179

36. Chronister CW, Drago RS et al (1993) Determination of hydrogen-bonding acid sites on silica using the Cal-Ad method. *J Am Chem Soc* 115: 4793-4798
37. Drago RS, Dias SC, Torrealba M, de Lima L et al (1997) Calorimetric and spectroscopic investigation of the acidity of HZSM-5. *J Am Chem Soc* 119: 4444-4452
38. Kob N, Drago RS, Young V et al (1997) Preparation, characterization, and acidity of a silica gel/tungsten oxide solid acid. *Inorg Chem* 36: 5127-5131
39. Drago RS, Dias CS, McGilvray JM, Mateus ALML et al (1998) Acidity and hydrophobicity of TS-1. *J Phys Chem B* 102: 1508-1514
40. Drago RS, Kob N et al (1997) Acidity and reactivity of sulfated zirconia and metal-doped sulfated zirconia. *J Phys Chem B* 101: 3360-3364
41. Arnet EM, Haaksma RA, Chawla B, Healy MH et al (1986) Thermochemical comparisons of homogeneous and heterogeneous acids and bases. 1. Sulfonic acid solutions and resins as prototype brønsted acids. *J Am Chem Soc* 108: 4888-4896
42. Arnet EM, Absan T, Amarnath K et al (1991) Thermochemical comparisons of solid and homogeneous acids and bases: pyridine and polyvinylpyridine as prototype bases. *J Am Chem Soc* 113: 6858-6861
43. Carniti P, Gervasini A, Biella S, Auroux A et al (2005) Intrinsic and effective acidity study of niobic acid and niobium phosphate by a multitechnique approach. *Chem Mater* 17: 6128-6136
44. Koujout S, Brown DR et al (2005) Calorimetric base adsorption and neutralisation studies of supported sulfonic acids. *Thermochim Acta* 434: 158-164
45. Guimon C, Martinez H (2003) *Recent Research Developments in Catalysis 2*. Research Signpost, Kerala
46. Knözinger H (1976) Specific poisoning and characterization of catalytically active oxide surfaces. In: Eley DD, Pines H, Weisz PB (ed) *Advances in catalysis*, vol 25. Academic Pres, Inc. San Diego, pp 184-271
47. Benesi HA, Winquist BH (1997) Surface acidity of solid catalysts. In: Eley DD, Pines H, Weisz PB (ed) *Advances in catalysis*, vol 27. Academic Pres, Inc. San Diego, pp 97-182

48. Mitani Y, Tsutsumi K, Takahashi H et al (1983) Direct measurement of the interaction energy between solids and gases. X. acidic properties of hydroxyl sites of H–Y zeolite determined by high-temperature calorimetry. *Bull Chem Soc Jpn* 56: 1917-1920
49. Tsutsumi K, Mitani Y, Takahashi H et al (1983) Direct measurement of the interaction energy between solids and gases. IX. heats of adsorption of ammonia and pyridine on several solids at high temperature. *Bull Chem Soc Jpn* 56: 1912-1916
50. Vèdrine JC, Auroux A, Coudurier G (1984) Combined physical techniques in the characterization of zeolite ZSM-5 and ZSM-11 acidity and basicity. In: Whyte TW Jr, Dalla Betta RA, Derouane EG, Baker RTK (ed) *Catalytic materials: relationship between structure and reactivity*. ASC Symposium Series, vol 248. American Chemical Society, Washington, pp 253-273
51. Damjanović Lj, Auroux A (2008) Heterogeneous catalysis on solids. In: Brown ME, Gallagher PK (ed). *Handbook of thermal analysis and calorimetry* vol 5. Elsevier, Amsterdam, pp 387-438
52. Auroux A, Chi ZC, Echoufi N, Ben Taarit Y (1989) Calorimetric investigation of the acidity of dealuminated Y-type zeolites using various basic probes. In: Karge HG, Weitkamp J (ed) *Zeolites as catalysts, sorbents and detergent builders*. Studies in surface science and catalysis, vol. 46, Elsevier, Amsterdam, pp 377-387
53. Auroux A (1988) New probes FOP an accurate calorimetric determination of the acidity of zeolites. In: Grobet PJ, Mortier WJ, Vansant EF, Schulz-Ekloff G (ed) *Innovation in zeolite materials science*. Studies in surface science and catalysis, vol. 37, Elsevier, Amsterdam, pp 385-391
54. Parrillo DJ, Gorte RJ, Farneth WE et al (1993) A calorimetric study of simple bases in H-ZSM-5: a comparison with gas-phase and solution-phase acidities. *J Am Chem Soc* 115: 12441-12445
55. Parrillo DJ, Biaglow A, Gorte RJ, White D (1994) Quantification of acidity in H-ZSM-5. In: Weitkamp J, Karge HG, Pfeifer H, Hölderich W (ed) *Zeolites and related microporous materials: state of the art*. Studies in surface science and catalysis, vol. 34, Elsevier, Amsterdam, pp 701-708
56. Parrillo DJ, Gorte RJ et al (1992) Characterization of stoichiometric adsorption complexes in H-ZSM-5 using microcalorimetry. *Catal Lett* 16: 17-25

57. Teraishi K et al (1995) Effect of Si to Al substitution at next-nearest neighbor sites on the acid strength: ab initio calculation of the proton affinity and the heat of ammonia adsorption. *Micropor Mater* 5: 233-244
58. Lavalley JC et al (1996) Infrared spectrometric studies of the surface basicity of metal oxides and zeolites using adsorbed probe molecules. *Catal Today* 27: 377-401
59. Cabrejas Manchado M, Guil JM, Perez Masia A, Ruiz Paniego A, Trejo Menayo JM et al (1994) Adsorption of H₂O, CO, and CO₂ on a γ -alumina: volumetric and calorimetric studies. *Langmuir* 10: 685-691
61. Witzel F, Karge HG, Gutze A et al (1992) Proc 9th Int Zeolite Conf Montreal Canada, July 5-10, (von Ballamos R, Higgins JB, Treacy MMJ eds), Butterworth-Heinemann, Boston, 1993, vol 2. p 283
61. Yang L, Kresnawahjuesa O, Gorte RJ (2001) A calorimetric study of oxygen-storage in Pd/ceria and Pd/ceria–zirconia catalysts. *Catal Lett* 72: 33-37

Characterization of acid-base sites in zeolites

Dušan Stošić^{1*} and Aline Auroux¹

¹Institut de Recherches sur la Catalyse et l'Environnement de Lyon, UMR 5256 CNRS/Université Lyon 1, 2 avenue Albert Einstein, 69626 Villeurbanne Cedex, France

*corresponding author: dušan.stosic@ircelyon.univ-lyon1.fr

9.1 Introduction

Zeolites are natural or synthetic microporous materials with an ordered structure: zeolite frameworks consist of 4-fold connected TO_4 tetrahedra ($T = Si, Al$) that form three-dimensional networks. In these networks, each oxygen atom is shared between two neighbouring tetrahedra; in other words, the linkage in between tetrahedra is accomplished through T-O-T bridges [1-3]. It should be mentioned that aluminate tetrahedra cannot be neighbours in the frameworks of zeolites. In other words Al-O-Al linkages are forbidden; this requirement being known as the Loewenstein rule [1-2]. In zeolitic network, the binding capability in between tetrahedra reaches its maximum; thus, ideal zeolite crystals should have terminal silanol groups only on their external surface[4].

The linkage of tetrahedra within zeolites leads to open network structures: the tetrahedra (primary building units) form rings of various sizes which are linked to form complex units (secondary building units). These secondary building units may be connected in many different ways to give a large number of different zeolite structure types. Thus formed network of interconnected tetrahedra results in the zeolite framework. From the other point of view, it can be told that zeolite crystals contain pore or channel systems of molecular dimensions with fixed geometry and size [3].

According to the pore size, zeolites are classified into small- (pore size up to 5 Å), medium- (pore size 5-6 Å), and large-pore types (pore size 7-8 Å). Typical representatives of the different types are zeolite A, ZSM-5, and the faujasites (X and Y), respectively [5]. According to the International Zeolite Association Website, about 190 different framework types of zeolites, zeolitic silicates and phosphates with precisely estimated structures are known to date (2010) [6].

In zeolite network, any tetrahedral T atom (Si^{4+} or Al^{3+}) is surrounded by four O^{2-} ions. Network constructed of SiO_2 units should be therefore, neutral, because each O^{2-} ion is shared by two tetrahedra. However, the isomorphous substitution of Si^{4+} by Al^{3+} causes a negative excess charge of the framework. This framework anionic charge is compensated by charge-balancing

cations located in the channels [7-9]. In contrast to the semipolar character of bonds within the zeolite framework, the interaction between cations and the framework is ionic. Oxygen atoms with radii of ca. 1.36 Å surround the smaller central atoms of the tetrahedra nearly completely [3]. Consequently, the interior surface of zeolites is nearly entirely composed of oxygen atoms. Nonframework charge-balancing cations and molecules within the pore system coordinate framework oxygen atoms. Water, if present, can coordinate these cations and interact with other sorbed molecules [1]. Finally, the overall composition of zeolitic unit cell is given by the formula:



where n denotes the Si/Al ratio and z is the number of water molecules adsorbed per framework Al atom.

Previously mentioned isomorphous substitution of Si^{4+} ions with Al^{3+} that provokes a negative excess charge of the framework is at the origin of their acidity [1-2], one of the most important characteristics of these materials which explains their numerous catalytic applications. Unlike framework T atoms, the charge-balancing cations can be exchanged by other cations from aqueous solutions [10-11]. If cations are exchanged by protons, the zeolite acquires considerable Brønsted acidic properties and for this reason they can be viewed as solid acids. Importantly, both Lewis and Brønsted acid sites can be found in the structure of zeolites [12]. The way to generate Brønsted acid sites (proton donor sites) is based either on the thermal decomposition of ammonium form of as-synthesized zeolites or on the direct ion exchange of Na^+ (usually) by H^+ (with mineral or organic acids). Brønsted acid sites can be converted into Lewis acid sites by dehydroxylation at elevated temperatures [5]. These processes are presented in Fig. 9.1. However, it is important to notice that charge-balancing cations can also play a role of Lewis acidity.

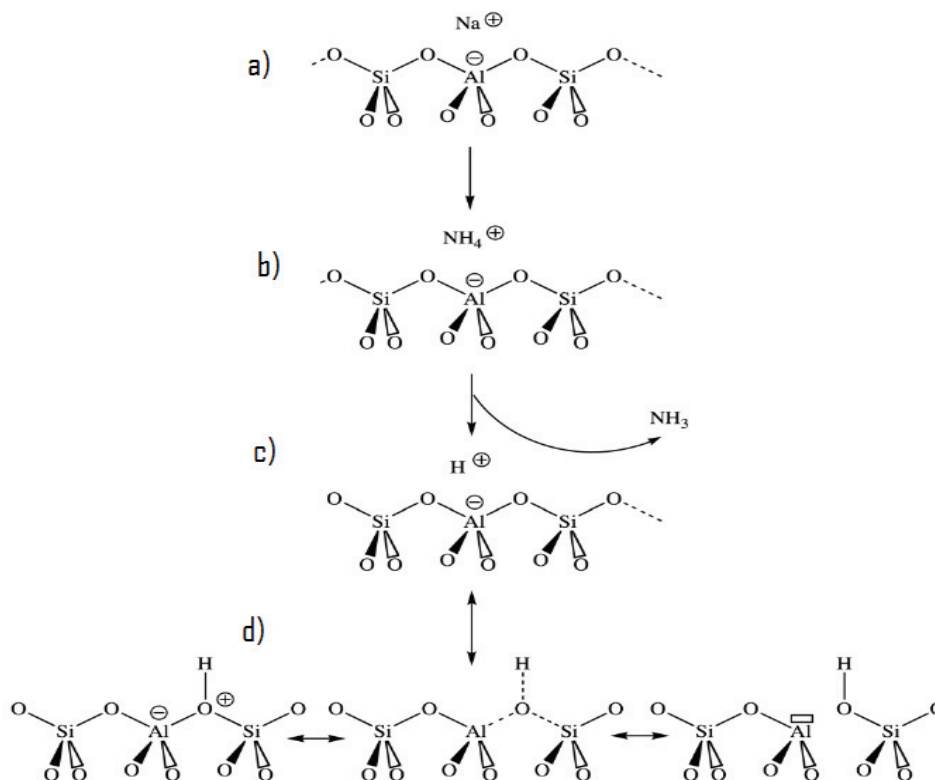


Fig. 9.1 Schematic presentation of generation of Brønsted and Lewis acidity in zeolites. a) the presentation of charge-balancing cation; b) cation-exchange Na^+ to NH_4^+ ; c) from NH_4^+ cation, isolated proton (proton-donor or Brønsted acid site) arises by calcination; d) Lewis acid site (Al atom with the empty electron orbital, electron acceptor) is formed by dehydroxylation.

Altogether, the structural diversity of zeolites discussed above is responsible for a wide range of interesting zeolite properties such as ion-exchange capacity, specific adsorption behaviour, and catalytic activity due to acidity, shape selectivity caused by size and polarity of molecules, high thermal stability and resistance against solvents, and wide flexibility for adjustments by post synthesis modification.

Because their thermal and mechanical stabilities are not enough to be used for the industrial purposes, and the zeolite synthesis requires too much cost and time, so many kinds of zeolite species are not available industrially. In fact, only about ten kinds of zeolites have been applied in industrial catalytic processes. In practice, Y-zeolite, ZSM-5, mordenite, MCM-22, and β zeolites are most typical zeolite catalysts [13]. Accordingly to the needs of specific catalytic reaction, they can be modified appropriately. For example, steaming, dealumination by HCl, cation-exchange or metal loading, are processes that can be applied to tune zeolites' features for their applications as industrial catalysts. In addition, since the remarkable developments of the mesoporous materials such as SBA-15, MCM-41 and FSM-16, many kinds of mesoporous materials also are synthesized and studied.

Evidently, many opportunities to develop a new catalyst based on zeolites and zeolite like materials are opened.

To summarize, industrial processes in which zeolites are used are mostly reactions catalysed by acid sites [14-26]. In other words, acidity with a controlled distribution of acid sites strengths is probably the most important property observed in the zeolite catalyst. Therefore, the estimation of features related to acidity is evidently crucial for understanding the reactivity of zeolites. The understanding of zeolites' acidity comprised knowledge of related concepts:

1. Nature of the acid sites.
2. Number of the acid sites.
3. Acid strength of the sites.
4. Distribution of the acid strength of the sites.

Experimentally, the physicochemical properties of the solid *per se*, obtained by solid-state NMR spectroscopy [27-31], or IR [32-33] spectroscopy, give insight into the surface properties related to the acidity. However, more detailed information is accessible if probe molecules are brought into contact with the surface sites and the mode of interaction is studied. Among techniques funded on adsorption of specific probe molecules, several methods such are: temperature-programmed desorption (TPD) of amines [34-37]; UV-Vis [38-40], IR [41-43] or XPS spectroscopy [44-45] of adsorbed probe molecules; and adsorption microcalorimetry [46-52] are applicable for the characterization of the solid materials' acidities. It is important to point out that none of mentioned methodologies can reveal all previously listed acidity concepts. In any case it has to be specified whether the concentration, strength or nature of acid sites is estimated.

Adsorption microcalorimetry allows an accurate determination of amount, strength and the strength distribution of surface sites, based on the heats of adsorption of appropriate probe molecules and differential heats as a function of surface coverage. Following text discuss the applicability of adsorption microcalorimetry for the determination of zeolites' acidity, and the estimation of different factors that can influence this important property.

9.2 Factors influencing the acid properties of zeolites

The strategy for estimation of zeolites' acidity comprises (includes) the adsorption and subsequent desorption of chosen probe molecules; both events can be studied by different physical methods. From the obtained results, the facts about acidic sites (such are: the strength, strength distribution...) can be derived. As it has been already discussed (Chapter III), the characteristics of

probe molecule (its nature and size), as well as the temperature dependence of the heats of adsorption have to be considered during the estimation of zeolite' acidity. However, additional parameters that are related to zeolite of interest might influence its acidity, and have to be taken into consideration. Here, the influence of:

- 1) zeolite topology;
- 2) pre-treatment parameters;
- 3) proton (cation) exchange level;
- 4) Si/Al ratio and dealumination;
- 5) the nature of framework T atom;

on acidity of zeolites and their determinations by the method of adsorption microcalorimetry will be discussed.

9.2.1 Influence of zeolite topology

Topology of zeolite structures plays an important role in the number on phenomena related to this important group of solid catalysts, such are selective adsorption and diffusion. It is well known that in the cases of adsorptions performed on the molecular sieves that possess same chemical composition but different pore systems, the topology of microporous solid (the structure of the pore system and the diameters of pores openings) is responsible for the phenomenon of selective adsorption [53-60]. Although other factors have additional impact on selective adsorption (the intensity of overall electrostatic field; outer surface acidity which can diminish adsorption and even cause pore blocking by coke formation), topology of zeolite structure is the most important factor responsible for the fact that in acid-catalyzed reactions, zeolites often show shape selectivity [61-67].

The topology of the zeolite host is also crucial for the diffusion of the guest through the interior; it controls the maximum uptake achievable. Zeolites with tridirectional structures are more accessible and allow diffusion readily, whereas diffusion in monodirectional zeolites is seriously affected [68].

Besides its significant role on the catalytic behavior of zeolites through the so called 'shape selectivity effects', the zeolite geometry plays an important role in determining the acidity of zeolites. From the overall knowledge concerning zeolitic structures, it is known that the distances and bond angles in the Al-OH-Si group can affect the acid strength of the hydroxyl group; besides, the zeolite structure may also cause preferential location of acid sites [69-70]. From the molecular orbital calculations for protonated Si-O-Al bridge it was suggested that the deprotonation energy decreases with the increase of the T-O-T bond angle, and consequently, the corresponding acidity

increases [71-75]. However, in the attempts to estimate the influence of zeolite structure on acidity, the difficulties in experimental work arise from the fact that it is not easy to obtain samples with the same chemical composition but with different homogenous distribution of Al atoms through the zeolitic particles. Nevertheless, there are results of investigation of zeolites' topology influence on the acidity reported in the literature. Here, the examples of such investigations done by adsorption microcalorimetry are summarized.

Influence of structure on the number and strength of available Brönsted acid sites was investigated on a series of delaminated zeolites (HY, mordenite, ZSM-5 and mazzite) with similar framework composition (Si/ Al ratios \approx 15). It is known that in the case of dealuminated zeolites, microporosity does not influence importantly on their acidity; while the bond angles play an important role. Differential heat curves plotted as a function of coverage, represented in Fig. 1, shows that the number of sites is higher on HY, but the strength of the sites is greater for the mazzite sample [46]. It seems therefore that these systems contain domains of more extensive dealumination than the other samples, including less accessible zones, thus leading to strength distributions of acid sites dependent on the samples.

Contrary to this behavior, various structures with high Si/Al ratio (H-ZSM-5, H-ZSM-12, HY and H-mordenite) were found to exhibit almost the same adsorption energies measured at 480 K, suggesting that the isolated Brönsted acid sites in these materials are identical [76]. Authors observed that the strength of Brönsted acid sites associated with framework Al atoms does not vary in a given zeolite, and they suggest that Brönsted acid sites in unsteamed zeolites are independent of the sample (what means, independent of Si/ Al ratio) and equal in concentration to the framework aluminum content [77].

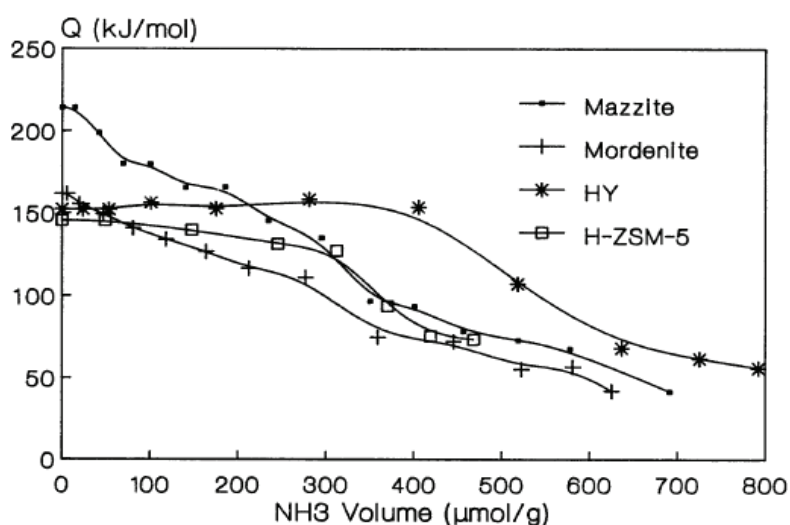


Fig. 1. Differential heat of ammonia adsorption versus the adsorbed amount for various zeolites [46].

A study performed by adsorption microcalorimetry of NH_3 and SO_2 on a series of milled Na zeolites [78-79] with different degrees of crystal collapse, revealed that losses in zeolite crystallinity cause a decrease in the number and strength of both Lewis acid sites and Lewis basic sites. It was observed that Lewis acid strength is strongly crystallinity dependent while Lewis basic strength is less so. Combined XPS and calorimetric results have shown that the extraframework Lewis acid sites (Na cations) are remarkably influenced by the long range stabilization effect of the zeolite lattice and gives a higher strength of Lewis acidity.

A similar study performed on crystals of HA, HX and HY zeolites [80] revealed that milling caused the destruction of the long-range symmetry of the crystal while the primary building units, namely Si(Al)-O_4 tetrahedra, remained intact. Microcalorimetry showed that the collapse in zeolite structure also caused decrease in the number and strength of acid sites, and that the Brønsted acid strength is strongly crystallinity-dependent. The destruction of long range crystal symmetry induces an increase of the population of weak Brønsted acid sites and a decrease of the population of strong Brønsted acid sites (Fig.9.2).

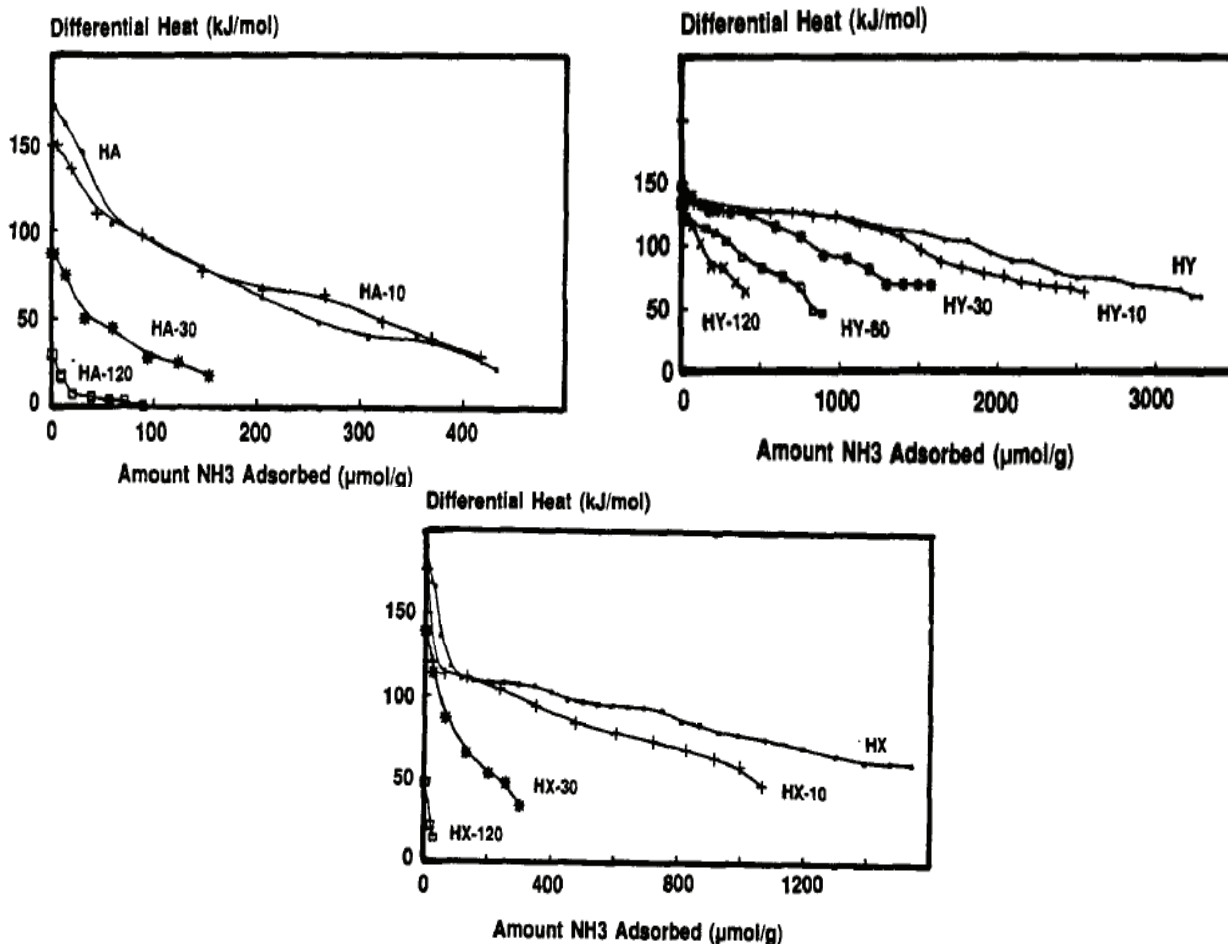


Fig.9.2. Differential heat NH₃ of adsorption on initial and ball-milled zeolite samples (each milled sample is designated by milling time noted behind the sample name) [80].

It can be concluded that the heat curves should be similar only when the solids contain exclusively isolated sites where the next-nearest neighbors (NNN) are identical. It appears that the NNN determines Brønsted acidity, in fact, it can be said that zeolite geometry has an influence on acidity due to long-range effects as well as on the local structure of the acid sites.

9.2.2 Influence of the Si/Al ratio

The Si/Al ratio has an important influence on the properties of zeolites. The Al content determines the number of cations in the framework and the properties such as the thermal and chemical stability or the polarity of internal species. Typically, zeolites with high Al content are thermally and chemically less stable, so that dehydration at high temperature may cause partial dealumination that happens together with water desorption, what results in a certain decrease of crystallinity[81]. The hydrophilicity / hydrophobicity of zeolites are related to the polarity of the pores. Zeolites without framework Al are the most hydrophobic[82-83].

The Si/ Al ratio plays also a significant role on acidic properties of zeolites. Aluminum atom is directly related to the acidic site, since a Brønsted site can result when the cation which balances

the negative charge associated with each framework Al is a “proton”. Because the “protons” are bonded to the bridging oxygen with considerable covalent character, the site should be viewed as a hydroxyl group, but with properties significantly different from that associated with pure silica [84]. Additionally, Al also accounts for the formation of carbenium and/ or carbonium ions or possibly cation radicals inside the zeolite.

An important aspect of zeolites and other acidic molecular sieves is that each of these materials contains a well defined, discrete number of acid sites. For high silica zeolites in which all bridging hydroxyls are accessible to adsorbates, such as H-ZSM-5, the site concentration is approximately equal to framework Al content[85-86]. In some other materials, such as HY, many of the sites are inaccessible to adsorbate molecule, so the measured site concentration is significantly lower than the Al content [87].

Tsutsumi et al. have studied heats of ammonia adsorption on mordenites with different Si / Al ratio [88]. The number of acid sites determined from the heat curves plotted against the theoretical number of protons (aluminum atoms) per unit cell of mordenites, shows a slope that deviates little from unity (Fig. 9.3); the deviation being smaller for higher Si / Al ratios. The authors suggested that the framework aluminium atoms participate in the formation of acid sites and that some of the generated Brønsted acid sites are converted to Lewis acid sites. Displacement of aluminium atoms from the zeolite framework may also be responsible for the observed deviation.

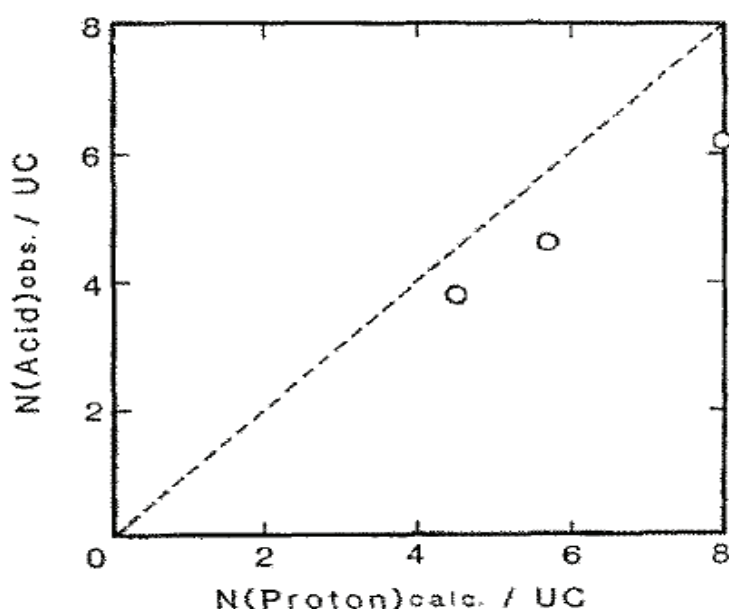


Fig. 9.3 Relationship between the number of acid sites calculated from calorimetric heat curves and the calculated number of protons on mordenite samples with different Si / Al ratio [88].

To investigate how Si/Al ratio influences the acidity for a given zeolite structure, several H-ZSM-5 samples have been prepared, with Si/ Al values varying between 50 and 14 [89]. Auroux et. al. found that the Al atoms progressively incorporated in larger proportion not only create new acid sites, but also modify the strength of pre-existing acid sites as well. The initial heat of ammonia adsorption goes through a maximum. When the Al content increases, the initial heat of adsorption, and thus the strength of the strongest acid sites increases, then remains constant (for Si/ Al between 35 and 18), and finally strongly decreases for low Si/ Al ratios. However, the integral heats of irreversible adsorption, representative of the overall acidity, increase sharply when the Al content increases from 0 to 2 atoms per unit cell, and then moderately for higher Al loadings. These results show that when relating the acidity of material to its catalytic properties, it is important to discriminate the strength of individual acid sites and the total acidity. It has been discovered that appropriate Si/Al ratio has to be discovered for a given reaction; so the importance of a careful selection of adequate zeolite sample is emphasized. For example, to prevent an excessive polymerization, the presence of very strong acid sites must be avoided, while the total acidity must be sufficient; for that purpose, ZSM-5 zeolites with a Si/Al ratio between 10 and 40 have been found to be best suited for this purpose.

The chemical composition of synthetic zeolites can be controlled either during synthesis (by varying the composition of mother gels) or by postsynthetic modifications. Dealumination process can promote modifications of porous structure, which may improve some important properties of zeolites, like: thermal and hydrothermal stability, acidity, catalytic activity, resistance to aging and low coking rate, and material transfer. Different dealumination processes have been proposed: steaming and acid treatments, as well as reactions with SiCl_4 or SiF_6^{2-} . From many theoretical and experimental investigations on the acidity of faujasites with different framework aluminium content, it was concluded that the number of bridging hydroxyl groups increases with the number of Al atoms in the lattice [90]. In contrast, the dependence of the acid strength on aluminium content is more complicated. From theoretical considerations, the acid strength is expected to increase with decreasing number of aluminium atoms, whereas from the studies of Al topology in the framework, a curve often presenting a maximum was derived from the number of strong sites [90].

Fig. 9.4 shows that on aluminium-deficient HY zeolites, dealumination generally causes a decrease in the acid sites concentration followed by an increase in strength [91].

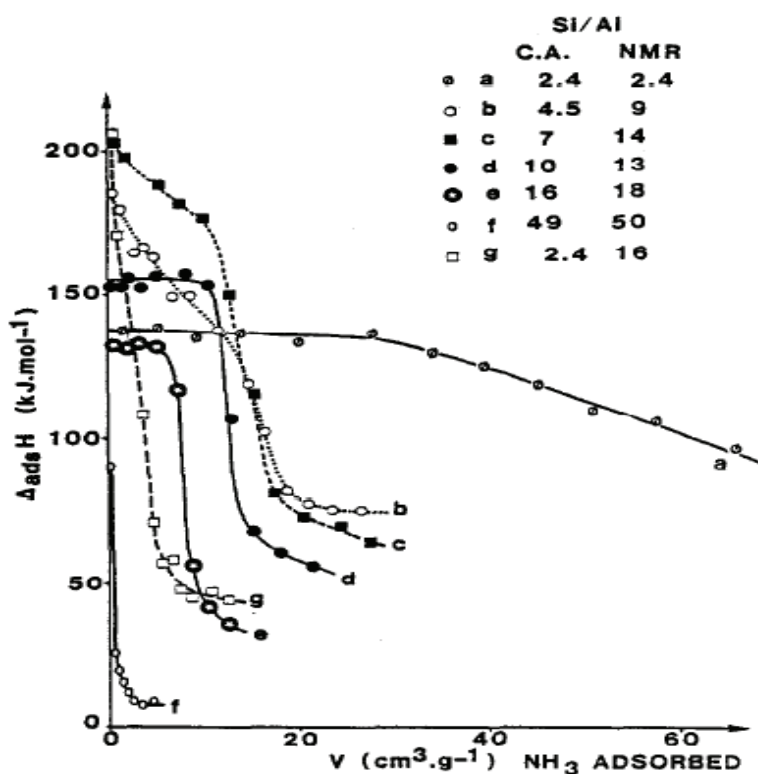


Fig. 9.4 Differential heats of ammonia adsorption over HY zeolites with various Al content as a function of coverage [91].

Mitani et al., in their work related to the investigation on the acidity of faujasites with different framework aluminium content, reported that the extent of the decrease in acid sites concentration varies with the kind of basic probe used in microcalorimetry experiments (see Fig. 9.5) [92]. The experimental results were explained by differences in molecular diameters of ammonia and pyridine, and the fact that pore size of zeolite becomes widely distributed as the dealumination proceeds; so OH groups in supercages have become available for adsorption of such large molecule as pyridine is.

In another study performed on steamed dealuminated faujasites presenting both framework and non framework Al, authors found no evidence for the presence of a small concentration of very strong acid sites [93]. For low coverage, differential heats of adsorption did not show any dependence on the Si/Al ratio of the samples or on the sample preparation. Since the samples with different degrees of dealumination showed considerable different catalytic activities, it was suggested that factors other than acid strength are responsible for this behaviour. It was concluded that when heterogeneity in the strength of sites is revealed by microcalorimetry (i.e. a fall of differential heat with coverage), this is the result of molecular interactions of molecules adsorbed at neighbouring sites, rather than a true indication of the differences between the sites. Strong repulsive

interactions between adsorbate molecules arising from ionic repulsion of two positively charged adsorbates, from steric interactions between neighbouring adsorbates, or from changes in a protonic site due to adsorption on adjacent sites, could lead to a large decrease in measured adsorption heats with coverage. The slope of this decrease depends on the adsorbate.

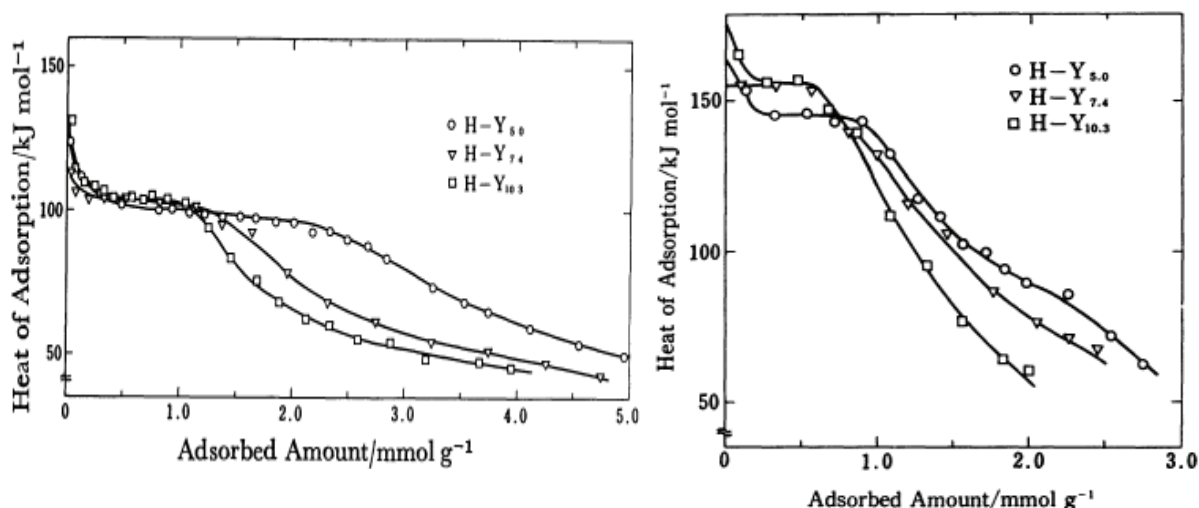


Fig. 9.5 Differential heats of adsorption of ammonia (left) and pyridine (right) at 473 K [92].

Generally, it can be seen that, when differential heats of adsorption of ammonia or pyridine are plotted as a function of the aluminium content of the samples, at least three domains of acidity are revealed, whose relative importance depends on the aluminum content, and whether aluminium is exclusively located in framework positions. First domain, with a sharp initial decrease in q_{diff} , is generally associated with non-framework Al and a very strong Lewis sites (heats of adsorption above ~ 150 kJ/mol). A region of intermediate heats, represented by a plateau, follows. This plateau corresponds to strong Brønsted acid sites associated with framework Al around 140-150 kJ/mol depending on the zeolite. At the end there is again a decrease of heat, corresponding to weak Lewis acid sites associated with alkali cations and weak Brønsted sites associated with non-framework Al or neighboring species.

The heats of adsorption of ammonia and the catalytic activity in isooctane cracking are reported by Mishin et al. [94] for high-silica Y zeolites with Si/Al ratios varying from 1.25 to 100. The aluminium-deficient Y zeolites have been found to possess stronger acid sites than the parent zeolites. It has been revealed using adsorption microcalorimetry measurements that even a minor increase in the Si/Al framework ratio results in an increase of the bond strength between NH_4^+ ions and the lattice. In agreement with the changes in acidity (number of sites with $q_{\text{diff}} \approx 130$ kJ/mol), progressive dealumination of Y zeolites results firstly in an increase followed by a decrease in catalytic activity, with a maximum for 25-30 Al atoms per unit cell. The increase in catalytic activity is associated with the appearance of strong acid sites ($q_{\text{NH}_3} > 120$ kJ/mol). The effect of acidity on

activity of dealuminated zeolites is explained in terms of isolated acid-site generation. It is postulated that nonframework Al atoms do not contribute to catalytic activity.

The effect of steaming on the number and strength of the acid sites is obvious from a comparison of differential heat curves for samples with different degrees of dealumination. The microcalorimetric curves show also that the strength of the sites corresponding to the intermediate plateau region first increases and then progressively decreases with steaming severity. The dependence of the acid strength distribution of dealuminated mordenites and dealuminated faujasites on the Si/Al ratio is depicted in Fig. 9.6. The number of strong acid sites presents a distinct maximum. The abscissa of the maximum corresponds to an Al content of 4.6 per unit cell (u.c.) (and Si/Al ratio equal to 9.5) for dealuminated mordenites and an Al content of about 29 / u.c. (and Si/Al ratio around 5.5) for dealuminated Y zeolites. These values are in good agreement with the values predicted theoretically [95], where the limit values, m_{lim} , for mordenite and H-Y zeolites were calculated. It was found that they correspond to $m_{lim} = 0.096$ (or Si/Al = 9.4) for mordenite and $m_{lim} = 0.150$ (Si/Al = 5.8) for H-Y zeolites. According to Barthomeuf [95], below this maximum no Al atom has another Al atom as a next-nearest neighbour, and therefore all acid sites show a high acid strength. Above these maxima, there are Al atoms in the second coordination sphere, with the consequence that some Brønsted sites show weak acidity (although the total number of acid sites is still increasing), and their concentration decreases with increasing of framework Al content. Measurements from Stach et al. [96-97] and Macedo et al. [98] were found to confirm this model and to be in very good agreement, though the dealumination and the measurements were not performed under the same conditions.

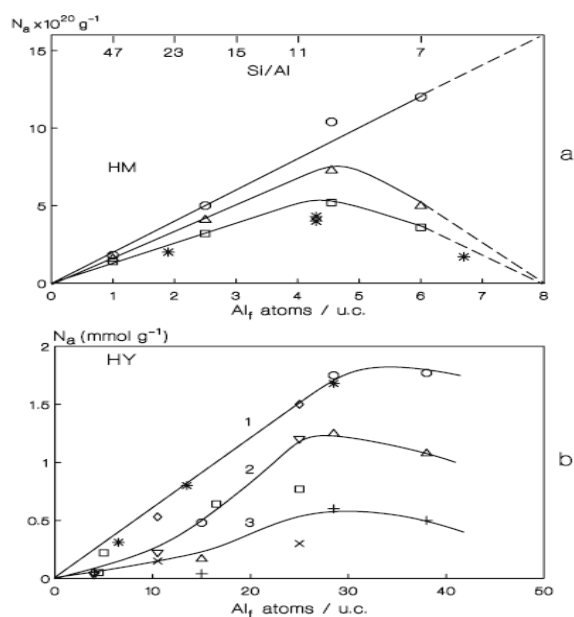


Fig. 9.6 a Acid strength distribution dependence on Al(IV) content per unit cell of dealuminated H-mordenites. N_a number of acid sites in molecules g⁻¹ with $Q > 80$ kJ mol⁻¹ (○), with $Q > 100$ kJ mol⁻¹ (Δ), with $Q > 120$ kJ mol⁻¹ (□, *) from [97]. Differential molar heats of ammonia adsorption were measured at 423 K. **b** Acid strength distribution dependence on the framework aluminum content per unit cell in dealuminated Y zeolites. *Curve 1*: total number of acid sites with $Q > 80$ kJ mol⁻¹ (*, ○, ◇). *Curve 2*: number of acid sites with $Q > 100$ kJ mol⁻¹ (Δ, ▽). *Curve 3*: number of acid sites with $Q > 120$ kJ mol⁻¹ (+, ×, □) from [96]. Differential molar heats of ammonia adsorption were measured at 423 K.

9.2.3 Influence of the pre-treatment parameters

It is known that increasing of the pre-treatment temperature modifies the surface acidity of the solids. High-temperature calcination is a well-known method of reducing total acidity of zeolites via dehydroxylation and dealumination. Although for the estimation of the real nature of an active site other techniques (spectroscopic investigation of adsorption/desorption of probe molecules) are needed, it can be told that, in principle, by using adsorption calorimetry technique it should be possible to determine the number of “strong” Brönsted sites, assuming that activation at 673K before NH_3 adsorption gives rise to a maximum in H^+ , i.e. that no dehydroxylation occurs at that temperature. This is a crude approximation but can be considered as valid for comparison of different samples [48]. After calcination at increasing temperatures, dehydroxylation of the zeolite is observed: above 675K, the number of Brönsted acid sites decreases, while that of strong Lewis acid sites increases. However, a limited dealumination occurs and the constraining character of the intracrystalline voids increases. Microcalorimetric studies of ammonia adsorption confirm the very strong acidic character of the acid sites and show their dependence in strength and heterogeneity upon calcination temperature [99-101].

In a ZSM-5 zeolite ($\text{Si}/\text{Al} = 19$), a thermal treatment at high temperatures leads to condensation of two OH groups (representative of two protons) to form a Lewis site. Changes in pre-treatment temperature modify the differential heat curve and thus allow identification of the nature (Lewis or Brönsted) of acid sites. Fig. 9.7 presents the acidity spectra (the values of dn_a/dq ratios) obtained for the adsorption of ammonia at 416 K on these ZSM-5 zeolites after the samples were pre-treated at various temperatures. The initial heat of adsorption increases as a function of outgassing temperature. From the results presented by Fig. 9.7, it is evident that the main band of the spectrum is progressively shifted towards higher adsorption heats, while its area (and thus the total number of sites) simultaneously decreases, when the sample is dehydrated at increasing temperatures (743, 923 or 1073 K). It follows that a high activation temperature (1073 K) decreases the total number of acid sites, while the acid strength of some of them is increased. The hypothesis of formation of Lewis sites stronger than Brönsted ones is thus confirmed [46].

However, the formation of Lewis acid sites cannot be revealed only from this shifting of the band in the acidity spectrum, since as already mentioned, calorimetry alone is not able to provide a simple procedure for identification of the nature of sites, and needs to be associated with another technique like infrared spectroscopy.

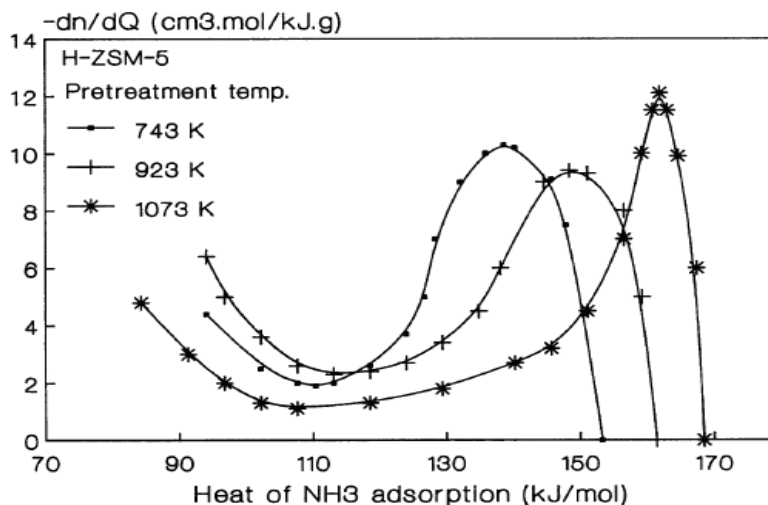


Fig. 9.7 Acidity spectra ($-dn_a/dq$ vs. q_{diff}) of a ZSM-5 sample for various pretreatment temperatures [46].

It is important to notice that the dehydroxylation at high temperatures produces an irreversible transformation; a sample outgased at 1073 K, rehydrated at room temperature and outgased again at 673 K, does not exhibit the initial acidity spectrum [46].

A similar microcalorimetric study has been performed by Karge et al. [102-103] on a well-crystallized H-ZSM-5 activated at 673 K which contains very few Lewis sites, i.e. with aluminium located almost exclusively in framework positions. The microcalorimetric curve of ammonia adsorption at 423 K showed a nearly horizontal plateau around 150 kJ/mol of homogeneous acidic strength due to the interaction of ammonia with Brönsted acid sites. After high temperature dehydroxylation in vacuum at 1073 K, true Lewis sites were created, inducing a large increase in the number of sites evolving differential heat over 150 kJ/mol. These were considered to be heats which have a contribution both from the Lewis sites induced by the high activation temperature and from the remaining Brönsted sites. The overall number of titrated strong and medium acidic sites had simultaneously decreased from 2.7 to 1.6 NH₃ molecules per u.c. while the width and the homogeneity of the plateau were considerably reduced. After dehydroxylation at high temperature, no Brönsted sites of homogeneous energy distribution remained on dealuminated ZSM-5 samples. Only the acidic sites of broad energy distribution remained unaffected by the high temperature treatment, i.e. the sites of strength between 140 and 80 kJ/mol.

Another example of pre-treatment influence on acidity is the study concerning high temperature calcination of H-mordenite (Si / Al = 13) in air at 1008 K, that has done by Chen et al. [104] using adsorption microcalorimetry of pyridine at 473 K. This treatment caused a significant

reduction in the total number and in the strength of the acid sites. The plateau characteristic of a large number of sites of uniform strength (near 200 kJ mol^{-1}), observed on the sample pre-treated at 673 K, also disappeared. High-temperature calcination is known to induce dealumination and dehydroxylation, both of which are expected to reduce the number of acid sites [104]. Dehydroxylation of an H-mordenite sample at 923 K caused the appearance of centres with heats of NH_3 adsorption between 170 and 175 kJ mol^{-1} which were not present in the same sample pre-treated at 703 K. Increasing the dehydroxylation temperature to 1023 K provoked the increasing of the concentration of centers characterized by a heat of ammonia adsorption of $175\text{--}170 \text{ kJ mol}^{-1}$ to 0.2 mmol g^{-1} , and sharply decreased the concentration of centres generating heats of $160\text{--}130 \text{ kJ mol}^{-1}$ [105]. It was shown that the latter values are typical of the dissociation of ammonia over Lewis acid centers.

The acidic properties of a mordenite zeolite with a Si/Al ratio of 10 were analyzed by Tsutsumi et al. [88] through calorimetric measurements of the heats of ammonia adsorption done at 473 K, on samples previously evacuated at temperatures varying from 703K to 1073 K. Drastic energy changes were observed between low and high coverage, with the exception of the sample evacuated at 1073 K. Both the number of the more energetic sites and their energy increased with an increase in the evacuation temperature, and reached a maximum at 773 K (around $170\text{--}175 \text{ kJ mol}^{-1}$); then a decline was observed. The heat curve of the sample evacuated at 1073 K did not exhibit a plateau, and its initial value was much less than those of the other samples (the value of 160 kJ mol^{-1} was obtained, instead of 175 kJ mol^{-1}). This may be attributed to the breakdown of part of the mordenite structure and/or to the local formation of amorphous species [88].

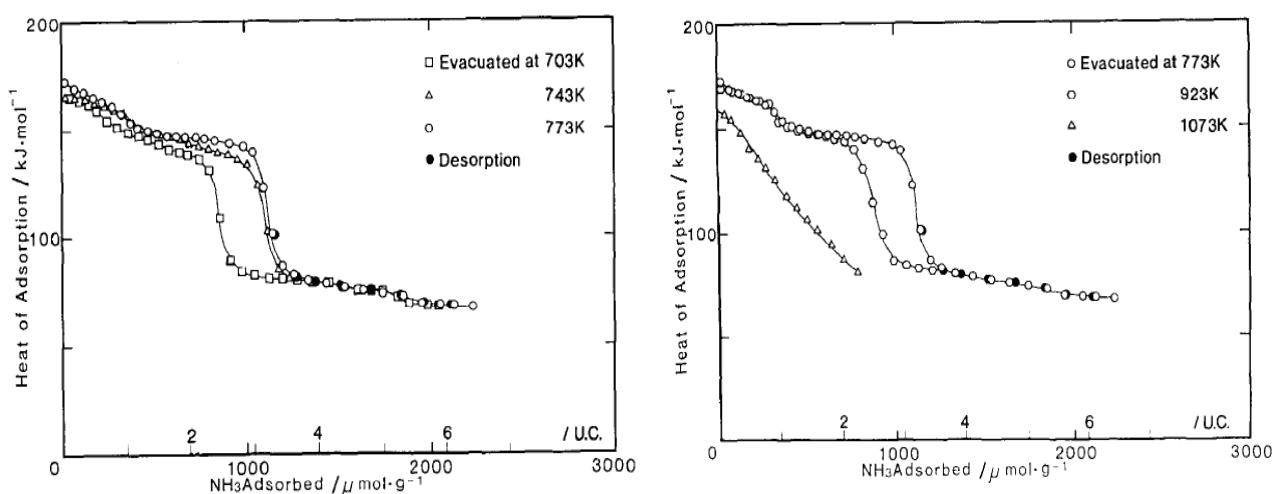


Fig. 9.8 Calorimetrically determined molar heats of adsorption of ammonia at 473 K on HM-20 evacuated at various temperatures. Filled symbols represent heats of re-adsorption on samples which were evacuated at 473 K after the first run of the adsorption measurement [106].

A sample of mordenite (98% degree of ammonium-ion exchange) deammoniated at various temperatures from 693 K to 923 K was studied at 573 K by NH₃ adsorption microcalorimetry by Bankos et al. [106]. On increasing the pre-treatment temperature, the number of acid sites passed through a maximum at 753 K as a result of simultaneous decationation and dehydroxylation. The heat of adsorption of NH₃ on Brønsted acid sites formed by decationation was 110–160 kJ mol⁻¹. During dehydroxylation, two types of Lewis sites were formed, characterized by heats of NH₃ adsorption of 170–185 kJ mol⁻¹ and 95–100 kJ mol⁻¹ respectively, and on which dissociative chemisorption of ammonia was evidenced by IR [105].

9.2.4 The effect of proton (cation) exchange level

Ion exchange is a characteristic property manifested by most molecular sieves. This property is used routinely for post synthesis modification during the preparation of molecular sieves for major industrial applications [10-11].

The origin of ion exchange properties resides in the fact that the net negative charge of zeolite network, equal to the number of the constituent aluminium atoms, is balanced by exchangeable cations, Mⁿ⁺, located in channels which normally also contain water. According to the synthetic procedures, these cations which neutralize the electrical charge of the aluminosilicate framework, are usually Na⁺, K⁺ or template cations. This charge –compensating entities can further be exchanged for other cations. Conventionally, ion exchange is carried out by suspending the zeolite powder in aqueous solutions of salts which contain the desired in-going cation, or in mineral acids to introduce protons into acid resistant zeolites [10-11]. The same can be done by solid state ion exchange, where dry powders of zeolites and salts or oxides containing the exchangeable cations are reacting [107].

Evidently, ion exchange capacities can be considered as functions of the quantity and distribution of aluminium atoms within the structure of zeolites. In addition, it is worth to notice that zeolites often possess high ion exchange selectivity for certain cations, and this can be used for their concentration and isolation. Molecular sieving and acid properties of zeolites are modified in this way, what gives possibility to tailor their catalytic activity. The framework anions and exchangeable cations form electrostatic fields which strongly interact with electronic structure of adsorbate molecules [108]. The reactivity of adsorbed species depends strongly on the number and kind of cations of the zeolite under investigation.

The exchange degree plays an important role in the heterogeneity of the acid sites of zeolites. From the study performed on NaY parent sample and NH₄NaY zeolites exchanged to 29, 56, 80, 90, and 94 % respectively, it was observed that acidity appears slowly at the early stages of replacement,

and that up to about 60% exchange, the number of acid sites present in the zeolites is four times lower than the amount of sodium replaced [109-110]. At higher extents of decationation, the density of acid sites increases rapidly and approaches a theoretical value [110]. A question is how the framework charge balance can be achieved at low exchange degree, if the number of cations that are removed is greater than that of the acid sites formed. Two alternative interpretations were offered: either the hydroxyls generated at low exchange levels are unstable and can be eliminated during pretreatment, or an incomplete decomposition of NH_4^+ ions occurs upon thermal activation, the latter hypothesis being supported by TPD spectra. To rationalize the observed acidity-exchange level profile a model was developed, extending the shielding power of a single Na^+ ion to several neighboring AlO_4^- tetrahedra. The catalytic activity of these decationated faujasites in the cracking of isooctane and the disproportionation of ethylbenzene was also found to vary in the same manner as the number of acid sites, increasing rapidly beyond 70% exchange degree. However, the observed discrepancy between the two increases (the catalytic activity increased much faster) prevented direct interpretation of the catalytic activity in terms of acid sites population. It is reasonable to assume that both the number and the strength of the acid sites are affected by the exchange level.

Similar study was performed on decationated mordenites [109], which have narrower pores and a higher Si/Al ratio than Y zeolites. From microcalorimetric measurements it was found that the number of acid sites increases nearly linearly with an increase of decationation level. Growth of the exchange level increased the acid strength, and removal of the last NH_4^+ ions resulted in the formation of strong sites ($q_{\text{diff}} > 130 \text{ kJ mol}^{-1}$). This increased concentration of strong acid sites explained that mordenites are more active in the cracking of n-octane than HY zeolites. However with bulkier reactants such as isooctane and ethylbenzene, the difference in catalytic activity decreases due to shape selectivity effects.

In a study by Muscas et al., a variety of NaHZSM-5 zeolites with varying extent of Na exchange was subjected to adsorption of various probe molecules in order to determine the selectivity of adsorption of various probe molecules on their acid centres of variable nature, such as Na^+ in Na forms and acidic OHs in the corresponding H forms [111]. Using ammonia as a basic probe it has been shown that the number of acid sites also increased quasi-linearly with the exchange level, while the acid strength increased monotonously and moderately up to about 40% of exchange level, remained almost constant at intermediate exchange level, and then dramatically increased when 80% of the original Na^+ ions were removed. The removal of residual Na^+ ions not only generated much stronger sites but resulted also in a general increase of the acid site population already present. Fig. 9.9 clearly shows that at low exchange levels, most of the acid sites were rather weak sites. While this population of weak sites remained almost constant as the exchange level

increased, the population of stronger sites increased progressively up to the point where, for extensively exchanged samples, the strongest sites became predominant. The population of sites, the heat of adsorption of which was above 150 kJ mol^{-1} , illustrated the effect of removal of the very last sodium ions on the acid strength, not only on that of newly created sites but also on that of pre-existing ones. This phenomenon, fairly common to those encountered with faujasites [110-112] and mordenites [109], was interpreted in terms of remote perturbation of the structure of the acid centers by the very few residual Na^+ ions modifying significantly the T-O-T bond angles. In addition, possible general cation redistribution induced by NH_3 adsorption may also affect the evolved heats of adsorption.

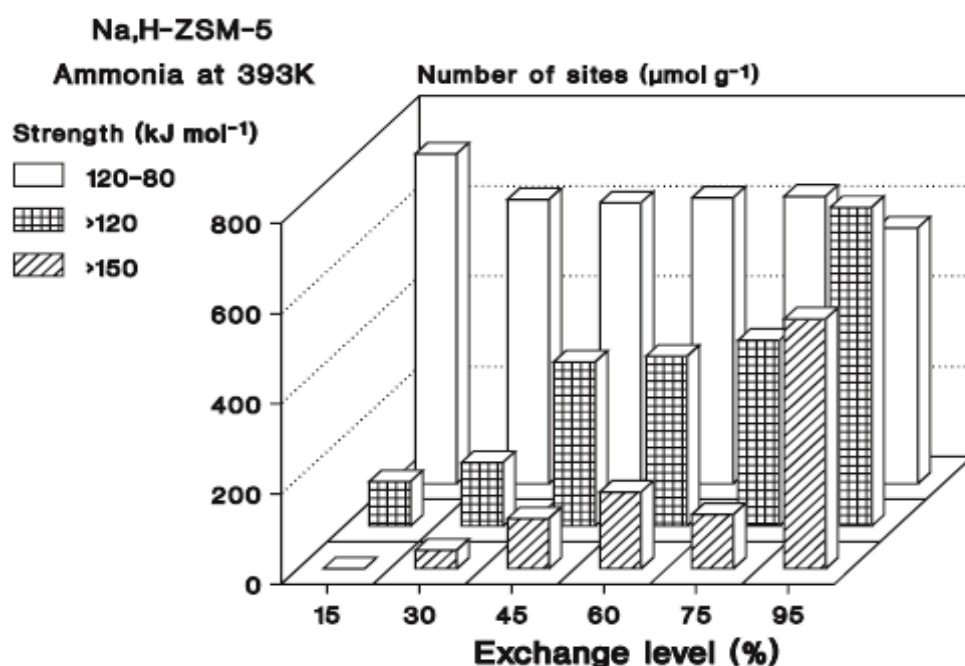


Fig. 9.9 Acid site strength distribution of Na,H-ZSM-5 zeolites as a function of the exchange level. Ammonia adsorption at 393 K, pretreatment at 673 K (111)

Fig. 9.10 presents the number of sites evolving heats above 110 kJ mol^{-1} upon NH_3 adsorption, as a function of the exchange level; for ZSM-5 [111], faujasite [109] and mordenite [110] samples. This number of strong sites increases in all cases, but in different proportions; almost linearly for mordenite and ZSM-5, and first slowly (for low exchange levels) and then sharply (at high exchange level) for faujasite. Concomitantly, the catalytic efficiency increases as does the acid strength. But it is not clear yet how the acid strength increases with increased exchange level.

The nature of the exchanged cation is one of the key points that determine acidity in zeolites. The acid-base properties of alkali-exchanged X and Y zeolites have been studied using microcalorimetry of ammonia, pyrrole or SO_2 probes. Generally, the alkali-exchanged X zeolites are more basic than the corresponding Y zeolites. It was shown that the basic strength increases quasi-

linearly with the negative charge of oxygen atom, calculated from the Sanderson electronegativity equivalence method. Pyrrole chemisorbed on the basic site creates a bonding between the framework oxygen (Lewis basic site) and the H atom of the NH group of the pyrrole molecule, so the stronger base (Cs) will produce a larger heat of adsorption. Briefly, a thermodynamic scale of the Lewis basic strength distribution of alkali-exchanged X and Y zeolites was obtained, supporting the conclusion that the Lewis basicity in alkali-exchanged zeolites is a local property, strongly influenced by the adjacent alkali cation [113].

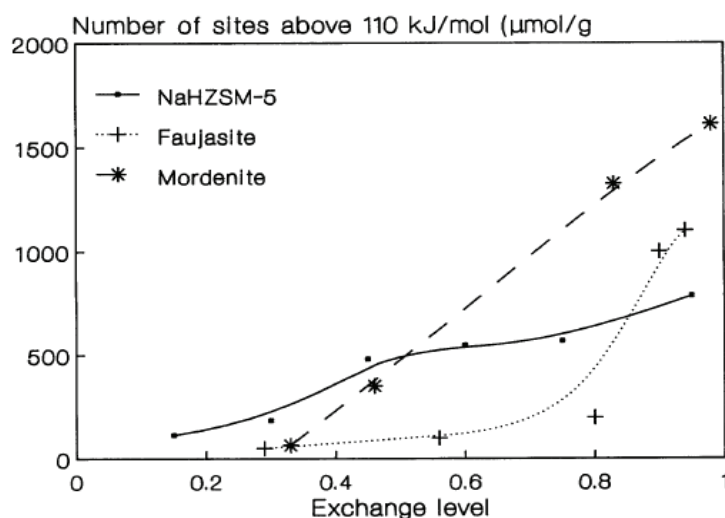


Fig. 9.10 Number of acid sites evolving heats above 110 kJ mol^{-1} upon NH_3 adsorption as a function of exchange level for HNa-ZSM-5 (■), HNaY (+) and HNaM (*) zeolites.

The acidic properties of a series of X faujasites exchanged with Li, Na, K, Rb and Cs have been studied by adsorption microcalorimetry, using ammonia as acidic probe. The heats of NH_3 adsorption were found to decrease in the sequence from Li to Cs (Fig. 9.11).

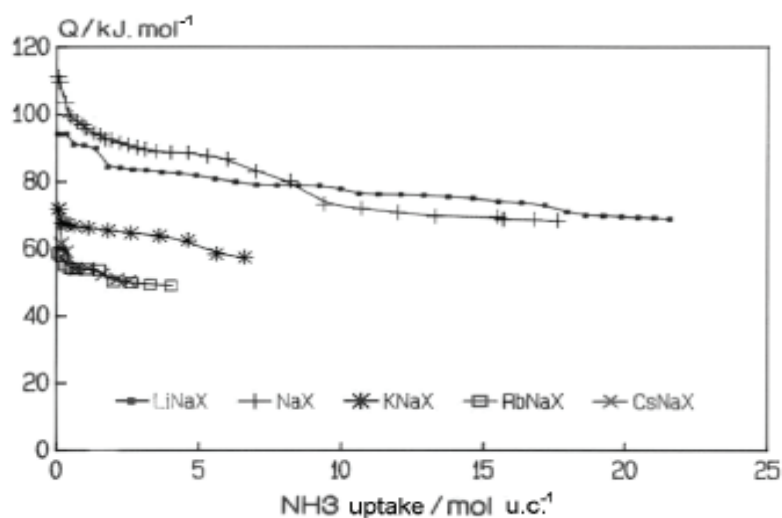


Fig. 9.11 Differential heats of NH_3 adsorption on alkaline X zeolites vs. coverage [90]

Li and Na zeolites presented much higher heats of NH₃ adsorption and greater coverage at the same pressure in comparison with the other zeolites. The acid-base properties of alkali-metal ion exchanged X and Y zeolites have also been investigated by ammonia and sulphur dioxide adsorption microcalorimetry, in parallel with the study of a catalytic reaction, viz. 4-methylpentan-2-ol conversion [114].

9.2.5 The influence of the framework T atom

Isomorphous substitution is an important way to modify zeolite properties for practical applications and have achieved considerable interest in the field of zeolite chemistry. The thermodynamics of isomorphous substitution have been considered by Barrer [115]. The phenomenon of isomorphous substitution is well-known in the field of mineralogy [1, 116]. By isomorphous substitution, framework atoms of crystalline compounds are replaced by atoms of other elements without changing the type of the crystal structure. Most elements can undergo substitution, at least to a very low degree. Even chromium, which prefers octahedral coordination, may substitute silicon in tetrahedral framework positions, at to a certain extent [117-118]. Extremely low degrees of substitution (0.2 atom %) can give rise to a remarkable change of properties.

The main factors governing isomorphous substitution are summarized in the following way [119]. a) The tendency of substitution depends on the ratio of radii of the atoms involved. With decreasing the difference of the radii Δr of atoms A and B, the substitution becomes energetically more favoured. b) If the replacement leads to a decrease of the coordination number of atom A, larger atom A will replace more easily smaller atom B. c) Electronegativity and ratio and the ionization potentials of exchanging atoms have an influence on substitution. d) During isomorphous replacement of A by B with preservation of local structure (coordination number), a minimum free energy is being achieved with $\Delta r/r = 0.025-0.03$, r denoting the radius of the atoms to be replaced in the framework by atoms of another element. e) Isomorphous substitution is facilitated as long as replacement of A by B does not change long range electrostatic interactions. f) Substitution may occur when the charges of exchanged atoms differ by 1, 2 or 3 units. g) Exchanging atoms should not react with each other.

The main criteria for the occurrence of isomorphous substitution, which are primarily derived from crystal chemistry and geometrical considerations, have been formulated by Pauling [120]. The basic idea is that framework of crystals, i.e., silicates including zeolites, consist of packages of negatively charged oxygen anions (O²⁻). Therefore, tetrahedral and octahedral vacancies are formed.

The size of these vacancies depends on the size of anions. According to Pauling, cations prefer tetrahedral coordination if $r_{Me}/r_{O2-} = 0.214-0.4$, and octahedral sites if $r_{Me}/r_{O2-} = 0.4-0.6$.

It should be said that all rules cited above are not strict laws. The ability of the framework to change its fine structure (bond angles and distances) by rotation of tetrahedra, by tilting, or by inversion is important in order to relax the strain resulting from the substituting atom [121]. The aim of substitution is to integrate the new element in the structure while preserving the structure type. Often a certain percentage of the modifier remains in the extra-framework positions.

The motivation to replace aluminium in aluminosilicate zeolite structures by other elements arose from the need to adjust their properties to intended applications. Since the nature and strength of the bridging hydroxyl groups (Si – OH – T, T = Al, Fe, Ga, B, ...) depend on T atom, and thus the proton – T distance and resulting acid strength of the modified material. At comparable bond angles, the proton – T distance decreases in order Fe, Ga, Al. This means that electrostatic repulsion between the proton and T increases in the same way, and that the acidity is expected to increase in the same order [48]. These changing in the acidity are easily accessible by adsorption calorimetry technique.

The use of organic templates has rendered possible the substitution of many elements, including other trivalent (Cr^{3+}), bivalent (Be^{2+}), and tetravalent ions (Ge^{4+} , Ti^{4+}). Most of these metallosilicate compositions have been synthesized with ZSM-5 crystal structure. Adsorption microcalorimetry enabled the studying of acidic properties of thus obtained materials, as in the case of parent zeolites.

A co-incorporation of aluminium and boron in the zeolite lattice has revealed weak acidity for boron-associated sites [122] in boron-substituted ZSM-5 and ZSM-11 zeolites. Ammonia adsorption microcalorimetry gave initial heats of adsorption of about 65 kJ mol^{-1} for H-B-ZSM-11 and showed that B-substituted pentasils have only very weak acidity [123]. Calcination at 1073 K increased the heat of NH_3 adsorption to about 170 kJ mol^{-1} by creating the strong Lewis acid sites. The lack of strong Brønsted acid sites in H-BZSM-11 was additionally confirmed by poor catalytic activity in methanol conversion and in toluene alkylation with methanol.

Gallium has been successfully introduced into numerous zeolite frameworks (β , MFI, offretite, faujasite, ...). The Ga^{3+} ions in zeolites can occupy both tetrahedral framework sites (T) and non-framework cationic positions. The isomorphous substitution of gallium into aluminosilicate zeolites results in modified acidity and subsequently modified catalytic activity such as enhanced selectivity towards aromatic hydrocarbons.

Microcalorimetric experiments with ammonia and pyridine as probe molecules have been used to investigate the effects of framework Ga on the acidic properties of several zeolites [124-130]. Experiments of NH_3 adsorption microcalorimetry, together with FTIR results from pyridine

thermodesorption, have shown that the isomorphous substitution of Al by Ga in various zeolite frameworks (offretite, faujasite, β) leads to reduced acid site strength, density, and distribution [125-128]. To a lower extent, a similar behaviour has also been observed in the case of a MFI framework [129, 130]. A drastic reduction in the acid site density of H,Ga-offretites has been reported, while the initial acid site strength remained high [125, 127].

For Ga- β zeolite it was found that, when the Si/Ga ratio increased from 10 to 40, the number of strong sites decreased drastically for Si/Ga between 10 and 25 and then reached a plateau above Si/Ga = 25 [124]. The strength and density of acid sites in H-(Ga,La)-Y have also been found to be lower than those in H-Y crystals of the type used in FCC preparation (LZY-82) [126].

Parrillo et al. [131] have used microcalorimetric measurements of ammonia and pyridine adsorption to compare the acid sites in H-[Fe]ZSM-5, H-[Ga]ZSM-5, and H-[Al]ZSM-5. On each of the molecular sieves, the differential heats of adsorption for both ammonia and pyridine were constant up to coverage of one molecule per Brönsted site. The differential heats at a coverage below 1 : 1 were identical on each of the materials, with values for ammonia of 145 ± 5 , 150 ± 5 , and 145 ± 5 kJ mol⁻¹ on H-[Fe]ZSM-5, H-[Ga]ZSM-5, and H-[Al]ZSM-5, respectively; and for pyridine of 195 ± 5 , 200 ± 5 , and 200 ± 5 kJ mol⁻¹ on H-[Fe]ZSM-5, H-[Ga]ZSM-5, and H-[Al]ZSM-5, respectively. The authors [131] concluded that the microcalorimetric heats of adsorption for ammonia and pyridine at Brönsted acid sites formed by framework Fe(III) and Ga(III) were very similar to heats of adsorption at Al(OH)Si sites, and that the three samples were effectively equivalent proton donors. By contrast, they found very different reactivity measurements for *n*-hexane cracking and propene oligomerization on the same materials. The authors claimed that heats of adsorption for strong bases do not reflect differences in inherent acid strength and may not be related to catalytic activity in a simple manner.

Iron silicates of MFI structure with various Si/Fe ratios have also been studied by NH₃ adsorption microcalorimetry [130, 132], and compared with the Al and Ga analogues. The intermediate strength sites (predominantly Brönsted sites) were found to correspond to a plateau around 145 kJ mol⁻¹ for H-[Al]-ZSM-5 (Si/Al = 19), 140 kJ mol⁻¹ for H-[Ga]-ZSM-5 (Si/Ga = 22), and 135 (Si/Fe = 41), 125 (Si/Fe = 26), or 120 (Si/Fe = 12) kJ mol⁻¹ for H-[Fe]-ZSM-5, respectively.

Besides, the adsorption of acetonitrile as a probe molecule has been studied using microcalorimetry at 400 K, in the case of H-[Fe] ZSM-5 and H-[Al] ZSM-5 [133]. The heats of formation of the complexes were found to differ slightly, ca. 95 kJ mol⁻¹ on H-[Fe] ZSM-5 compared to ca. 110 kJ mol⁻¹ on H-[Al] ZSM-5; suggesting that the hydrogen bonds at FeOHSi sites may be slightly weaker.

Ga- and Fe-substituted MFI zeolites have been investigated using adsorption microcalorimetry of different alkanes at 353 K by Auroux et al. [134]. The acid strength of the zeolite protons decreased following the sequence H-[Al]MFI > H-[Ga]MFI > H-[Fe]MFI. The heats of adsorption decreased with the basicity of the alkane in the order *n*-butane > isobutane > propane.

The active sites of isomorphously substituted MFI structures activated at 673 K have been characterized by Jänchen et al. [135] using microcalorimetric measurements carried out at 423 K with ammonia as a probe. In accordance with decreasing heats of NH₃ adsorption, the Brönsted acid site strength of the modified MFI was reported to decrease in the sequence Al > Fe > In > silicalite. In addition to these strong sites, weaker Lewis centres due to the non-framework material were found (Fig. 9.12).

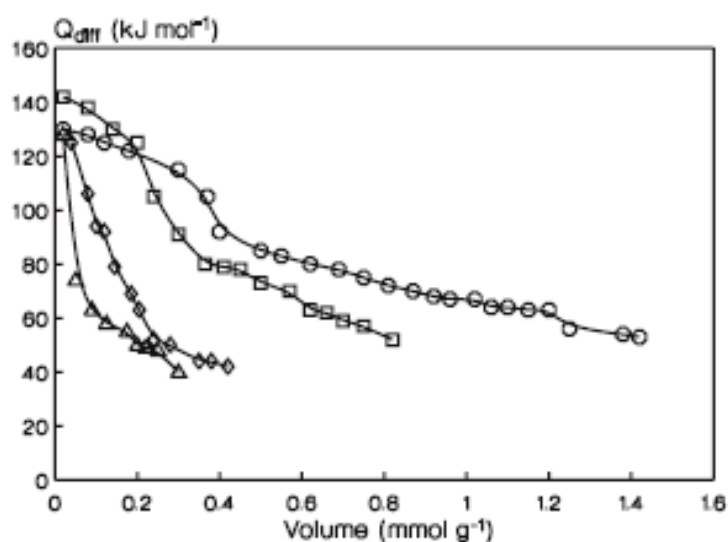


Fig. 9.12 Differential molar heats of ammonia chemisorption at 423K on MFI zeolites as a function of the adsorbed amount: □ Al-Sil, ○ Fe-Sil, ◇ In-Sil, △ silicalite. Pretreatment temperature 673 K ([135])

Crystalline MFI-type indosilicates containing indium ions in framework positions were hydrothermally synthesized by Vorbeck et al. [136] and characterized by adsorption microcalorimetry of NH₃ at 423 K (after activation of the sample at 670 K). They exhibited rather weak acidity attributed to Brönsted sites. However, the number of acid sites with a sorption heat between 80 and 110 kJ mol⁻¹ was significantly higher than for silicalite [136].

Titanium-substituted silicalite can be prepared with a homogeneous distribution of Ti ions in the crystal. The Ti⁴⁺ ions seem to be all surrounded by four NNN Si ions and, thus, the catalytic site is an isolated Ti⁴⁺ ion. For TS-1 (titanium silicate molecular sieve, zeolite of pentasil family), relatively low heats of adsorption due to coordinatively bonded ammonia were detected by Jänchen et al. [135]. Moreover, the amounts of adsorption with heats higher than found for silicalite correlated with the amount of Ti in the sample [135].

Similarly, the acidity of titanium-silicalites with different titanium contents was characterized by adsorption calorimetry at 353K of various probe molecules by Muscas et al. [137]. These molecular sieves had a molar composition $x\text{TiO}_2(1 - x)\text{SiO}_2$, where x ranged from 0 to 0.02. Subjected to ammonia adsorption, these solids showed an acidic character compared to a pure silicalite-1 sample. A small amount of titanium induced a high increase in the strong acid sites ($Q_{\text{init}} = 160\text{--}170 \text{ kJ mol}^{-1}$ instead of 75 for silicalite-1). The integral heat and the total amount of acid sites increased with increasing titanium loading and then reached a plateau for $x \geq 0.014$. All the curves showed a sharp decrease in Q_{diff} at very low coverage. The next region corresponded to a plateau with heats evolving around 70 kJ mol^{-1} , instead of 40 kJ mol^{-1} found for silicalite-1. Other basic probes such as pyridine and substituted pyridines (DMP) were also used in an attempt to identify by selective adsorption the different sites of these catalysts [137]. The heats and amounts adsorbed were in the order: pyridine > 3.5 lutidine > 2.6 lutidine.

The adsorption properties of titanium silicalites-1 synthesized via two different routes (in the presence or the absence of sodium in the precursor gel) have been compared by Auroux et al. [138]. Adsorption calorimetric measurements of a basic probe (NH_3) and an acidic probe (SO_2) showed that these solids were very acidic compared to a silicalite-1 sample. The presence of Na in the different samples decreased the number and the strength of the acid sites. The modification strongly depended on the synthesis procedure [138].

The treatment of Ti-silicalite-1 (TS-1) and silicalite by aqueous solutions of ammonium acetate has been shown to suppress the most energetic sites on these two catalysts, as evidenced by the heats of adsorption which were much lower for the treated samples than for the untreated ones [139], while the number of NH_3 molecules absorbed per Ti atom was unaffected by the treatment in the case of TS-1.

In another study, the heterogeneity of framework Ti (IV) atoms in Ti-silicalite (TS-1) was studied by NH_3 adsorption calorimetry [140] and compared to a Ti-free silicalite taken as reference material. The evolution of the heat of adsorption with coverage was found to be typical of heterogeneous surfaces, due not only to the presence of sites active towards ammonia on the silicalite matrix but also to the heterogeneous distribution of Ti (IV) sites. This suggests that a considerable number of framework sites (among the 12 available in the MFI framework) is occupied in a nearly equally distributed manner.

9.3 Correlation between adsorption heat and catalytic activity

Finding correlations in between catalysts surface properties and catalytic behaviour is the main reason to study adsorption of probe molecules on catalysts surfaces. If the probe molecules are chosen to resemble possible reaction intermediates of the catalytic cycle, measurements of heat of adsorption of such probe molecules can provide essential information about reaction mechanisms.

Finding correlations between the heats of adsorption and the catalytic behaviour (activity and/or selectivity) of the solid catalysts is not an easy task. Surface sites may exist in different configurations what typically brings to the distribution of adsorption sites' strengths. Among the active sites present on the surface of catalyst certain number may possess adequate strength to activate the adsorbed molecule and to form a reactive intermediate [52]. In other words, some of the sites may be too weak to activate the reactants or they can be too strong, leading to strongly held species which block and deactivate these sites or cause excessive fragmentation of reactants or products.

Therefore, the determination of the strength and strength distribution of surface active sites is of fundamental importance, because in this way one can distinguish the undesired sites from the desired ones. This further gives possibility of creating novel catalysts, which properties can be tuned/back-optimized for the target reaction. In revealing these very important features, adsorption microcalorimetry plays one irreplaceable role.

In a study performed by Auroux et. al. [114] microcalorimetry experiments of ammonia and sulfur dioxide were performed in order to analyze the possible correlations between the acidity and basicity of the alkali-metal ion-exchanged X and Y zeolite structures and their catalytic properties. The catalytic results for the 4-methylpentan-2-ol conversion show that activity and selectivity are both affected to some extent by the acid-base character of the catalysts. The activity was found to increase in order Cs > Rb > K > Na > Li for both X and Y zeolites. The dehydrogenation reaction occurs only on CsX+Cs₂O, which presents very strong basicity. The product selectivity of the reaction depends on both Lewis acidity and basicity; Lewis basic or acidic sites of zeolites can be considered as acid-base pairs, in which both framework basic oxygens and neighboring cations are important. The selectivity ratio between the 1-alkene and (2-alkene+isomers) increases linearly with the ratio between basic and acid sites number, n_{SO_2}/n_{NH_3} , for both X and Y zeolites, as shown in Fig. 9.13.

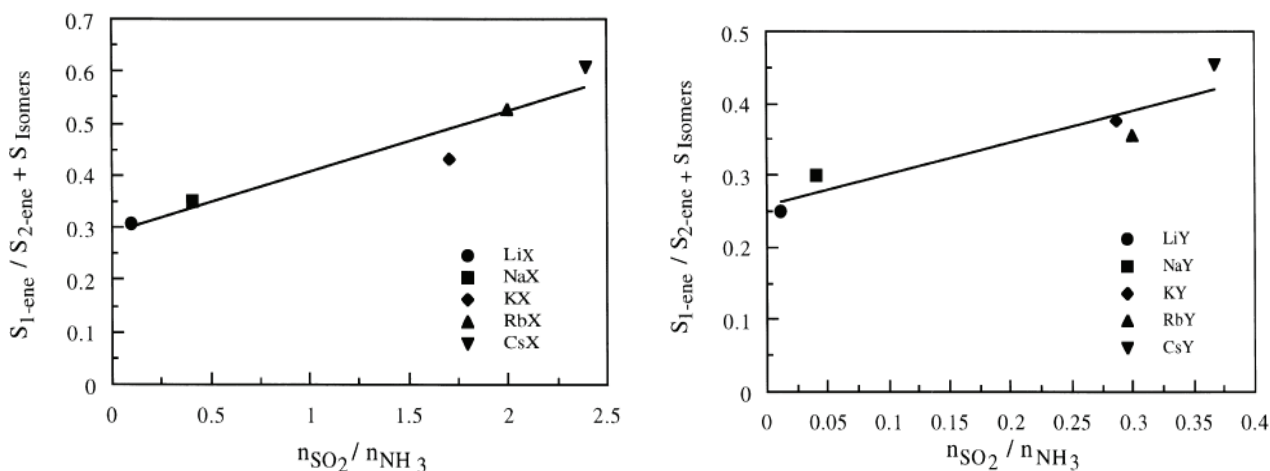


Fig. 9.13 1-ene/(2-ene+isomers) selectivity ratio versus the basic/acidic site number for X samples left and for Y samples right.

In another study [141], authors presented evidence that heats of adsorption of ammonia on three different kinds of zeolite structure (Y, mordenite, ZSM-5) can be used to obtain the correlation plots that describe relationships between acidic and catalytic properties of these catalysts. Catalytic properties were tested in simple carbonium ion reactions. An approach to search “acidity-catalytic activity” correlations was based on the straightforward concept which implies that the heat of adsorption of the base is directly related to the energy needed for the protonation of hydrocarbon molecules leading to the carbocation formation. For example it was found that the variation of strong acidity and the change of activity with progressing dealumination of Y zeolites show similar trend (Fig. 9.14).

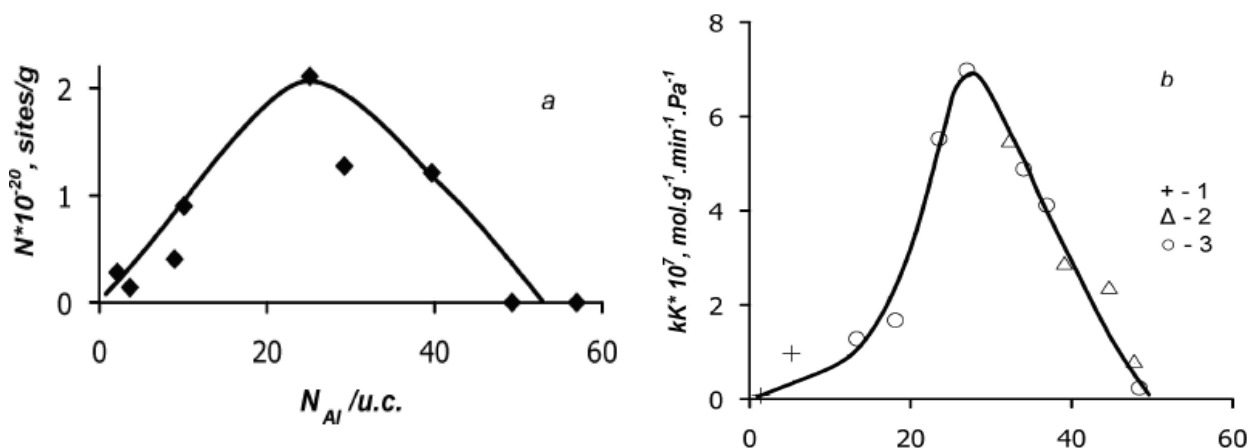


Fig. 9.14 Variation in the number of strong acid sites with $Q_{NH_3} = 122-136$ kJ/mol (a) and activity in cracking of isooctane as a function of N_{Al} for Y zeolites (b): prepared by treating the stabilized Y zeolites with HCl (1), prepared by thermal dealumination at 600–700°C (2) and produced by treatment of sodium faujasites with $SiCl_4$ (3).

In a study on ZSM-5 based materials [142], Nicolaidis et. al. have shown that the number of Brönsted acid sites, determined by adsorption microcalorimetry of ammonia, increases with

increasing XRD crystallinity. A strong correlation was observed between the catalytic activity of these materials, in *n*-hexane cracking reaction, and the number of strong acid sites, as presented in Fig.9.15.

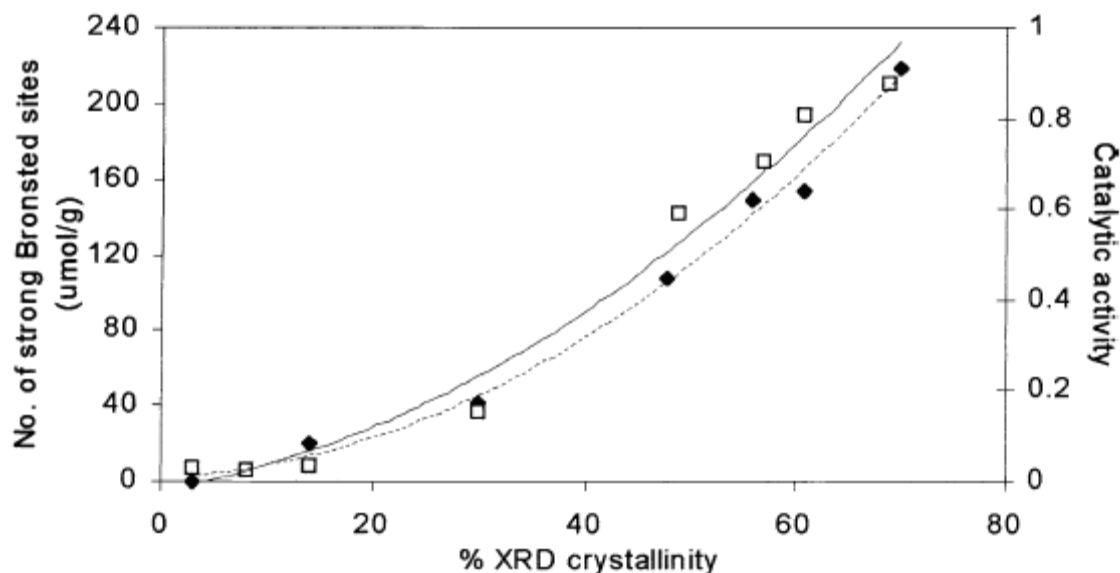


Fig. 9.15 Plots of number of strong Brønsted acid sites (◆) and catalytic activity for *n*-hexane cracking (□) as a function of percentage XRD crystallinity of ZSM-5-based samples.

Microcalorimetry study of NH_3 adsorption has been used to characterize the acid sites of H-USY zeolite and another USY sample in which the strong Lewis sites were poisoned with ammonia. Poisoning of Lewis acid sites did not affect the rate of deactivation, the cracking activity, or the distribution of cracked products during 2-methylpentene cracking. From these findings it was concluded that strong Lewis sites do not play any important role in cracking reactions [143].

The effect of the Si/Al ratio of HZSM-5 zeolite-based catalysts on surface acidity and on selectivity in the transformation of methanol into hydrocarbons has been studied using adsorption calorimetry of ammonia and tert-butylamine. The observed increase in light olefin selectivity and decrease in methanol conversion with increasing Si/Al ratio can be explained by a decrease in total acidity [144].

However, it is worth noting that experiments aimed at directly comparing the cracking activity and the enthalpy of adsorption of basic probe molecules have sometimes failed to make correlative conclusions. For example, Gorte et al. [145] detected no difference in the enthalpies of ammonia or pyridine adsorption on H-[Al] ZSM5, H-[Ga] ZSM5 and H-[Fe] ZSM5 samples whose cracking activities were quite different. Likewise, in a study on dealuminated Y zeolites, no significant differences in the highest enthalpies of adsorption could be detected by microcalorimetry

for samples of different cracking activities [93]. Kuehne et al. [146] confirm these conclusions by the results of another study where a 57 kJ mol^{-1} difference in the enthalpy of ammonia adsorption was detected between HY and an (H, NH₄)- USY sample, although the latter was 33 times more active than HY. It means that there is only a certain category of sites with a given strength that are active in the reaction.

References:

- [1] D. W. Breck in: *Zeolite Molecular Sieves: Structure, Chemistry and Use*, John Wiley & Sons Inc, New York, 1974.
- [2] P. A. Jacobs in: *Carboniogenic Activity of Zeolites*, Elsevier Science Ltd., Amsterdam, 1977.
- [3] J. V. Smith, Chem. Rev. 88(1988) 149.
- [4] W. M. Meier in: *Molecular sieves*, Society of Chemical industry, London, 1968.
- [5] R. Fricke, H. Kosslick, G. Lische, M. Richter, Chem. Rev. 100 (2000) 2303.
- [6] Ch. Baerlocher, L.B. McCusker, Database of zeolite structures. <http://www.iza-structure.org/databases/>
- [7] A. Dyer in: *An introduction to zeolite molecular sieves*, John Wiley and sons, New York, 1988.
- [8] W. M. Meier in: *Stud. Surf. Sci. Catal.*, Vol. 28 (Elsevier, Amsterdam, 1986), p13.
- [9] J. B. Uytterhoven, L. C. Christner, W. K. Hall, J. Phys. Chem. 69 (1965) 2117.
- [10] R. P. Townsend, R. Harjula, in: *Molecular Sieves—Science and Technology: Ion exchange in molecular sieves by conventional techniques*, eds. H. Karge and J. Weitkamp Vol. 3 (Springer-Verlag, Berlin Heidelberg, New York, 2002) p 1.
- [11] P. Townsend in: *Stud. Surf. Sci. Catal.*, Vol. 58 (Elsevier, Amsterdam, 1991) p 359.
- [12] W. E. Farneth, R. J. Gorte, Chem. Rev. 95 (1995) 615.
- [13] M. Niva, N. Katada, K. Okumura in: *Characterization and Design of Zeolite Catalysts*, Springer-Verlag, Berlin, Heidelberg, 2010.
- [14] H. Ichihashi, M. Ishida, A. Shiga, M. Kitamura, T. Suzuki, K. Suenobu, K. Sugita, Catal. Surv. Asia 7 (2003) 261.
- [15] S. Shimizu, N. Abe, A. Iguchi, H. Sato, Catal. Surv. Jpn. 2 (1998) 71.
- [16] H. Ishida, Catal. Surv. Jpn. 1 (1997) 241.
- [17] H. Tsuneki, M. Kirishiki, T. Oku, Bull. Chem. Soc. Jpn. 80 (2007) 1075.
- [18] M. Iwamoto, H. Yahiro, K. Tanda, N. Mizuno, Y. Mine, S. Kagawa, J. Phys. Chem. 95 (1991) 3727.
- [19] X.B. Feng, W.K. Hall, J. Catal. 166 (1997) 368.

- [20] Y.J. Li, J.N. Armor, *Appl. Catal. B Environ.* 1 (1992) L31.
- [21] D.J. Wang, J.H. Lunsford, M.P. Rosynek, *J. Catal.* 169 (1997) 347.
- [22] Y. Ashina, T. Fujita, M. Fukatsu, K. Niwa, J. Yagi, in : *Stud. Surf. Sci. Catal.*, Vol. 28 (Elsevier, Amsterdam, 1986), p. 779
- [23] A. Corma, V. Martinez-Soria, E. Schnoefeld, *J. Catal.* 192 (2000) 163.
- [24] U. Freese, F. Heinrich, F. Roessner, *Catal. Today* 49 (1999) 237.
- [25] T.R. Hughes, W.C. Buss, P.T. Tamm, R.L. Jacobson, in : *Stud. Surf. Sci. Catal.*, Vol. 28 (Elsevier, Amsterdam, 1986), p. 725
- [26] R. E. Jentoft, M. Tsapatsis, M. E. Davis, B. C. Gates, *J. Catal.* 179 (1998) 565.
- [27] H. Pfeifer, D. Freude, J. Kärger in : *Catalysis and Adsorption by Zeolites*, Elsevier, Amsterdam, 1991.
- [28] M. Hunger, D. Freude, D. Fenzke, H. Pfeifer, *Chem. Phys. Lett.* 191 (1992) 391.
- [29] T. J. Gluszak, D. T. Chen, S. B. Sharma, J. A. Dumesic, T. W. Root, *Chem. Phys. Lett.* 190 (1992) 36.
- [30] P. Batamack, C. Doremieux-Morin, J. Fraissard, *J. Chim. Phys.* 89 (1992) 423.
- [31] A.L. Blumenfeld, J. J. Fripiat, *Magn. Reson. Chem.* 37 (1999) S118.
- [32] A. G. Pelmenchikov, E. A. Paukshtis, V. G. Stepanov, V. I. Pavlov, E. N. Yurchenko, K. G. Ione, S. Beran, *J. Phys. Chem.* 93 (1989) 6725.
- [33] K.-P. Schröder, J. Sauer, M. Leslie, C. R. A. Catlow, J. M. Thomas, *Chem. Phys. Lett.* 188 (1992) 320.
- [34] K. Suzuki, T. Noda, N. Katada, M. Niwa, *J. Catal.* 250 (2007) 151.
- [35] N. Katada, H. Igi, J. H. Kim, M. Niwa, *J. Phys. Chem. B*, 101 (1997) 5969.
- [36] J. R. Anderson, K. Foger, T. Mole, R. A. Rajadhyaksan, J. V. Sanders, *J. Catal.* 58 (1979) 114.
- [37] V. S. Nayak, V. R. Choudhary, *J. Catal.* 81 (1983) 26.
- [38] D. Atkinson, G. Curthoys, *Chem. Soc. Rev.* 8 (1979) 475.

- [39] B. S. Ujmansky, W. K. Hall J. Catal. 124 (1990) 97.
- [40] D. Farcasiu, A. Ghenciu, J. Am. Chem. Soc. 115 (1993) 10901.
- [41] E. P. Parry, J. Catal. 2 (1963) 371.
- [42] C. A. Emeis, J. Catal. 141 (1993) 347.
- [43] O. Cairon, T. Chevreau, J. Chem. Soc. Faraday Trans. 94 (1998) 323.
- [44] R. Borade, A. Sayari, A. Adnot, S. Kaliaguine, J. Phys. Chem. 94 (1990) 5989.
- [45] C. Guimon, A. Boreave, G. Pfister-Guillouzo, Surf. Interface Anal. 22 (1994) 407.
- [46] A. Auroux, Top.Catal. 4 (1997) 71.
- [47] A. Auroux, Top.Catal. 19 (2002) 205.
- [48] A. Auroux, in: *Molecular Sieves—Science and Technology: Acidity and Basicity*, eds. H. Karge and J. Weitkamp Vol. 6 (Springer-Verlag, Berlin Heidelberg, New York, 2000) Vol. 6, 2000.
- [49] N. Cardona-Martinez, J.A. Dumesic, Adv. Catal. 38 (1992) 149.
- [50] V. Solinas, I. Ferino, Catal. Today 41 (1998) 179.
- [51] A. Auroux, in: *Catalyst Characterization: Physical Techniques for Solid Materials*, eds. B. Imelik and J.C. Vedrine, Plenum Press, New York, 1994, p. 611.
- [52] P.C. Gravelle, Adv. Catal. 22 (1972) 191.
- [53] A. Corma, Chem. Rev. 95 (1995) 559.
- [54] P. B. Weisz, Chemtech 3 (1973) 498.
- [55] P. B. Weisz, V. J. Frilette, J. Phys. Chem. 64 (1960) 382.
- [56] W. O. Haag, R. M. Lago, P. B. Weisz, Faraday Discuss. 72 (1982) 317.
- [57] V. J. Frilette, W. O. Haag, R. M. Lago, J. Catal. 67 (1981) 218.
- [58] S. M. Csicsery, in: *ACS Monograph*, Vol.171 (American Chemical Society, Washington DC, 1976) p 680.
- [59] S. M. Csicsery, Zeolites 4 (1984) 202.

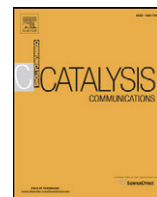
- [60] S. M. Csicsery, *J. Catal.* 108 (1987) 433.
- [61] E. G. Derouane, *J. Catal.* 100 (1986) 541.
- [62] E. G. Derouane, in : *Stud. Surf. Sci. Catal.*, Vol. 4 (Elsevier, Amsterdam, 1980), p 5.
- [63] E. G. Derouane, in: *Stud. Surf. Sci. Catal.*, Vol. 19 (Elsevier, Amsterdam, 1984), p 1.
- [64] J. Dwyer, *Chem. Ind.* 7 (1984)
- [65] P. A. Jacobs, J. A. Martens, in: *Stud. Surf. Sci. Catal.*, Vol. 28 (Elsevier, Amsterdam, 1986), p 23.
- [66] U. Hammon, G. T. Kokotailo, L. Riekert, J. Q. Zhou, *Zeolites* 8 (1988) 338.
- [67] E. G. Derouane, Z. Gabelica, *J. Catal* 65 (1980) 486.
- [68] J. Kärger, D. M. Ruthven, *Diffusion in Zeolites and Other Microporous Solids*, John Wiley and Sons, New York, 1992.
- [69] J. Datka, M. Boczar, P. Rymarowicz, *J. Catal.* 114 (1988) 168.
- [70] A. Chatterjee, T. Iwasaki, T. Ebina, H. Tsuruya, T. Kanougi, Y. Oumi, M. Kubo, A. Miyamoto, *Appl. Surf. Sci.* 130-132 (1998) 555.
- [71] J. Sauer, *Chem. Rev.* 89 (1989) 89.
- [72] J. Sauer, C. M. Kölmel, J. R. Hill, R. Ahlrichs, *Chem. Phys. Lett.* 164 (1989) 193.
- [73] J. B. Nicholas, R. E. Winans, R. J. Harrison, L. E. Iton, L. A. Curtiss, A. J. Hopfinger, *J. Phys. Chem.* 96 (1992) 10247.
- [74] J. Limtrakul, S. Hannongbua, *J. Mol. Struct. (Theochem)* 280 (1993) 139.
- [75] R. Carson, E. M. Cooke, J. Dwyer, A. Hinchliffe, P. J. O'Malley, in: *Zeolites as Catalysts, Sorbents and Detergent Builders*, Eds. H. G. Karge, J. Wietkamp, Elsevier, Amsterdam, 1989, p 39.
- [76] D. J. Parrillo, R. J. Gorte, *J. Phys. Chem.* 97 (1993) 8786.
- [77] D.J. Parrillo, C. Lee, R.J. Gorte, *Appl. Catal. A* 110 (1994) 67.
- [78] M. Huang, S. Kaliaguine, A. Auroux, *J. Phys. Chem.* 99 (1995) 9952.

- [79] M. Huang, S. Kaliaguine, A. Auroux, in: *Stud. Surf. Sci. Catal.*, Vol. 97 (Elsevier, Amsterdam, 1995) p. 311.
- [80] M. Huang, A. Auroux, S. Kaliaguine, *Micropor. Mater.* 5 (1995) 17.
- [81] C. V. McDaniel, P. K. Maher, in: *ACS Monograph*, Vol.171 (American Chemical Society, Washington DC, 1976) p 171.
- [82] M. A. Camblor, A. Corma, S. Valencia, *Chem. Commun.* (1996) 2265.
- [83] M. A. Camblor, A. Corma, A. Mifsud, J. Perez-Pariente, S. Valencia, in: *Stud. Surf.Sci. Catal.*, Vol. 105 (Elsevier, Amsterdam, 1997) p. 341.
- [84] P.A. Jacobs, R. von Ballmoos, *J. Phys. Chem.* 86 (1982) 3050.
- [85] T.J. Gricus Kofke, R. J. Gorte, W. E. Farneth, *J. Catal.* 114 (1988) 34.
- [86] T. J. Gricus Kofke, R. J. Gorte, G. T. Kokotailo, W. E. Farneth, *J. Catal.* 115 (1989) 265.
- [87] A. I. Biaglow, D. J. Parrillo, R. J. Gorte, *J. Catal.* 144 (1993) 193.
- [88] K. Tsutsumi, K. Nishimiya, *Thermochim. Acta*, 143 (1989) 299.
- [89] A. Auroux, P.C. Gravelle, J.C. Vedrine and M. Rekas, *Proc. 5th Int. Conf. on Zeolites*, ed. L.V. Rees (Heyden, London, 1980) p. 443.
- [90] H. Stach, J. Jänchen, U. Lohse, *Catal. Lett.* 13 (1992) 389.
- [91] A. Auroux, Y. Ben Taarit, *Thermochim. Acta* 122 (1987) 63.
- [92] Y. Mitani, K. Tsutsumi, H. Takahashi, *Bull. Chem. Soc. Jpn.* 56 (1983) 1921.
- [93] A.I. Biaglow, D.J. Parrillo, G.T. Kokotailo, R.J. Gorte, *J. Catal.* 148 (1994) 213.
- [94] I.V. Mishin, A.L. Klyachko, T.R. Brueva, O.P. Tkachenko, H.K. Beyer, *Kinet. Catal.* 34 (1993) 502.
- [95] D. Barthomeuf (1987) In: *Stud. Surf. Sci. Catal.*, Vol. 38 (Elsevier, Amsterdam, 1987) p 177.
- [96] H. Stach, J. Jänchen, U. Lohse, *Catal. Lett.* 13 (1992) 389.
- [97] H. Stach, J. Jänchen, H. G. Jerschke, U. Lohse, B. Parlitz, M. Hunger, *J. Phys. Chem.* 96 (1992) 8480.

- [98] A. Macedo, A. Auroux, F. Raatz, E. Jacquinot, R. Boulet, In: *ACS Symposium Series*, Vol. 368 (American Chemical Society, Washington DC, 1988) p 98.
- [99] A. Auroux, P.C. Gravelle, J. C. Védrine, M. Rekas (1980) In: Rees LVC (ed) Proc 5th Int Zeolite Conf, Naples, Italy, June 2–6, 1980, LV, Heyden, London, p 433.
- [100] J. C. Védrine, A. Auroux, G. Coudurier (1984) In: *ACS Symposium Series* Vol. 13 (American Chemical Society, Washington DC, 1984) p 254.
- [101] J. C. Védrine, A. Auroux, V. Bolis, P. Dejaifve, C. Naccache, P. Wierzchowski, E. G. Derouane, J. C. H. van Hoff, *J. Catal.* 59 (1979) 248.
- [102] H.G. Karge and L.C. Jozefowicz, in: *Stud. Surf. Sci. Catal.*, Vol. 84 (Elsevier, Amsterdam, 1994) p. 685.
- [103] L.C. Jozefowicz, H.G. Karge, E.N. Coker, *J. Phys. Chem.* 98 (1994) 8053.
- [104] D.T. Chen, S.B. Sharma, I. Filimonov, J.A. Dumesic, *Catal. Lett.* 12 (1992) 201.
- [105] G. I. Kapustin, L. M. Kustov, G. O. Glonti, T. R. Brueva, V. Y. Borovkov, A. L. Klyachko, A. M. Rubinshtein, V. B. Kazanskii, *Kinet. Katal.* 25 (1984) 959.
- [106] I. Bankós, J. Valyon, G. I. Kapustin, D. Kallo, A. L. Klyachko, T. R. Brueva, *Zeolites* 8 (1988) 189.
- [107] H. G.Karge , H. K. Beyer, in: *Molecular Sieves—Science and Technology: Solid-State Ion Exchange in Microporous and Mesoporous Materials*, eds. H. Karge and J. Weitkamp Vol. 3. (Springer-Verlag, Berlin Heidelberg, New York, 2002).
- [108] H. Garcia, H. D. Roth, *Chem.Rev.* 102 (2002) 3947.
- [109] I.V. Mishin, A.L. Klyachko, G.I. Kapustin, H.G. Karge, *Kinet. Catal.* 34 (1993) 828.
- [110] I.V. Mishin, A.L. Klyachko, T.R. Brueva, V.D. Nissenbaum, H.G.Karge, *Kinet.Catal.* 34 (1993) 835.
- [111] M. Muscas, J.F. Dutel, V. Solinas, A. Auroux and Y. Ben Taarit, *J.Mol.Catal.*106 (1996) 169.
- [112] H. Stach, J. Jänchen, H.G. Jerschke, U. Lohse, B. Parltitz, *J. Phys. Chem.* 96 (1992) 8480.
- [113] M. Huang, S. Kaliaguine, M. Muscas, A. Auroux, *J. Catal.* 157 (1995) 266.

- [114] A. Auroux, P. Artizzu, I. Ferino, R. Monaci, E. Rombi, V. Solinas, *Micropor. Mater.* 11 (1997) 117.
- [115] Barrer, R. M. *Hydrothermal Chemistry of Zeolites*; Academic Press: London, 1982.
- [116] R. Szostak, *Molecular Sieves: Principle of Synthesis and Identification*; Van Nostrand Reinhold: New York, 1989.
- [117] T. Chapus, A. Tuel, Y. Ben Taarit, C. Naccache, *Zeolites* 14 (1994) 349.
- [118] K. G. Ione, L. A. Vostrikova, M. Mastikin, *J. Mol. Catal.* 31 (1985) 355.
- [119] K. G. Ione, L. A. Vostrikova, *Uspechi. Chimii.* 56 (1987) 393.
- [120] L. Pauling, *The Nature of the Chemical Bond*, 3rd ed.; Cornell University Press: Ithaca, NY, 1967.
- [121] F. Liebau, *Structural Chemistry of Silicates*; Springer-Verlag: Berlin, 1985.
- [122] M. Sayed, A. Auroux, J. C. Védrine, *J. Catal.* 116 (1989) 1.
- [123] G. Coudurier, A. Auroux, J. C. Védrine, R. D. Farlee, L. Abrams, R. D. Shannon, *J. Catal.* 108 (1987) 1.
- [124] M. L. Occelli, H. Eckert, A. Wölker, A. Auroux, *Micropor. Mesopor. Mat.* 30 (1999) 219.
- [125] M. L. Occelli, H. Eckert, C. Hudalla, A. Auroux, P. Ritz, P. S. Iyer, *Stud. Surf. Sci. Catal.* 105 (1997) 1981.
- [126] M. L. Occelli, G. Schwering, C. Fild, H. Eckert, A. Auroux, P. S. Iyer, *Micropor. Mesopor. Mat.* 34 (2000) 15.
- [127] H. Eckert, C. Hudalla, A. Wölker, A. Auroux, M. L. Occelli, *Solid State NMR* 9 (1997) 9.
- [128] M. L. Occelli, A. E. Schweizer, C. Fild, G. Schwering, H. Eckert, A. Auroux, *J. Catal.* 192 (2000) 119.
- [129] B. Ducourty, M. L. Occelli, A. Auroux, *Thermochim. Acta* 312 (1998) 27.
- [130] E. Dumitriu, V. Hulea, I. Fechete, C. Catrinescu, A. Auroux, J. F. Lacaze, C. Guimon, *Appl. Catal. A-Gen.* 181 (1999) 15.
- [131] D. J. Parrillo, C. Lee, R. J. Gorte, D. White, W. E. Farneth. *J. Phys. Chem.* 99 (1995) 8745.

- [132] E. Dumitriu, V. Hulea, I. Fechete, A. Auroux, J. F. Lacaze, C. Guimon, 43 (2001) 341.
- [133] J. Kotrla, L. Kubelkova, C. C. Lee, R. J. Gorte, J. Phys. Chem. B 102 (1998) 1437.
- [134] A. Auroux, A. Tuel, J. Bandiera, Y. Ben Taarit, J. M. Guil, Appl. Catal. 2 (1993) 181.
- [135] J. Jänchen, G. Vorbeck, H. Stach, B. Parlitz, J. H. C. van Hooff, (1995) In: *Stud. Surf. Sci. Catal.*, Vol. 94 (Elsevier, Amsterdam, 1995) p108.
- [136] G. Vorbeck, J. Jänchen, B. Parlitz, M. Schneider, R. Fricke, J. Chem. Soc. Chem. Com. (1994) 123.
- [137] M. Muscas, V. Solinas, S. Gontier, A. Tuel, A. Auroux, in: *Stud. Surf. Sci. Catal.*, Vol. 94 (Elsevier, Amsterdam, 1995) p 101.
- [138] A. Auroux, A. Gervasini, E. Jorda, A. Tuel (1994) In: *Stud. Surf. Sci. Catal.*, Vol. 84 (Elsevier, Amsterdam, 1994) p 653.
- [139] V. Bolis, S. Bordiga, C. Lamberti, A. Zecchina, A. Carati, F. Rivetti, G. Spano, G. Petrini, *Micropor. Mater.* 30 (1999) 67.
- [140] V. Bolis, S. Bordiga, C. Lamberti, A. Zecchina, A. Carati, F. Rivetti, G. Spano, G. Petrini, *Langmuir* 15 (1999) 5753.
- [141] I. V. Mishin, T. R. Brueva, G. I. Kapustin, *Adsorption* 11(2005) 415.
- [142] C. P. Nicolaidis, H. H. Kung, N. P. Makgoba, N. P. Sincadu, M. S. Scurrrell, *Appl. Catal. A-Gen.* 223 (2002) 29.
- [143] S.M. Babitz, M.A. Kuehne, H.H. Kung, J.T. Miller, *Ind. Eng. Chem. Res.* 36 (1997) 3027.
- [144] A.G. Gayubo, P.L. Benito, A.T. Aguayo, M. Olazar, J. Bilbao, *J. Chem. Tech. Biotechnol.* 65 (1996) 186.
- [145] D.J. Parrillo, C. Lee, R.J. Gorte, D. White, W.E. Farneth, *J. Phys. Chem.* 99 (1995) 8745.
- [146] M.A. Kuehne, H.H. Kung, J.T. Miller, *J. Catal.* 171 (1997) 293.



Short Communication

Influence of surface acid–base properties of zirconia and titania based catalysts on the product selectivity in gas phase dehydration of glycerol

Dušan Stošić^a, Simona Bennici^a, Jean-Luc Couturier^b, Jean-Luc Dubois^c, Aline Auroux^{a,*}^a Université Lyon 1, CNRS, UMR 5256, IRCELYON, Institut de recherches sur la catalyse et l'environnement de Lyon, 2 avenue Albert Einstein, F-69626 Villeurbanne, France^b ARKEMA, Centre de Recherche Rhône Alpes, Pierre Bénite, 69493 cedex, France^c ARKEMA, Direction Recherche & Développement, 420 Rue d'Estienne d'Orves, 92705 Colombes France

ARTICLE INFO

Article history:

Received 1 August 2011

Received in revised form 29 September 2011

Accepted 4 October 2011

Available online 13 October 2011

Keywords:

Adsorption microcalorimetry

Acid–base properties

Glycerol conversion

Acrolein

Acetol

ABSTRACT

Acid–base properties of zirconia and titania based materials were investigated by adsorption microcalorimetry of NH_3 and SO_2 probe molecules. Catalytic performance of the catalysts was also tested in the gas phase dehydration of glycerol with the intention of finding correlations between catalytic activity and surface acid–base features. Results show that the number of basic sites directly affects the selectivity in gas phase dehydration of glycerol to produce acrolein. Therefore, in order to realize the target reaction it is necessary to control not only the strength and the amount of the desired sites (acidic ones), but also to hinder as much as possible the number/strength/action of the undesired ones (basic ones).

© 2011 Elsevier B.V. All rights reserved.

1. Introduction

Glycerol is a significant by product derived from the production of biodiesel [1]. It is predicted that by 2015, 1.54 million tonnes of glycerol will be generated worldwide [2], all of which should be efficiently processed in order to achieve sustainability of the biodiesel sector. Crude glycerol obtained from biodiesel process contains 80 wt.% of glycerol, but also contains water, methanol, traces of fatty acids, and various inorganic and organic compounds [3]. As a consequence, it needs to be purified by an expensive distillation step prior to further use.

Glycerol is a molecule with a large functionalisation potential that opens numerous opportunities for chemical and biochemical conversions to produce value-added chemicals. More detailed information is available in recent review articles [3–8]. The percentage of glycerol that is being refined is now decreasing due to high cost of necessary distillation step and because of the absence of any market able to absorb the overproduction.

Promising route to glycerol valorisation is its catalytic dehydration to produce acrolein and hydroxyacetone (acetol), which are important industrial intermediates for the chemical and agrochemical industries [7, 8]. However, the selective catalytic conversion to acrolein and/or hydroxyacetone remains very challenging.

Adsorption microcalorimetry is a direct method for describing in detail the features of surface sites simultaneously from a quantitative and from an energetic point of view. Determination of the strength of

the acidic and basic sites exposed on the solid surface as well as their distribution is a necessary requirement to understand the catalytic properties of materials. Heat flow calorimetry linked to sensitive volumetric system is the most commonly used technique for this purpose.

Zirconium and titanium oxides are important catalytic materials with medium high Lewis acidity, significant basicity, and weak Brønsted acidity [9–12]. The acid–base properties of ZrO_2 are easily adjusted by making its mixtures with other oxides, such as CeO_2 and La_2O_3 . Furthermore, the presence of tungstate species on both titania and zirconia causes full disappearance of the surface anions acting as basic sites, and the appearance of a very strong Brønsted acidity [13–16].

In this work we report the preparation and investigation of the acid–base properties of zirconia and titania based materials by adsorption microcalorimetry of NH_3 and SO_2 probe molecules. The catalysts were also tested in the gas phase dehydration of glycerol with the intention of finding correlations between catalytic activity and surface acid–base features to better understand the nature of active sites for the dehydration reaction, which could help to develop more efficient solid catalysts for a sustainable use of biomass-derived glycerol by chemical industry. The aim was also the tuning of a desirable ratio of acidic to basic sites especially active for a given reaction.

2. Experimental

2.1. Preparation of catalysts

$\text{WO}_3\text{-ZrO}_2$ (10 wt.% of WO_3), $\text{La}_2\text{O}_3\text{-ZrO}_2$ (30 wt.% of La_2O_3) and $\text{CeO}_2\text{-ZrO}_2$ (25 wt.% of CeO_2) were commercial samples purchased

* Corresponding author. Tel.: +33 472445398; fax: +33 472445399.

E-mail address: aline.auroux@ircelyon.univ-lyon1.fr (A. Auroux).

from Dai Ichi Kigenso Kabushiki Kaisha. They were calcined in air at 500 °C for 5 h before use. ZrO₂, TiO₂ anatase and TiO₂ rutile were purchased from Saint-Gobain Norpro, and were calcined in air at 500 °C for 5 h before use.

HPW/TiO₂ (10 wt.% of HPW) was prepared by incipient wetness impregnation with an aqueous solution of phosphotungstic acid on to the TiO₂ anatase. The sample was dried in air at 110 °C overnight, followed by calcination in air at 500 °C.

HPW/WO₃-ZrO₂ (4 wt.% of HPW) was prepared by incipient wetness impregnation with an aqueous solution of phosphotungstic acid on to the WO₃-ZrO₂ sample. The sample was subsequently dried in air at 110 °C overnight and calcined in air at 450 °C.

2.2. Measurement of catalyst acidity and basicity

The acid–base properties were studied by adsorption microcalorimetry of NH₃ and SO₂. Experiments were performed at 423 K in a heat flow calorimeter (C80 from Setaram) linked to a conventional volumetric apparatus equipped with a Barocel capacitance manometer for pressure measurements. The samples were pretreated in a quartz cell by heating overnight under vacuum at 573 K; this temperature was reached using a heating rate of 1 K min⁻¹. The differential heats of adsorption were measured as a function of coverage by repeatedly sending small doses of respective gas on to the sample until an equilibrium pressure of around 67 Pa was reached. The sample was then out-gassed for 30 min at the same temperature, and a second adsorption run was performed at 423 K on each sample, until an equilibrium pressure of about 27 Pa was attained. The difference between the amounts adsorbed in the first and second adsorptions at 27 Pa represents the irreversibly adsorbed amount (V_{irr}) of a respective gas, which provides an estimation of the number of strong acidic/basic sites.

2.3. Catalytic reaction

The gas phase dehydration reaction of glycerol was carried out at 280 °C under atmospheric pressure in fixed-bed Pyrex reactor (420 mm length × 8 mm inside diameter). The reaction temperature was monitored by a thermocouple inserted into the middle of the catalyst bed. The catalyst was first crushed and sieved (300–500 μm), then mixed with quartz sand (50–80 mesh) and loaded in the middle of reactor with quartz wool packed in both ends. The catalysts were initially pretreated at 573 K in a flow of nitrogen (30 mL min⁻¹) for 2 h. Glycerol solution was composed by 30 wt.% of glycerol in water and was introduced in the flow of nitrogen with help of syringe pump at a flow of 0.48 g h⁻¹. The composition of fed gas was N₂:H₂O:glycerol, equal to 18.7:75:6.3 in vol.%. The catalytic performance of the solid catalysts was evaluated at a gas hourly space velocity (GSHV) of reaction stream of 4400 h⁻¹. The sampling time, after

Table 1
BET surface area and chemical composition.

Sample	Calcination temperature (°C)	BET surface area (m ² g ⁻¹)	Composition
ZrO ₂	400	53	/
WO ₃ -ZrO ₂	400	45	10 wt.% WO ₃
HPW/WO ₃ -ZrO ₂	400	45	10 wt.% WO ₃ , 4 wt.% HPW (H ₃ PW ₁₂ O ₄₀ - Keggin structure)
CeO ₂ -ZrO ₂	500	50.7	25 wt.% CeO ₂
La ₂ O ₃ -ZrO ₂	500	67.4	30 wt.% La ₂ O ₃
TiO ₂ anatase	500	39	/
TiO ₂ rutile	500	3.7	/
HPW/TiO ₂	500	40	10 wt.% HPW (H ₃ PW ₁₂ O ₄₀ - Keggin structure)

Table 2

V_{irr} and V_{tot} calculated from adsorption isotherms of SO₂ and NH₃ on different materials.

Sample name	SO ₂ adsorbed amount		NH ₃ adsorbed amount	
	V_{total}^a (μmol/m ²)	V_{irr}^b (μmol/m ²)	V_{total}^a (μmol/m ²)	V_{irr}^b (μmol/m ²)
ZrO ₂	3.93	3.59	1.99	1.05
WO ₃ -ZrO ₂	0.37	0.26	2.52	1.54
HPW/WO ₃ -ZrO ₂	0.13	0.09	2.73	1.41
CeO ₂ -ZrO ₂	4.19	3.78	1.66	0.72
La ₂ O ₃ -ZrO ₂	3.53	3.22	1.05	0.43

^a Amount of NH₃ or SO₂ adsorbed under an equilibrium pressure of 0.2 Torr (27 Pa).

^b Amount of chemisorbed NH₃ or SO₂ under an equilibrium pressure of 0.2 Torr (27 Pa).

stabilization of temperature at 280 °C, was 90 min. Products were collected after the reactor in a cold trap. The concentrations of products obtained in the liquid phase (glycerol, acrolein, acetol) were measured by gas chromatography using a flame ionization detector (Column Alltec ECTM-1000 FFAP 30 m × 0.53 mm × 1.2 μm). Quantification was done by using the external standards. Volatile products running outside the cold trap (CO, CO₂) were analyzed online with a two columns Varian Chrompack micro-GC. The first column, silica plot, allows the CO analysis, while the second column, packed with molecular sieve, allows CO₂ analysis.

3. Results and discussion

Table 1 displays the list of catalysts investigated in this work, their chemical compositions and their surface areas. Among zirconia based catalysts, La₂O₃-ZrO₂ presents largest surface area, while ZrO₂ and CeO₂-ZrO₂ express smaller and similar surface areas. It can be seen from the same table that impregnation of ZrO₂ with WO₃ and WO₃/HPW leads to a slight decrease in this property. As it can be expected TiO₂ anatase possess significantly higher surface area in comparison with rutile sample. Impregnation of anatase sample with WO₃ does not change the surface area of thus obtained material.

3.1. Acid/base properties

The adsorption of probe molecules was used to determine the acid/base features of investigated catalysts by microcalorimetry technique. Ammonia was used as a basic molecule to determine the acid character, while sulfur dioxide was used for titration of the basic sites.

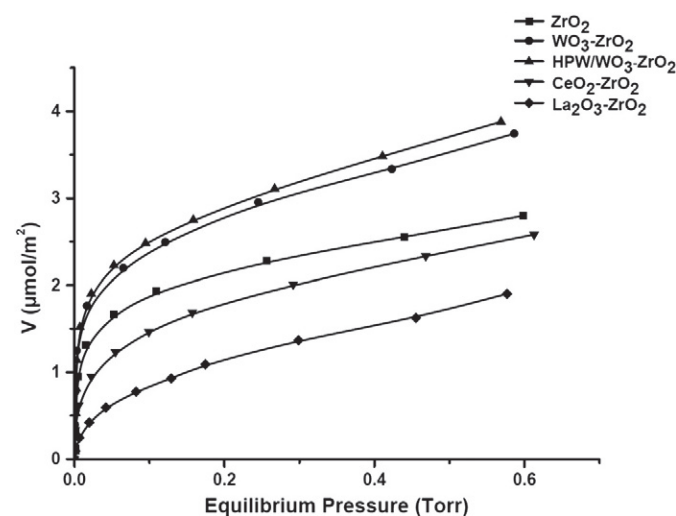


Fig. 1. Volumetric isotherms of NH₃ adsorption on zirconia based materials.

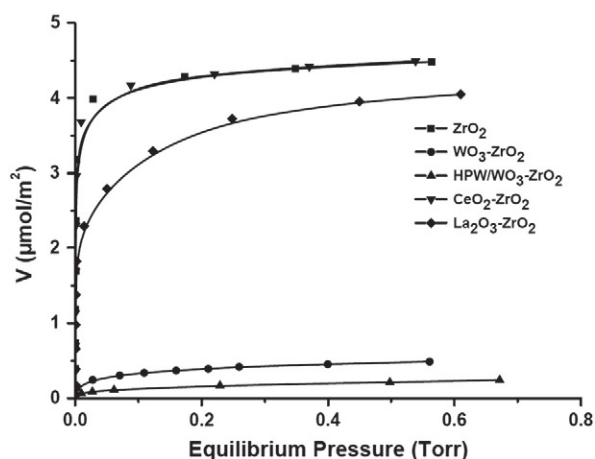


Fig. 2. Volumetric isotherms of SO₂ adsorption on zirconia based materials.

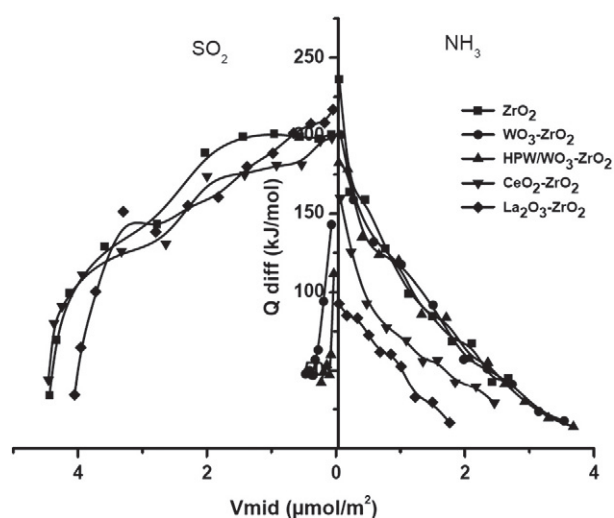


Fig. 3. Differential heats of NH₃ and SO₂ adsorption as a function of surface coverage.

3.2. Zirconia based catalysts

Zirconia belongs to the group of amphoteric oxides, whose acid–base properties are easily adjusted by making its mixtures with other oxides. Here, pure zirconia and its mixtures with La₂O₃, CeO₂, WO₃, and with both WO₃–HPW (H₃PW₁₂O₄₀) have been investigated.

Table 2 summarizes the data obtained for SO₂ and NH₃ adsorption on zirconia based materials. This table presents total and irreversibly adsorbed (chemisorbed) amounts of gasses. As the investigated samples display differences in BET surface areas (Table 1), the calorimetric results are presented in μmol m⁻² rather than in μmol g⁻¹. NH₃ adsorption isotherms of ZrO₂ based catalysts are presented in Fig. 1. The vertical parts of the isotherms correspond to irreversible adsorption, whereas the horizontal parts can be assigned to reversible adsorption. It is evident that addition of WO₃ and HPW increased

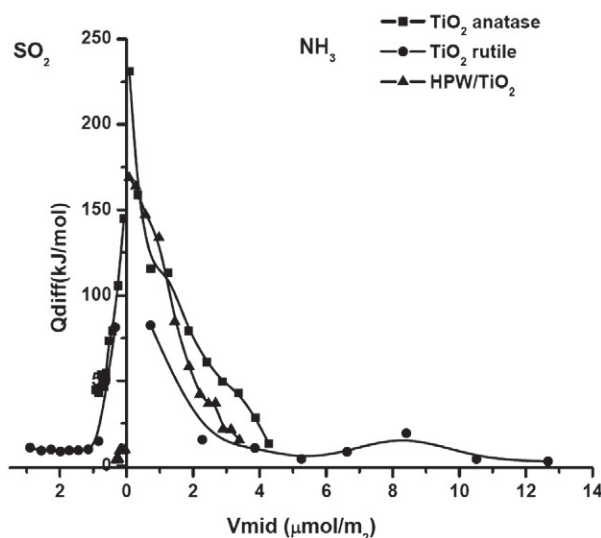


Fig. 4. Differential heats of NH₃ and SO₂ adsorption as a function of surface coverage.

the number of acid sites (see also Table 2), as can be expected from previously reported results [13–18]. Quite surprisingly, the presence of ceria and lanthania decreased the amount of adsorbed ammonia, indicating that the acidic character was decreased in the case of these mixed oxides, when compared to pure zirconia. The lowest adsorption of NH₃ was found on the sample containing La₂O₃ oxide; what means that, among all investigated samples, this one is the least acidic one.

The volumetric data for SO₂ adsorption are also summarized in Table 2 whereas the corresponding adsorption isotherms are presented in Fig. 2. It is easy to see that the addition of WO₃ and HPW led to a significant decrease of chemisorbed SO₂. The addition of lanthania also decreases SO₂ uptake, but to a much lower extent. Adsorption isotherms of zirconia and mixed ceria–zirconia are almost identical.

Fig. 3 displays the differential heats of adsorption as a function of surface coverage for both SO₂ and NH₃ probe molecules. These curves can provide data concerning the amount, strength and strength distribution of active sites. Furthermore, the initial heats of adsorption are characteristic of the strongest acid or base sites involved in adsorption process.

All the investigated materials express energetic heterogeneity of both acidic and basic active sites present on their surface. Evidently among the investigated samples, WO₃–ZrO₂ and HPW/WO₃–ZrO₂ showed prominent acidic character. The other solid materials adsorbed significant amounts of both SO₂ and NH₃, which is a clear indication of their amphoteric nature.

From these results it becomes evident that mixing of lanthania and ceria with the starting material (ZrO₂) has as a consequence the decrease in acidic character, while the distribution of basic sites is only slightly affected. The addition of WO₃ and WO₃–HPW to zirconia significantly decreases the amount of adsorbed SO₂ and the corresponding heats of adsorption.

Table 3

V_{irr} and V_{tot} calculated from adsorption isotherms of SO₂ and NH₃ on different materials.

Sample name	SO ₂ adsorbed amount		NH ₃ adsorbed amount	
	V _{total} ^a (μmol/m ²)	V _{irrev} ^b (μmol/m ²)	V _{total} ^a (μmol/m ²)	V _{irrev} ^b (μmol/m ²)
TiO ₂ anatase	0.69	0.43	3.62	2.03
TiO ₂ rutile	1.89	1.73	7.59	4.37
HPW/TiO ₂	0.20	0.15	2.61	1.85

^a Amount of NH₃ or SO₂ adsorbed under an equilibrium pressure of 0.2 Torr (27 Pa).

^b Amount of chemisorbed NH₃ or SO₂ under an equilibrium pressure of 0.2 Torr (27 Pa).

Table 4
Catalytic performance of investigated catalysts for gas phase dehydration of glycerol at 280 °C.

Catalyst	Conversion (%)	Product selectivity (mol%)			
		Acrolein	Acetol	CO _x	Others
ZrO ₂	59	5	25	2	68
WO ₃ -ZrO ₂	100	72	8	1	20
HPW/WO ₃ -ZrO ₂	100	73	11	1	16
CeO ₂ -ZrO ₂	16	2	40	1	58
La ₂ O ₃ -ZrO ₂	19	3	14	3	80
TiO ₂ anatase	20	21	39	5	35
TiO ₂ rutile	5	50	17	18	15
HPW/TiO ₂	100	74	7	1	19

3.3. Titania based catalysts

Table 3 presents total and irreversibly adsorbed amounts of gases obtained from adsorption isotherms of SO₂ and NH₃.

It is easy to see that the TiO₂ rutile adsorbed the highest amount of sulfur dioxide. TiO₂ adsorbed less of the gas probe molecule compared to rutile sample, while addition of HPW to anatase led to a decrease of SO₂ adsorption capacity.

If about NH₃ adsorption, the situation is similar; amount of the adsorbed probe gas decreases in order TiO₂ rutile > TiO₂ anatase > HPW/TiO₂ (Table 3).

Differential heats of SO₂ and NH₃ adsorption as a function of surface coverage are presented in Fig. 4. It is evident that titania, although amphoteric, expresses more prominent acidic than basic character. The addition of heteropolyacid (HPW) to this oxide results in a decreasing of both the amounts of adsorbed probes and the strengths of interactions. Moreover, is important to notice that this modification leads to suppression of basic character of titania. Differential heat of adsorption for both probe molecules, on titania rutile sample, after the first doses decreases fast and reaches a constant value.

3.4. Catalytic activity

Gas phase dehydration of glycerol was carried out at 280 °C with a GHSV of 4400 h⁻¹ (GHSV of glycerol 277 h⁻¹). Using high GHSV shortened the induction period for obtaining the steady acetol and acrolein selectivity and reduced the possibility of acetol conversion into undesired byproducts [19, 20]. The possibility that

very different glycerol conversions could make comparison of the selectivity unreliable was examined by Chai et al [21]. It was shown that after the induction period, the selectivity in glycerol dehydration reaction becomes insensitive to the conversion level of the glycerol reactant. Prior to catalytic testing, blank reaction test was performed at the same temperature without catalyst to determine the reactivity of the reactor. The results showed that conversion of glycerol was less than 2%, without any detectable amounts of acetol or acrolein.

The results given in Table 4 show that among the tested catalysts, glycerol is completely converted on WO₃-ZrO₂, HPW/WO₃-ZrO₂ and HPW-TiO₂ at the beginning of the reaction. The same catalysts exhibited the highest selectivity to acrolein (72–74%). Presented data clearly indicate that the conversion of glycerol decreased in the order WO₃-ZrO₂, HPW/WO₃-ZrO₂, HPW/TiO₂ > ZrO₂ > TiO₂ anatase > La₂O₃-ZrO₂ > CeO₂-ZrO₂ > TiO₂ rutile. The acrolein selectivity decreased according to: HPW/TiO₂ > HPW/WO₃-ZrO₂ > WO₃-ZrO₂ > TiO₂ rutile > TiO₂ anatase > ZrO₂ > La₂O₃-ZrO₂ > CeO₂-ZrO₂. From these results it is evident that although high acidity is important to achieve complete conversion of glycerol, it is not the only requirement. When compared to HPW/TiO₂, titania anatase shows higher number of acid sites (Table 3), and displays higher overall acidity (Fig. 4). Overall acidity strength (heat of adsorption) of ZrO₂ is also higher than of WO₃-ZrO₂ and HPW/WO₃-ZrO₂ catalysts (Fig. 3), but the number of acid sites is lower (Table 2). The differences in glycerol conversion and selectivity to acrolein could be explained by the nature of acid sites present on the surface of these catalysts. On the surface of pure titania and zirconia only Lewis acid sites are present [9–12], while impregnation with HPW and WO₃ on its surface would create significant Brønsted acidity [13–18]. Alhanash et al. showed that Lewis acid catalysts need a higher reaction temperature to be activated, due to a higher activation energy compared to Brønsted acid catalysts [22]. Thus, glycerol conversion is lower on the catalysts possessing mainly Lewis acidity. It should be stated here that, although Brønsted acid sites were not present on the fresh zirconia and titania, the possibility that they could be generated by the interaction of the Lewis sites with steam present in the system cannot be neglected [22]. The low conversion observed for TiO₂ rutile sample can be explained by its low surface area, while the low conversion of glycerol on CeO₂-ZrO₂ and La₂O₃-ZrO₂ catalysts can easily be explained by their lower acidity. It should be mentioned here that samples that expressed a lower reactivity towards glycerol also possess significant basicity.

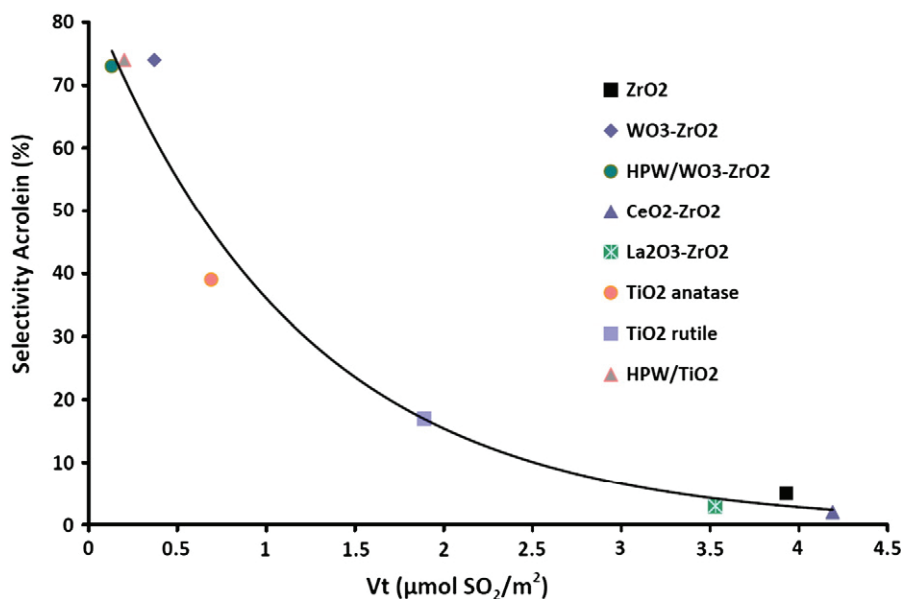


Fig. 5. Selectivity to acrolein as function of density of basic sites.

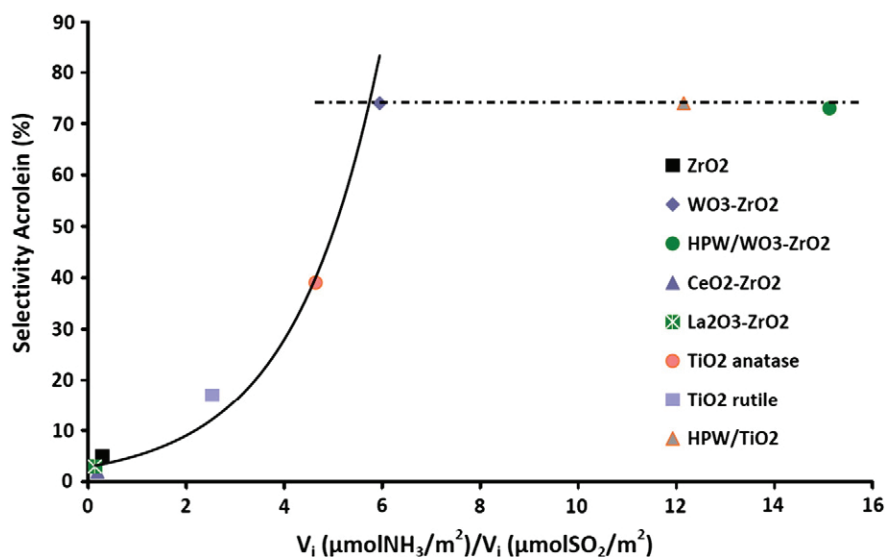


Fig. 6. Selectivity to acrolein as a function of $V_i (\mu\text{molNH}_3/\text{m}^2)/V_i (\mu\text{molSO}_2/\text{m}^2)$ ratio.

Previous work on glycerol dehydration suggests that acrolein forms on strong Brønsted acid sites [3, 6, 19, 22]; protonation occurs at the central hydroxyl group of glycerol, a water molecule and a proton are eliminated from the protonated glycerol, and then 3-hydroxypropanal is produced by tautomerism, which is unstable and readily dehydrated into acrolein. It is easy to see from Table 4 that Brønsted acid catalysts showed high acrolein selectivity. As the catalysts usually contain both acidic and basic sites, the influence of basicity must also be considered. Results presented in Fig. 5 show that the selectivity to produce acrolein is decreasing with increasing number of basic sites on the catalysts surface. Besides Fig. 6 presents acrolein selectivity as a function of the ratio of acid to basic sites ($V_{\text{irr}}(\text{SO}_2)/V_{\text{irr}}(\text{NH}_3)$). This ratio has been calculated for each catalyst from microcalorimetry results by dividing the amount of irreversibly adsorbed NH_3 by the amount of irreversibly adsorbed SO_2 . As can be observed in Fig. 6, the higher this parameter is (which corresponds to a decrease in basicity) the higher the selectivity towards acrolein is, and after a certain value further increase of this ratio does not influence selectivity which remains constant. On contact with the surface of bifunctional catalysts substrate can react both on basic and acidic sites, thus undergoing competitive reactions. Evidently, a larger number of basic sites would increase the possibility of glycerol interaction with them and reduce acrolein selectivity. Therefore it is logical to suggest that catalytic performances observed on $\text{WO}_3\text{-ZrO}_2$, $\text{HPW}/\text{WO}_3\text{-ZrO}_2$ and HPW-TiO_2 are not only due to high Brønsted acidity induced by addition of tungstate species, but also because of hindering the number/strength/action of the basic sites. In contrast to acrolein, no obvious correlation between selectivity and acid/base features of the catalysts can be observed in the case of second desired product – acetol. From Table 4 it is evident that better selectivity to acrolein is observed on the catalysts that possess basic and/or Lewis acid sites. It is proposed that on Lewis acid sites protonation proceeds at the terminal hydroxyl group of glycerol and acetol is produced through dehydration and deprotonation accompanied by tautomerism [22]. In contrast to the mechanism proposed over Lewis acid sites, the reaction over basic ones does not start with a dehydration step, but with a dehydrogenation step. The resulting 2,3-dihydroxypropanal can either further react *via* consecutive dehydration and hydrogenation to yield acetol, or can form – *via* a retro-aldol reaction – formaldehyde and hydroxyacetaldehyde, which can be subsequently hydrogenated to ethylene glycol [23]. Another possibility is that reaction over basic sites proceeds through dehydration starting from a terminal hydroxyl

group. This leads to formation of enol intermediate, which can undergo rapid rearrangement to acetol. Having in mind that transformation of glycerol to acetol could proceed in parallel according to the different mechanisms over the bifunctional catalysts, finding direct correlation with surface acid/base properties is not likely to be done.

4. Conclusions

The glycerol dehydration activity is dependent not only on the total acidity of the catalysts, but also on the nature of acid sites present on their surface. Selectivity in the reaction is largely governed by the balance between acidic and basic active sites, but also by the ratio of Lewis to Brønsted acid sites.

Results show that the number of basic sites directly affects the selectivity in gas phase dehydration of glycerol to produce acrolein. Therefore, in order to realize the target reaction it is necessary to control not only the strength and the amount of the desired sites (acidic ones), but also to hinder as much as possible the number/strength/action of the undesired ones (basic ones). Direct correlations between surface acid–base properties and selectivity to acetol were not observed due to the fact that production of acetol could proceed simultaneously through different independent pathways.

Acknowledgments

Authors acknowledge the support from the French National Research Agency (ANR-09-CP2D-19).

References

- [1] G.W. Huber, S. Iborra, A. Corma, Chemical Reviews 106 (2006) 4044.
- [2] Global Industry Analysts, http://www.strategyr.com/Glycerin_Market_Report.asp.
- [3] B. Katryniok, S. Paul, V. Bellière-Baca, P. Rey, F. Dumeignil, Green Chemistry 12 (2010) 2079.
- [4] D.T. Johnson, K.A. Taconi, AIChE Journal 26 (2007) 338.
- [5] C.-H. Zhou, J.N. Beltrami, T.-X. Fan, G.Q. Lu, Chemical Society Reviews 37 (2008) 527.
- [6] B. Katryniok, S. Paul, M. Capron, F. Dumeignil, ChemSusChem 2 (2009) 719.
- [7] M. Pagliaro, R. Ciriminna, H. Kimura, M. Rossi, C. Della-Pina, Angewandte Chemie, International Edition 46 (2007) 4434.
- [8] Y. Zheng, X. Chen, Y. Shen, Chemical Reviews 108 (2008) 5253.
- [9] V. Bolis, G. Cerrato, G. Magnacca, C. Morterra, Thermochimica Acta 312 (1998) 63.
- [10] Z. Luan, J.A. Fournier, Microporous and Mesoporous Materials 79 (2005) 235.
- [11] G. Busca, H. Saussey, O. Saur, J.C. Lavalley, V. Lorenzelli, Applied Catalysis 14 (1985) 245.
- [12] L. Ferretto, A. Glisenti, Chemistry of Materials 15 (2003) 1181.

- [13] G. Ramis, G. Busca, V. Lorenzelli, *Studies in Surface Science and Catalysis* 48 (1989) 777.
- [14] G. Ramis, G. Busca, C. Cristiani, L. Lietti, P. Forzatti, F. Bregani, *Langmuir* 8 (1992) 1744.
- [15] A. Gutierrez-Alejandre, P. Castillo, J. Ramirez, G. Ramis, G. Busca, *Applied Catalysis A: General* 216 (2001) 181.
- [16] D.C. Calabro, J.C. Vartuli, J.G. Santiesteban, *Topics in Catalysis* 18 (2002) 231.
- [17] A. Ulgen, W. Hoelderich, *Catalysis Letters* 131 (2009) 122.
- [18] W. Ji, J. Hu, Y. Chen, *Catalysis Letters* 53 (1998) 15.
- [19] F. Wang, J.-L. Dubois, W. Ueda, *Applied Catalysis A: General* 376 (2010) 25.
- [20] W. Suprun, M. Lutecki, T. Haber, H. Papp, *Journal of Molecular Catalysis A: Chemical* 309 (2009) 71.
- [21] S.-H. Chai, H.-P. Wang, Y. Liang, B.-Q. Xu, *Green Chemistry* 9 (2007) 1130.
- [22] A. Alhanash, E.F. Kozhevnikova, I.V. Kozhevnikov, *Applied Catalysis A: General* 378 (2010) 11.
- [23] A.K. Kinage, P.P. Upare, P. Kasinathan, Y.K. Hwang, J.-S. Chang, *Catalysis Communications* 11 (2010) 620.



Contents lists available at SciVerse ScienceDirect

Applied Catalysis A: General

journal homepage: www.elsevier.com/locate/apcata

Glycerol dehydration over calcium phosphate catalysts: Effect of acidic–basic features on catalytic performance

Dušan Stošić^a, Simona Bennici^a, Sergey Sirotnin^b, Christophe Calais^c, Jean-Luc Couturier^c, Jean-Luc Dubois^d, Arnaud Travert^b, Aline Auroux^{a,*}

^a Université Lyon 1, CNRS, UMR 5256, IRCELYON, Institut de Recherches sur la Catalyse et l'Environnement de Lyon, 2 Avenue Albert Einstein, F-69626 Villeurbanne, France

^b Laboratoire Catalyse et Spectrochimie, CNRS-ENSICAEN, Université de Caen, 6 Boulevard du Maréchal Juin, 14050 Caen Cedex, France

^c ARKEMA, Centre de Recherche Rhône Alpes, 69493 Pierre Bénite Cedex, France

^d ARKEMA, Direction Recherche & Développement, 420 Rue d'Estienne d'Orves, 92705 Colombes, France

ARTICLE INFO

Article history:

Received 31 July 2012

Received in revised form

10 September 2012

Accepted 11 September 2012

Available online xxx

Keywords:

Calcium phosphate catalysts

Acid–base properties

Glycerol conversion

Acrolein

Acetol

ABSTRACT

This work focuses on investigation of calcium phosphate compounds with different Ca/P ratios (1.39–1.77). Additionally, hydroxyapatite impregnated with tungsten oxide was also investigated. The structural, textural, and surface properties of these materials have been fully characterized using appropriate techniques (low-temperature adsorption–desorption of nitrogen, X-ray diffraction analysis (XRD), X-ray photoelectron spectroscopy (XPS), Raman spectroscopy and temperature-programmed reduction (TPR)). Adsorption microcalorimetry of NH₃ or SO₂ was used to estimate the population, strength and strength distribution of acid and basic sites. The nature of acidic sites was determined through the adsorption/desorption of pyridine, followed by infrared spectroscopy. Catalytic performance of the catalysts was tested in the gas phase dehydration of glycerol with the intention of finding correlations between catalytic activity and surface acid–base features. Results show that Ca/P ratio, beside the already known influence on acidic/basic features, also influences red-ox properties of these materials. The investigation performed here proved that, in order to get acrolein – with high selectivity – which is formed on acid sites, it is not only necessary to provide acidity, but also to hinder basic sites. Our results also show that reducing of number and strength of acid centers increases the yield of other desired product, acetol.

© 2012 Elsevier B.V. All rights reserved.

1. Introduction

Glycerol is the main by-product obtained in triglyceride methanolysis for biodiesel production [1]. During this process glycerol is normally generated at a rate of 1 mol of glycerol for every 3 mol of methyl ester synthesized, which accounts for approximately 10 wt% of the total product [1]. It is estimated that by 2015, 1.54 million tons of glycerol will be generated worldwide [2], all of which could be efficiently processed in order to increase the value generated from biodiesel production and to achieve a sustainable industry.

Glycerol has a multifunctional structure and properties that give numerous opportunities for chemical and biochemical conversions to produce value-added chemicals. More detailed information is available in recent review articles [3–8]. Therefore, using glycerol for the synthesis of value-added chemicals is of great industrial

importance, not only because glycerol can be formed in large amounts during the biodiesel process, but also because glycerol is a nontoxic, edible, renewable and biodegradable compound [9,10].

One of the promising route to glycerol valorization is its catalytic dehydration to produce acrolein and hydroxyacetone (acetol), which are important industrial intermediates for the chemical and agrochemical industries [7,8]. The acidity of the active phase is considered as a crucial factor that influences the catalytic performance in this process to produce acrolein [11,12]. Especially Brønsted acid catalysts give high acrolein selectivity [13]. On the other hand, catalysts that showed higher selectivity to acetol possess significant Lewis acidity, but also possess strong basic sites on their surface [14–18]. Direct correlation between selectivity to acetol and catalyst basicity or Lewis acidity has not been found. Therefore, it remains very challenging topic to explain in more detailed way the selective catalytic conversion of glycerol to hydroxyacetone [19].

Calcium phosphates are compounds of significant interest in an interdisciplinary field of sciences involving chemistry, biology, medicine and geology. Hydroxyapatites [HAP; Ca₁₀(PO₄)₆(OH)₂], are the most stable among known calcium phosphates at normal temperatures [20,21]. In the field of catalysis these materials gained

* Corresponding author. Tel.: +33 472445398; fax: +33 472445399.

E-mail address: aline.auroux@ircelyon.univ-lyon1.fr (A. Auroux).

increasing interest in catalysis due to their unusual property of containing both basic and acid sites in a single crystal lattice [22–24]. The stoichiometric form of HAP is presented as $\text{Ca}_{10}(\text{PO}_4)_6(\text{OH})_2$ with Ca/P ratio of 1.67 [25]. The ionic radius of HAP's constituent elements (Ca, P) allows a fair degree of transfer or loss of ions within its crystal structure [26]. Thus HAP is a highly nonstoichiometric calcium phosphate compound with a Ca/P molar ratio ranging from 1.50 to 1.67. It is known that at a Ca/P ratio 1.5, highly crystalline HAP acts as an acid catalyst, while at a Ca/P ratio of 1.67 it acts as a basic catalyst [22,23]. If this ratio is between 1.50 and 1.67 HAPs possess both acid and basic character [22,23]. The ability to finely tune the acidic–basic properties of these materials by changing Ca/P ratio makes them appropriate catalysts for investigation of reactions where the yield and selectivity to desired products is largely governed by the balance between acidic and basic active sites. Furthermore, the properties of hydroxyapatites can be tuned by modification of the $\text{Ca}_{10}(\text{PO}_4)_6(\text{OH})_2$ lattice composition through the numerous possible ionic substitutions [27], on either the Ca cationic position (Ba, Mg, Cd, Sr, etc.), or the ionic sites, PO_4^{3-} (VO_4^{3-} , HPO_4^{2-} , CO_3^{2-}) or OH^- (CO_3^{2-} , F^-). These substitutions influence the thermal stability, textural properties and catalytic activity. Due to all of these appropriate properties calcium phosphate materials have been used as catalysts in various reactions; in dehydration and dehydrogenation [28–30] of alcohols, in oxidation of alkanes [31], and for water gas shift reaction [32], for Knoevenagel condensation [33] and Friedel–Crafts alkylation [34].

In the present work calcium phosphates with different Ca/P ratios have been characterized with respect to their structural, textural and red-ox properties. Acidic/basic features of these materials are thoroughly explored here by microcalorimetry of ammonia and sulfur dioxide adsorption, as well as by FTIR (Fourier Transform Infrared Spectroscopy) of pyridine adsorption. Additionally, in order to investigate the influence of wolframate species on acidic–basic properties and catalytic activity of hydroxyapatites; HAP impregnated with tungsten oxide was also investigated in this work. It is known that the presence of wolframate species on the surface of solid catalysts causes both an increase of the Lewis acidity, almost full disappearance of the surface anions acting as basic sites, and the appearance of a very strong Brønsted acidity [35]. Catalytic behavior of studied materials was tested in the gas phase dehydration of glycerol. Special attention is given to the correlation between catalytic activity and surface acid–base properties, which are essential to the mechanism of the reaction. Understanding the nature of active sites for dehydration reaction could help in development of more efficient solid catalysts for a sustainable use of biomass-derived glycerol by chemical industry.

2. Experimental

2.1. Sample preparation

Hydroxyapatite samples with Ca/P ratios of 1.50 (product reference: nanoXIM.TCP202) and 1.66 (nanoXIM.HAp402) were commercial samples purchased from Fluidinova S.A. They were calcined in air at 450 °C for 5 h before use.

Sample 1.66 HAP was modified by incipient wetness impregnation, at room temperature, with aqueous solutions of calcium acetate and phosphoric acid to form a Ca-rich (Ca/HAP) and a Ca-deficient (P/HAP) calcium phosphates respectively. Subsequently, samples were dried in air at 110 °C overnight, followed by calcination in air at 450 °C.

W/HAP sample was prepared by incipient wetness impregnation, at room temperature, with an aqueous solution of tungstic acid on 1.66 HAP. The sample was dried in air at 110 °C overnight and calcined in air at 450 °C.

2.2. Characterization

Chemical compositions of investigated materials were determined by inductively coupled plasma optical emission spectroscopy (ICP-OES) with an ACTIVA spectrometer from Horiba JOBIN YVON, after they were digested using a mixture of inorganic acids (H_2SO_4 and HNO_3).

Surface areas were determined by low temperature nitrogen adsorption performed at –196 °C, on a Micromeritics 2020 apparatus, after pretreatment performed for 2 h at 300 °C under vacuum. The BET method was used to derive surface areas (S_{BET}) from the resulting isotherms.

The structural characteristics of samples were examined by XRD, Raman and DRIFT (Diffuse Reflectance Infrared Fourier Transform) spectroscopy techniques. XRD patterns were recorded on a Bruker (Siemens) D5005 diffractometer at room temperature using $\text{Cu K}\alpha$ radiation (0.154 nm) from 4 to 70° in 0.02° steps with 1 s per step. Raman spectra were collected under the ambient conditions on a LabRAMHR (Jobin Yvon) spectrometer. The excitation was provided by the 514.5 nm line of an $\text{Ar}^+ \text{Kr}^+$ ion laser (Spectra Physics), keeping the sample under microscope. The power of the incident beam on the sample was 100 μW . Because the laser beam can be precisely focused, it was possible to perform quantitative evaluation of band intensities between the samples studied. The laser beam was focused through microscope objective lenses (100 \times) down to a 1 μm spot on the sample. The acquisition time was adjusted according to the intensity of the Raman scattering. The wavenumber values reported from the spectra are accurate to within 2 cm^{-1} . For each solid, the spectra were recorded at several points of the sample to ascertain the homogeneity of the sample; the averages of these spectra were plotted and presented in this paper. Diffuse reflectance infrared (DRIFT) spectra were collected with a Nicolet 8700 THERMO SCIENTIFIC instrument by co-addition of 100 scans at 2 cm^{-1} resolution. The instrument was equipped with a Praying Mantis accessory (Harrick) and a liquid nitrogen-cooled MCT detector. The samples were diluted in KBr, and a spectrum of KBr was used as a reference.

Surface concentrations of Ca, P and O were determined by means of XPS technique, which was done using KRATOS AXIS Ultra DLD spectrometer equipped with a hemispherical electron analyzer and an Al anode (Al $\text{K}\alpha = 1486.6 \text{ eV}$) powered at 150 W, with a pass energy of 20 eV, and in a hybrid lens mode. The detection area analyzed was 700–300 μm . Charge neutralization was required for all samples. The peaks were referenced to the C–(C, H) components of the C 1s band at 284.6 eV. Shirley background subtraction and peak fitting to theoretical Gaussian–Lorentzian functions were performed using an XPS processing program (vision 2.2.6 KRATOS). The residual pressure in the spectrometer chamber was 5×10^{-9} mbar during data acquisition.

Red-ox properties of investigated samples were revealed by TPR technique using a TPD/R/O-1100 (ThermoFisher) instrument. Prior to the TPR run, the fresh sample was treated in a O_2/He stream (0.998% v/v, with a flow rate of 20 ml min^{-1}), ramping the temperature at 10 °C min^{-1} from room temperature to 350 °C and maintaining it at this temperature for 60 min. Subsequently, sample was cooled down to 40 °C. The TPR measurements were carried out using H_2/Ar (4.98% v/v) as reducing gas mixture, with flow rate of 20 ml min^{-1} . The heating rate was 10 °C min^{-1} from 40 °C to 850 °C. The consumption of H_2 was detected by a thermal conductivity detector (TCD). The TPR peak areas were calibrated with given H_2/Ar (4.98% v/v) mixture injections.

The acid–base properties were studied by adsorption microcalorimetry of NH_3 and SO_2 . Experiments were performed at 150 °C in a heat flow calorimeter (C80 from Setaram) linked to a conventional volumetric apparatus equipped with a Barocel capacitance manometer for pressure measurements. The samples

were pretreated in a quartz cell by heating overnight under vacuum at 300 °C; this temperature was reached using a heating rate of 1 °C min⁻¹. The differential heats of adsorption were measured as a function of coverage by repeatedly sending small doses of respective gas on to the sample until an equilibrium pressure of around 67 Pa was reached. The sample was then outgassed for 30 min at the same temperature, and a second adsorption run was performed at 150 °C on each sample, until an equilibrium pressure of about 27 Pa was attained. The difference between the amounts adsorbed in the first and second adsorptions at 27 Pa represents the irreversibly adsorbed amount (V_{irr}) of a respective gas, which provides an estimation of the number of strong acidic/basic sites.

The nature of acid sites on the surface of investigated solids was determined by FTIR of adsorbed pyridine. Infrared transmission spectra were recorded on self-supporting wafers (2 cm², 8–15 mg) which were placed into an infrared quartz cell (KBr windows) connected to a vacuum line. They were activated under vacuum (10⁻⁴ Pa) by slowly heating (1 K min⁻¹) them up to 723 K and then outgassing them at this temperature for a period of 2 h. Addition of accurately known amount of pyridine (133.3 Pa) into the cell was made by using a calibrated volume of a volumetric line and measuring the pressure inside the IR cell. Spectra were recorded at room temperature after desorption was carried out by evacuation for 30 min at 50, 100, 150, 200, 250 and 300 °C, with a spectral resolution of 4 cm⁻¹. The Nicolet Nexus IR spectrometer equipped with an extended KBr beam splitter and a mercury cadmium telluride (MCT) detector was used to collect spectra. Pyridine (Aldrich, 99+% grade) was dried on molecular sieves prior to use.

2.3. Catalytic reaction

The gas phase dehydration reaction of glycerol was carried out at 350 °C under atmospheric pressure in fixed-bed Pyrex reactor (420 mm length × 8 mm inside diameter). The reaction temperature was monitored by a thermocouple inserted into the middle of the catalyst bed. The catalyst was first crushed and sieved (300–500 μm), then mixed with quartz sand (50–80 mesh) and loaded in the middle of reactor with quartz wool packed in both ends. The catalysts were initially pretreated at 573 K in a flow of nitrogen (30 mL min⁻¹) for 2 h. Glycerol solution (30 wt% in water) was introduced in the flow of nitrogen with help of syringe pump at a flow of 0.48 g h⁻¹. The composition of fed gas was N₂:H₂O:glycerol, equal to 18.7:75:6.3 in vol.%. The catalytic performance of the solid catalysts was evaluated at a gas hourly space velocity (GSHV) of reaction stream of 4400 h⁻¹. The sampling time, after stabilization of temperature at 350 °C, was 90 min. Products were collected after the reactor in a cold trap. The concentrations of reactants and products obtained in the liquid phase (glycerol, acrolein, acetol) were measured by gas chromatography using a flame ionization detector (Column Alltec ECTM-1000 FFAP column 30 m × 0.53 mm × 1.2 μm). Quantification was done by using the external standards. Volatile products running outside the cold trap (CO, CO₂) were analyzed online with a two columns Varian Chrompack micro-GC. The first column, silica plot, allows the CO analysis, while the second column, packed with molecular sieve, allows CO₂ analysis.

3. Results and discussion

3.1. Chemical composition, structure and morphology of the samples

Table 1 presents the list of samples synthesized in this work, their chemical composition, obtained by ICP technique, surface concentrations obtained by XPS technique, and the values of BET

Table 1

Chemical analysis (CA), XPS results and BET surface areas of investigated samples.

Catalyst	S_{BET} (m ² /g)	Ca/P molar ratio		W (wt.%)
		Surface (XPS)	Bulk (CA)	
1.5 HAP	81	1.26	1.50	–
1.66 HAP	69	1.47	1.66	–
Ca/HAP	151	1.67	1.77	–
P/HAP	71	0.93	1.39	–
W/HAP	85	1.49	1.5	15.45

surface areas. It is easy to see that 1.66 HAP possess slightly lower surface area than 1.5 HAP. Impregnation of 1.66 HAP with a solution of phosphoric acid does not change this property, while addition of extra Ca to the structure of this material brings about a significant increase of S_{BET} . Addition of tungsten species to 1.66 HAP leads to a slight increase of surface area.

The results of XPS analysis (Table 1) show that Ca/P ratios found for the surfaces of investigated samples were lower than the bulk ones, with the exception of W/HAP. Similar behavior was noted in previous studies and is generally attributed to the nonstoichiometric composition of hydroxyapatites [36]. Same bulk and surface Ca/P ratios for the W/HAP sample could be attributed to replacement of some phosphate groups with tungsten oxide species on the surface of the catalyst.

X-ray diffractograms of materials investigated in this work are presented in Fig. 1. XRD patterns of 1.5 and 1.66 HAP samples are in good agreement with reported data [30], and confirm that these samples are composed of crystalline HAP, with no other phases. In the Ca/HAP and P/HAP samples the apatite phase is the dominant one. However, additional diffractions are present which could be assigned to possible formation of small amount of brushite (dicalcium phosphate di-hydrate, DCPD) and octa-calcium phosphate (OCP, Ca₈H₂(PO₄)₆5H₂O) phase [37,38]. Diffractograms of W/HAP show the presence of hydroxyapatite as well as crystalline tungsten oxide phases.

Structural properties of materials presented in this work were also investigated by means of vibrational spectroscopy (Raman and FTIR). It is known that complex ionic crystals have two distinct kinds of vibrational modes: external modes, in which well-defined complex ionic groups vibrate as rigid units, and internal modes, which involve atomic vibrations of the complex ionic groups that leave their center of mass stationary [39]. It is reported that the peaks that originate from the internal modes dominate the Raman spectra of calcium phosphate compounds [40].

Raman spectra of investigated oxide systems are presented in Fig. 2. 1.5 HAP and 1.66 HAP display vibrational frequencies that are in agreement with the literature [40]. The bands were observed

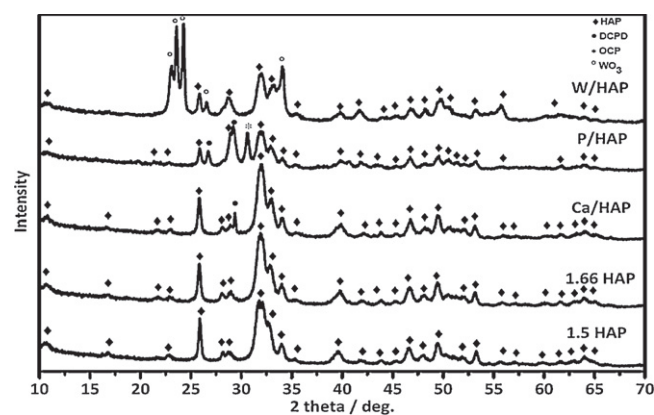


Fig. 1. Wide XRD patterns of investigated materials.

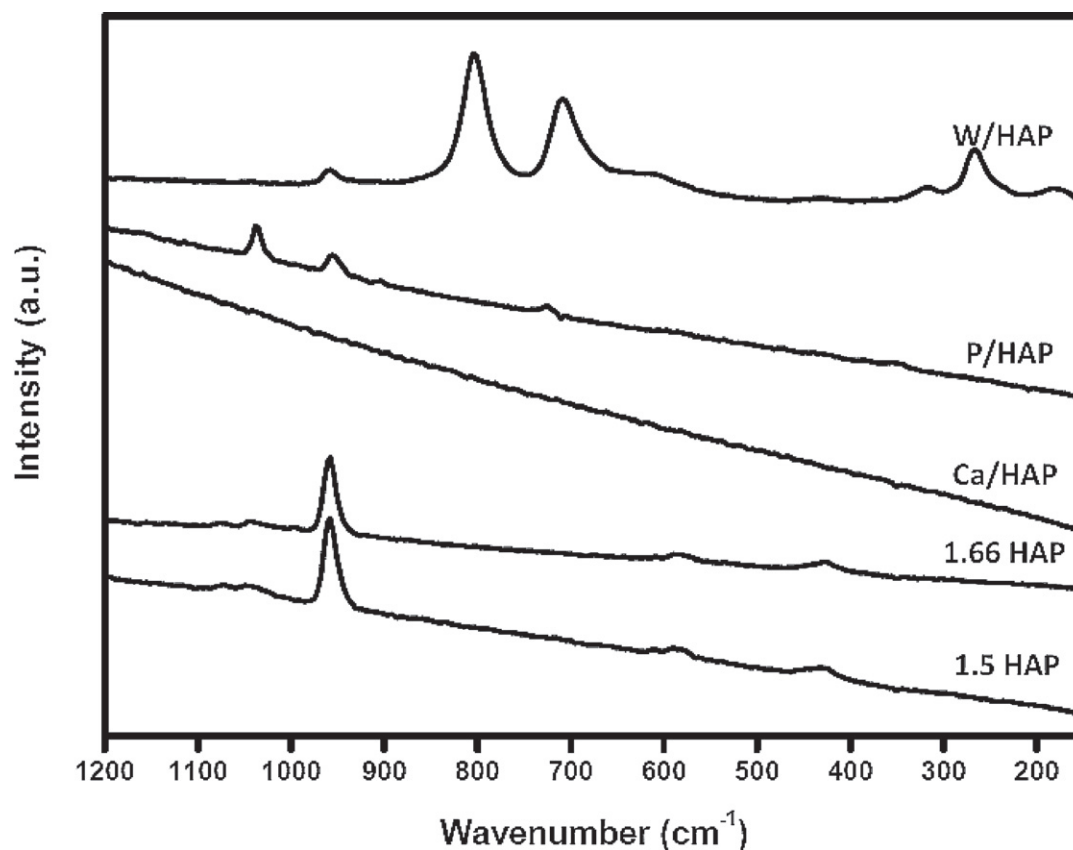


Fig. 2. Raman spectra of investigated materials.

at around 959 cm^{-1} for the symmetric P–O stretching ν_1 , at 1045 and 1075 cm^{-1} for the asymmetric P–O stretching ν_3 , and at two peaks centered at 428 and 583 cm^{-1} for the O–P–O bending modes ν_2 and ν_4 . No Raman band was observed for Ca/HAP sample, most probably due to the strong fluorescence of background. It is known that this effect can disturb the Raman measurements, since the intensity of fluorescence is generally much stronger than that of a non-resonance Raman scattering [41,42]. The spectrum of P/HAP contains bands similar to those observed in the HAP (at 959 , 1045 , 428 and 583 cm^{-1}), as well as band at 360 cm^{-1} assigned to the ν_2 (HPO_4) $^{2-}$ bending mode [40]. The Raman spectrum of W/HAP is dominated by typical features of parent materials. The peak at around 959 cm^{-1} , broad band at 428 cm^{-1} and a shoulder at 609 cm^{-1} have already been described as typical features of hydroxyapatites. On the other hand, the band around 959 cm^{-1} can also be assigned to the W=O stretching mode characteristic of two-dimensional tungsten oxide surface species. The major vibrational modes of WO_3 are located at 808 , 714 , and 276 cm^{-1} and have been assigned to the W–O stretching mode, the W–O bending mode, and the W–O–W deformation mode, respectively [43]. The band at 808 cm^{-1} is considered as the evidence of the presence of crystalline WO_3 species. Furthermore, the absence of any other Raman bands provides additional evidence that WO_3 is not forming any compound with hydroxyapatite. These findings are consistent with XRD measurements.

Fig. 3 compares IR spectra of materials investigated in this work. All spectra possess a weak band at 3690 cm^{-1} , a sharper band at 3572 cm^{-1} , a broad band at $3500\text{--}2500\text{ cm}^{-1}$, several bands around 2000 , 1500 and rich spectrum below 1300 cm^{-1} . The 3572 cm^{-1} band is due to the stretching mode ν_s of terminal OH $^-$ groups and the broad band at $3500\text{--}2500\text{ cm}^{-1}$ to strongly adsorbed and/or bound H_2O respectively [25]. The band at 3690 cm^{-1} can be assigned to stretching vibrations of P–OH generated by the

protonation of surface anions to maintain the surface PO_4^{3-} charge balance of hydroxyapatites. Similarly, in the case of W/HAP sample it could be also attributed to surface W–OH [44]. A group of bands around 1500 cm^{-1} is assignable to CO_3^{2-} vibrations. From Fig. 3 it can be noticed that the intensity of these bands is increasing with increasing the Ca content in samples. The absence of bands around 1500 cm^{-1} in the spectrum of P/HAP sample and low intensity for 1.5 HAP sample indicates that these samples do not contain large quantities of carbonate ions. It is known that in the synthetic calcium phosphates some fractions of PO_4^{2-} as well as OH^- can be replaced by CO_3^{2-} groups. The presence of carbonate in the structure of calcium phosphates influences the decomposition, sinterability, solubility and other properties of these materials [45]. Skeletal vibrations of the lattice phosphate

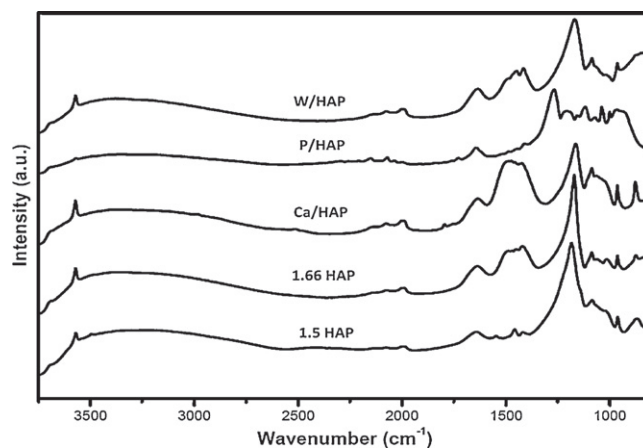


Fig. 3. DRIFT spectra of studied materials.

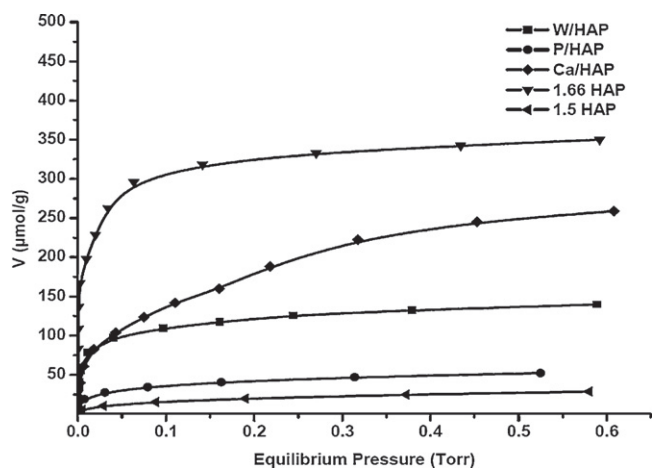


Fig. 4. Volumetric isotherms of SO_2 adsorption on investigated catalysts.

groups give rise to intense and rich spectrum below 1300 cm^{-1} . For 1.5 HAP, 1.66 HAP, Ca/HAP and W/HAP the bands around 870 , 963 , 1022 and 1092 cm^{-1} confirm the presence of monohydrogen phosphate (HPO_4^{2-}), whereas the peak at 1057 cm^{-1} is assigned to the vibrations of phosphate group. The dominant peak in this region centered around 1181 cm^{-1} has been interpreted as a combination band in the literature [46]. It should also be mentioned here that for the W/HAP sample, the vibrations characteristic for tungsten oxide species ($\text{W}=\text{O}$ stretching vibration) are usually found at 1020 cm^{-1} , and at 1400 , 1260 and 1100 cm^{-1} [47]. These bands are assigned to the well crystallized WO_3 phase and overlap with peaks of hydroxyapatite phase; therefore they could not be differentiated. For the P/HAP, the region below 1300 cm^{-1} is more complicated than in the case of other samples investigated in this work. The bands recorded at 960 , 1038 and 1070 cm^{-1} can be assigned to the presence of HPO_4^{2-} ; while the band 1210 cm^{-1} is due to the vibration of the hydrogen atoms belonging to the hydrogen phosphate group ($-\text{O}_3\text{PO}-\text{H}\cdots\text{O}-\text{PO}_3$) [48]. The peaks at 1000 , 1117 and 1270 cm^{-1} could be attributed to formation of small amount of octa-calcium phosphate phase [48]. This finding is in accordance with XRD measurements.

3.2. Acid/base properties

The adsorption of probe molecules was followed by FTIR and calorimetry method in order to investigate the acid–base character. The principles of these two techniques are not the same and obtained information should be considered as complementary, rather than as a basis for comparison of results. FTIR of pyridine adsorption is generally used to differentiate the types of acid sites (Lewis or Brønsted), whereas microcalorimetry measurements of NH_3 or SO_2 adsorption allows precise determination of density and strength distribution of active sites (basic or acidic) present on the catalyst surface.

3.2.1. Microcalorimetry results

Table 2 compiles the data obtained from microcalorimetric measurements of SO_2 and NH_3 adsorption on all investigated samples. The total amounts of adsorbed gases and the amounts of irreversibly adsorbed gases, expressed as a $\mu\text{mol}/\text{m}^2$ and $\mu\text{mol}/\text{g}$, are given in Table 2. All comments concerning the microcalorimetry results refer to $\mu\text{mol}/\text{g}$, and it should be mentioned here that there are slight differences when compared to the results presented in $\mu\text{mol}/\text{m}^2$. Fig. 4 presents the isotherms obtained for SO_2 adsorption on the investigated samples. The vertical parts of the isotherms correspond to irreversible adsorption, whereas the horizontal parts

Table 2
 V_{irrev} and V_{total} calculated from adsorption isotherms of SO_2 and NH_3 on the different materials.

Sample name	SO_2 amount adsorbed		NH_3 amount adsorbed				Ratio of total acidic to total basic sites		Ratio of strong acidic to strong basic sites	
	V_{total}^a ($\mu\text{mol}/\text{g}$)	V_{irrev}^b ($\mu\text{mol}/\text{g}$)	V_{total}^a ($\mu\text{mol}/\text{g}$)	V_{irrev}^b ($\mu\text{mol}/\text{g}$)	V_{total}^a ($\mu\text{mol}/\text{m}^2$)	V_{irrev}^b ($\mu\text{mol}/\text{m}^2$)	V_{total}^a ($\mu\text{mol NH}_3/\text{g}/V_{\text{total}}$ ($\mu\text{mol SO}_2/\text{g}$))	V_{irrev}^b ($\mu\text{mol NH}_3/\text{g}/V_{\text{irrev}}^b$ ($\mu\text{mol SO}_2/\text{g}$))	V_{total}^a ($\mu\text{mol NH}_3/\text{g}/V_{\text{total}}$ ($\mu\text{mol SO}_2/\text{g}$))	V_{irrev}^b ($\mu\text{mol NH}_3/\text{g}/V_{\text{irrev}}^b$ ($\mu\text{mol SO}_2/\text{g}$))
1.5 HAP	17.7	9.5	113.1	47.4	1.4	0.6	6.4	4.9	0.1	0.3
1.66 HAP	315.5	272.4	218.3	40.3	3.2	0.6	0.7	0.1	0.3	0.3
Ca/HAP	166.9	146.4	148.8	48.3	1.0	0.3	0.9	0.3	1.4	1.4
P/HAP	39.0	24.2	127.9	35.1	1.8	0.5	3.3	1.4	1.4	1.4
W/HAP	117.2	96.4	155.9	51.9	1.8	0.6	1.3	0.5	0.5	0.5

^a Amount of NH_3 or SO_2 adsorbed under an equilibrium pressure of 0.2 Torr (27 Pa).

^b Amount of chemisorbed NH_3 or SO_2 under an equilibrium pressure of 0.2 Torr (27 Pa).

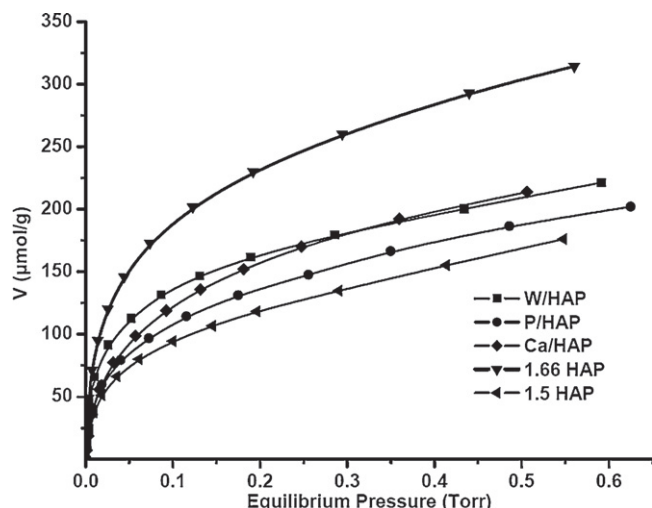


Fig. 5. Volumetric isotherms of NH_3 adsorption on studied materials.

can be assigned to reversible adsorption. It is visible from the results presented in Table 2 and in Fig. 4 that the Ca/P ratio has a decisive role for a basic character of investigated mixed oxides. The lowest adsorbed amount of SO_2 was found for 1.5 HAP, while the highest was observed on 1.66 HAP sample. All three modifications of the starting material (1.66 HAP) lead to a decrease of adsorbed amount of ammonia, especially significant decrease was found on P/HAP material. It is also important to notice that addition of tungsten oxide did not provoke a full disappearance of the surface anions acting as basic sites, what was noted in literature in cases of some other starting materials for preparation of catalysts by impregnation [35]. This would indicate that the wolframate (tungstate) species are not only present on the surface, but also in the bulk of the catalyst. Additionally, the shape of the SO_2 isotherm of the Ca/HAP, which is different when compared to the other isotherms presented in Fig. 4, is indicative of the reaction of sulfur dioxide with the surface of this catalyst.

The volumetric data obtained for NH_3 adsorption is also summarized in Table 2, whereas the isotherms of ammonia adsorption are shown in Fig. 5. Evidently, total amount of adsorbed NH_3 was highest on 1.66 HAP. Surprisingly, 1.5 Ca/HAP adsorbed lower, both total and irreversible, amounts of NH_3 in comparison with 1.66 HAP. However, from the ratio of strong acidic to strong basic sites presented in Table 2 (corresponding to irreversibly adsorbed NH_3 and SO_2 , respectively), it can be concluded that hydroxyapatite 1.5 will act mostly as an acid catalyst, whereas the 1.66 one will act mostly as a basic catalyst. Modification of 1.66 HAP leads to a decrease of V_{total} adsorbed ammonia in all three cases. Furthermore, it is important to notice that V_{irrev} amounts are decreasing in a different way ($\text{W/HAP} > \text{Ca/HAP} > 1.5 \text{ HAP} > 1.66 \text{ HAP} > \text{P/HAP}$), as amount of irreversibly adsorbed ammonia roughly represents the number of strong acid sites.

Fig. 6 displays differential heats of SO_2 (left) and NH_3 (right) adsorption on the investigated samples. The profiles of differential heats vs. uptake of the gas probe are multi-indicative; they provide data concerning the amount, strength, and strength distribution of the active sites. Besides, the values of initial heats of adsorption characterize the strongest sites active for adsorption. Evidently, 1.5 HAP showed prominent acidic character, while all other investigated solids adsorbed both NH_3 and SO_2 , what is a clear indication of their amphoteric character. Profile of differential heat curve for sulfur dioxide adsorption on Ca/HAP indicates, as previously mentioned, that surface reaction is taking place. These results could be assigned to the formation of calcium sulfite or sulfate species. Moreover, it should be emphasized here that titration of basic sites on

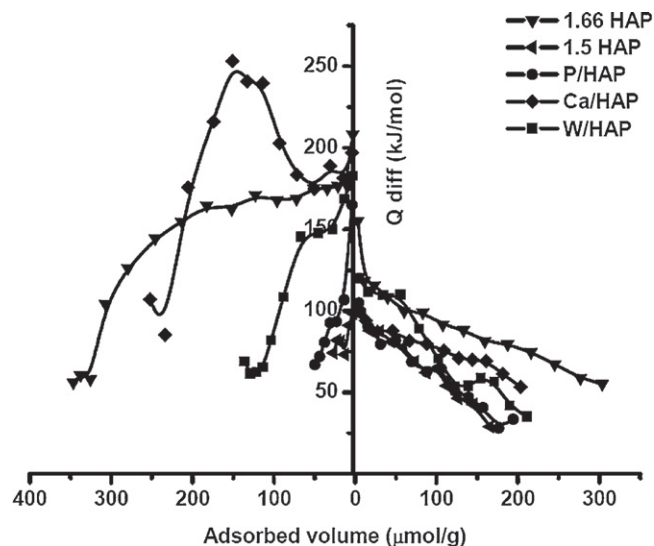


Fig. 6. Differential heats of SO_2 (left) and NH_3 (right) adsorption as a function of surface coverage.

the Ca/HAP sample by CO_2 molecule would also lead to a surface reaction and formation of calcium carbonate species. It is known that sulfur dioxide, as a strong acid, is able to cover all types of basic sites, from strong to weak ones, while carbon dioxide is not able to titrate all basic sites [49]. Additionally, CO_2 is also a soft Lewis base and can be molecularly coordinated in a linear form on the strongest Lewis acid sites present on the surface of solid catalysts [50]. 1.66 HAP material has strongest basic and acid sites on its surface. Changing the Ca/P ratio from 1.66 to 1.5 evidently leads to a decrease in strength of surface acid and basic sites. Moreover, impregnation of 1.66 HAP with calcium acetate, phosphoric acid and tungstic acid gives materials with weaker basic and acidic character.

3.2.2. FTIR of pyridine adsorption

For the potential catalytic applications of solid materials, presence of Brønsted (proton donor OH groups) and Lewis (coordinatively unsaturated metal atoms) acid sites on their surface is of a primary demand. FTIR of adsorbed probe molecules, such as pyridine, is a well established and powerful surface analytical technique for the determination of the nature of surface acid sites.

The relevant parts ($1700\text{--}1400 \text{ cm}^{-1}$) of collected spectra are shown in Fig. 7. All reported spectra were obtained by subtracting the spectrum collected for the fresh catalyst (without pyridine adsorption at room temperature) from those obtained after pyridine adsorption.

Admission of pyridine on the investigated samples gives rise to bands typical for pyridine adsorption positioned at around 1440 , 1490 , 1575 , 1600 and 1627 cm^{-1} . The exception is Ca/HAP catalyst where the existence of band at 1490 cm^{-1} cannot be confirmed due to a strong distortion of spectra. Of these, the peaks at 1440 cm^{-1} (19b vibrational mode) and 1600 cm^{-1} (8a vibrational mode) are characteristic of pyridine coordinated to Lewis acid sites, while the band at 1627 cm^{-1} (v8a) is characteristic of pyridine ions bonded to Brønsted acid sites [51]. The bands around 1490 cm^{-1} (v19a) and 1575 cm^{-1} (v8b) are associated simultaneously to both Brønsted and Lewis acid sites [51]. It should be noted here that absence of the band that is usually found around 1540 cm^{-1} and attributed to Brønsted acid sites [51], is indication that the acidity of these materials is preferentially of a Lewis type. From the relative intensities of the bands at 1627 and 1440 cm^{-1} it is obvious that at elevated evacuation temperatures, pyridine is desorbed preferentially from Brønsted acid sites which completely disappear from the surface of

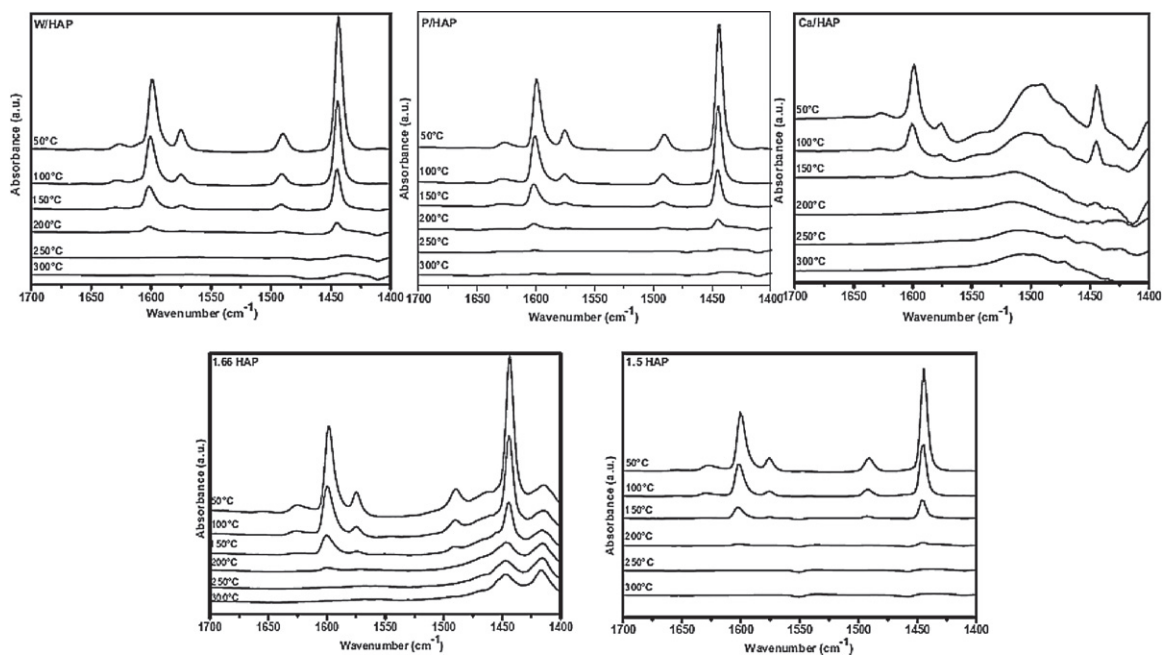


Fig. 7. FTIR spectra of pyridine desorption on investigated materials recorded at different temperatures.

catalysts at 200 °C. Total disappearance of Lewis sites is observed at 250 °C for 1.5 HAP, W/HAP and P/HAP samples, whereas for 1.66 HAP the band at 1440 cm^{-1} is still visible at 300 °C. On Ca/HAP sample pyridine coordinated to Lewis of Brønsted sites is absent from the spectra at 200 °C. From comparison of the relative intensity of the spectra at 50 °C it is evident that 1.66 HAP adsorbed the highest amount of pyridine which shows that it is the most acidic material of the catalysts investigated in this work. Furthermore, it can be said that modification of 1.66 HAP led to a decrease of acidity in all cases, while there is no changes in the nature of acidic sites. These findings are in accordance with adsorption microcalorimetry results.

3.3. Red-ox properties

Normalized TPR spectra of investigated materials are presented in Fig. 8, which shows H_2 consumption (a.u.) as a function of temperature. H_2 consumption of 1.66 HAP ($156 \mu\text{mol H}_2/\text{g}$) showed two maxima at 766 and 825 °C. This red-ox behavior of hydroxyapatites was not mentioned before in the literature, due to the lower temperatures up which TPR was done [32,52]. When parent

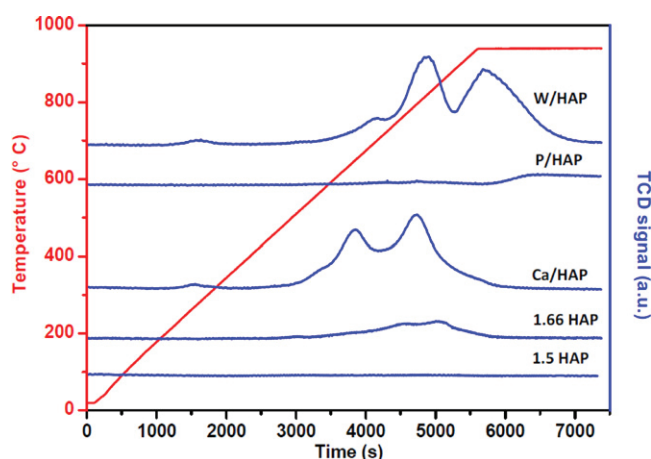


Fig. 8. TPR profiles of investigated materials.

material was modified by calcium acetate (Ca/HAP), the peaks moved to lower temperatures and increased in intensity ($539 \mu\text{mol H}_2/\text{g}$). Opposite behavior was observed for P/HAP; the reducibility was diminished with the addition of phosphorous. In the case of 1.5 HAP no red-ox peaks were observed. The tendency of increasing the reducibility of these materials with increasing the Ca/P ratio is evident.

W/HAP sample showed four peaks in the temperature range of the experiment ($969 \mu\text{mol H}_2/\text{g}$). In accordance with already published data, the peak with a maximum at around 300 °C is due to reduction of polytungstate species [53], while the peaks at 700 °C, 814 °C, and the one that started at 880 °C (without reaching the maximum until 950 °C), can be assigned to crystalline WO_3 species [53]. This red-ox behavior is similar to the red-ox properties of HPW/ ZrO_2 and HPW/ TiO_2 [53]. It should also be mentioned that red-ox peaks of tungstate species are overlapping with the peaks attributed to pure 1.66 HAP, which have significantly lower intensity.

In order to determine which species in the structure of 1.66 HAP and Ca/HAP were reduced during the TPR measurements, XPS analysis was performed on the fresh (before reduction) and on reduced samples. The samples were reduced in H_2 up to 600 °C with a rate of heating equal to $10^\circ\text{C min}^{-1}$.

Fig. 9 shows the O 1s core level spectra for Ca/HAP sample fitted with two components for non reduced sample (Fig. 9a) and with three for the reduced sample (Fig. 9b). The component positioned at 531.1 eV for the fresh sample was attributed to the oxygen bonded to phosphorous in apatite structure [54]. After the reduction, this component is slightly shifted to lower binding energy (530.7 eV) and has a lower contribution to O 1s spectrum. The O 1s photoelectron peak component at 532.6 eV corresponds to the binding energy of hydroxyl groups in Si–OH, P–OH and C–OH bonds [55,56]. Upon reduction this component is shifted to higher binding energy (532.9 eV); its relative contribution in the reduced sample is increased compared to fresh sample. The component at 535.0 eV could be assigned to molecularly bonded water [54].

The O 1s XPS spectra of 1.66 HAP sample (Fig. 10) displays two components for fresh sample: peak at 530.9 eV is assigned to the oxygen bonded to phosphorous in apatite structure, whereas the

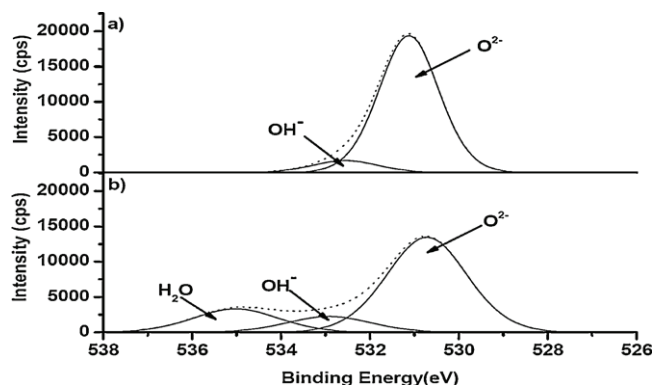


Fig. 9. XPS O 1s spectra of Ca/HAP sample (a) before reduction and (b) after reduction. Dotted lines present overall spectra, while solid lines correspond to specific surface species and have been obtained by deconvolution.

other peak (532.6 eV) corresponds to oxygen in hydroxyl group. Upon reduction, the peak at 532.6 eV disappears, while the O^{2-} peak remains at the same position.

Positions of Ca 2p and P 2p XPS peaks (not presented here) for 1.66 HAP and Ca/HAP samples are recognized in the literature as characteristic for hydroxyapatites [54]. Upon reduction, the spectra of 1.66 HAP remain unchanged, while in the spectra of Ca/HAP new satellite peaks are present at 354.1 eV for Ca 2p and at 135.5 eV for P 2p.

From above presented XPS results, it can be concluded that calcium and phosphorous remain in their starting oxidation states after reduction, with the possible formation of new phase in Ca/HAP sample. From the change in relative contributions of components in O 1s spectra and appearance of new peak upon reduction of Ca/HAP, it can be inferred that during TPR, hydrogen was consumed by O^{2-} from phosphate groups to form OH^- groups; and by hydroxyl groups to form water. In these materials, the charge that is created by excess of calcium, which is in oxidation state of +2, is compen-

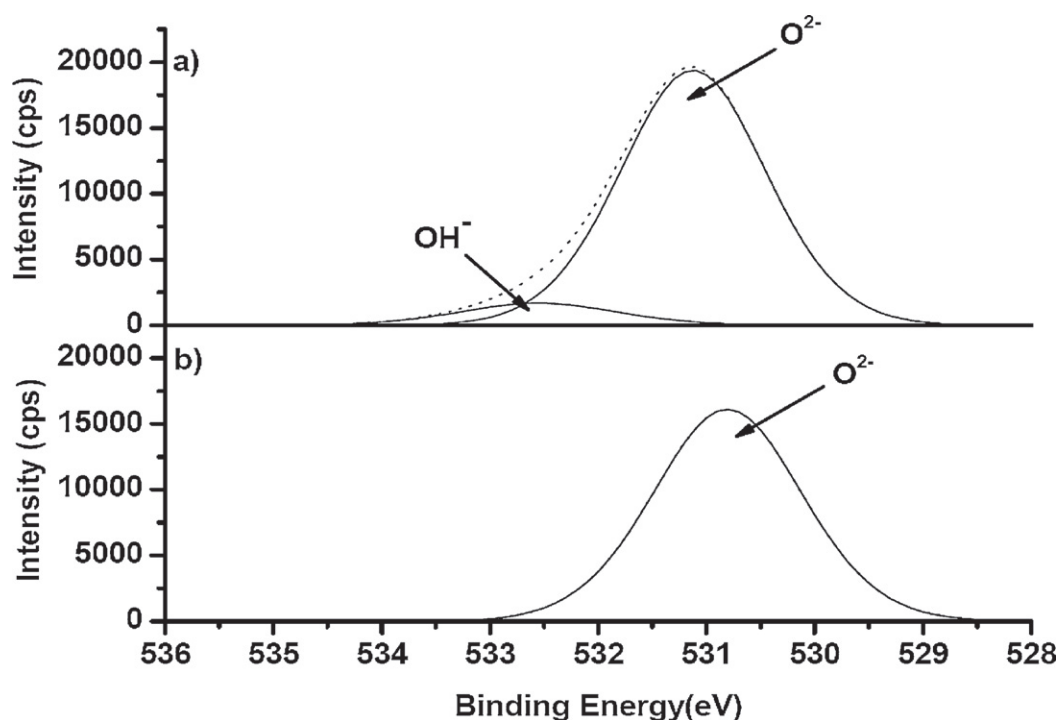


Fig. 10. XPS O 1s spectra of 1.66 HAP sample (a) before reduction and (b) after reduction. Dotted lines present overall spectra, while solid lines correspond to specific surface species and have been obtained by deconvolution.

Table 3

Catalytic performance of investigated catalysts for gas phase dehydration of glycerol at 350 °C.

Catalyst	Conversion (%)	Product selectivity (mol%)				Product yield (mol%)	
		Acrolein	Acetol	CO _x	Others	Acrolein	Acetol
1.5 HAP	63	51	23	<1	26	32	14
1.66 HAP	88	21	29	<1	49	18	25
Ca/HAP	85	9	22	1	69	7	19
P/HAP	97	35	19	<1	46	34	18
W/HAP	100	33	13	<1	54	33	13

sated by OH^- groups. Therefore, there is a tendency in increasing the H_2 consumption with increasing the Ca content.

3.4. Catalytic activity

Gas phase dehydration of glycerol was carried out at 350 °C with a GHSV of 4400 h⁻¹ (GHSV of glycerol 277 h⁻¹). High GHSV shortened the induction period for obtaining the steady acetol and acrolein selectivity and reduced the possibility of acetol conversion into undesired byproducts. The possibility that very different glycerol conversions could make comparison of the selectivity unreliable was examined by Chai et al. [14]. It was shown that after the induction period, the selectivity toward acrolein in glycerol dehydration reaction becomes insensitive to the conversion level of the glycerol reactant. Prior to catalytic testing, blank reaction test was performed at the same temperature without catalyst. The results showed that conversion of glycerol was less than 2%, without any detectable amounts of acetol or acrolein.

The results given in Table 3 show that among the tested catalysts, glycerol is completely converted only on W/HAP sample at the beginning of the reaction. Presented data clearly indicate that the conversion of glycerol decreased in the order W/HAP > P/HAP > 1.66 HAP > Ca/HAP > 1.5 HAP. The low glycerol conversion on 1.5 HAP sample, when compared to other samples, can be explained by the

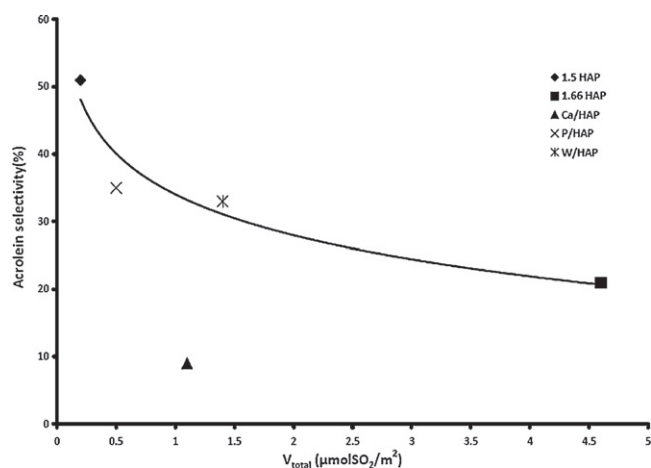


Fig. 11. Selectivity to acrolein as function of density of basic sites.

low total number of active sites on its surface, since glycerol can be converted on acidic as well as on basic sites [14,57]. Moreover, the energy of active sites (expressed as differential heats of SO_2 and NH_3 adsorption as a function of surface coverage, Fig. 6) is the lowest among investigated samples. Additionally TPR revealed that this sample does not possess red-ox centers which may promote catalyst surface clean-up.

Previous work on glycerol dehydration suggests that acrolein is formed on strong Brønsted acid sites [18]; protonation occurs at the central hydroxyl group of glycerol, a water molecule and a proton are eliminated from the protonated glycerol, and then 3-hydroxypropanal is produced by tautomerism, which is unstable and readily dehydrated into acrolein. It is also proposed that on Lewis acid sites protonation proceeds at the terminal hydroxyl group of glycerol and acetol is produced through dehydration and deprotonation accompanied by tautomerism [18]. It should be mentioned here that state of Lewis acid sites is not known under the reaction conditions. Possibility that Brønsted acid sites could be generated by the interaction of the Lewis sites with steam present in the system cannot be neglected [17,18], especially with the huge amount of steam in the reactor. The proposed mechanism of glycerol dehydration which happens on Lewis acid sites implies dehydration as initial step; while the reaction which goes on basic sites starts with a dehydrogenation step. The resulting 2,3-dihydroxypropanal can either further react via consecutive dehydration and hydrogenation to yield acetol, or can form – via a retro-aldol reaction – formaldehyde and hydroxyacetaldehyde, which can be subsequently hydrogenated to ethylene glycol [18]. Another possibility is that, on basic centers, reaction proceeds through dehydration, starting from a terminal hydroxyl group [14–16]. This leads to formation of enol intermediate, which can undergo rapid rearrangement to acetol.

In the case of catalysts investigated in this work, the selectivity to acrolein decreased according to: 1.5 HAP > P/HAP > W/HAP > 1.66 HAP > Ca/HAP. It is evident from Tables 2 and 3 that the catalysts that have the highest number of acid sites did not show highest selectivity toward acrolein. Since these materials contain both acidic and basic sites, the influence of basicity must also be considered. Results presented in Fig. 11 show that the selectivity to produce acrolein is decreasing with increasing number of basic sites on the catalysts surface. Besides, Fig. 12 presents acrolein selectivity as a function of the ratio of acid to basic sites ($V_{total}(\text{NH}_3)/V_{total}(\text{SO}_2)$). This ratio has been calculated for each catalyst from microcalorimetry results by dividing the amount of total adsorbed NH_3 by the amount of total adsorbed SO_2 , and corresponds to a decrease in basicity. As can be observed in Fig. 11, the

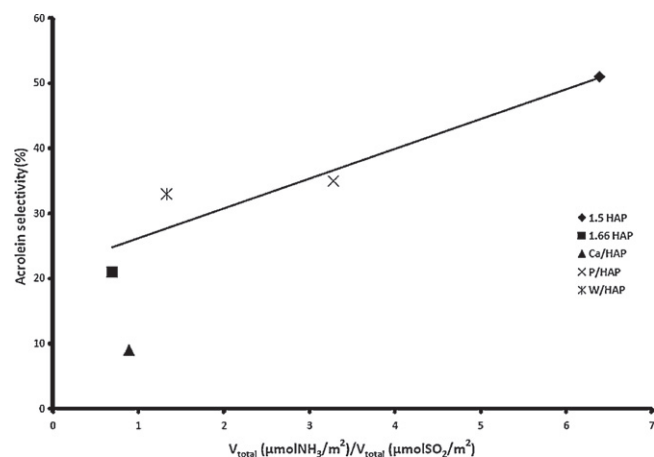


Fig. 12. Selectivity to acrolein as a function of $V_{total}(\mu\text{molNH}_3/\text{m}^2)/V_{total}(\mu\text{molSO}_2/\text{m}^2)$ ratio.

higher this parameter is, the higher the selectivity toward acrolein is. Significant deviation of Ca/HAP sample from both correlations could be provoked by error in determining the number of basic sites due to the reaction with SO_2 during adsorption in microcalorimetry experiments. Another possibility is that its red-ox properties could be the cause of different reaction pathways. Although W/HAP also possesses red-ox features, it is known from the literature that acidic properties of tungsten oxide species are decisive for its chemical reactivity [58].

Since it is not proved that selectivity for acetol formation can be compared in the case of significantly different conversions, contrary to the other product, acrolein (as previously mentioned), the authors find that correlations in the case of acetol are more correct if its amount is presented as a yield instead of selectivity. Results presented in Fig. 13 show that acetol yield is increasing with increasing number of basic centers. Additionally, Fig. 14 presents acetol yield as a function of the ratio of acidic to basic sites ($V_{total}(\text{NH}_3)/V_{total}(\text{SO}_2)$). Contrary to the case of acrolein, the higher this ratio is, the lower the acetol yield is. Aberrations of W/HAP sample from the presented correlations are most probably due to crystalline clusters of WO_3 species, as evidenced by XRD and Raman measurements. These agglomerates can hinder the accessibility to basic sites for glycerol molecules, while these centers remain accessible to small SO_2 molecule.

The results presented in this work indicate that the application of such bifunctional catalysts as investigated here allows the substrate to react with both basic and acidic sites, thus undergoing

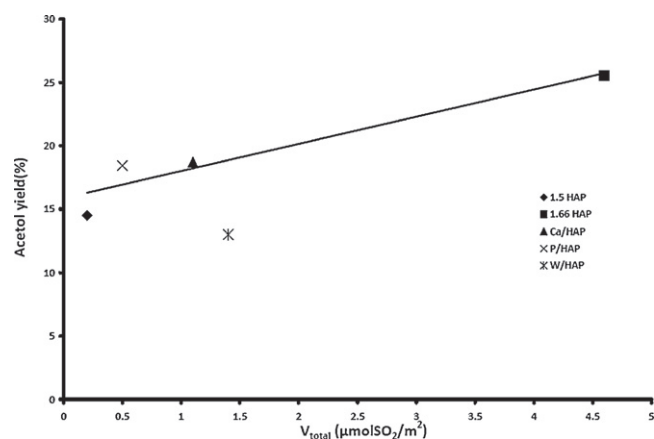


Fig. 13. Acetol yield as function of density of basic sites.

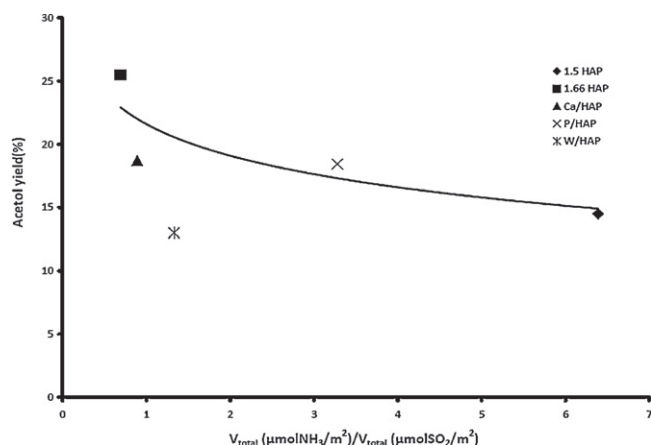


Fig. 14. Acetol yield as a function of $V_{\text{total}} (\mu\text{mol NH}_3/\text{m}^2)/V_{\text{total}} (\mu\text{mol SO}_2/\text{m}^2)$ ratio.

competitive reactions. Furthermore, glycerol can react through a complex reaction network with numerous consecutive and side reactions [59–61]. These reactions lead to formation of coke deposits on the surface of the catalysts, which brings about the deactivation of the catalysts [14]. Generally, it is accepted that acidic sites are responsible for the formation of coke precursors and coke. However, a role of basic sites in catalyzing the formation of heavy compounds that also lead to coke deposits can not be neglected. Secondary products can be formed by retroaldol reaction (probably catalyzed by basic sites) of 3-hydroxypropanal to produce formaldehyde and acetaldehyde [59–61]. Acetalization, catalyzed by acidic sites, may occur to produce glycerol acetals as byproduct [62]. At lower temperatures intermolecular dehydration (acid catalyzed), yielding oligomers of glycerol, is thermodynamically favored over the desired intramolecular dehydration forming acrolein [63] and is triggered by the high concentration of glycerol in the aqueous solution. Furthermore, dehydrogenation and hydrogen transfer reaction (acetone, allyl alcohol...), catalyzed by basic sites, are also possible and therefore may promote the formation of coke [59–61]. Also formation of heavy compounds has been reported. These heavy compounds may form either by direct glycerol transformation (to give linear, cyclic and branched oligomers), or as consecutive transformations from both acrolein and acetol; these heavy compounds, which may also include oxygenated aromatics, such as phenol [11] are precursors for coke formation [64]. Evidently, a larger number of basic sites would increase the possibility of glycerol interaction with them, promote a number of unwanted side reactions, increase the coking of the catalyst and reduce acrolein production, while increasing acetol yield. In addition, it can be suggested that catalytic ability of the selected catalysts to produce acrolein is not controlled only by the surface acidity but also by hindering the number/strength/activity of the basic sites, and thus limiting the side reactions which affect the selectivity of acrolein.

4. Conclusion

Results presented in this work show that the addition of cations: Ca, P or W into the layered structure of hydroxyapatites enables the modification of their features important for catalytic behavior. Ca/P ratio is the directing parameter which crucially determines textural, acid–base and red–ox characteristics, thus giving the possibility to tune the properties of these materials and their modification. The modification of parent 1.66 HAP enabled creation of catalysts which are characterized by more prominent acidity. In addition to already known importance of Ca/P ratio for acid–base features

of these materials, in this work it has been shown that this value influences the red–ox properties, as well.

The obtained results show that the number of basic sites directly affects the dehydration of glycerol and the production of acrolein and acetol. The investigation performed here proved that, in order to get acrolein which is formed on acid sites, it is not only necessary to provide acidity, but also to hinder basic sites. Our results also show that reducing of number and strength of acid centers increases the yield of other desired product, acetol.

Acknowledgments

French National Research Agency (ANR-09-CP2D-19) is greatly acknowledged for financial support. Special thanks are addressed to the technical services of IRCALYON (Institut de Recherches sur la Catalyse et l'Environnement de Lyon) for valuable technical contributions in Raman, XRD, BET, XPS, and chemical analysis.

References

- [1] G.W. Huber, S. Iborra, A. Corma, *Chem. Rev.* 106 (2006) 4044–4098.
- [2] Global Industry Analysts, <http://www.strategyr.com/Glycerin.Market.Report.asp>
- [3] B. Katryniok, S. Paul, V. Bellière-Baca, P. Rey, F. Dumeignil, *Green Chem.* 12 (2010) 2079–2098.
- [4] D.T. Johnson, K.A. Taconi, *AIChE J.* 26 (2007) 338–359.
- [5] C.-H. Zhou, J.N. Beltrami, T.-X. Fan, G.Q. Lu, *Chem. Soc. Rev.* 37 (2008) 527–549.
- [6] B. Katryniok, S. Paul, M. Capron, F. Dumeignil, *ChemSusChem* 2 (2009) 719–730.
- [7] M. Pagliaro, R. Ciriminna, H. Kimura, M. Rossi, C. Della-Pina, *Angew. Chem. Int. Ed.* 46 (2007) 4434–4440.
- [8] Y. Zheng, X. Chen, Y. Shen, *Chem. Rev.* 108 (2008) 5253–5277.
- [9] Z.Z.J. Wang, J. Zhuge, H. Fang, B.A. Prior, *Biotechnol. Adv.* 19 (2001) 201–233.
- [10] J. Chowdury, K. Fouky, *Chem. Eng.* 100 (1993) 35–41.
- [11] J.-L. Dubois, C. Duquenne, W. Hoelderich, J. Kervennal (Arkema), WO 2006087084, 2006.
- [12] J.-L. Dubois, C. Duquenne, W. Hoelderich (Arkema), WO 2006087083, 2006.
- [13] S.-H. Chai, H.-P. Wang, Y. Liang, B.-Q. Xu, *J. Catal.* 250 (2007) 342–349.
- [14] S.-H. Chai, H.-P. Wang, Y. Liang, B.-Q. Xu, *Green Chem.* 9 (2007) 1130–1136.
- [15] D. Stošić, S. Bennici, J.-L. Couturier, J.-L. Dubois, A. Auroux, *Catal. Commun.* 17 (2012) 23–28.
- [16] P. Lauriol-Garbey, G. Postole, S. Loridant, A. Auroux, V. Bellière-Baca, P. Rey, J.M.M. Millet, *Appl. Catal. B: Environ.* 106 (2011) 94–102.
- [17] B. Katryniok, S. Paul, M. Capron, C. Lancelot, V. Bellière-Baca, P. Rey, F. Dumeignil, *Green Chem.* 12 (2010) 1922–1925.
- [18] A. Alhanash, E.F. Kozhevnikova, I.V. Kozhevnikov, *Appl. Catal. A: Gen.* 378 (2010) 11–18.
- [19] C.-W. Chiu, A. Tekeci, W.R. Sutterlin, J.M. Ronco, G.J. Suppes, *AIChE J.* 54 (2008) 2456–2463.
- [20] S. Weiner, L. Addadi, *J. Mater. Chem.* 7 (1997) 689–702.
- [21] S. Weiner, H.D. Wagner, *Annu. Rev. Mater. Sci.* 28 (1998) 271–298.
- [22] J.S. Joris, H.C. Amberg, *J. Phys. Chem.* 75 (1971) 3167.
- [23] S.A.J. Bett, K.W. Hall, *J. Catal.* 10 (1968) 105–113.
- [24] L.C. Kibby, K.W. Hall, *J. Catal.* 29 (1973) 144–159.
- [25] J.C. Elliott, *Structure and Chemistry of the Apatites and Other Calcium Orthophosphates*, Elsevier Science B.V., Amsterdam, 1994.
- [26] R.E. Kreidler, A.F. Hummel, *Am. Mineral.* 55 (1970) 170–184.
- [27] S. Sazalbou, C. Combes, D. Eichert, C. Rey, *J. Mater. Chem.* 14 (2004) 2148–2153.
- [28] C.L. Kibby, W.K. Hall, *J. Catal.* 29 (1973) 144–159.
- [29] H. Monma, *J. Catal.* 75 (1982) 200–203.
- [30] T. Tsuchida, J. Kuboa, T. Yoshioka, S. Sakuma, T. Takeguchi, W. Ueda, *J. Catal.* 259 (2008) 183–189.
- [31] S. Sugiyama, T. Minami, H. Hayashi, M. Tanaka, N. Shigemoto, J.B. Moffat, *J. Chem. Soc. Faraday Trans.* 92 (1996) 293–299.
- [32] A. Venugopal, M.S. Scurrell, *Appl. Catal. A: Gen.* 245 (2003) 137–147.
- [33] S. Sebti, R. Tahir, R. Nazih, A. Saber, S. Boulaajaj, *Appl. Catal. A: Gen.* 228 (2002) 155–159.
- [34] S. Sebti, R. Tahir, R. Nazih, S. Boulaajaj, *Appl. Catal. A: Gen.* 218 (2001) 25–30.
- [35] G. Ramis, G. Busca, V. Lorenzelli, *Stud. Surf. Sci. Catal.* 48 (1989) 777–786.
- [36] M. Yoshinari, Y. Ohtsuka, T. Derand, *Biomaterials* 15 (1994) 529–535.
- [37] H.-C. Hsu, W.-H. Tuan, H.-Y. Lee, *Mater. Sci. Eng. C* 29 (2009) 950–954.
- [38] M.J. Arellano-Jiménez, R. García-García, J. Reyes-Gasga, *J. Phys. Chem. Solids* 70 (2009) 390–395.
- [39] S. Martínez-Ramírez, L. Fernández-Carrasco, in: S.G. Dayle (Ed.), *Construction and Building: Design, Materials and Techniques*, Nova Science Publishers, Inc., New York, 2011, pp. 234–244.
- [40] C.C. Silva, A.S.B. Sombra, *J. Phys. Chem. Solids* 65 (2004) 1031–1033.
- [41] A. Aminzadeh, *Spectrochim. Acta A* 53 (1997) 693–697.
- [42] T. Hasegawa, J. Nishijo, J. Umemura, *Chem. Phys. Lett.* 317 (2000) 642–646.
- [43] E.I. Ross-Medgaard, W.V. Knowles, T. Kim, M.S. Wong, W. Zhou, C.J. Kiely, I.E. Wachs, *J. Catal.* 256 (2008) 108–125.

- [44] S.M. Kanan, Z. Lu, J.K. Cox, G. Bernhardt, C.P. Tripp, *Langmuir* 18 (2002) 1707–1711.
- [45] D. Tadic, F. Peters, M. Epple, *Biomaterials* 23 (2002) 2553–2559.
- [46] C.B. Badiel, E.E. Berry, *Spectrochim. Acta* 22 (1966) 1407–1416.
- [47] M.A. Cortes-Jacome, J.A. Toledo, C. Angeles-Chavez, M. Aguilar, J.A. Wang, *J. Phys. Chem. B* 109 (2005) 22730–22739.
- [48] S. Koutsopoulos, *J. Biomed. Mater. Res.* 62 (2002) 600–612.
- [49] A. Auroux, A. Gervasini, *J. Phys. Chem.* 94 (1990) 6371–6379.
- [50] V. Bolis, G. Magnacca, G. Cerrato, C. Morterra, *Thermochim. Acta* 379 (2001) 147–161.
- [51] E.P. Parry, *J. Catal.* 2 (1963) 371–379.
- [52] P.A. Kumar, M.P. Reddy, L.K. Ju, H.H. Phil, *Catal. Lett.* 126 (2008) 78–83.
- [53] J. Engweiler, J. Harf, A. Baiker, *J. Catal.* 159 (1996) 259–269.
- [54] S. Simon, R. Ciceo-Lucacel, T. Radu, L. Baia, O. Ponta, A. Iepure, V. Simon, *J. Mater. Sci. Mater. Med.* 23 (2012) 1193–1201.
- [55] M. Textor, L. Ruiz, R. Hofer, A. Rossi, K. Feldman, N.D. Spencer, *Langmuir* 16 (2000) 3257–3271.
- [56] G. Zorn, I. Gotman, E.Y. Gutmanas, R. Aladi, G. Salitra, C.N. Sukenik, *Chem. Mater.* 17 (2005) 4218–4226.
- [57] A.K. Kinage, P.P. Upare, P. Kasinathan, Y.K. Hwang, J.-S. Chang, *Catal. Commun.* 11 (2010) 620–623.
- [58] M. Badlani, I.E. Wachs, *Catal. Lett.* 75 (2001) 137–149.
- [59] M.R. Nimols, S.J. Blanksby, X. Qian, M.E. Himmel, D.K. Johnson, *J. Phys. Chem. A* 110 (2006) 6145–6156.
- [60] J.B. Paine III, Y.B. Pithawalla, J.D. Naworal, C.E. Thomas Jr., *J. Anal. Appl. Pyrolysis* 80 (2007) 297–311.
- [61] F. Wang, J.-L. Dubois, W. Ueda, *J. Catal.* 268 (2009) 260–267.
- [62] J. Deleplanque, J.-L. Dubois, J.-F. Devaux, W. Ueda, *Catal. Today* 157 (2010) 351–358.
- [63] A. Ulgen, W. Hoelderich, *Catal. Lett.* 131 (2009) 122–128.
- [64] F. Cavani, S. Guidetti, L. Marinelli, M. Piccinini, E. Ghedini, M. Signoretto, *Appl. Catal. B: Environ.* 100 (2010) 197–204.



CeO₂–Nb₂O₅ mixed oxide catalysts: Preparation, characterization and catalytic activity in fructose dehydration reaction

Dušan Stošić^a, Simona Bennici^a, Vesna Rakić^b, Aline Auroux^{a,*}

^a Université Lyon 1, CNRS, UMR 5256, IRCELYON, Institut de recherches sur la catalyse et l'environnement de Lyon, 2 avenue Albert Einstein, F-69626 Villeurbanne, France

^b Faculty of Agriculture, Department of Chemistry, University of Belgrade, Nemanjina 6, 11080 Zemun, Serbia

ARTICLE INFO

Article history:

Received 5 July 2011

Received in revised form 9 September 2011

Accepted 19 October 2011

Available online 5 December 2011

Keywords:

Ceria–niobia mixed oxide catalysts

Acid/base properties

Adsorption calorimetry

Fructose dehydration

5-Hydroxymethylfurfural

ABSTRACT

In this work, ceria–niobia mixed oxides have been prepared by coprecipitation. The structural, textural, and surface properties of these materials have been fully characterized using appropriate techniques (low-temperature adsorption–desorption of nitrogen, thermogravimetric analysis, X-ray diffraction analysis (XRD), X-ray photoelectron spectroscopy (XPS), Raman spectroscopy and temperature-programmed reduction/oxidation (TPR/O)). The acid–base properties were estimated by the adsorption of appropriate probe molecules – NH₃ or SO₂ were used to estimate the population, strength and strength distribution of acid or basic sites, by means of adsorption microcalorimetry. The nature of acidic sites was determined through the adsorption/desorption of pyridine, studied by infrared spectroscopy. New phases between the oxides were not formed, while there is evidence of interaction between them, as revealed by XRD and Raman spectroscopy. All investigated mixed oxide samples are amphoteric and possess red-ox centers on their surface. Both red-ox and acid–base properties are dependent on the ratio of ceria to niobia in the samples. Both Lewis and Brønsted acid sites are present on the surface of the mixed oxides. In order to check catalytic abilities of these materials, reaction of fructose dehydration has been performed. All the investigated materials are catalytically active in fructose dehydration; conversion of fructose and selectivity to 5-hydroxymethylfurfural (5-HMF) improved with increasing content of niobia in the samples.

© 2011 Elsevier B.V. All rights reserved.

1. Introduction

Ceria and niobia are important catalytic materials that are used in numerous catalytic processes. Ceria is included in materials used in automotive emissions control as an active component of three-way catalysts [1–8], in fuel cell processes as a part of electrode or as a part of a composite electrolyte film [9–12], in oxygen permeation membrane systems [13–16], and in fluid catalytic cracking processes as a promoter [4]. It is also used in several groups of industrially important catalytic processes: oxidation of different hydrocarbons [1,4,17,18], wet oxidation processes of organic compounds [4,19,20], photo-catalytic degradation of phenolic compounds [21], removal of total organic carbon from wastewaters [19,20] and removal of heavy metals from drinking water [22], automotive exhaust gas conversion [2–4], water–gas shift reaction [23,24], methane reforming with CO₂ [25–29], SO₂ reduction with CO [5], and deNO_x catalysis [30–33]. These applications are based on a number of appropriate properties that ceria expresses which are all characteristic of fluorite type structures:

chemical and physical stability, high oxygen vacancy concentration and high oxygen mobility. Cerium can cycle easily between reduced and oxidized states (Ce³⁺ ↔ Ce⁴⁺), which permits the reversible addition and removal of O₂ from CeO₂ [1–4,8], this feature being crucial for the application of this material in the domain of catalysis. However, catalytic activity of pure ceria may be affected by some of its properties: at elevated temperatures, the catalytic efficiency of ceria may be reduced as a consequence of sintering and loss of surface area [34]; sintering also causes a loss of oxygen storing capacity.

The unique properties of compounds containing niobia have led to catalytic applications in various reactions [35,36]. Hydrated niobium oxide (Nb₂O₅·*n*H₂O; niobic acid) possesses both Lewis acid sites and relatively strong Brønsted acid sites on its surface [37]. On the other hand, niobia and its mixed oxides have very interesting properties acting as supports and promoters [38,39] for catalytically active phase. Bulk niobia or niobia containing catalysts are used in various processes such as fructose dehydration reaction [40–43], selective oxidation of hydrocarbons [44–47], hydrogenation and dehydrogenation [48–51], hydrocarbon conversion [52], photocatalysis [53,54] and polymerization processes [55]. Among these heterogeneous reactions, those in which water participates as a reactant, product or solvent, are of particular importance. In

* Corresponding author. Fax: +33 472445399.

E-mail address: aline.auroux@ircelyon.univ-lyon1.fr (A. Auroux).

fact, only very few solids offer the required activity, stability and insolubility to properly catalyze reactions in aqueous media [56]. This feature makes niobia-based materials attractive for industrial use, and is very important for the establishment of less expensive and environmentally clean processes.

From all above mentioned properties of cerium and niobium oxides, it can be assumed that ceria–niobia mixed oxides could be interesting materials in the field of so-called green catalysis. Mixing the oxides results in formation of new materials with modified physical and chemical features and different catalytic properties in comparison with parent materials. Importantly, this approach offers also a possibility of adjusting these properties by changing the relative amounts of one component to another. However, in order to get mixed oxides as competitive catalysts, it is required to apply a preparation method that is easy to handle and results in materials with high surface area, good dispersion and homogeneous distribution in the bulk. Among the other known techniques, such as hydrothermal and surfactant-templated synthesis [57], sol–gel [58], and ultrasound irradiation [59]; coprecipitation is still the most straightforward method known to provide the above mentioned required features [4,60–62].

In this work, cerium–niobium mixed oxides have been prepared by coprecipitation. Having in mind that catalytic functions of solid materials are governed by their surface features, in order to predict their activity and selectivity in various reactions, we fully characterized the synthesized samples with respect to their structural, textural, acid–base, and red-ox properties. Their catalytic behavior was tested in the reaction of fructose dehydration; reaction of great environmental importance, which yields to 5-hydroxymethylfurfural (5-HMF), compound recognized as a bio-refining intermediate for the production of alternative fuels [63].

2. Experimental

2.1. Sample preparation

In this work ceria–niobia mixed oxides with a wide range of niobia content were prepared by coprecipitation from ammonium–niobium oxalate complex (99.99%, Aldrich) and cerium nitrate (99.9%, Strem Chemicals) aqueous solutions. The requested quantities of these precursors were dissolved in deionized water at room temperature. The solutions were mixed with continuous monitoring of pH. Ammonia solution (16 wt.%) was added gradually dropwise to the mixture of two solutions with vigorous stirring, until precipitation was completed (pH = 9). Pure ceria was obtained by precipitation from pure solution of cerium nitrate by ammonia in the same way. All the precipitates were then filtered and washed with hot distilled water (0.5 L), dried overnight in an oven at 110–120 °C and calcined in air at 400 °C for 10 h. The calcination temperature has been chosen on the basis of thermogravimetric measurements. Nb₂O₅ was purchased from H.C. Starck company and calcined at the same temperature.

2.2. Characterization

Chemical compositions of prepared materials (the contents of metals and metal oxides) were determined by inductively coupled plasma–optical emission spectroscopy (ICP–OES) with an ACTIVA spectrometer from Horiba JOBIN YVON, after they were digested using a mixture of inorganic acids (H₂SO₄ and HNO₃).

After the preparation, crude samples were calcined, with the intention of decomposing the nitrates and removing the water and impurities from the bulk. Thermogravimetry (TG–dTG, performed on a “Labsys-TG” instrument from Setaram) was used in order to determine the lowest temperature needed for calcination of fresh

samples, at which no significant loss of mass occurred with further increase of temperature. The crude samples (~50 mg) were heated from 25 °C to 800 °C with a heating rate of 5 °C min⁻¹ in a flow of air, which was chosen as a soft oxidizing agent for calcination.

Surface areas were determined by low temperature nitrogen adsorption performed at –196 °C, on a Micromeritics 2020 apparatus, after pretreatment performed for 2 h at 300 °C under vacuum. The BET method was used to derive surface areas from the resulting isotherms.

The structural characteristics of samples were examined by XRD and Raman spectroscopy techniques. XRD patterns were recorded on a Bruker (Siemens) D5005 diffractometer at a room temperature using Cu K α radiation (0.154 nm) from 4° to 70° in 0.02° steps with 1 s per step. Raman spectra were collected under the ambient conditions on a LabRAMHR (Jobin Yvon) spectrometer. The excitation was provided by the 514.5 nm line of an Ar⁺ Kr⁺ ion laser (Spectra Physics), keeping the sample under microscope. The power of the incident beam on the sample was 100 μ W. Because the laser beam can be precisely focused, it was possible to perform quantitative evaluation of band intensities between the samples studied. The laser beam was focused through microscope objective lenses (100 \times) down to a 1 μ m spot on the sample. The acquisition time was adjusted according to the intensity of the Raman scattering. The wavenumber values reported from the spectra are accurate to within 2 cm⁻¹. For each solid, the spectra were recorded at several points of the sample to ascertain the homogeneity of the sample; the averages of these spectra were plotted and presented in this paper.

Surface concentrations of Nb, Ce and O were determined by means of XPS technique, which was done using KRATOS AXIS Ultra DLD spectrometer equipped with a hemispherical electron analyzer and an Al anode (Al K α = 1486.6 eV) powered at 150 W, a pass energy of 20 eV, and a hybrid lens mode. The detection area analyzed was 700–300 μ m. Charge neutralization was required for all samples. The peaks were referenced to the C–(C, H) components of the C 1s band at 284.6 eV. Shirley background subtraction and peak fitting to theoretical Gaussian–Lorentzian functions were performed using an XPS processing program (vision 2.2.6 KRATOS). The residual pressure in the spectrometer chamber was 5 \times 10⁻⁹ mbar during data acquisition.

Redox properties of investigated samples were revealed by TPR (temperature programmed reduction) technique using a TPD/R/O-1100 (ThermoFisher) instrument. Prior to the TPR run, the fresh sample was treated in a O₂/He stream (0.998%, v/v, with a flow rate of 20 ml min⁻¹), ramping the temperature at 10 °C min⁻¹ from room temperature to 850 °C and maintaining it at this temperature for 60 min. Subsequently, sample was cooled down to 40 °C. The TPR measurements were carried out using H₂/Ar (4.98%, v/v) as reducing gas mixture, with flow rate of 20 ml min⁻¹. The heating rate was 10 °C min⁻¹ from 40 °C to 850 °C. The consumption of H₂ was detected by a thermal conductivity detector (TCD). The TPR peak areas were calibrated with given H₂/Ar (4.98%, v/v) mixture injections.

The acid–base properties were studied by adsorption microcalorimetry of NH₃ and SO₂. Experiments were performed at 150 °C in a heat flow calorimeter (C80 from Setaram) linked to a conventional volumetric apparatus equipped with a Barocel capacitance manometer for pressure measurements. The samples were pretreated in a quartz cell by heating overnight under vacuum at 300 °C; this temperature was reached using a heating rate of 1 °C min⁻¹. The differential heats of adsorption were measured as a function of coverage by repeatedly sending small doses of respective gas on to the sample until an equilibrium pressure of around 67 Pa was reached. The sample was then outgassed for 30 min at the same temperature, and a second adsorption run was performed at 150 °C on each sample, until an equilibrium pressure

Table 1
Chemical analysis, XPS results and BET surface areas of investigated samples.

Sample	S_{BET} (m ² /g)	CA %					XPS
		Nb (wt.%)	Ce (wt.%)	Nb ₂ O ₅ (wt.%)	CeO ₂ (wt.%)	Ce/Nb (wt.% ratio)	Ce/Nb (wt.% ratio)
CeO ₂	88	–	–	–	–	–	–
75% CeO ₂ –25% Nb ₂ O ₅	99	13.7	59.5	19.6	72.9	4.3	1
50% CeO ₂ –50% Nb ₂ O ₅	79	29.2	42.8	52.6	41.8	1.5	0.4
25% CeO ₂ –75% Nb ₂ O ₅	41	47.4	22.0	67.8	27.1	0.5	0.2
Nb ₂ O ₅	93	–	–	–	–	–	–

of about 27 Pa was attained. The difference between the amounts adsorbed in the first and second adsorptions at 27 Pa represents the irreversibly adsorbed amount (V_{irr}) of a respective gas, which provides an estimation of the number of strong acidic/basic sites.

The nature of acid sites on the surface of investigated solids was determined by FTIR of adsorbed pyridine. Infrared spectra were recorded, in the 4000–400 cm⁻¹ spectral range, with a resolution of 2 cm⁻¹, using a Bruker Vector 22 FT-IR spectrophotometer equipped with DTGS detector, collections of 100 scans were recorded. The self-supporting wafer (30–50 mg of catalyst, 18 mm diameter) was first activated in situ at 300 °C in oxygen flow for 14 h, subsequently evacuated at the same temperature for 2 h and then exposed to pyridine (Air Liquide, 99.8%, vapor pressure 3.3 kPa) at room temperature for 5 min. The desorption was carried out by evacuation for 30 min each at room temperature, 100 °C, 200 °C and 300 °C. The IR spectra were recorded at room temperature after desorption at each temperature.

2.3. Catalytic reaction

The catalytic abilities of investigated materials were probed through fructose dehydration reaction. The batch catalytic experiments were performed in a 100 ml stainless steel autoclave, at 130 °C. In a typical procedure, 600 mg of fructose was dissolved in 60 ml of water and then 80 mg of solid catalyst was added. Water was chosen as a green and appropriate solvent for dehydration of fructose to 5-HMF. Starting time of the reaction was taken when the reaction mixture reached 130 °C. Time needed to reach this temperature was 30 min. Samples were withdrawn from the reaction mixtures at 1 h intervals; the changes of fructose, 5-HMF, levulinic acid (LA) and formic acid (FA) concentrations with time were followed by collecting ¹H NMR spectra, using liquid NMR technique (Bruker AVANCE 250 spectrometer equipped with a multinuclear 10 mm Probe). After the reaction, solids were separated from reaction solution by simple decantation, washed 3–4 times with deionized water and dried at 60 °C for 12 h. Catalytic activities of previously used catalysts were probed in repeated reaction. Reactant conversion (mol %), and product selectivity (%) were defined as follows:

$$\text{Conversion (mol\%)} = \frac{\text{moles of } x \text{ reacted}}{\text{moles of } x \text{ initial}} \times 100\%$$

$$\text{Selectivity (\%)} = \frac{\text{moles of } y \text{ produced}}{\text{moles of } x \text{ reacted}} \times 100\%$$

3. Results and discussion

3.1. Chemical composition, structure and morphology of the samples

Table 1 presents the list of samples synthesized in this work, their chemical composition, obtained by ICP technique, surface concentrations obtained by XPS technique, and the values of BET surface areas. It can be seen that adding a small amount of niobia at

first increases the surface areas of mixed oxides; while with further increase of the niobia content surface areas of mixed oxides become lower. It appears that the surface areas of materials containing Nb₂O₅ as a major component are very sensitive to the final calcination temperature; this behavior was also noted in other cases where niobia was used in mixed oxide formulations [64–66].

XR diffractograms of pure and mixed oxides investigated in this work are presented in Fig. 1. It is visible that in the case of ceria, only the diffraction lines of fluorite structure of CeO₂ are visible, with no evidence of Ce₂O₃ patterns, while formation of hexagonal structure is observed in the case of niobia. The XRD patterns of mixed oxide samples show only the diffraction peaks of already mentioned fluorite structure of CeO₂. This is in accordance with the data that have already been reported in the literature for the case of ceria mixed with silica, titania, zirconia, or with group III metal oxides [67,68]. From comparison of the diffractograms assigned to pure Nb₂O₅ and to mixed oxides it can be inferred that in the case of mixed oxides the crystallinity of niobia is influenced by its interactions with ceria, since the resulting structure of Nb₂O₅ is different upon sample calcination at the same temperature. A similar behavior was noted for SiO₂–Nb₂O₅ mixed oxides, where it has been found that silica inhibits the crystallization of niobia after a heat treatment at 500 °C for 2 h [37].

Generally it can be said that the poor crystallinity is characteristic for all mixed oxides investigated here. Importantly, the intensities of XR diffraction lines specific to CeO₂ found for mixed oxides samples are lower in comparison with those found for pure ceria; the peak intensities are becoming lower with increasing the relative amount of niobia. It is also important to notice that the recorded XRD patterns showed no evidence of compounds or mixed phases formed between ceria and niobia.

Raman spectra of investigated oxide systems are reported in Fig. 2. The spectrum of pure niobia is dominated by a broad band at 690 cm⁻¹, which is typical for all niobium oxides and is assigned to

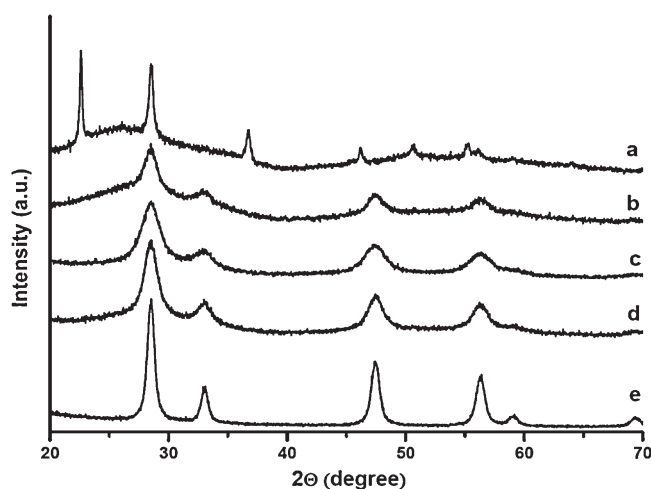


Fig. 1. Wide angle XRD patterns of (a) Nb₂O₅, (b) 75% Nb₂O₅/25% CeO₂, (c) 50% Nb₂O₅/50% CeO₂, (d) 25% Nb₂O₅/75% CeO₂, and (e) CeO₂.

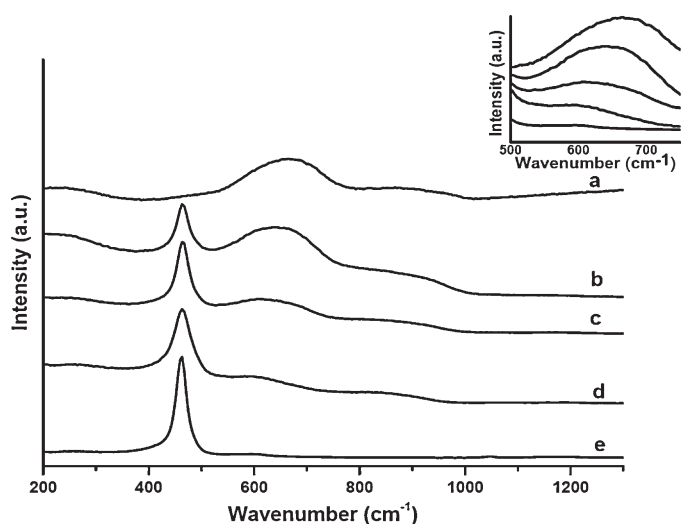


Fig. 2. Raman spectra of (a) Nb₂O₅, (b) 75% Nb₂O₅/25% CeO₂, (c) 50% Nb₂O₅/50% CeO₂, (d) 25% Nb₂O₅/75% CeO₂, and (e) CeO₂.

the vibrations of Nb–O–Nb bridges from slightly distorted octahedral NbO₆ connected with sharing corners [69,70]. The weak band around 850 cm⁻¹ can be assigned to the symmetric stretching mode of Nb=O surface species, this kind of bond being present in highly distorted octahedral NbO₆ structures. Raman band between 150 and 300 cm⁻¹ is due to the bending modes of Nb–O–Nb linkages [69,71].

The Raman spectrum of pure CeO₂ is also shown in Fig. 2. This spectrum exhibits peaks at 270, 464 and 600 cm⁻¹. The sharp peak at 464 cm⁻¹ is assigned to F_{2g} mode due to symmetrical stretching of Ce–O vibrational unit in eightfold coordination [67]. The presence of two other peaks might be due to perturbations of the fluorite structure; in fact it is known from the literature that a band recorded at 600 cm⁻¹ is associated with oxygen vacancies in the CeO_{2-x} lattice, and that these sites might be active in combustion reactions [67,72]. Therefore, it is important to notice that this band in mixed oxide samples is masked by the more intensive vibration of Nb₂O₅ in the same region, and its existence cannot be confirmed.

Evidently, the spectra of mixed oxide samples are dominated by the typical features of parent materials. Furthermore, the absence of any other Raman bands provides additional evidence that Nb₂O₅ is not forming any compound with cerium oxide, which is consistent with XRD measurements. For each sample, the spectra were recorded at several points and no shift in the band position or difference of width was noted. This observation shows clearly that CeO₂–Nb₂O₅ samples are homogeneous. It should also be mentioned that broad bands, found for Nb₂O₅ prepared in this work, are characteristic of Raman scattering from amorphous materials [73]. The intensity of the peak at 464 cm⁻¹, assigned to CeO₂ phases, decreases upon decreasing the amount of ceria in the sample. The shift and intensity changes of the Raman band at 690 cm⁻¹, associated with vibrations of Nb–O–Nb bridges, suggest that the structures of the niobium oxide species are dependent on the relative concentration of the two component oxides.

XPS technique was used to obtain a better understanding of chemical states for all elements on the surface, additionally to determination of their concentration. The electron binding energies (BE (eV)) of the photoelectron peaks pertaining to O 1s, Nb 3d and Ce 3d together with the corresponding atomic percentages are shown in Table 2.

The XPS spectra of Ce 3d core electron levels for mixed oxides samples are given in Fig. 3. There are six peaks corresponding to the three pairs of spin–orbit doublets of oxidized CeO₂ [1] and two

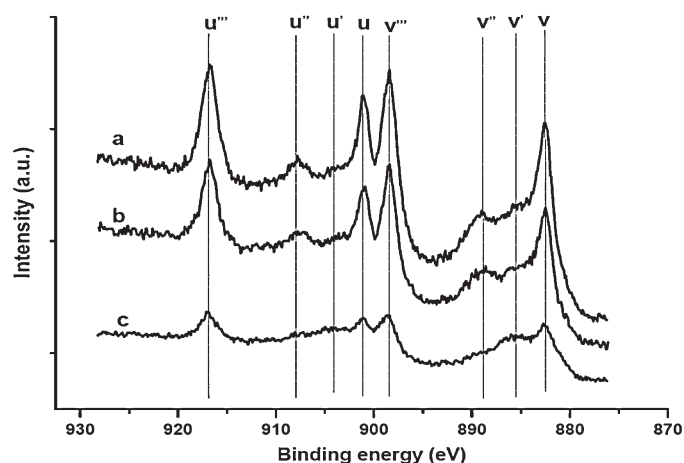


Fig. 3. Ce 3d XPS spectra of (a) 25% Nb₂O₅/75% CeO₂, (b) 50% Nb₂O₅/50% CeO₂, and (c) 75% Nb₂O₅/25% CeO₂.

peaks corresponding to the doublet of oxidized Ce₂O₃. The intensities of all peaks decrease with decreasing the ceria content. For each doublet, 3d_{5/2} corresponds to the label v and 3d_{3/2} to u. Explanation of the origin of each doublet is given in details in the work of Reddy et al. [67]. The peaks labelled v/u, v''/u'', v'''/u''' have been assigned to Ce⁴⁺ and v'/u' to Ce³⁺. The main band of Ce3d_{5/2} at 882.6 eV (v) corresponds to Ce⁴⁺, while the band at 885.4 eV (v') corresponds to Ce³⁺; these bands were observed for all samples (Fig. 3).

As XRD could not detect any visible Ce₂O₃ diffraction lines, its concentration in the samples has to be lower than that detectable by this technique. At the surface, cerium is mainly present in the Ce⁴⁺ oxidation state (from XPS, it is present up to 70–80 at.%). The presence of Ce (III) can be mainly attributed to removal of surface hydroxyl groups and oxygen from CeO₂ surface during exposure of the samples to the X-ray in an ultrahigh vacuum chamber what presents mild reduction conditions [74]. This phenomenon is confirmed by an increase in the intensity of the components corresponding to Ce (III) with the irradiation time of the sample.

Fig. 4 shows the Nb 3d XPS spectra for mixed oxides samples. All of them produce a single symmetric 3d_{5/2} component which, on the basis of its BE, can be assigned to Nb⁵⁺ [73], with no evidence for the presence of Nb⁴⁺. The 3d_{5/2} BE values are around 206.8 eV (Table 2), and remain practically unchanged with changes of the niobium content, while it is known from the literature that BE for bulk Nb₂O₅ is at 207.5 eV [75]. This shift could be attributed to an

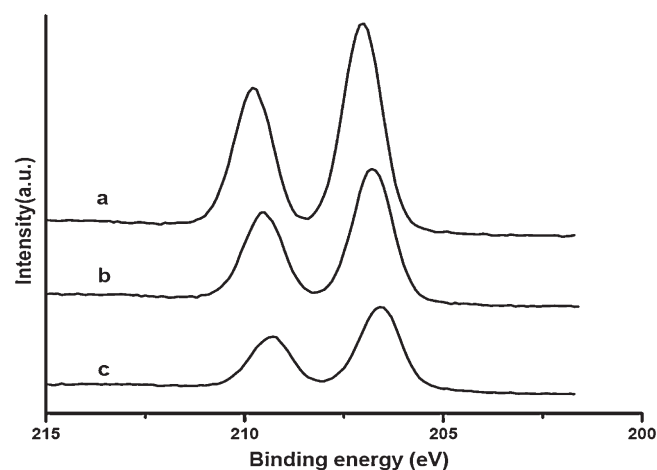


Fig. 4. Nb 3d XPS spectra of (a) 75% Nb₂O₅/25% CeO₂, (b) 50% Nb₂O₅/50% CeO₂, and (c) 25% Nb₂O₅/75% CeO₂.

Table 2
XPS data for mixed oxide samples.

Sample	Ce 3d _{5/2}		Nb 3d _{5/2}		O1s							
	at.%	BE (eV)	at.%	BE (eV)	Nb–O		Ce–O		O–H		O _{chemisorbed}	
					at.%	BE (eV)	at.%	BE (eV)	at.%	BE (eV)	at.%	BE (eV)
75% CeO ₂ –25% Nb ₂ O ₅	20.84	882.5	11.76	206.6	12.80	530.1	39.08	529.5	5.39	532.1	10.10	531.2
50% CeO ₂ –50% Nb ₂ O ₅	13.60	882.6	17.11	206.8	27.72	530.1	30.48	529.5	4.15	532.1	6.92	531.2
25% CeO ₂ –75% Nb ₂ O ₅	6.14	882.6	23.54	207.0	44.29	530.2	14.06	529.6	4.92	532.2	7.03	531.2

atomic dispersion of niobium on the surface of the samples and/or to a change of coordination number of niobium, which would be indicative of some interaction between Nb and Ce atoms in the oxides.

As shown in Fig. 5, O 1s peak is broad and complicated which could be a consequence of the non-equivalence of the surface oxygen ions. It is important to notice that the O 1s BE peaks do not change their positions with the different compositions of the Nb₂O₅–CeO₂ system. As reported in the literature [76], the oxygen ions in pure CeO₂ exhibit intense peaks at 528.0, 528.8, 529.0 and 530.1 eV while the oxygen ions in pure Nb₂O₅ show intense peaks at 530.0 and 533.0 eV [77]. The observation of the peak shape in Fig. 5 suggests that the O 1s spectrum is composed of more than one peak arising from the overlapping contributions of oxygen in different chemical states. The peaks at 529.5 and 530.1 eV are ascribed to oxide ions (lattice oxygen) from ceria and niobia, respectively. The bands at 531.2 eV and 532.1 eV are assigned to chemisorbed oxygen and to the oxygen from hydroxyl groups, respectively.

Surface Ce/Nb ratios are obtained from the quantitative XPS results (Table 1). The difference between surface and bulk ratios clearly shows the relative enrichment in Nb of surfaces of mixed oxides samples. Furthermore, it is interesting to note that the amount of surface oxygen in the mixed oxides increases upon increasing the niobia content. The possibility of the presence of Ce³⁺ which favours the formation of oxygen vacancies in the mixed oxide surface cannot be ignored [78]. It can be speculated that chemical pumping effect causes oxygen to diffuse up to the surface, reaching the vacant sites. As discussed in the literature [79], the reduction of ceria is presumably controlled by the nature of the oxygen vacancies, since oxygen diffusion, the rate-controlling step, depends on the type, size and concentration of oxygen vacancies.

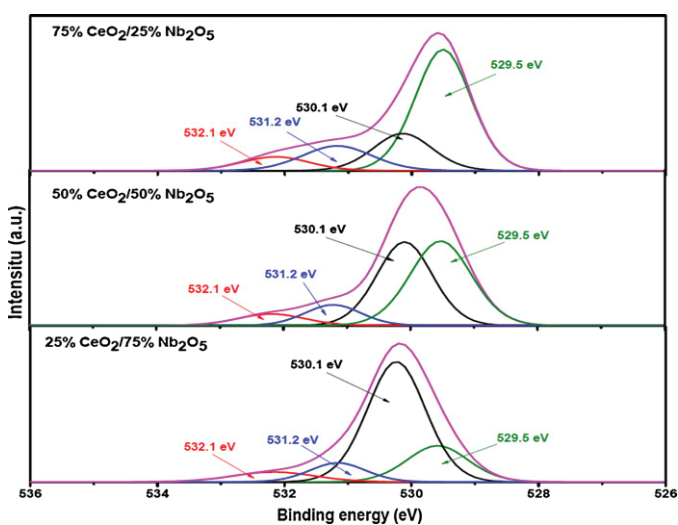


Fig. 5. O 1s XPS spectra of mixed oxide samples (experimental O 1s spectrum: pink line, O 1s spectrum of Nb₂O₅: black line, O 1s spectrum of CeO₂: green line, O 1s spectrum of surface hydroxyl groups: red line, O1s spectrum of chemisorbed oxygen: blue line). (For interpretation of the references to color in this figure legend, the reader is referred to the web version of this article.)

3.2. Redox properties

The mobility of surface oxygen species in ceria is found to be higher compared to conventional oxides such as SiO₂, Al₂O₃ and ZrO₂ [80]. These mobile surface oxygen species can be removed easily under reduction atmosphere leading to formation of non-stoichiometric ceria, CeO_{2-x} (0 ≤ x ≤ 0.5) [81]. On the other hand, the reduction of niobia is more difficult than that of cerium oxide. Nb₂O₅ reduction is initiated at ~800 °C and only very mild reduction occurs until ~1300 °C, when bulk Nb₂O₅ is reduced to bulk Nb₂O₄ [82].

Normalized TPR spectra of investigated materials are presented in Fig. 6, which shows H₂ consumption (a.u.) as a function of temperature. The reduction of ceria takes place in two temperature regions: the first one is from 250 to 590 °C with T_{max} around 430 °C; while the second region starts at 610 °C and is not achieved in the temperature scale of the experiment. These two reduction regions are characteristic of ceria and are attributed to surface and bulk reduction, respectively [81]. Overlapping of peaks is evident in lower temperature region, what might be due to the fact that surface may contain O²⁻ at different positions and with different coordination numbers. For example, the oxide surfaces can have imperfections such as steps, kinks, and corners projecting O²⁻ ions of different coordination number.

The 75% CeO₂–25% Nb₂O₅ sample shows similar red-ox profile as pure ceria in the lower temperature region, while a new peak is arising with T_{max} at 660 °C. This peak can be attributed to niobia species on the catalyst surface and is centered at temperature which is lower than that found for pure Nb₂O₅. This result points out the good dispersion of niobium oxide species and confirms that ceria promotes the reduction of niobia. This effect is obviously dependent on niobia content and H₂ consumption decreases with further increase in Nb content, which indicates lower reducibility.

3.3. Acid/base properties

The adsorption of probe molecules was used to investigate the acid–base character by FTIR and calorimetry method. The

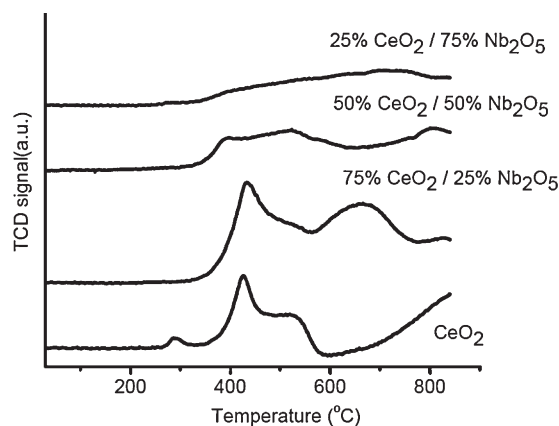


Fig. 6. TPR profiles of investigated materials.

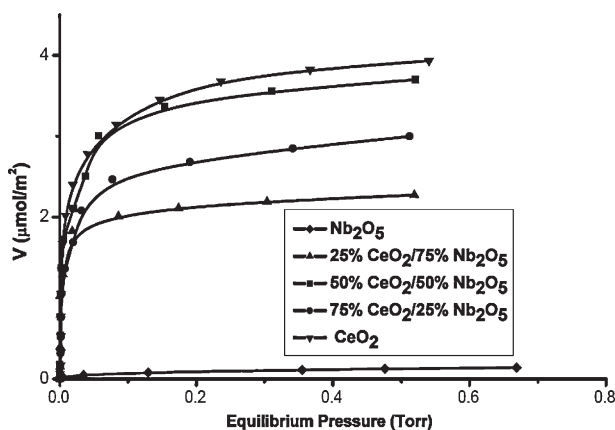


Fig. 7. Volumetric isotherms of SO_2 adsorption on investigated materials.

information obtained from these investigations are considered as complementary, rather than as a basis for comparison of results, because the principles of these two techniques are not the same. Adsorption calorimetry of NH_3 or SO_2 molecules allows precise determination of concentration and strength distribution of surface active sites (basic or acidic), whereas FTIR measurements of adsorbed pyridine can help to differentiate the types of acid sites (Lewis or Brønsted).

3.3.1. Microcalorimetric results

Table 3 compiles the data obtained from microcalorimetric measurements of SO_2 and NH_3 adsorption on all investigated samples. The total amounts of adsorbed gases, the amounts of irreversibly adsorbed (chemisorbed) and the amounts of reversibly adsorbed (physisorbed) gases are given in Table 3. As the investigated samples display noticeable differences in BET surface areas (Table 1), the calorimetric results are presented in $\mu\text{mol}/\text{m}^2$ rather than in $\mu\text{mol}/\text{g}$. The vertical parts of the isotherm correspond to irreversible adsorption, whereas the horizontal parts can be assigned to reversible adsorption.

Fig. 7 presents the isotherms obtained for SO_2 adsorption on the investigated samples. It is visible from the results presented in Table 3 and in Fig. 7 that the ratio of niobia to ceria has a decisive role for a basic character of investigated mixed oxides. The lowest adsorbed amount was found for pure niobia; an increase of niobia content in the mixed oxide samples produced a decrease of the amount of adsorbed gas (both total and irreversible).

The volumetric data obtained for NH_3 adsorption are also summarized in Table 3, whereas the isotherms of ammonia adsorption are shown in Fig. 8. It is evident that increasing the niobia loading in mixed oxides increases the number of acid sites, which can be clearly recognized through the increase of total and irreversibly adsorbed amounts of ammonia.

Fig. 9 displays differential heats of SO_2 (right) and NH_3 (left) adsorption on the investigated samples. The profiles of differential heats vs. uptake of the gas probe are multi-indicative; they provide data concerning the amount, strength, and strength distribution of the active sites. Besides, the values of initial heats of adsorption characterize the strongest sites active for adsorption. Evidently, niobia showed prominent acidic character, while all other investigated solids adsorbed both NH_3 and SO_2 , what is a clear indication of their amphoteric character. The addition of niobia to ceria has as a consequence an increase of the acidic character while the distribution of acidic sites is only slightly affected by niobia content. All investigated mixed oxides exhibited high initial differential heats of ammonia adsorption ($\geq 150 \text{ kJ mol}^{-1}$), with a continuous decrease with increasing surface coverage. If about basic sites, the addition of a small niobia amount importantly affected their strength; while

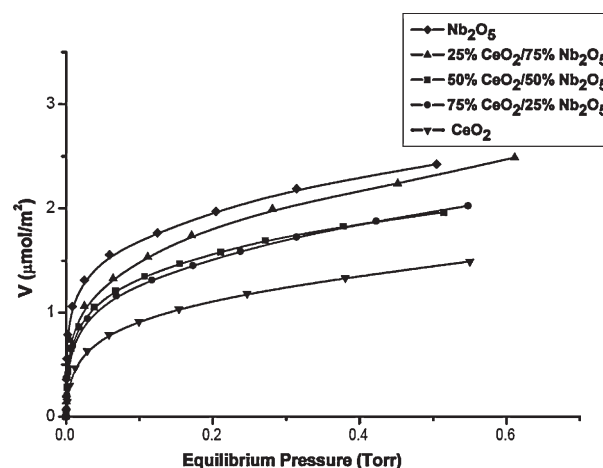


Fig. 8. Volumetric isotherms of NH_3 adsorption on investigated materials.

with further increase of niobia content the strength of basic sites decreased. Such results could be the indication of an interaction in between ceria and niobia, but also the indication of changes in the surface morphology of ceria as a result of mixing with niobia.

3.3.2. FTIR of pyridine adsorption

Presence of Lewis (coordinatively unsaturated metal atoms) and Brønsted (proton donor OH groups) acid sites on solid surfaces is a prime demand for potential catalytic applications. FTIR of adsorbed probe molecules, such as pyridine, is a well established and powerful surface analytical technique for determination of surface acid sites nature.

The relevant parts ($1700\text{--}1400 \text{ cm}^{-1}$) of collected spectra are shown in Fig. 10. All reported spectra were obtained by subtracting the spectrum of the fresh catalyst (without pyridine adsorption at room temperature) from those after pyridine adsorption. In FTIR spectra of pyridine adsorbed on pure Nb_2O_5 (Fig. 10), intense adsorption was observed at about 1445 , 1489 , 1542 , 1575 , 1606 and 1637 cm^{-1} . Of these, the peaks at 1445 cm^{-1} (19b vibrational mode) and 1606 cm^{-1} (8a vibrational mode) are characteristic of pyridine coordinated to Lewis acid sites, while the bands at 1637 (v8a) and 1542 cm^{-1} (v19b) are characteristic of pyridine ions bonded to Brønsted acid sites [83]. The bands around 1489 (v19a) and 1575 cm^{-1} (v8b) are associated simultaneously to both Brønsted and Lewis acid sites [83]. From the relative intensities of the bands

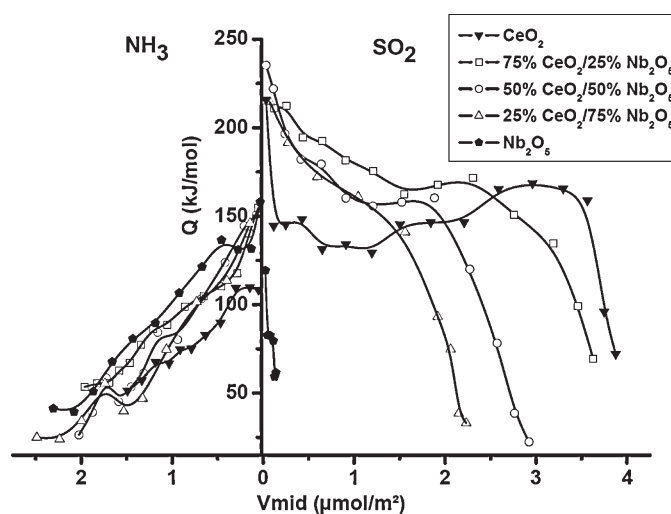


Fig. 9. Differential heats of NH_3 and SO_2 adsorption as a function of surface coverage.

Table 3 V_{irr} and V_{tot} calculated from adsorption isotherms of SO_2 and NH_3 on the different materials.

Sample name	SO_2 amount adsorbed		NH_3 amount adsorbed	
	$V_{\text{tot}}^{\text{a}}$ ($\mu\text{mol}/\text{m}^2$)	$V_{\text{irr}}^{\text{b}}$ ($\mu\text{mol}/\text{m}^2$)	$V_{\text{tot}}^{\text{a}}$ ($\mu\text{mol}/\text{m}^2$)	$V_{\text{irr}}^{\text{b}}$ ($\mu\text{mol}/\text{m}^2$)
CeO_2	3.4	2.9	1.0	0.3
75% CeO_2 /25% Nb_2O_5	3.2	2.9	1.5	0.5
50% CeO_2 /50% Nb_2O_5	2.6	2.2	1.4	0.5
25% CeO_2 /75% Nb_2O_5	2.1	1.7	1.7	0.9
Nb_2O_5	0.1	0.05	1.9	1.1

^a Amount of NH_3 or SO_2 adsorbed under an equilibrium pressure of 0.2 Torr (27 Pa).

^b Amount of chemisorbed NH_3 or SO_2 under an equilibrium pressure of 0.2 Torr (27 Pa).

at 1542 and 1445 cm^{-1} it is obvious that at elevated evacuation temperatures, pyridine is desorbed preferentially from Brønsted acid sites.

On the CeO_2 sample, pyridine adsorption gave rise to five bands in the 1400–1700 cm^{-1} region (Fig. 10). The peaks at around 1443 cm^{-1} (v19b) and 1596 (v8a), are assignable to pyridine coordinated on Lewis acid sites, while the peak at 1630 cm^{-1} is proof of Brønsted sites existence. The bands at 1573 (v8b) and 1486 (v19a) cm^{-1} are, as previously mentioned, associated simultaneously to both Brønsted and Lewis acid sites. Gradual weakening in intensity of the bands characteristic for pyridine species adsorbed at room temperature was observed, as the thermo-evacuation temperature increased. However, the appearance of new lines occurred at 1551 and 1283 cm^{-1} (not shown in Fig. 10), when the temperature of evacuation was increased to 200 °C. The band at 1551 cm^{-1} can be attributed to formation of carboxylate species [84], while the peak at 1283 cm^{-1} is assigned to N–O surface species [85]. Conversion of pyridine coordinated to Lewis acid sites into carboxylate species at high temperature implies the presence of basic OH groups, whereas its conversion into N–O is considered to be indicative of basic O^{2-} sites [85].

In the case of the mixed oxide samples, pyridine adsorption gave bands that are characteristic of pyridine interaction with Brønsted and Lewis acid sites. The bands at 1445 and 1606 cm^{-1} show a complex structure due to overlapping of components assigned to pyridine bonded to niobium or cerium sites. The presence of a small peak at 1542 cm^{-1} , characteristic of protonated pyridine, is clearly dependent on the niobia content. Among mixed oxide samples this

peak was found only for the sample containing the highest percentage of Nb_2O_5 .

Thermoevacuation caused gradual weakening of the bands present at the room temperature with the appearance of new ones (around 1546, 1371 and 1358 cm^{-1}) at 200 °C. The band at 1551 cm^{-1} was already assigned to the formation of carboxylate species, while the peaks at 1371 and 1359 cm^{-1} are indicative of the presence of carbonate species on surfaces of these mixed oxides [85].

According to Boehm and Knözinger, high temperature interactions, leading to selective oxidation of pyridine coordinated to Lewis acid sites must be preceded by sufficient activation of pyridine ligands for the nucleophilic attack [84]. Therefore, oxidation would require availability of both basic and strong Lewis acid sites functioning in a concerted mechanism. These results, thus, account for the presence of acid–base site pairs on the surface of ceria and mixed oxides samples. Presence of both kinds of sites was previously proven by adsorption microcalorimetry technique.

3.4. Catalytic activity

As already explained in Section 2, the changes in fructose and its product concentrations were monitored by ^1H liquid NMR technique. Product of major interest in fructose dehydration reaction, 5-HMF, was identified through the lines at 6.5, 7.4 and 9.3 ppm.

All investigated materials appear active in dehydration of fructose to 5-HMF. Fig. 11 shows the trend of fructose conversion as a function of reaction time. Maximum conversion of fructose after 6 h of reaction was 82% on Nb_2O_5 , while minimum of conversion, 39%, was found for CeO_2 sample. Activity in this reaction seems to increase with niobia loading in the mixed oxide samples, since the conversion of fructose and selectivity to HMF increased in the same manner (Fig. 12). Results presented in Fig. 13 show that the density of strong acid sites (represented by V_{irr} in $\mu\text{mol NH}_3/\text{m}^2$), favours the selectivity to HMF in fructose dehydration reaction. As shown in

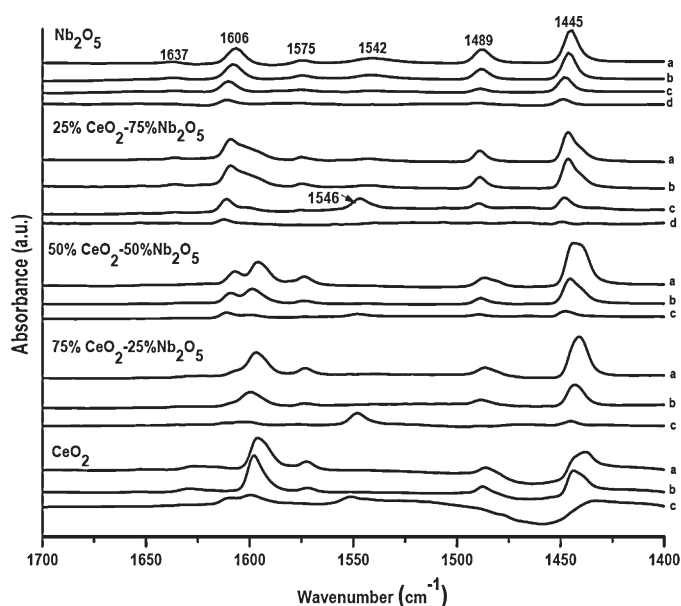


Fig. 10. FTIR spectra for pyridine desorption on investigated materials at different temperatures: (a) 25 °C, (b) 100 °C, (c) 200 °C, and (d) 300 °C.

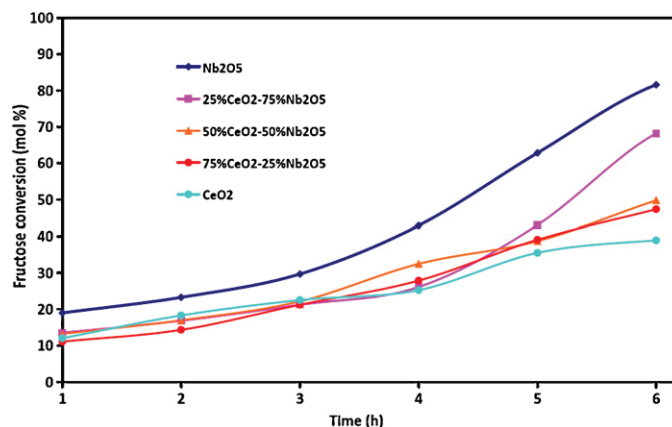


Fig. 11. Fructose conversion as a function of reaction time on investigated materials.

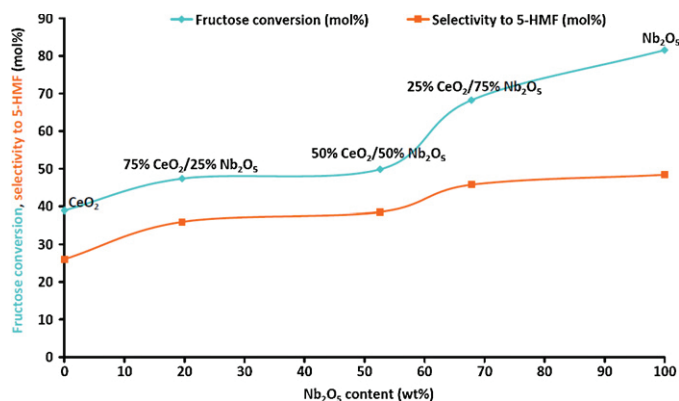


Fig. 12. Conversion of fructose and selectivity to 5-HMF as a function of Nb₂O₅ loading, after 6 h of reaction.

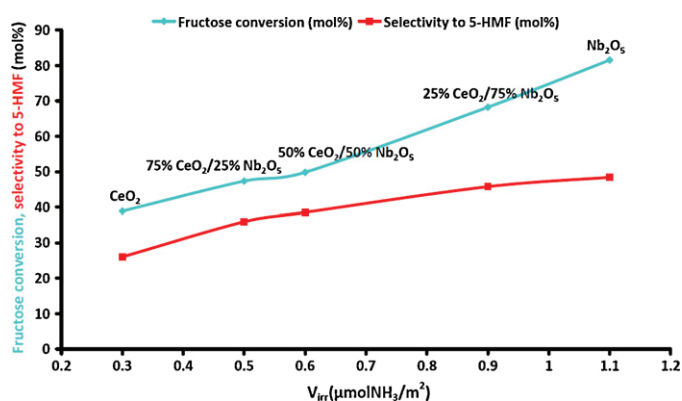


Fig. 13. Conversion of fructose and selectivity to 5-HMF as a function of density of strong acid sites, after 6 h of reaction.

Table 3, the number of strong acid sites per surface area of the samples increases with increasing the amount of Nb₂O₅ in the samples, leading to the conclusion that niobia is the main active component in dehydration of fructose in mixed oxide samples. These findings are in agreement with literature, where it is found that higher number of surface acid sites leads to a better catalytic performance in this reaction [86].

After 6 h, samples were separated from reaction solution by simple decantation. Catalytic activity of sample that showed the best activity and selectivity to 5-HMF was probed in a repeated reaction. Table 4 gives results obtained for reused catalyst; it is evident that catalytic activity of the reused sample decreases significantly after the first run. Deactivation further progresses with each new run, but in a slower manner. The observed behavior indicates a fast deactivation of an active sites part which is evidently the most active in dehydration of fructose. The loss of activity could be caused by a deposition of coke on the catalyst surface, but it could be also attributed to deposition of insoluble polymeric side products and humins as already reported in the literature [87]. Coke deposition on the surface of solid-acid catalysts used in analogous reaction of glucose dehydration in aqueous solutions was found to be significant at temperature over 120 °C [88].

Table 4

Catalytic activity of the fresh and reused 25% CeO₂/75% Nb₂O₅ sample for the dehydration of fructose.

	1st run	2nd run	3rd run	4th run	5th run
TON ^a (s ⁻¹)	0.16	0.061	0.06	0.058	0.05

^a TON was expressed as: (mol of 5-HMF/number of strong acid sites × time (s)).

However, as it has been already reported for aqueous systems [89], unwanted products, namely levulinic (LA, 2.1 ppm) and formic acids (FA, 8.1 ppm), that are formed by rehydration of 5-HMF, have been noticed in this work. FA was formed in relatively low yield, ranging from 0.9% on 50% Nb₂O₅–50% CeO₂ to 2.2% on pure niobia. On the other hand a small amount, <1%, of LA was identified for all the materials used in this work. The mass balance i.e. the sum of total carbon of identified products and non-reacted fructose accounts for 60–80% of total carbon of initial fructose in the reaction. The difference could be attributed to the soluble polymeric condensation products and insoluble humins or other reaction products or intermediates not identified in this work, similarly as already reported in the literature [87,89]. It should be mentioned here that, in the case of fructose dehydration catalyzed by solid acids, absence of these by-products was reported [90]. Nevertheless, it has to be underlined that reaction conditions (temperature and design of catalytic reactor) applied in our work and that of Carniti et al. [90], were importantly different. In the present work we performed the reaction in an autoclave, and observed small amounts of LA and FA products which were not observed in Ref. [90], when working in flow conditions over Nb₂O₅ catalyst at 100 °C in aqueous phase. Besides, rehydration reactions that lead to LA and FA formation could be more easily avoided in flow conditions, as the products are continuously removed from the reactor. Moreover, it is worth to notice that a higher temperature (130 °C in our work) has as a consequence an increase in the yield of LA, as previously reported [89,91,92].

It is important to mention also that after dehydration of fructose, the structure of solid samples was checked by XRD and Raman techniques. No significant changes of structure before and after reaction were observed, thus indicating the stability of samples under the reaction conditions.

4. Conclusions

Coprecipitation, the method applied for preparation of our samples allowed good homogeneity and dispersion of the two components in ceria–niobia mixed oxides formulations. Results obtained from XRD and Raman spectroscopy showed that there is no formation of any new phase between the two components of this mixed oxide system, while there are clear indications of their interaction. Furthermore, enrichment of the surface in niobia was observed by XPS technique, particularly, with increasing niobia content in the mixed oxide. Exposure of niobia on the surface can be of interest in applications where its unique properties, such as water insolubility, activity and stability in water phase are important.

Amphoteric character and red-ox properties of ceria have been confirmed in this work. However, it is important to point out here that all mixed oxides investigated have also shown amphoteric behavior and red-ox features, depending on the relative amounts of ceria and niobia present in them.

All oxides investigated here were active in fructose dehydration reaction. The activity and selectivity to desired product were found to be dependent on the amount of strong acid sites present on the surface of the catalyst; fact that is related to the amount of niobia.

Acknowledgments

French National Research Agency (ANR-09-CP2D-19) is greatly acknowledged for financial support. Special thanks are addressed to the technical services of IRCÉLYON (Institut de Recherches sur la Catalyse et l'Environnement de Lyon) for valuable technical contributions in Raman, XRD, BET, XPS, and chemical analysis.

References

- [1] S. Damyanova, J.M.C. Bueno, *Appl. Catal. A* 253 (2003) 135.
- [2] T. Ozaki, T. Masui, K.-I. Machida, G.-Y. Adachi, T. Sakata, H. Mori, *Chem. Mater.* 12 (2000) 643.
- [3] E. Aneggi, C. de Leitenburg, G. Dolcetti, A. Trovarelli, *Catal. Today* 114 (2006) 40.
- [4] A. Trovarelli, C. de Leitenburg, M. Boaro, G. Dolcetti, *Catal. Today* 50 (1999) 353.
- [5] T. Zhu, L.J. Kundakov, A. Dreher, M. Flytzani-Stephanopoulos, *Catal. Today* 50 (1999) 381.
- [6] V. Solinas, E. Rombi, I. Ferino, M.G. Cutrufello, G. Colón, J.A.J. Navio, *J. Mol. Catal. A: Chem.* 204–205 (2003) 629.
- [7] L.G. Appel, J.G. Eon, M. Schmal, *Phys. Status Solidi* 163 (1997) 107.
- [8] R.J. Gorte, *AIChE J.* 56 (2009) 1126.
- [9] F. Calise, G. Restuccia, N. Sammes, *J. Power Sources* 196 (2011) 301.
- [10] Z. Shao, S.M. Halle, *Nature* 431 (2004) 170.
- [11] E. Ramirez-Cabrero, N. Laosiripojana, A. Atkinson, D. Chadwick, *Catal. Today* 78 (2003) 433.
- [12] A. Kumar, P.S. Devi, H.S. Maiti, *Chem. Mater.* 16 (2004) 5562.
- [13] V.V. Kharton, A.V. Kovalevsky, A.P. Viskup, A.L. Shaula, F.M. Figueiredo, E.N. Naumovich, F.M.B. Marques, *Solid State Ionics* 160 (2003) 247.
- [14] C. Levy, C. Guizard, A. Julbe, *Sep. Purif. Technol.* 32 (2004) 327.
- [15] X. Yin, L. Hong, Z.-L. Liu, *Appl. Catal. A* 300 (2006) 75.
- [16] X. Yin, L. Hong, Z.-L. Liu, *J. Membr. Sci.* 268 (2006) 2.
- [17] S. Zhao, R.K. Gorte, *Appl. Catal. A* 277 (2004) 129.
- [18] J. Kašpar, F. Graziani, *Catal. Today* 50 (1999) 285.
- [19] S. Imamura, I. Fukuda, S. Ishida, *Ind. Eng. Chem. Res.* 27 (1988) 718.
- [20] V.S. Mishra, V.V. Mahajani, J.B. Joshi, *Ind. Eng. Chem. Res.* 34 (1995) 2.
- [21] C. Wang, Y. Ao, P. Wang, J. Hou, J. Quian, *J. Hazard. Mater.* 184 (2010) 1.
- [22] S. Recillas, J. Colón, E. Casals, E. González, V. Puentes, A. Sánchez, X. Font, *J. Hazard. Mater.* 184 (2010) 425.
- [23] M. Weibel, F. Garin, P. Bernhardt, G. Maire, M. Prigent, *Stud. Surf. Sci. Catal.* 71 (1991) 195.
- [24] G. Jacobs, S. Khalid, P.M. Patterson, D.E. Sparks, B.H. Davis, *Appl. Catal. A* 268 (2004) 255.
- [25] S. Wang, G.Q. Lu, *Appl. Catal. B* 19 (1998) 267.
- [26] A. Trovarelli, *Catal. Rev. Sci. Eng.* 48 (1996) 439.
- [27] J.A. Montoya, E. Romero-Pascual, C. Gimon, P. Del Angel, A. Monzon, *Catal. Today* 63 (2000) 71.
- [28] R. Craciun, W. Daniell, H. Knözinger, *Appl. Catal. A* 230 (2002) 153.
- [29] K. Asami, X. Li, K. Fujimoto, Y. Koyama, A. Sakurama, N. Kometani, Y. Yonezawa, *Catal. Today* 84 (2003) 27.
- [30] S. Kawi, Y.P. Tang, K. Hidajat, L.E. Yu, *J. Metastable Nanocryst. Mater.* 23 (2005) 95.
- [31] M.K. Neylon, M.J. Castagnola, N.B.Ch. Castagnola, L. Marshall, *Catal. Today* 96 (2004) 53.
- [32] F. Baudin, P. Da Costa, C. Thomas, S. Calvo, Y. Lendresse, S. Schneider, F. Delacroix, G. Plassat, G. Djega-Mariadassou, *Top. Catal.* 30/31 (2004) 97.
- [33] J. Kašpar, P. Fornasiero, *J. Solid State Chem.* 171 (2003) 19.
- [34] S.J. Schmieg, D.N. Belton, *Appl. Catal. B* 6 (1995) 127.
- [35] K. Tanabe, *Catal. Today* 8 (1990) 1.
- [36] K. Tanabe, S. Okazaki, *Appl. Catal. A* 133 (1995) 191.
- [37] J.M. Jehng, I.E. Wachs, *Catal. Today* 8 (1990) 37.
- [38] M. Ziolek, *Catal. Today* 78 (2003) 47.
- [39] I. Nowak, M. Ziolek, *Chem. Rev.* 99 (1999) 3603.
- [40] F. Yang, Q. Liu, X. Bai, Y. Du, *Bioresour. Technol.* 102 (2011) 3424.
- [41] P. Carniti, A. Gervasini, S. Biella, A. Auroux, *Catal. Today* 118 (2006) 373.
- [42] T. Armaroli, G. Busca, C. Carlini, M. Giuttari, A.M.R. Galletti, G. Sbrana, *J. Mol. Catal. A: Chem.* 151 (2000) 233.
- [43] C. Carlini, M. Giuttari, A.M.R. Galletti, G. Sbrana, T. Armaroli, G. Busca, *Appl. Catal. A* 183 (1999) 295.
- [44] S.H. Taylor, J.S.J. Hargreaves, G.J. Hutschings, R.W. Joyner, *Appl. Catal. A* 12 (1995) 287.
- [45] J.M. Jehng, H. Hu, X. Gao, I.E. Wachs, *Catal. Today* 28 (1996) 335.
- [46] K. Ruth, R. Burch, R. Kieffer, *J. Catal.* 175 (1998) 27.
- [47] K. Ruth, R. Burch, R. Kieffer, *J. Catal.* 175 (1998) 16.
- [48] K. Kunimori, H. Oyanagi, H. Shindo, *Catal. Lett.* 21 (1993) 283.
- [49] D.A.G. Aranda, A.L.D. Ramos, F.B. Passos, M. Schmal, *Catal. Today* 28 (1996) 119.
- [50] D.A. Aranda, F.B. Noronha, M. Schmal, F.B. Passos, *Appl. Catal.* 100 (1993) 77.
- [51] F.B. Passos, D.A. Aranda, R.R. Soares, M. Schmal, *Catal. Today* 43 (1998) 3.
- [52] M. Schmal, D.A.G. Aranda, R.R. Soares, F.B. Noronha, A. Frydman, *Catal. Today* 57 (2000) 169.
- [53] A. Esteves, L.C.A. Oliveira, T.C. Ramalho, M. Goncalves, A.S. Anastacio, H.P.W. Carvalho, *Catal. Commun.* 10 (2008) 330.
- [54] A.G.S. Prado, L.B. Bolzon, C.P. Pedroso, A.O. Moura, L.L. Costa, *Appl. Catal. B* 82 (2008) 219.
- [55] I.E. Wachs, J.-M. Jehng, G. Deo, H. Hu, N. Arora, *Catal. Today* 28 (1996) 199.
- [56] T. Okuhara, *Chem. Rev.* 102 (2002) 3641.
- [57] R. Craciun, W. Daniell, H. Knozinger, *Appl. Catal. A* 230 (2002) 153.
- [58] C. Laberty-Robert, J.W. Long, E.M. Lucas, K.A. Pettigrew, R.M. Stroud, M.S. Doescher, D.R. Rolison, *Chem. Mater.* 18 (2006) 50.
- [59] J.C. Yu, L. Zhang, J. Lin, *J. Colloid Interface Sci.* 260 (2003) 240.
- [60] A. Pintar, J. Batista, S. Hočvar, *J. Colloid Interface Sci.* 285 (2005) 218.
- [61] J.-S. Lee, K.-H. Choi, B.-K. Ryu, B.-C. Shin, I.-S. Kim, *Mater. Res. Bull.* 39 (2004) 2025.
- [62] S. Letichevsky, A. Tellez, R.R. de Avillez, M.I.P. da Silva, M.A. Fraga, L.G. Appel, *Appl. Catal. B* 58 (2005) 203.
- [63] Y. Roman-Leshkov, C.J. Barret, Z.Y. Liu, J.A. Dumesic, *Nature* 447 (2007) 982.
- [64] P.A. Burke, E.I. Ko, *J. Catal.* 129 (1991) 38.
- [65] P. Carniti, A. Gervasini, M. Marzo, *Catal. Today* 152 (2010) 42.
- [66] F.M.T. Mendes, C.A. Perez, R.R. Soares, F.B. Noronha, M. Schmal, *Catal. Today* 78 (2003) 449.
- [67] B. Reddy, A. Khan, Y. Yamada, T. Kobayashi, S. Loridant, J.-C. Volta, *J. Phys. Chem. B* 107 (2003) 11475.
- [68] T. Yuzhakova, V. Rakic, C. Guimon, A. Auroux, *Chem. Mater.* 19 (2007) 2970.
- [69] J.-M. Jehng, I.E. Wachs, *Chem. Mater.* 3 (1991) 100.
- [70] A.A. McConnel, J.S. Anderson, C.N.R. Rao, *Spectrochim. Acta A* 23 (1976) 1067.
- [71] X. Gao, S.R. Bare, B.M. Weckhuysen, I.E. Wachs, *J. Phys. Chem. B* 102 (1998) 10842.
- [72] A. Matinez-Arias, M. Fernández-García, L.N. Salamanca, R.X. Valenzuela, J.C. Conesa, J. Soria, *J. Phys. Chem. B* 104 (2000) 4038.
- [73] B.M. Reddy, A. Khan, *Catal. Surv. Asia* 9 (2005) 155.
- [74] S. Damyanova, C.A. Perez, M. Schmal, J.M.C. Bueno, *Appl. Catal. A* 234 (2002) 271.
- [75] A. Meerchaut, J. Rijnsdorp, J.C.W. Folmer, R. Jellinek, *Stud. Inorg. Chem.* 3 (1983) 777.
- [76] K.I. Seo, P.C. McIntyre, H. Kim, K.C. Saraswat, *Appl. Phys. Lett.* 86 (2005) 082904.
- [77] L. Dragonem, P. Moggi, G. Predieri, R. Zannoni, *Appl. Surf. Sci.* 187 (2002) 82.
- [78] X. Liang, X. Wang, Y. Zhuang, B. Xu, S. Kuang, Y. Li, *J. Am. Chem. Soc.* 130 (2008) 2736.
- [79] G. Balucci, J. Kaspar, P. Fornasiero, M. Graziani, M. Saiful Islam, *J. Phys. Chem. B* 102 (1998) 557.
- [80] C. Hardacre, R.M. Ormerod, R.M. Lambert, *J. Phys. Chem.* 98 (1994) 10901.
- [81] M. Ricken, J. Nolting, I. Riess, *J. Solid State Chem.* 54 (1984) 89.
- [82] I.E. Wachs, L.E. Briand, J.M. Jehng, L. Burcham, X. Gao, *Catal. Today* 57 (2000) 323.
- [83] G. Busca, *Phys. Chem. Chem. Phys.* 1 (1999) 723.
- [84] H.P. Boehm, H. Knözinger, in: J.R. Anderson, M. Boudart (Eds.), *Catalysis-Science and Technology*, vol. IV, Springer-Verlag, Berlin, 1983, p. 39.
- [85] M.I. Zaki, G.A.M. Hussein, S.A.A. Mansour, H.A. El-Ammawy, *J. Mol. Catal.* 51 (1989) 209.
- [86] P. Carniti, A. Gervasini, S. Biella, A. Auroux, *Chem. Mater.* 17 (2005) 6128.
- [87] T. Armaroli, G. Busca, C. Carlini, M. Giuttari, A.M. Raspolli Galletti, G. Sbrana, *J. Mol. Catal. A* 151 (2000) 233.
- [88] K. Lourvanij, G.L. Rorrer, *Ind. Eng. Chem. Res.* 32 (1993) 11.
- [89] H.E. Van Dam, A.P.G. Kieboom, H. Van Bekkum, *Starch/Stärke* 38 (1986) 95.
- [90] P. Carniti, A. Gervasini, M. Marzo, *Catal. Commun.* 12 (2011) 1122.
- [91] T.S. Hansen, J.M. Woodley, A. Riisager, *Carbohydr. Res.* 344 (2009) 2568.
- [92] L. Peng, L. Lin, J. Zhang, J. Zhuang, B. Zhang, Y. Gong, *Molecules* 15 (2010) 5258.

-Submitted to ChemCatChem-

Tuning the acidity of niobia: characterization and catalytic activity of Nb₂O₅-MeO₂ (Me = Ti, Zr, Ce) mesoporous mixed oxides

Dušan Stošić^a, Simona Bennici^a, Vladimir Pavlović^b, Vesna Rakić^b, Aline Auroux^{a}*

^a Université Lyon 1, CNRS, UMR 5256, IRCELYON, Institut de recherches sur la catalyse et l'environnement de Lyon, 2 avenue Albert Einstein, F-69626 Villeurbanne, France

^b Faculty of Agriculture, Department of Chemistry, University of Belgrade, Nemanjina 6, 11080 Zemun, Serbia

*Corresponding author: Fax: +33 472445399, Tel: +33 472445398

E-mail address: aline.auroux@ircelyon.univ-lyon1.fr (A. Auroux)

Abstract

Well ordered mesoporous Nb₂O₅-MeO₂ (Me = Ti, Zr, Ce) mixed oxides were successfully prepared using evaporation-induced self-assembly method. The structural and textural properties of these materials have been fully characterized using appropriate techniques (low-temperature adsorption-desorption of nitrogen, thermogravimetric analysis, X-ray diffraction analysis (XRD), scanning electron microscopy (SEM) and Raman spectroscopy). The acid-base properties were estimated by the adsorption of appropriate probe molecules – NH₃ or SO₂ were used to estimate the population, strength and strength distribution of acid or basic sites, by means of adsorption microcalorimetry. Formation of mesoporous structure was confirmed by the results of XRD and BET techniques. Results of adsorption microcalorimetry technique showed that that the type of transition metal oxide added to niobia has a decisive role for acidic-basic character of investigated mixed oxides. Among the investigated mixed oxide formulations only Nb₂O₅-CeO₂ was amphoteric, while the other samples showed prominent acidic character. All the investigated materials are catalytically active in fructose dehydration; conversion of fructose and selectivity to 5-hydroxymethylfurfural (5-HMF) and levulinic acid (LA) are proved to be dependant on the number of acidic sites on the surface of catalysts. Furthermore, presence of the basic sites on the surface of the catalyst decreases the activity in the fructose dehydration reaction, as in the case of Nb₂O₅-CeO₂ sample.

Keywords: mesoporous Nb₂O₅-MeO₂ (Me = Ti, Zr, Ce) mixed oxides, adsorption microcalorimetry, acidic-basic properties, fructose dehydration

1. Introduction

From the discovery of ordered mesoporous silicates by Mobil Corporation in 1992 (material denoted as M41S), these substances have attracted considerable attention [1, 2]. Over the last two decades there has been increasing interest in exploiting and improving their unique properties, such as controlled pore sizes, high surface area and high thermal stability, which are of great importance in heterogeneous catalysis and gas separation processes [3, 4]. Of particular importance is the existence of their large pores, what should lead to fast diffusion to the active sites during catalytic process, even for large molecules. High catalytic performance of porous materials can be also attributed to capillary condensation: reactants can be effectively incorporated into the pores by capillary action and converted to products over active sites [5, 6].

Among other mesoporous materials, aluminosilicates have been extensively investigated and these topics are covered in several review articles [7-9]. However, such materials do not possess sufficient number and strength of acidic active sites to be useful in many catalytic applications. Therefore, synthesizing mesoporous materials from acidic transition metal oxides recently got significant attention. Mesoporous transition metal oxides have superior properties in many applications as compared to their traditional silica analogues due to their high acidities and the variable oxidation states afforded by the empty transition metal d orbitals, which allow electron transfer to occur between the reactants and active sites during any given catalytic process [10, 11]. Compared to so-called “bulk” transition metal oxides, characterized primarily by low surface area, mesoporous ones should have larger surface areas and higher number of active sites. Mesoporous mixed metal oxides are particularly promising as heterogeneous catalysts because of their tunable surface compositions, metal oxidation states (via organic-inorganic interfacial chemistry), and wall structures. Furthermore, mixing the oxides results in formation of new materials with modified physical and chemical features and different catalytic properties in comparison with parent materials.

Niobium-based mesostructured materials are of significant importance in heterogeneous catalysis which had attracted considerable attention due to its superior features. The unique properties of these compounds have led to catalytic applications in various reactions [12, 13]. Hydrated niobium oxide ($\text{Nb}_2\text{O}_5 \cdot n\text{H}_2\text{O}$; niobic acid) possesses both Lewis acid sites and relatively strong Brønsted acid sites on its surface [14]. Niobia belongs to a group of a few solids that offer the required acidity, activity, stability and insolubility to properly catalyze reactions in aqueous media [15]. This feature makes niobia-based materials attractive for industrial use, and is very important for the establishment of low-cost and environmentally

clean processes. However, deactivation of niobia during processes such as fructose dehydration reaction, due to the formation of large amounts of solid products (humins or coke) has been reported [16, 17]. For real catalytic applications, besides a balanced activity–selectivity pattern, the maintenance of a stable activity is an essential requisite. It was proposed that the strong acid nature of the Nb_2O_5 sites could be responsible of such deactivation [16, 17].

Zirconium and titanium oxides are important catalytic materials with medium-to-high Lewis acidity, significant basicity, and weak Brønsted acidity [18–21]. In the field of catalysis, TiO_2 is mainly used as a support due to its good mechanical properties, inertness and low price. In many cases titania interacts strongly with the supported active phase. This interaction is decisive for the catalytic activity of such materials [22]. Zirconia is used in catalysis as active material and support. As a carrier, it gives rise to an unique kind of interaction between the active phase and support, this being manifested in both the catalytic activity and the selectivity pattern of the system, and it is more chemically inert than the classical supports (e.g. Al_2O_3 and SiO_2) [23].

Numerous applications of cerium oxide in heterogeneous catalysis are based on a number of appropriate properties that ceria expresses which are all characteristic of fluorite type structures: chemical and physical stability, high oxygen vacancy concentration and high oxygen mobility. Cerium can cycle easily between reduced and oxidized states ($\text{Ce}^{3+} \leftrightarrow \text{Ce}^{4+}$), which permits the reversible addition and removal of O_2 from CeO_2 [24, 25], this feature being crucial for the application of this material in the domain of catalysis.

In this work mesoporous $\text{Nb}_2\text{O}_5\text{-MeO}_2$ ($\text{M} = \text{Ce}, \text{Zr}, \text{Ti}$) mixed metal oxides were prepared by evaporation-induced self-assembly (EISA) method with the aim of investigating the change in properties of niobia with the presence of another component oxide. It is known that the catalytic functions of solid materials are governed by their surface features. Thus, in order to predict their activity and selectivity in various reactions, we fully characterized the synthesized samples with respect to their structural, textural and acid–base properties. Their catalytic behavior was tested in the reaction of fructose dehydration; reaction of great environmental importance, which yields to 5-hydroxymethylfurfural (5-HMF), compound recognized as a bio-refining intermediate for the production of alternative fuels [26].

2. Experimental

2.1. Sample preparation

Mixed mesoporous oxides were prepared from niobium pentachloride NbCl_5 (99.99, Strem Chemicals INC.), zirconium tetrachloride ZrCl_4 (99.99, Sigma-Aldrich), cerium trichloride CeCl_3 (99.99, Sigma-Aldrich) and titanium dichloride TiCl_2 (99.99, Sigma-Aldrich). Triblock copolymer surfactant (PE 105, Sigma-Aldrich) was used as a structure directing agent. Mixed oxides were synthesized by dissolving 1 g of surfactant in 10 g of dehydrated ethanol, and by adding 7 mmol of metal chloride salts into the solution with vigorous stirring. The molar ratio of niobium to other metals was 1. Water (0.333 mol) was added to the solution with further stirring. The resulting sol was gelled in a Petri dish at 30 °C for 14 days. The aged gel samples were then calcined at 500 °C for 5 h in air for removal of the surfactant. The calcination temperature has been chosen on the basis of thermogravimetric measurements [27, 28].

2.2. Characterization

Chemical compositions of prepared materials (the contents of metals and metal oxides) were determined by inductively coupled plasma-optical emission spectroscopy (ICP-OES) with an ACTIVA spectrometer from Horiba JOBIN YVON, after they were digested using a mixture of inorganic acids (H_2SO_4 and HNO_3).

After the preparation fresh samples were calcined at 500 °C, with the intention of removing the structure directing agent. Thermogravimetry (TG-dTG, performed on a “Labsys-TG” instrument from Setaram) was used in order to determine this lowest temperature at which no significant loss of mass occurred with further heating. The crude samples (~50 mg) were heated from 25 °C to 800 °C with a heating rate of 5 °C min^{-1} in a flow of air, which was chosen as a soft oxidizing agent for calcination.

Surface areas were determined by low temperature nitrogen adsorption performed at -196 °C, on a Micromeritics 2020 apparatus, after pretreatment performed for 2 h at 300 °C under vacuum. The BET (Brunauer – Emmet – Teller) method was used to derive surface areas from the resulting isotherms. Pore size distributions were obtained from analysis of the adsorption branch of the isotherms using Barrett – Joyner – Halenda (BJH) method.

The structural characteristics of samples were examined by XRD, scanning electron microscopy (SEM) and Raman spectroscopy techniques. XRD patterns were recorded on a Bruker (Siemens) D5005 diffractometer at a room temperature using $\text{Cu K}\alpha$ radiation (0.154 nm) from 1° to 10°, for low angle X-ray diffraction (LAXRD) measurements, and from 4° to 70°, for wide angle XRD (WAXRD), in 0.02° steps with 1 s per step. Raman spectra were

collected under the ambient conditions on a LabRAMHR (Jobin Yvon) spectrometer. The excitation was provided by the 514.5 nm line of an Ar⁺ Kr⁺ ion laser (Spectra Physics), keeping the sample under microscope. The power of the incident beam on the sample was 100 μW. Because the laser beam can be precisely focused, it was possible to perform quantitative evaluation of band intensities between the samples studied. The laser beam was focused through microscope objective lenses (100×) down to a 1 μm spot on the sample. The acquisition time was adjusted according to the intensity of the Raman scattering. The wavenumber values reported from the spectra are accurate to within 2 cm⁻¹. For each solid, the spectra were recorded at several points of the sample to ascertain the homogeneity of the sample; the averages of these spectra were plotted and presented in this paper. The morphology of samples was investigated by scanning electron microscopy (SEM, JEOL JSM-6390 LV). Prior to the analysis the samples were covered with Au using a sputter coater Baltec scd 005 accessory. Time of sputtering was 100 ms using a current of 30 mA.

The acid–base properties were studied by adsorption microcalorimetry of NH₃ and SO₂, using well known methodology described already in the literature [29]. Briefly, experiments were performed at 150 °C in a heat flow calorimeter (C80 from Setaram) linked to a conventional volumetric apparatus equipped with a Barocel capacitance manometer for pressure measurements. The samples were pretreated in a quartz cell by heating overnight under vacuum at 300 °C; this temperature was reached using a heating rate of 1 °C min⁻¹. The differential heats of adsorption were measured as a function of coverage by repeatedly sending small doses of respective gas onto the sample until an equilibrium pressure of around 67 Pa was reached. The sample was then outgassed for 30 min at the same temperature, and a second adsorption run was performed at 150 °C on each sample, until an equilibrium pressure of about 27 Pa was attained. The difference between the amounts adsorbed in the first and second adsorptions at 27 Pa represents the irreversibly adsorbed amount (V_{irr}) of a respective gas, which provides an estimation of the number of strong acidic/basic sites.

2.3. Catalytic reaction

The catalytic abilities of investigated materials were probed through fructose dehydration reaction. The batch catalytic experiments were performed in a 100 ml stainless still autoclave, at 130 °C. In a typical procedure, 600 mg of fructose was dissolved in 60 ml of water and then 80 mg of solid catalyst was added. Water was chosen as a green and appropriate solvent for dehydration of fructose to 5-HMF. Starting time of the reaction was taken when the reaction mixture reached 130 °C. Time needed to reach this temperature was 30 min. Samples were withdrawn from the reaction mixtures at 1 h intervals; the changes of fructose, 5- HMF,

levulinic acid (LA) and formic acid (FA) concentrations with time were followed by collecting ^1H NMR spectra, using liquid NMR technique (Bruker AVANCE 250 spectrometer equipped with a multinuclear 10 mm Probe). Reactant conversion (mol %) and product selectivity (%) were defined as follows:

$$\text{Conversion (mol \%)} = (\text{moles of x reacted})/(\text{moles of x initial}) \times 100\%$$

$$\text{Selectivity (\%)} = (\text{moles of y produced})/(\text{moles of x reacted}) \times 100\%$$

3. Results and discussion

3.1 Chemical composition, structure and morphology of the samples

Table 1 presents the list of samples synthesized in this work, their chemical composition, obtained by ICP technique, values of BET surface areas, and pore structure parameters.

As it is well-known that the temperature of calcination can influence the morphology of a final product, it was important to determine the lowest temperature which is high enough to achieve the complete removal of structure directing agent and impurities from the bulk of a sample. In this work, thermogravimetric analysis was performed in order to determine this minimal temperature needed for calcination of crude samples. These experiments indicated that the block copolymers are completely removed from the as synthesized mesoporous oxides upon calcination at 500 °C (Fig. 1).

From the Table 1 it can be seen that specific surface area of Nb_2O_5 single oxide is lower than those of $\text{Nb}_2\text{O}_5\text{-TiO}_2$ and $\text{Nb}_2\text{O}_5\text{-ZrO}_2$ binary oxides. The interaction between two component oxides may have suppressed the particle growth of each component, making the binary oxides that possess higher surface areas. $\text{Nb}_2\text{O}_5\text{-CeO}_2$ has the same surface area as pure Nb_2O_5 .

The N_2 adsorption/desorption isotherms and the corresponding pore size distributions of the investigated catalysts are shown in Fig. 2. It can be seen that the isotherms presented in Figure 2 are classical type IV, characteristic for mesoporous materials as defined by IUPAC [30]. To describe precisely adsorption isotherms, it can be told that they express “hydrogen type” hysteresis loop, which is an additional characteristic of mesoporous materials. These hysteresis loops have triangular shape and a steep desorption branches [30]. The sharp N_2 uptake over a narrow range ($P/P_0 \approx 0.4\text{-}0.6$) of the adsorption isotherm for Nb_2O_5 , $\text{Nb}_2\text{O}_5\text{-TiO}_2$ and $\text{Nb}_2\text{O}_5\text{-ZrO}_2$ samples indicates uniform mesopores (~ 4.5 nm) with a narrow size range in the corresponding pore size distribution span, as can be seen in the insets of Fig. 2 for BJH pore size distribution. On the other hand, gradual N_2 uptake over a wide range ($P/P_0 \approx$

0.4-1) implies that $\text{Nb}_2\text{O}_5\text{-CeO}_2$ has broad pore size distribution (3 – 13 nm). It is also easy to see from Table 1 that $\text{Nb}_2\text{O}_5\text{-TiO}_2$ has a lower wall thickness than pure Nb_2O_5 , whereas $\text{Nb}_2\text{O}_5\text{-CeO}_2$ and $\text{Nb}_2\text{O}_5\text{-ZrO}_2$ samples have higher. It is considered that lower wall-thickness results in better thermal stability of mesoporous materials [31, 32].

Fig. 3 shows small angle X-ray scattering patterns of mesoporous oxides investigated in this work. XRD spectra clearly indicate the formation of mesoporous structure with the first diffraction peak, tentatively indexed as the (100) reflection at $d(100)$ 6.6 – 8.2 nm [33] (Table 1). With the mixing of niobia with zirconia, the intensity of this peak increased, indicating that the percent of ordered mesostructure increased. In the case of $\text{Nb}_2\text{O}_5\text{-TiO}_2$ and $\text{Nb}_2\text{O}_5\text{-CeO}_2$ intensity decreased indicating the opposite effect. Furthermore, the secondary broad shoulder is present only in the diffractions of $\text{Nb}_2\text{O}_5\text{-ZrO}_2$ sample. This secondary broad shoulder implies the formation of an ordered mesoporous structure. As can be seen in Table 1, $\text{Nb}_2\text{O}_5\text{-CeO}_2$ showed a larger d -spacing value than pure Nb_2O_5 , whereas $\text{Nb}_2\text{O}_5\text{-TiO}_2$ and $\text{Nb}_2\text{O}_5\text{-ZrO}_2$ samples have lower values. Wide angle XRD (Fig. 4) patterns reveal that among investigated samples only mesoporous $\text{Nb}_2\text{O}_5\text{-CeO}_2$ is crystalline; the reflections correspond to the fluorite type structure of CeO_2 . Absence of any crystallite peaks for $\text{Nb}_2\text{O}_5\text{-TiO}_2$ sample indicates that this catalyst is amorphous. In XRD of $\text{Nb}_2\text{O}_5\text{-ZrO}_2$ small peaks that correspond to ZrO_2 crystalline phase appear, indicating the coexistence of amorphous mesoporous phase and ZrO_2 crystalline phase in this sample. The peaks of very low intensity in XRD patterns of pure niobia give evidence of poor crystallinity of this sample.

SEM images presented in Fig. 5 amend the insight into the morphology of investigated samples. Imaging of niobia sample has shown that this material exists in the form of some compact blocked particles (Fig. 5a). It seems that, even after the calcinations done in the flow of air, some residual amount of structure-directing agent remains in this sample. SEM micrographs of mixed-oxides samples give evidence about the existence of two different phases, and about more or less pronounced homogeneous mixing of related components. The forming of spherical particles is visible in the case of both niobia mixed with ceria and niobia mixed with titania (Fig. 5b and 5c); while it seems that zirconia particles have rectangular shapes (5d). Higher uniformity explains the higher BET surface area found for $\text{Nb}_2\text{O}_5\text{-ZrO}_2$ and for $\text{Nb}_2\text{O}_5\text{-TiO}_2$, in comparison with pure niobia. Although the BET surface area of $\text{Nb}_2\text{O}_5\text{-CeO}_2$ is the same as this one found for pure niobia, this material expresses pretty high mixing of rectangular (niobia) and spherical (ceria) particles (Fig. 5b).

Raman spectra of investigated oxide systems are reported in Fig. 6. For each sample, the spectra were recorded at several points and no shift in the band position or difference of width

was noted. This observation shows clearly that investigated samples are homogeneous. The spectrum of pure niobia is dominated by a broad band at 676 cm^{-1} , which is typical for all niobium oxides and is assigned to the vibrations of Nb–O–Nb bridges from slightly distorted octahedral NbO_6 connected with sharing corners [34, 35]. The weak band around 850 cm^{-1} can be assigned to the symmetric stretching mode of Nb=O surface species, this kind of bond being present in highly distorted octahedral NbO_6 structures. Raman band between 150 and 300 cm^{-1} is due to the bending modes of Nb–O–Nb linkages [34, 36].

Evidently, the spectrum of Nb_2O_5 - CeO_2 mixed oxide sample is dominated by the typical features of parent materials. The sharp peak at 459 cm^{-1} is assigned to F_{2g} mode due to symmetrical stretching of Ce–O vibrational unit in eightfold coordination [37]. Low intensity band at 600 cm^{-1} , which is usually recorded for pure cerium oxide, is covered by the peak of higher intensity of Nb_2O_5 , and its presence cannot be unequivocally confirmed. It is known from the literature that a band recorded at 600 cm^{-1} is associated with oxygen vacancies in the CeO_{2-x} lattice, and that these sites might be active in combustion reactions [37, 38]. Furthermore, it is easy to see that the bands assigned to niobia are lower in intensity when compared to pure Nb_2O_5 sample.

The spectrum of Nb_2O_5 - TiO_2 is dominated by a broad band located around 635 cm^{-1} , which is formed by overlapping of the peak at similar positions already assigned to niobia, and E_g mode that is attributed to titania in anatase phase [39]. Band at 850 cm^{-1} , characteristic for Nb_2O_5 , is also present. No other peaks that are usually observed for titania phases were found. In the spectrum of Nb_2O_5 – ZrO_2 sample bands are present at 477, 639 and 850 cm^{-1} . The peaks at 477 and 639 cm^{-1} can be attributed to monoclinic zirconia [40]. Furthermore, there are no bands that could be assigned to tetragonal ZrO_2 . It should be mentioned that the band at 639 cm^{-1} could also have a contribution of Nb_2O_5 peak. The band at 850 cm^{-1} is higher in intensity than in pure niobia, showing the increase of highly distorted octahedral NbO_6 structures.

It should be also mentioned here that the absence of any other Raman bands provides evidence that Nb_2O_5 is not forming any compound with other component oxides. Furthermore, broad bands, found for materials prepared in this work are characteristic of Raman scattering from amorphous structures [41].

3.3. Acid/base properties

The adsorption of probe molecules was used to investigate the acid–base character by calorimetry method. Adsorption calorimetry of NH_3 or SO_2 molecules allows precise

determination of concentration and strength distribution of surface active sites (basic or acidic).

Table 2 compiles the data obtained from microcalorimetric measurements of SO₂ and NH₃ adsorption on all investigated samples. The total amounts of adsorbed gases and the amounts of irreversibly adsorbed (chemisorbed) gases are given in Table 2. As the investigated samples display noticeable differences in BET surface areas (Table 1), the calorimetric results are presented in mol/m² rather than in mol g⁻¹. The vertical parts of the isotherms correspond to irreversible adsorption, whereas the horizontal parts can be assigned to reversible adsorption.

Fig. 7 presents the isotherms obtained for SO₂ adsorption on the investigated samples. It can be concluded from the results presented in Table 2 and in Fig. 7 that the type of transition metal oxide added to niobia has a decisive role for a basic character of investigated mixed oxides. The highest adsorption of SO₂ is found on Nb₂O₅-CeO₂ mixed oxide sample, while the lowest was on Nb₂O₅ catalyst. In the case of Nb₂O₅-TiO₂ and Nb₂O₅-ZrO₂, values are slightly higher, but comparable with those obtained for pure niobia.

The volumetric data obtained for NH₃ adsorption are also summarized in Table 2, whereas the isotherms of ammonia adsorption are shown in Fig. 8. It is evident that addition of titania increased the number of acidic sites, while mixing niobia with ceria and zirconia decreased their amount.

Fig. 9 displays differential heats of SO₂ (right) and NH₃ (left) adsorption on the investigated samples. The profiles of differential heats vs. uptake of the gas probe are multi-indicative; they provide data concerning the amount, strength, and strength distribution of the active sites. Besides, the values of initial heats of adsorption characterize the strongest sites active for adsorption. Among the investigated samples Nb₂O₅-CeO₂ adsorbed both NH₃ and SO₂, what is a clear indication of its amphoteric character, while other samples showed prominent acidic character. Evidently mixing niobia with other oxides increased the basic character of thus obtained materials and this effect is highest in the case of ceria. If about acidic sites the addition of zirconia to Nb₂O₅ increased the acidic character while the distribution of acidic sites is only slightly affected. Nb₂O₅-ZrO₂ sample displays similar curve of differential heats vs. surface coverage as that of pure niobium oxide. Nb₂O₅-TiO₂ shows the same acidity as Nb₂O₅ for lower coverage, while for higher coverage shows acidic sites of higher strength. It should also be noticed that all differential heats of adsorption profiles showed continuous decreases with increasing surface coverage; what was found for both probe molecules and for all investigated materials; what is a clear evidence of surface active sites heterogeneity.

3.4. Catalytic activity

As already explained in Section 2, the changes in concentrations of reactants and products in fructose dehydration reaction were monitored by ^1H liquid NMR technique. Product of major interest in fructose dehydration reaction, 5-HMF, was identified through the lines at 6.5, 7.4 and 9.3 ppm. Levulinic (LA) and formic (FA) acid, possible products of fructose dehydration were identified by the lines at 2.1 and 8.1 ppm respectively.

All investigated materials appear active in dehydration of fructose to 5-HMF. Fig. 10 shows the trend of fructose conversion as a function of reaction time. Maximum conversion of fructose after 10 h of reaction was 87 % on Nb_2O_5 , while minimum of conversion, 71 %, was found for $\text{Nb}_2\text{O}_5\text{-CeO}_2$ sample. Evidently, at the beginning of the reaction conversion of fructose is highest on the $\text{Nb}_2\text{O}_5\text{-TiO}_2$ (3h), the sample that has the highest number of acidic sites on its surface (Table 2). After the 4th hour the conversion is highest and of similar value on Nb_2O_5 and $\text{Nb}_2\text{O}_5\text{-ZrO}_2$ catalysts. These materials also possess similar number of acidic sites (Table 2). This behavior might be caused by deactivation of most active sites for fructose conversion on $\text{Nb}_2\text{O}_5\text{-TiO}_2$ mixed oxide.

Fig. 11 presents selectivity to 5-HMF as a function of reaction time on materials investigated in this work. Highest selectivity overall was observed on $\text{Nb}_2\text{O}_5\text{-TiO}_2$ (mol 39 %) at the 7th hour of reaction. For pure Nb_2O_5 and $\text{Nb}_2\text{O}_5\text{-ZrO}_2$ catalysts best selectivity to 5-hydroxymethylfurfural was after 6th hour of reaction; 36 and 32 % respectively. After this peak, the selectivity for these samples is getting lower, and is followed by the increase in the yield of LA (Fig. 12). Decrease in 5-HMF selectivity with reaction time was already reported in the cases where this reaction is performed in batch catalytic systems [42]. On the other hand, constant increase in 5-HMF selectivity was observed on $\text{Nb}_2\text{O}_5\text{-CeO}_2$ sample, and levulinic acid is appearing only after 8th hours of reaction. It should also be mentioned here that quantifiable amount of FA was only found when pure niobia was used as catalyst, and selectivity was 4 % at the 10th hour of fructose dehydration reaction.

It is known from the literature that LA and FA are formed by rehydration of 5-HMF on the acidic sites [42, 43]. Evidently, when using batch catalytic system wanted products of the reaction are spending more time in the presence of strong acid sites undergoing further chemical transformations and reducing selectivity, in this case of 5-HMF [42-45]. Furthermore, results presented in this work show that adjusting the acidity, i.e. reducing the number of acid sites, slows down these consecutive reactions, constantly increasing the selectivity to 5-HMF, as in the case of $\text{Nb}_2\text{O}_5\text{-CeO}_2$ catalyst.

4. Conclusions

Well ordered mesoporous Nb₂O₅-MeO₂ (Me = Ti, Zr, Ce) mixed oxides were successfully prepared by evaporation-induced self-assembly (EISA) method. Formation of mesoporous structure was confirmed by the results of XRD and BET techniques. Acidic-basic properties of synthesized materials proved to be dependent on the nature of the oxide that was mixed with niobia. Among the investigated mixed oxide formulations only Nb₂O₅-CeO₂ was amphoteric, while the other samples showed prominent acidic character.

All oxides investigated here were active in fructose dehydration reaction. The activity and selectivity to desired product were found to be dependent on the amount of strong acid sites present on the surface of the catalyst. Furthermore, presence of the basic sites on the surface of the catalyst decreases the activity in the fructose dehydration reaction, as in the case of Nb₂O₅-CeO₂ sample.

Acknowledgments

French National Research Agency (ANR-09-CP2D-19) is greatly acknowledged for financial support. Special thanks are addressed to the technical services of IRCELYON (Institut de Recherches sur la Catalyse et l'Environnement de Lyon) for valuable technical contributions in Raman, XRD, BET, and chemical analysis.

References

- [1] C.T. Kresge, M.E. Leonowicz, W.J. Roth, J.C. Vartuli, J.S. Beck, *Nature* 359 (1992) 710.
- [2] J.S. Beck, J.C. Vartuli, W.J. Roth, M.E. Leonowicz, C.T. Kresge, K.D. Schmitt, C.T.W. Chu, D.H. Olson, E.W. Sheppard, S.B. Mccullen, J.B. Higgins, J.C. Schlenker, *J. Am. Chem. Soc.* 114 (1992) 10834.
- [3] Y. Ma, W. Tong, H. Zhou, S.L. Suib, *Micropor. Mesopor. Mater.* 37 (2000) 243.
- [4] A.K. Cheetham, G. Ferey, T. Loiseau, *Angew. Chem. Int. Ed.* 38 (1999) 3269.
- [5] K. Nakajima, T. Fukui, H. Kato, M. Kitano, J. N. Kondo, S. Hayashi, M. Hara, *Chem. Mater.* 22 (2010) 3332.
- [6] A. Corma, *Chem. Rev.* 97 (1997) 2373.
- [7] U. Ciesla, F. Schüth, *Micropor. Mesopor. Mat.* 27 (1999) 131.
- [8] J. Y. Ying, C. P. Mehnert, M. S. Wong, *Angew. Chem., Int. Ed.* 38 (1999) 56.
- [9] M. Linden, S. Schacht, F. Schüth, A. Steel, K. K. Unger, *J. Porous Mater.* 5 (1998) 177.
- [10] C. Yue, M.L. Trudeau, D.M. Antonelli, *Chem. Commun.* (2006) 1918.
- [11] C. Yue, M.L. Trudeau, D.M. Antonelli, *Can. J. Chem.* 83 (2005) 308.
- [12] K. Tanabe, *Catal. Today* 8 (1990) 1.
- [13] K. Tanabe, S. Okazaki, *Appl. Catal. A* 133 (1995) 191.
- [14] K. Tanabe, *Catal. Today* 78 (2003) 65.
- [15] T. Okuhara, *Chem. Rev.* 102 (2002) 3641.
- [16] C. Carlini, M. Giuttari, A.M. Raspolli Galletti, G. Sbrana, T. Armaroli, G. Busca, *Appl. Catal. A* 183 (1999) 295.
- [17] T. Armaroli, G. Busca, C. Carlini, M. Giuttari, A.M. Raspolli Galletti, G. Sbrana, *J. Mol. Catal. A* 151 (2000) 233.
- [18] V. Bolis, G. Cerrato, G. Magnacca, C. Morterra, *Thermochimica Acta* 312 (1998) 63.
- [19] Z. Luan, J.A. Fournier, *Microporous and Mesoporous Materials* 79 (2005) 235.
- [20] G. Busca, H. Saussey, O. Saur, J.C. Lavalley, V. Lorenzelli, *Applied Catalysis* 14 (1985) 245.
- [21] L. Ferretto, A. Glisenti, *Chem. Mater.* 15 (2003) 1181.
- [22] K. Hadjiivanov, D. G. Klissurski, *Shem. Soc. Rev.* 25 (1996) 61.
- [23] P.D.L. Mercera, J.G. van Ommen, E.B.M. Doesburg, A.J. Burggraaf, J.R.H. Ross, *Appl. Catal.* 71 (1991) 363.
- [24] S. Damyanova, J.M.C. Bueno, *Appl. Catal. A* 253 (2003) 135.
- [25] T. Ozaki, T. Masui, K.-I. Machida, G.-Y. Adachi, T. Sakata, H. Mori, *Chem. Mater.* 12 (2000) 643.

- [26] Y. Roman-Leshkov, C.J. Barret, Z.Y. Liu, J.A. Dumesic, *Nature* 447 (2007) 982.
- [27] P. Yang, D. Zhao, D. I. Margolese, B. F. Chmelka, G. D. Stucky, *Chem. Mater.* 11 (1999) 2813.
- [28] T. Katou, D. Lu, J. N. Kondo, K. Domen, *J. Mater. Chem.* 12 (2002) 1480.
- [29] A. Auroux, *Top. Catal.* 4 (1997) 71.
- [30] K. S. W. Sing, D. H. Everett, R. A. W. Haul, L. Moscou, R. A. Pierotti, J. Rouquerol, T. Siemieniewska, *Pure Appl. Chem.* 57 (1985) 603.
- [31] K. Nakajima, D. Lu, M. Hara, K. Domen, J. N. Kondo, in: J. Čejka, N. Žilková, P. Nachtigall (Eds.), *Molecular Sieves: From Basic Research to Industrial Applications, Part 2*, ELSEVIER B. V., Amsterdam, 2005, pp. 1477-1484.
- [32] H.-P. Lina, Y.-H. Liu, C.-Y. Moub, in: Z. Tang, P. Sheng, (Eds.), *Nano Science and Technology: Novel Structures and Phenomena*, Taylor & Francis, London, 2003, pp. 214-217.
- [33] B. Lee, D. Lu, J. N. Kondo, K. Domen, *Chem. Commun.* (2001) 2118.
- [34] J.-M. Jehng, I.E. Wachs, *Chem. Mater.* 3 (1991) 100.
- [35] A.A. McConnel, J.S. Anderson, C.N.R. Rao, *Spectrochim. Acta A* 23 (1976) 1067.
- [36] X. Gao, S.R. Bare, B.M. Weckhuysen, I.E. Wachs, *J. Phys. Chem. B* 102 (1998) 10842.
- [37] B. Reddy, A. Khan, Y. Yamada, T. Kobayashi, S. Loridant, J.-C. Volta, *J. Phys. Chem. B* 107 (2003) 11475.
- [38] A. Matinez-Arias, M. Fernández-Garcia, L.N. Salamanca, R.X. Valenzuela, J.C. Conesa, J. Soria, *J. Phys. Chem. B* 104 (2000) 4038.
- [39] H. Yoshitake, D. Abe. *Micropor. Mesopor. Mater.* 119 (2009) 267–275.
- [40] T. Remier, D. Spielbauer, M. Hunger, G.A.H. Mekhemer, H. Knozinger, *J. Chem. Soc., Chem. Commun.* (1994) 1181.
- [41] B.M. Reddy, A. Khan, *Catal. Surv. Asia* 9 (2005) 155.
- [42] H.E. Van Dam, A.P.G. Kieboom, H. Van Bekkum, *Starch/Stärke* 38 (1986) 95.
- [43] L. Peng, L. Lin, J. Zhang, J. Zhuang, B. Zhang, Y. Gong, *Molecules* 15 (2010) 5258.
- [44] T.S. Hansen, J.M. Woodley, A. Riisager, *Carbohydr. Res.* 344 (2009) 2568.
- [45] F. Yang, Q. Liu, X. Bai, Y. Du, *Bioresour. Technol.* 102 (2011) 3424.

Figure captions

Fig. 1. TG profiles obtained for uncalcined investigated samples.

Fig. 2. N₂ adsorption–desorption isotherms and BJH pore size distributions (inset) of different samples: a) pure Nb₂O₅, b) Nb₂O₅-TiO₂, c) Nb₂O₅-ZrO₂ and d) Nb₂O₅-CeO₂.

Fig. 3. LAXRD patterns of investigated samples.

Fig. 4. WAXRD patterns of investigated samples.

Fig. 5. SEM images of investigated samples. a) Nb₂O₅, b) Nb₂O₅-CeO₂, c) Nb₂O₅-TiO₂, d) Nb₂O₅-ZrO₂.

Fig. 6. Raman spectra of studied samples.

Fig. 7. Volumetric isotherms of SO₂ adsorption on investigated materials.

Fig. 8. Volumetric isotherms of NH₃ adsorption on investigated materials.

Fig. 9. Differential heats of NH₃ and SO₂ adsorption as a function of surface coverage.

Fig. 10. Fructose conversion as a function of reaction time on investigated materials.

Fig. 11. Selectivity to 5-HMF as a function of reaction time.

Fig. 12. Selectivity to LA as a function of reaction time.

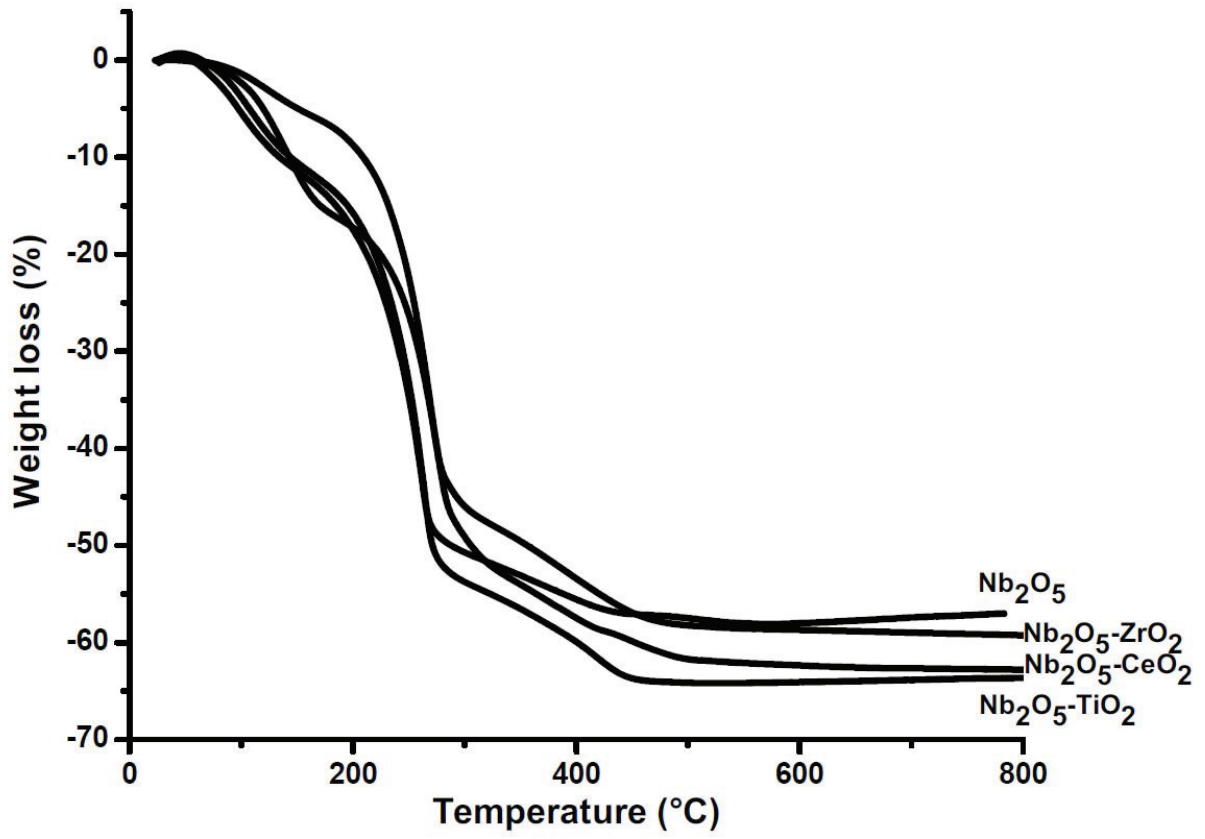


Fig. 1. TG profiles obtained for uncalcined investigated samples.

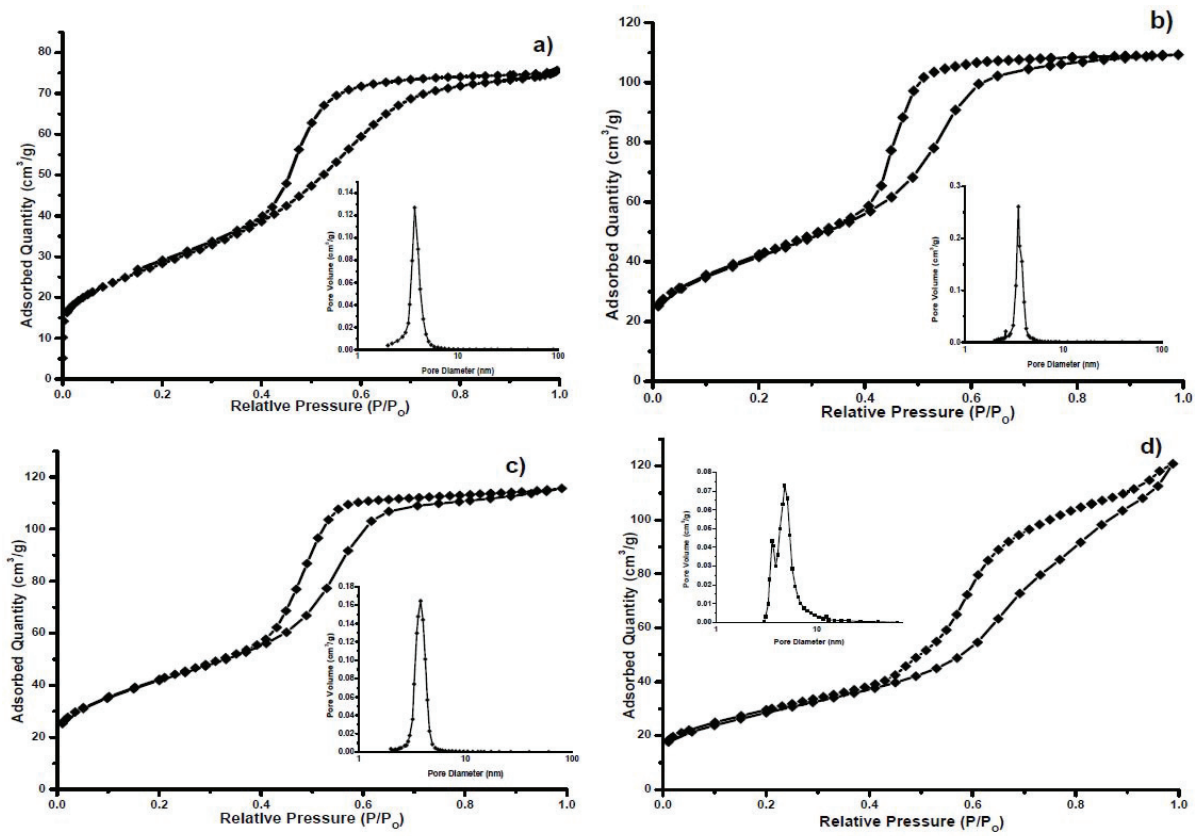


Fig. 2. N₂ adsorption–desorption isotherms and BJH pore size distributions (inset) of different samples: a) pure Nb₂O₅, b) Nb₂O₅-TiO₂, c) Nb₂O₅-ZrO₂ and d) Nb₂O₅-CeO₂.

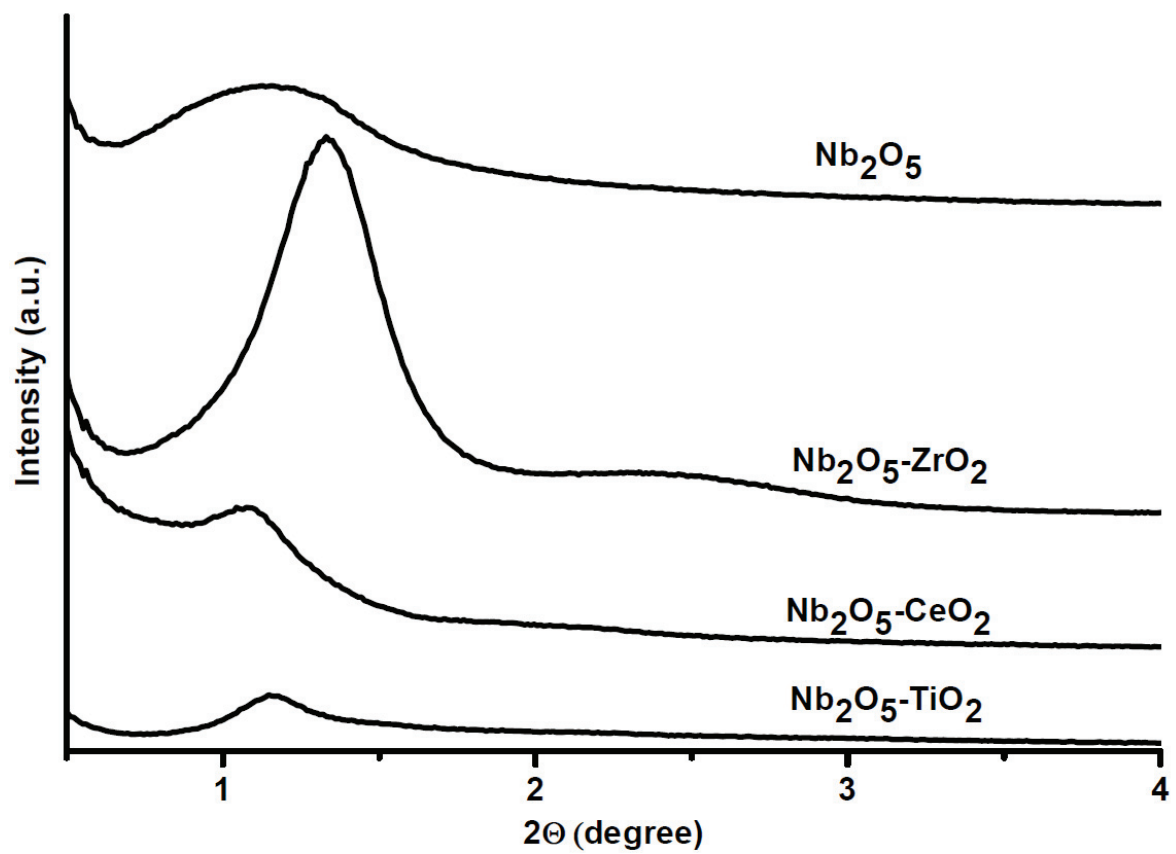


Fig. 3. LAXRD patterns of investigated samples.

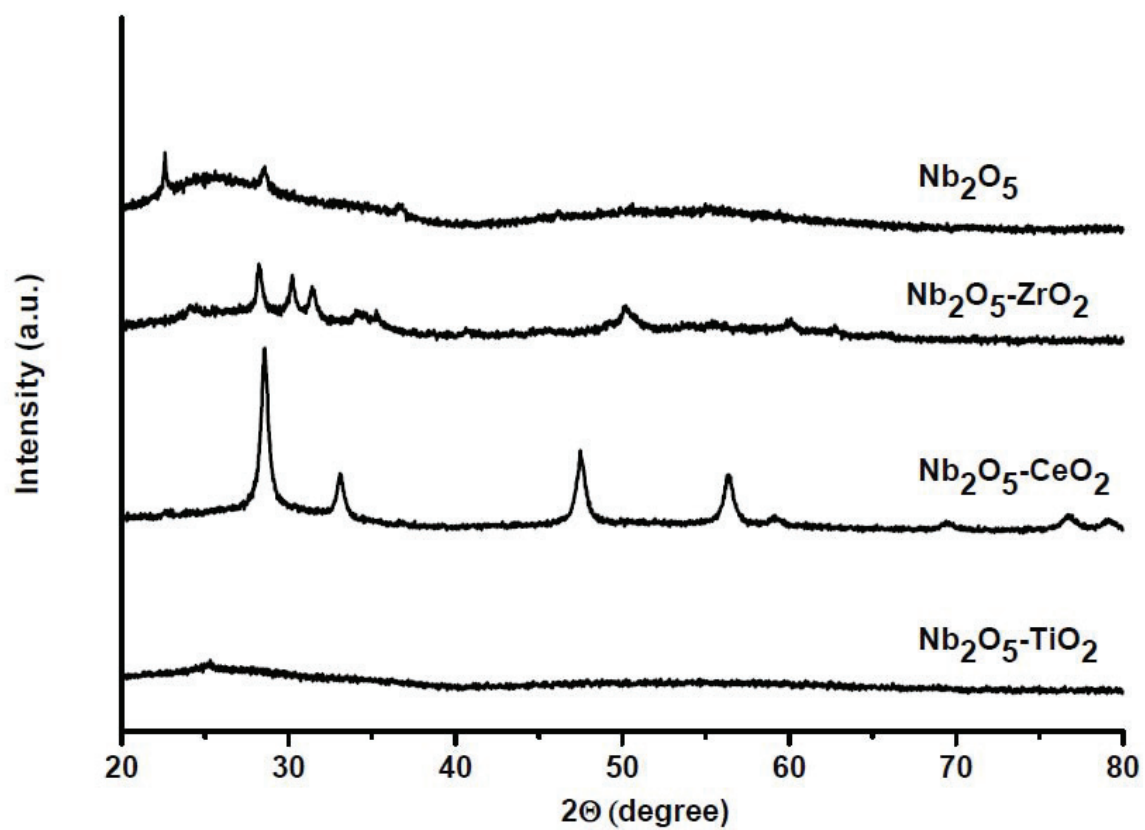


Fig. 4. WAXRD patterns of investigated samples.

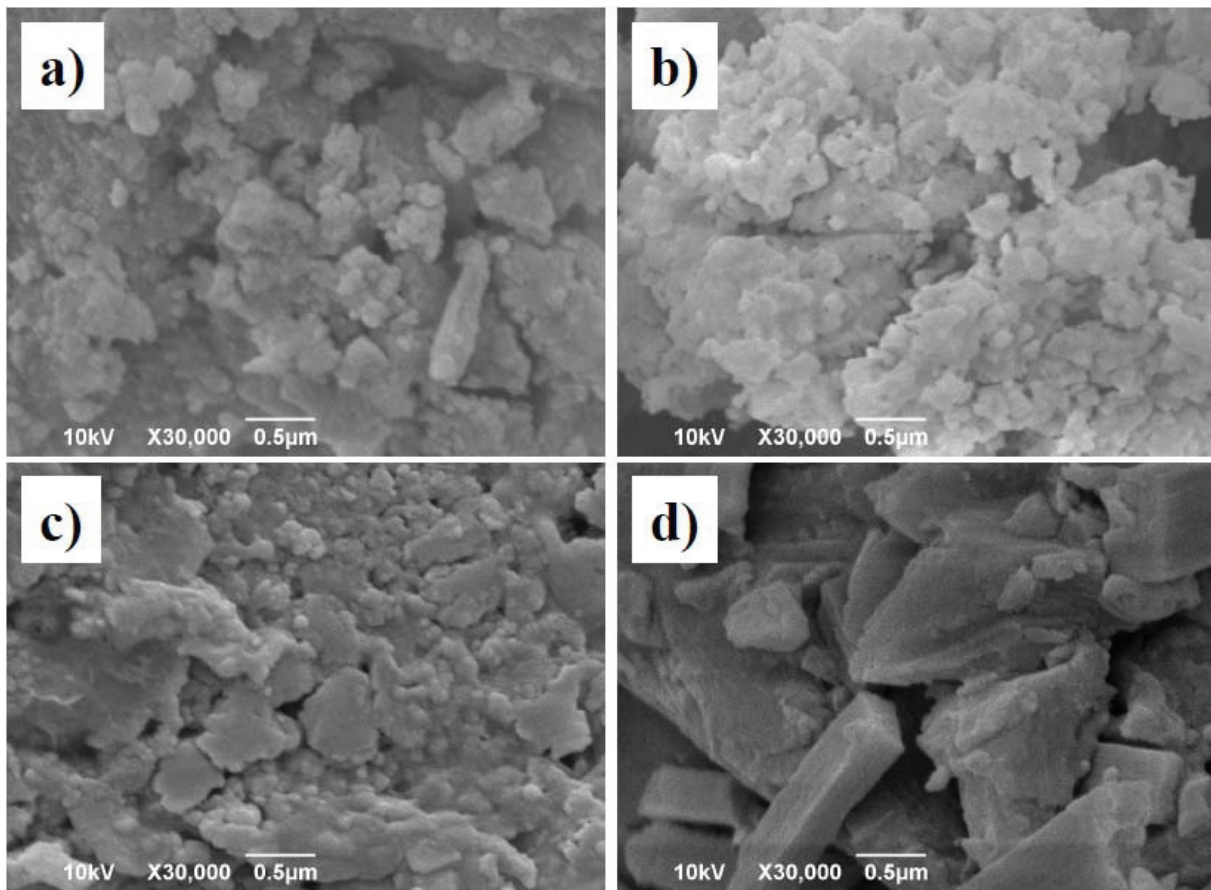


Fig. 5. SEM images of investigated samples. a) Nb_2O_5 , b) $\text{Nb}_2\text{O}_5\text{-CeO}_2$, c) $\text{Nb}_2\text{O}_5\text{-TiO}_2$, d) $\text{Nb}_2\text{O}_5\text{-ZrO}_2$.

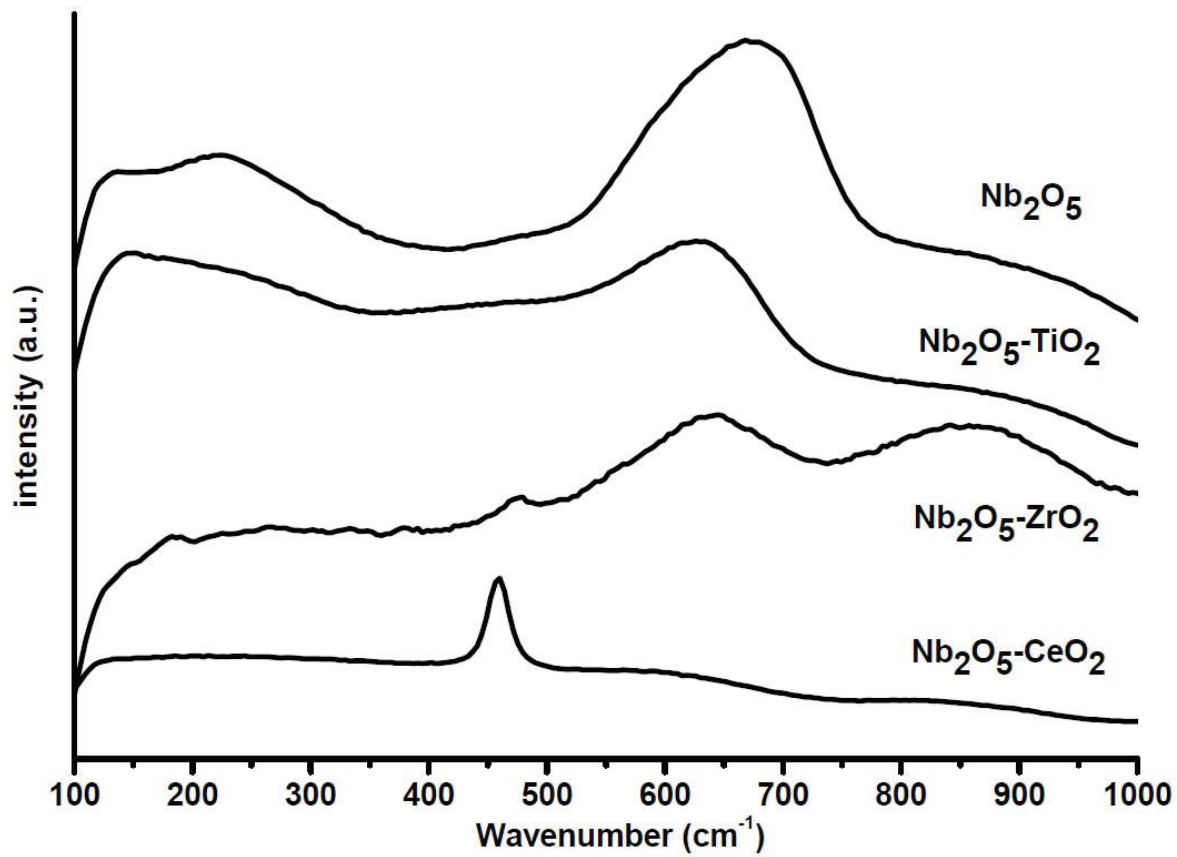


Fig. 6. Raman spectra of studied samples.

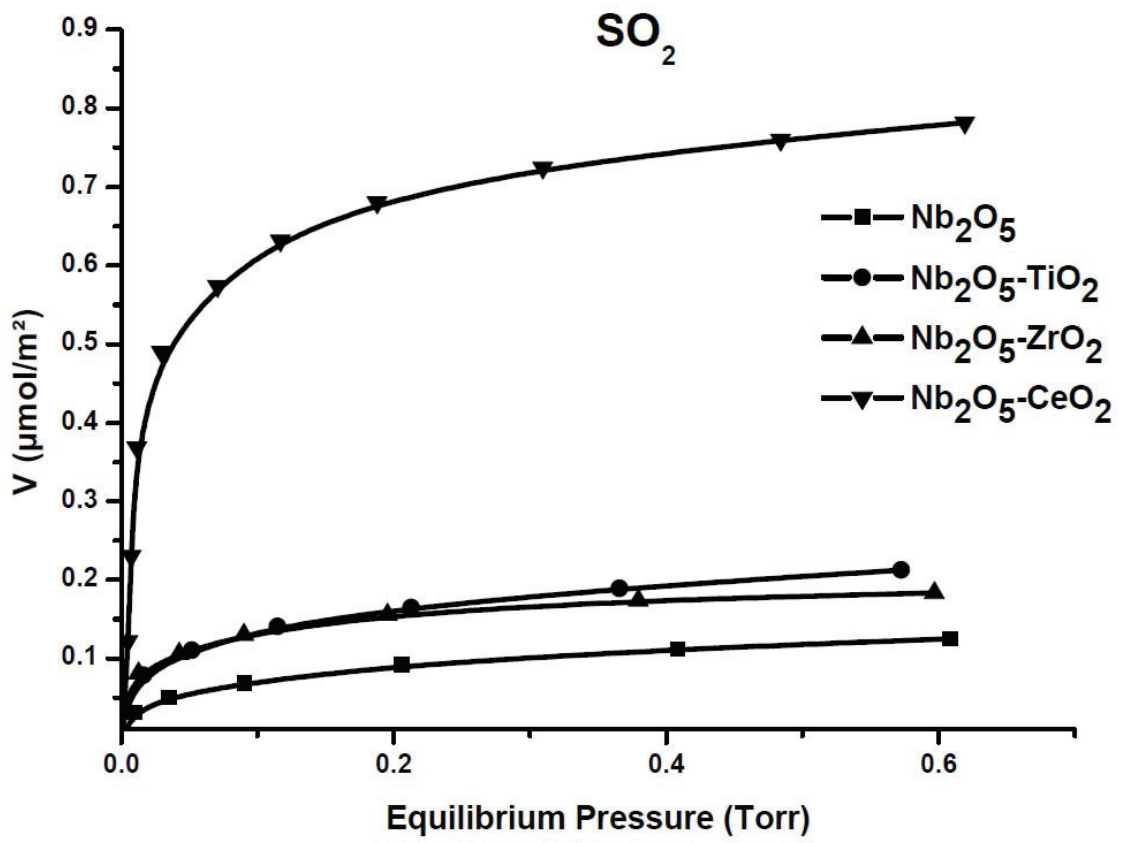


Fig. 7. Volumetric isotherms of SO₂ adsorption on investigated materials.

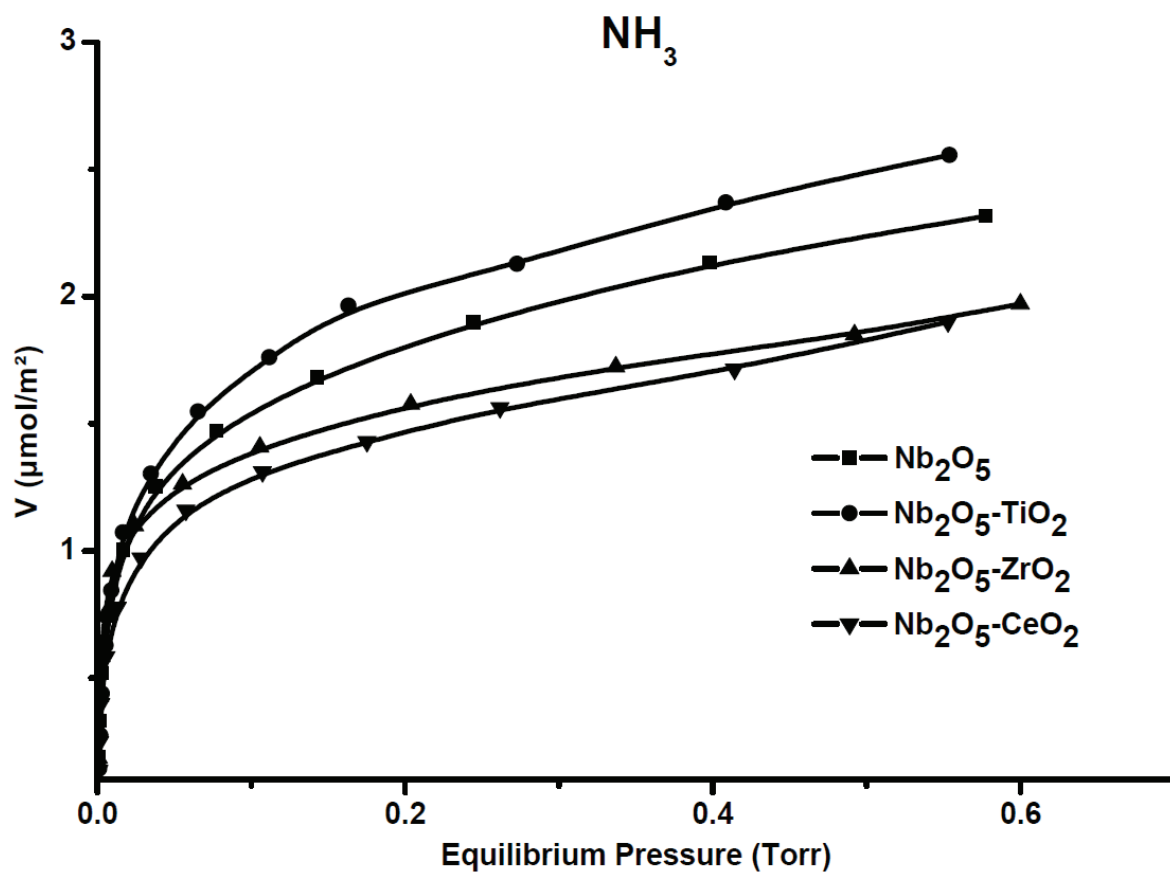


Fig. 8. Volumetric isotherms of NH_3 adsorption on investigated materials.

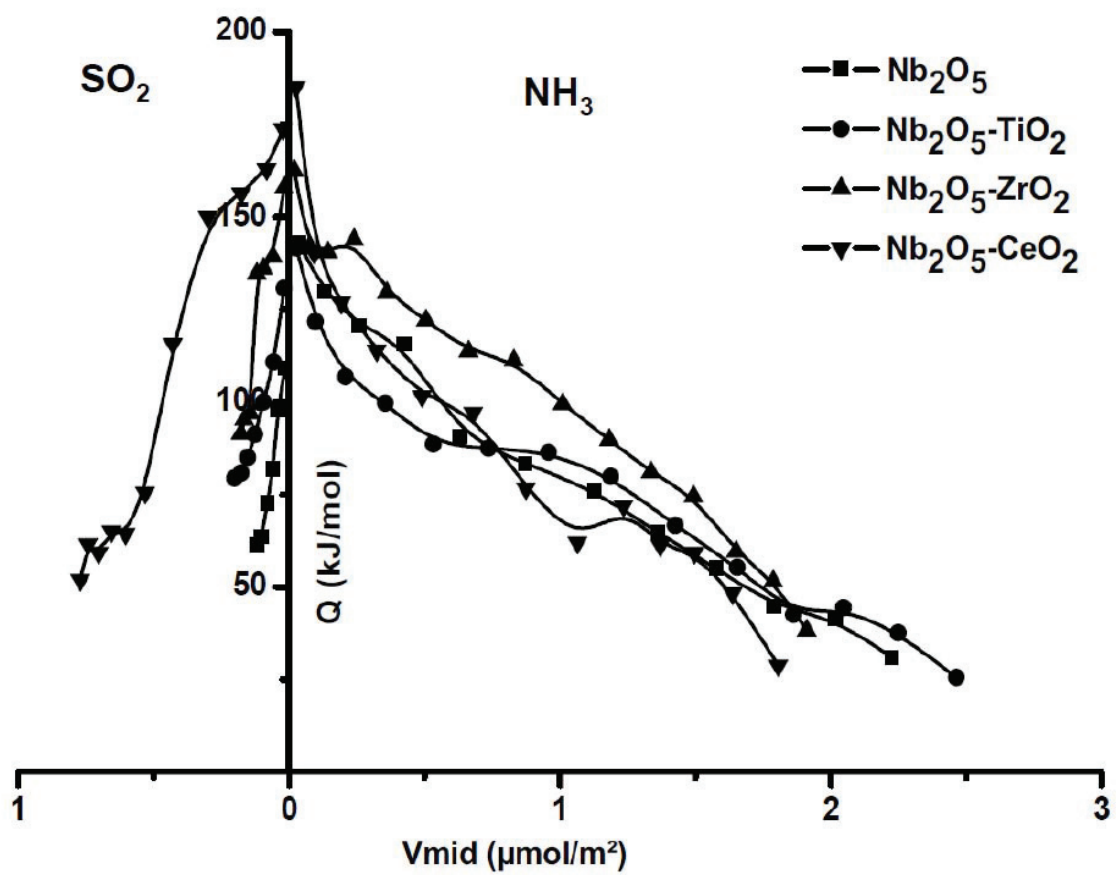


Fig. 9. Differential heats of NH_3 and SO_2 adsorption as a function of surface coverage.

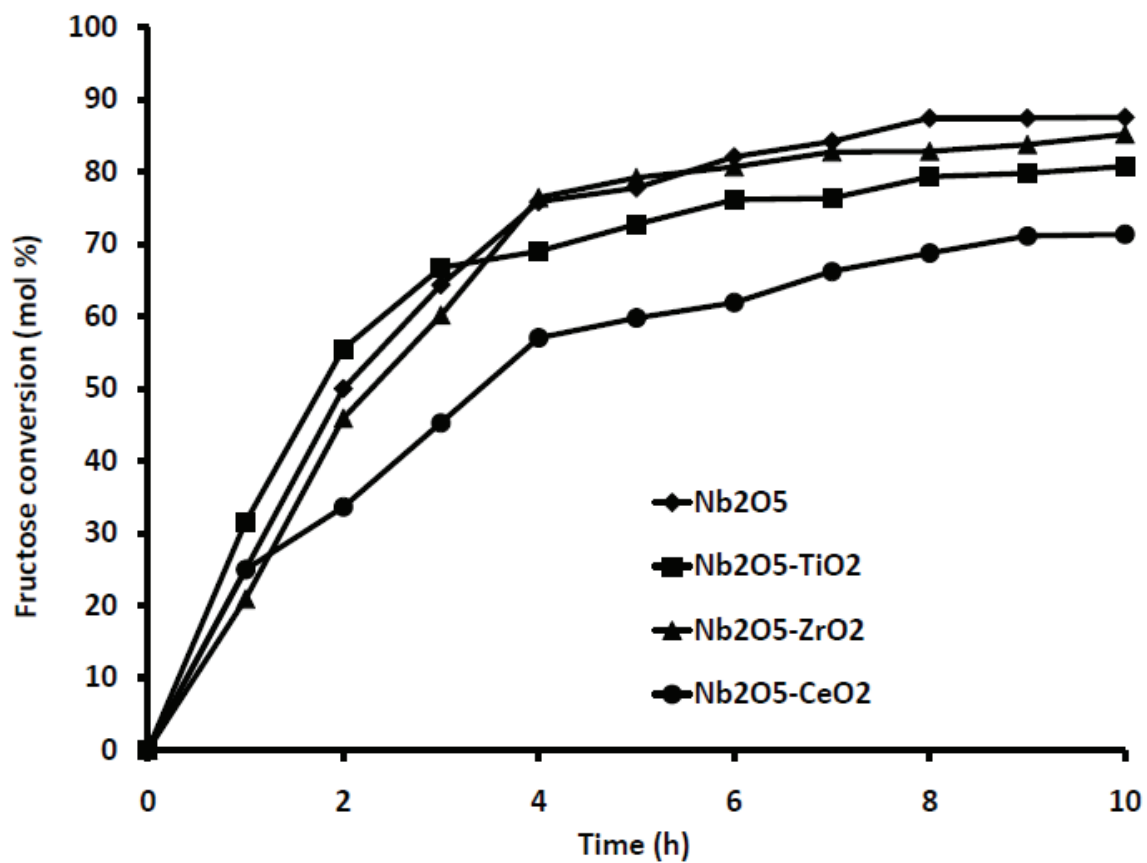


Fig. 10. Fructose conversion as a function of reaction time on investigated materials.

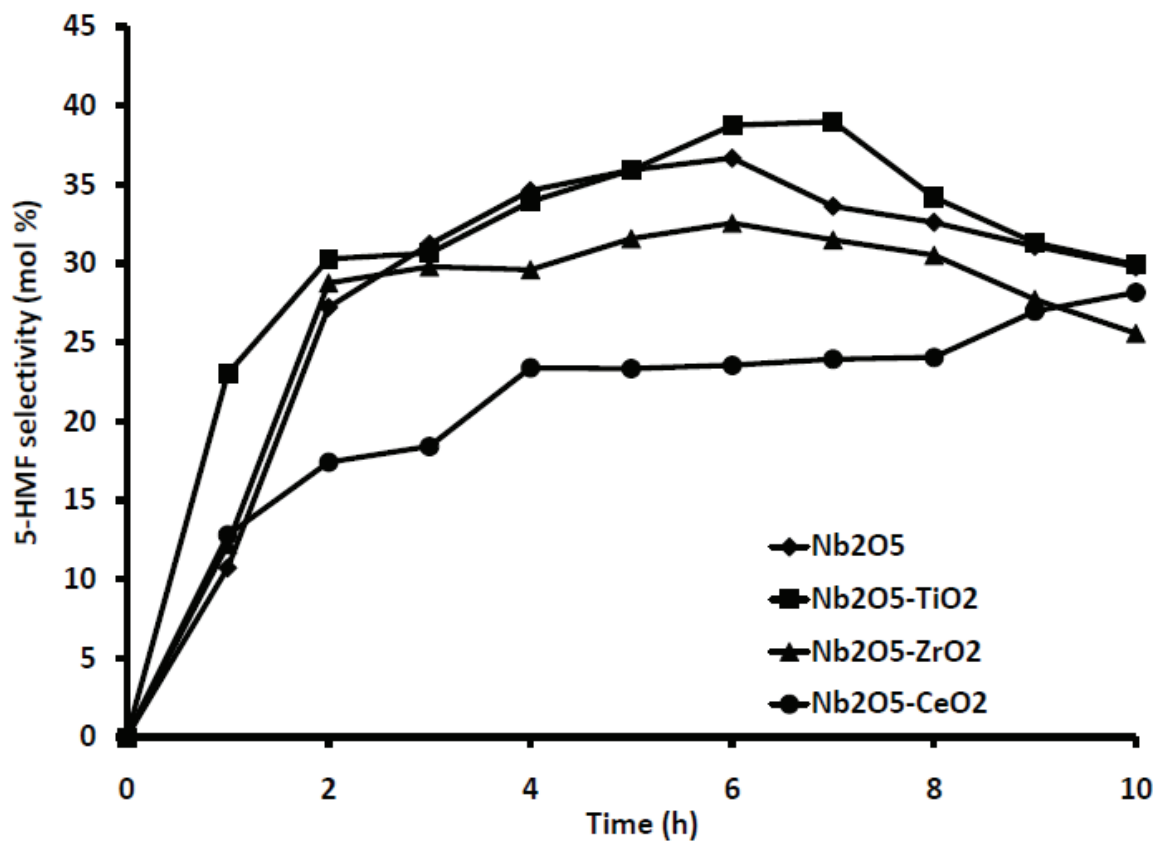


Fig. 11. Selectivity to 5-HMF as a function of reaction time.

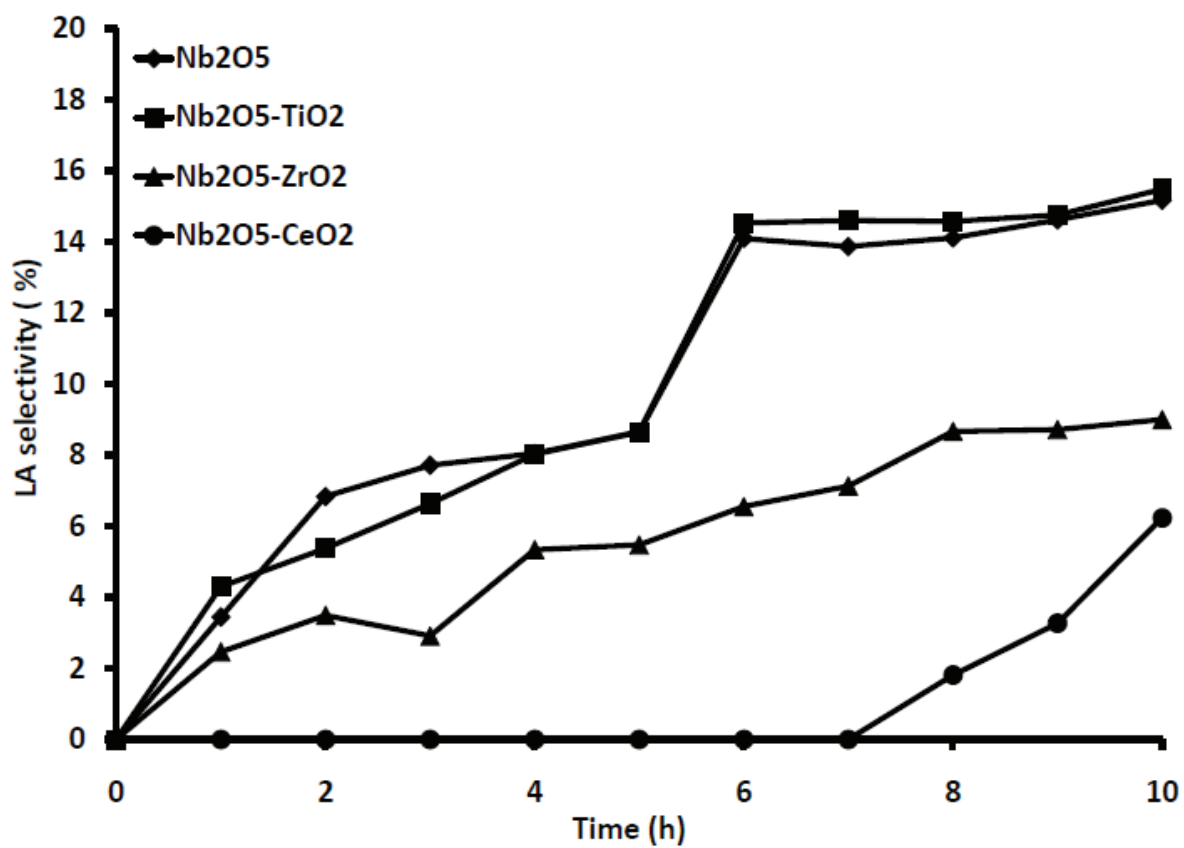


Fig. 12. Selectivity to LA as a function of reaction time.

Table 1. Chemical composition and structural properties of mesoporous mixed oxides catalysts.

Sample	S_{BET} ($\text{m}^2 \text{g}^{-1}$)	Mesopore volume (ml g^{-1})	Mesopore size (nm)	d_{100} (nm)	Wall thickness (nm)	CA %			
						Nb_2O_5	ZrO_2	CeO_2	TiO_2
Nb_2O_5	103	0.12	3.8	7.8	5.2	/	/	/	/
Nb_2O_5 - ZrO_2	151	0.18	3.9	6.6	3.7	53.3	43.2	/	/
Nb_2O_5 - CeO_2	103	0.19	5.7	8.2	3.7	50.2	/	46.0	/
Nb_2O_5 - TiO_2	151	0.17	3.5	7.6	5.3	42.4	/	/	54.9

Table 2. V_{irr} and V_{tot} calculated from adsorption isotherms of SO_2 and NH_3 on the different materials.

Sample	SO_2 adsorbed amount		NH_3 adsorbed amount	
	V_{total}^a ($\mu\text{mol}/\text{m}^2$)	V_{irrev}^b ($\mu\text{mol}/\text{m}^2$)	V_{total}^a ($\mu\text{mol}/\text{m}^2$)	V_{irrev}^b ($\mu\text{mol}/\text{m}^2$)
Nb_2O_5	0.08	0.05	1.69	1.01
Nb_2O_5 - ZrO_2	0.14	0.10	1.65	0.96
Nb_2O_5 - CeO_2	0.66	0.55	1.40	0.72
Nb_2O_5 - TiO_2	0.15	0.09	1.92	1.40

^a Amount of NH_3 or SO_2 adsorbed under an equilibrium pressure of 0.2 Torr (27 Pa).

^b Amount of chemisorbed NH_3 or SO_2 under an equilibrium pressure of 0.2 Torr (27 Pa).

INFLUENCE OF THE DESILICATION PROCESS ON THE ACIDITY OF HZSM-5 ZEOLITE

Vladislav Rac^{1*}, *Vesna Rakić*¹, *Zoran Miladinović*², *Dušan Stošić*³, *Aline Auroux*³

¹Faculty of Agriculture, Department of Chemistry, University of Belgrade, Belgrade, Serbia

²Zoran Miladinović, Institute of General and Physical Chemistry, Belgrade, Serbia

³Institut de Recherches sur la Catalyse et l'Environnement de Lyon (IRCELYON), Villeurbanne, France

*Corresponding author: Tel: +381112615315; Nemanjina 6, 11080 Zemun, Belgrade, Serbia.

E-mail: vrac@ffh.bg.ac.rs

Abstract

Introduction of mesopore regions into initially micropore zeolite structures may increase the range of molecules the zeolite can potentially interact with and influence the conversion rates of catalyzed reactions. In recent years, a novel route for mesopore formation via silicon extraction by hydroxides has been proposed. In this work, the influence of the alkaline treatment on the acidity of zeolite ZSM-5 ($\text{SiO}_2/\text{Al}_2\text{O}_3 = 23, 50$ and 80) modified by desilication was investigated. A detailed microcalorimetric, volumetric and thermokinetic study was performed. The samples were characterized by X-ray diffraction, low temperature adsorption of nitrogen and solid-state ^{27}Al MAS NMR. The desilication process was shown to be Si/Al ratio dependant, with significant efficiency and almost full preservation of acid sites strength and distribution achieved for $\text{SiO}_2/\text{Al}_2\text{O}_3 = 50$ and 80 .

Keywords

Hierarchical ZSM-5, desilication, microcalorimetry, acidity

1. Introduction

Zeolites are microporous crystalline aluminosilicate materials well known for their catalytic and adsorptive activity and selectivity. They also possess high surface area, high thermal and chemical stability and as such they have found application in a great number of processes ranging from petrochemical industry to environmental separations [1,2]. The activity of zeolites is determined by their intrinsic acidity, of both Lewis and Bronsted nature, or by active species (mostly metal ions or oxides) that can be introduced into the zeolite

structure. Their selectivity is governed by the structure of the channels and/or cages which form the zeolitic frameworks, with micropores ranging from 3 to 15 Å [3]. However, the sole microporosity of zeolites, which plays a crucial role in their shape selectivity, can also be their biggest drawback [4,5]. Molecules with diameters larger than the framework pore openings are restricted from entering and approaching the active sites. This imposes significant limitations in terms of the range of reactions that can be efficiently catalyzed. Furthermore, even for molecules that readily enter the zeolite, the intracrystalline diffusion is often reduced which can influence the rate, conversion level and yield of certain catalytic process. It has been shown that, in a diffusion-controlled reaction, the effectiveness may correspond to less than 10% of the zeolite actually being used, compared to a situation with no diffusion limitations, just because of the mass transfer problem [5]. On the other hand, known mesoporous materials, such as MCM-41 and SBA-15, which do not exhibit the pore size constraint found for microporous zeolites, possess framework acidity much inferior to zeolites [6,7].

Introduction of mesopores into originally microporous zeolitic structures is one approach to obtaining the best of both worlds, i.e. creating materials with lower diffusion restrictions, which are able to host larger molecular species, while still retaining the desired acidity of the active sites within the structure [5,8]. Such microporous/mesoporous zeolites are called hierarchical, a term which designates a zeolitic material with at least one additional level of porosity besides the intrinsic micropore system. The development of mesoporosity can be achieved by both synthetic and post-synthetic routes. The synthetic methods are, however, not the scope of this paper [9,10,11]. Historically, the most widely used post-synthetic method for mesopore creation in zeolites was steaming combined with acid leaching [4]. In the past decade, a different route for post-synthetic mesopore formation in zeolitic material - desilication by alkaline treatment was proved to be the most promising one, in terms of simplicity and efficiency [12,13,14]. The method consists on silicon extraction by a base, usually sodium hydroxide, although the effects of weaker bases, such as organic ones, were investigated [15]. The desilication treatment was successfully applied to various zeolite families (MFI, MTW, BEA, FAU) [16,17,18,19]. Different structures, as well as zeolites that belong to the same zeolite family while having different silica to alumina ratios, exhibit distinct susceptibility to desilication and consequent mesopore formation. Several routes for fine tuning the process for a specific zeolite were proposed, the most important being the initial dealumination with either mild or strong acids, acid washing after the desilication and the use of pore directing agents [20].

One of the zeolites well investigated as a potential material for mesopore formation is ZSM-5. It was shown that ZSM-5 samples with various silica to alumina ratios can be desilicated to yield hierarchical frameworks with significant mesopore surface areas (more than 200 m²/g) and preserved microporous structures [21]. The resulting mesopore materials exhibit enhanced ability to host large molecular species and significantly higher catalytic activity when tested in reactions typical for ZSM-5 zeolite [22,23]. However, although hierarchical ZSM-5 have been otherwise thoroughly characterized, their acidity and the effect of the alkaline treatment on the nature, number and strength of the acid sites have not yet been investigated in details – only the results of TPD of ammonia and IR spectroscopy in the OH stretching region are available in literature [21]. In this work, we present quantitative microcalorimetric, volumetric and thermokinetic characterization of acid sites in three different mesoporous ZSM-5 zeolites (SiO₂/Al₂O₃ = 23, 50 and 80) and analyse the influence of the desilication process on their acidity.

2. Experimental

2.1 Materials

Commercial MFI type zeolites (HZSM-5) chosen for the desilication process were supplied by Zeolyst International. Samples characterized by three different silica to alumina ratios were used and denoted as Z_x, where Z and x mark ZSM-5 and silica to alumina ratio, respectively: Z23 (producer's code CBV 2314, SiO₂/Al₂O₃=23), Z50 (CBV 5524G, SiO₂/Al₂O₃=50) and Z80 (CBV 8014, SiO₂/Al₂O₃=80). Parent zeolite samples, designated as Z_xP were prepared by calcination in air at 773 K during 5 h, in order to obtain their hydrogen forms. Silicone extraction was performed using the alkaline treatment proposed by Groen *et al.*[16]. In a typical experiment, 5g of the ammonium form of a ZSM-5 sample was introduced to 150 ml of 0.2M NaOH solution at 363K and stirred for the duration of 30 minutes. The sample was then filtrated, thoroughly washed with deionized water until a neutral pH was reached and dried at 393 K overnight. Subsequently, an acid washing was performed using hydrochloric acid (0.1 M, 150 ml) for 6 h at room temperature. The samples were then filtered, washed and dried again. Following the acid treatment, the samples were converted to their ammonium forms by three-fold ion-exchange (0.1 M ammonium nitrate at 363 K during 1 hour). The resulting zeolitic materials were filtered, washed with deionized water, dried at 393 K and finally converted to hydrogen form by calcination in air at 773 K

for 5h. The obtained samples were coded ZxM , where x has the same meaning as in the names of the parent zeolites.

2.2 Methods

The crystallinity of parent and alkaline treated samples was checked by X-ray diffraction. Powder X-ray diffraction patterns were recorded on a Bruker (Siemens) 5005 diffractometer at room temperature using CuK_α radiation (0.154 nm) from $3 - 80 2\theta$ in a 0.02° steps with 1 s per step.

Nitrogen adsorption isotherms were measured at 77 K after pretreatment at 673 K for 4 h under vacuum. The total surface area was determined by the BET method, the total pore volume was obtained as the amount of nitrogen adsorbed at $p/p^0 = 0.99$, and the t-plot method was used to distinguish micropores from mesopores.

Solid-state ^{27}Al MAS NMR spectra were acquired on a Bruker MSL-400 (9.39 T) spectrometers upgraded with Apollo console (Tecmag, USA) operating at 104.27 MHz. MAS probes (7 mm) were used and the spinning speeds were 4.7 kHz. Single-pulse excitations of 2 μs were used for the ^{27}Al MAS NMR experiments. All the spectra were accumulated with a 3 s recycle time. Obtained chemical shift was determined in ppm relative to $\text{AlCl}_3 \cdot 6\text{H}_2\text{O}$ solution as an external standard.

Microcalorimetry – volumetry of ammonia adsorption was performed in order to obtain the distribution of strength of acidic sites within the samples. A heat-flow calorimeter of the Tian-Calvet type from Setaram, linked to a glass volumetric line was used and both thermal effects and volumetric isotherms were detected. A well-established stepwise procedure, previously fully described [24] was followed. Before the adsorption of ammonia the samples were pretreated under vacuum at 673 K overnight. Successive small doses of NH_3 were introduced onto the samples until a final equilibrium pressure of 66 Pa was achieved. The equilibrium pressure corresponding to each adsorbed amount was measured by means of a differential pressure gauge from Datametrics. During the experiment the calorimetric cell was maintained at 423 K. Differential heats of NH_3 adsorption were calculated based on the measured values of the evolved heat and the amount of ammonia adsorbed for each admitted dose of gas. Furthermore, after the completion of the adsorption experiment, the samples were pumped at 423 K and a secondary adsorption was carried out at the same temperature. The irreversibly chemisorbed amounts of ammonia (V_{irr}) were then calculated as the difference between the primary and the secondary isotherms. The kinetics of

heat release during ammonia adsorption was monitored by the thermokinetic parameter (τ). During the adsorption of a single dose of ammonia, the calorimetric signal first increases and, after reaching a maximum value, decreases exponentially with time. This decrease is expressed as $D=D_m e^{-t/\tau}$, where D and D_m are deviation at time t and the maximum deviation of the calorimetric signal, respectively [25]. The thermokinetic parameter was calculated as the inverse of the slope of the logarithm of the evolved heat curve during the return to equilibrium, for each dose of ammonia.

3. Results and discussion

The nitrogen adsorption isotherms (Figure 1) indicate that changes in the pore structure occurred after the alkaline treatment of all the investigated ZSM-5 samples. The total adsorbed amount of nitrogen increased and the shapes of the isotherms themselves had changed for the desilicated samples, compared to the corresponding parent zeolites. The increase of the total nitrogen amount adsorbed is very pronounced for the samples with $\text{SiO}_2/\text{Al}_2\text{O}_3$ ratio of 50 and 80 - a twofold and a more than twofold increase for Z80M and Z50M, respectively. In the case of Z23M, this increase is also present, but to a much smaller extent. Also, the resulting shapes of the nitrogen isotherms of the desilicated samples show a distinction between the ZSM-5 zeolite with $\text{SiO}_2/\text{Al}_2\text{O}_3 = 23$ and the samples with silica to alumina ratios of 50 and 80. The latter isotherms are of type IIb, with a steep slope at higher values of p/p^0 , and a H3 hysteresis, which is typical for materials containing slit-like mesopores [26], while the former exhibits a shape that could be described as an intermediate between type I and type IIb isotherms. All the isotherms of the parent samples are of the type I, typical for microporous materials, with H4 hysteresis which is, in the case of type I isotherm behaviour, also a sign of microporosity [27].

Fig. 1.

The observed difference in the pore structure changes among the samples with different silica to alumina ratios is also evident from the textural data presented in Table 1. Alkaline treatment resulted in increased BET surface and mesopore surface and volume for all the investigated samples. However, in the case of Z23, these effects are much less pronounced than for the other two samples. Mesopore formation was most effectively achieved in the Z50M sample, where mesopore surface increased from 65 to 173 m^2/g , and mesopore volume from 0.085 to 0.38 cm^3/g . Although the highest value of mesopore surface

was achieved for Z80M (212 m²/g), this is due to the significant S_{meso} of the parent Z80P sample, and the relative increase is the greatest for Z50M. It is important to emphasize that the microporous structure was not significantly affected by the treatment: only a slight decrease in the micropore volume was observed for all samples. These results are consistent with those found in literature [22].

The pore size distributions of all ZSM-5 samples are presented in Figure 2. Although all alkaline treated zeolites developed mesoporosity, there is a remarkable difference in the distribution of pore sizes between the three samples with different silica to alumina ratios. In the case of Z23M there is a fairly narrow peak at 7.5 nm, for Z50M the peak is broader and its center is shifted to 14 nm, while Z80M exhibits a very broad pore size distribution with no distinct peak center. In general, it seems that the mesopore distribution in figure 2 tends to broaden with increasing SiO₂/Al₂O₃ ratio.

Fig. 2.

XRD patterns, presented in Figure 3, show that all the investigated samples preserved their MFI structure. However, the alkaline treatment did influence the degree of crystallinity in the mesopore samples. The variations in crystallinity of the desilicated zeolites (table 1) was calculated based on the relative intensities of the reflection at 23° 2θ, taking the crystallinity of the parent sample to be 100%. The results indicate that the degree of crystallinity decreases with increasing mesoporosity. In fact, when crystallinity is plotted vs the relative increase of mesopore surface, a linear relationship is observed, with a R² of 0.98045 (graph not shown). This effect was also reported in literature and is explained by local Si extraction from the zeolite lattice without significant destruction of the framework, thus preserving long range ordering and microporous structure in the material [21].

Fig. 3.

Solid-state ²⁷Al MAS NMR spectra, presented in Figure 4, were recorded in order to investigate the influence of desilication treatment on the coordination state of Al in the zeolite samples. The obtained results indicate that the parent zeolites predominantly contain tetrahedral Al (peak at 54 ppm), which is attributed to framework aluminum. Some octahedrally coordinated Al (peak at 0 ppm), ascribed to extraframework species, is also found in the spectra of all parent samples, and the intensity of the corresponding peak decreases with the increase of silica to alumina ratio. Spectra of mesoporous samples show

that the alkaline treatment of samples with $\text{SiO}_2/\text{Al}_2\text{O}_3$ ratio of 50 and 80 did not result in significant extraframework Al buildup, while there is a noticeable increase of the peak at 0 ppm for Z23M. Also, a broadening of the band at 54 ppm is observed for Z23M, which is attributed to a partial reintegration of Al in the zeolite framework [28].

Fig. 4.

Microcalorimetric and volumetric investigations of ammonia adsorption were used to evaluate the effects of mesopore formation induced by the alkaline treatment on the acidity of the zeolitic materials. The obtained distributions of strength of the acidic sites, presented in Figure 5, support previously observed differences in susceptibility to mesopore creation via desilication between Z23 and the other two samples with higher silica to alumina ratios. Namely, the profiles of differential heats vs. ammonia uptake recorded for Z50M and Z80M and their corresponding parent samples indicate that the distributions of strength of the acidic sites did not change significantly after the alkaline treatment. The shapes of the calorimetric curves are similar for mesoporous and parent zeolites and the values of the differential heats of adsorption only slightly differ. However, in the case of the samples with $\text{SiO}_2/\text{Al}_2\text{O}_3 = 23$, it is obvious that the acidity of the zeolite was greatly altered by desilication. The shape of the calorimetric curve of Z23M differs markedly for the one obtained for Z23P, and the strengths of the existing acidic sites in Z23M are reduced, compared to the parent material, especially in the middle region of the curve which represents the heats released during adsorption on the predominant sites. The observed effects of alkaline treatment on the acidity of the investigated samples is also corroborated by the values of the irreversibly adsorbed amounts of ammonia. Table 2 summarizes measured V_{irr} as well as the differences of V_{irr} calculated for corresponding parent and mesoporous samples (denoted as ΔV_{irr}). From the presented data, it can be observed that the reduction of irreversibly adsorbed amount of ammonia, found in mesoporous samples, increases with decreasing silica to alumina ratio.

Fig. 5.

The changes in the zeolite samples structure were additionally investigated considering the thermokinetic parameter of ammonia adsorption (Figure 6) which is a measure of the time needed to reach the equilibrium state during the adsorption of a single dose of ammonia. It is generally considered [29] that lower values of the thermokinetic parameter arise from either irreversible adsorption on the strongest sites, giving short equilibrium times, or from fast exchange of molecules on weakest sites. Higher values are expected at surface coverages at

which the number of strong sites still available decreases, and a competition between strong and weak sites takes place: molecules firstly adsorbed on weak sites tend to migrate to the strong ones, causing the time to reach the equilibrium to grow longer. Also, accessibility of the adsorption sites and surface diffusion greatly influence the value of the thermokinetic parameter [25,30]. This factor is of importance in explaining the thermokinetic parameter differences between mesoporous and parent (microporous) samples with silica to alumina ratios of 50 and 80 investigated in this work. As mentioned earlier, the changes in the distribution of strength of the acidic sites brought upon by desilication are not pronounced, and yet the values of τ have decreased for Z50M and Z80M when compared to the parent material, especially in the region of lower coverages. These results indicate that the existence of mesopores enhances accessibility for the adsorbing molecules which results in shorter equilibrium times. In the case of Z23, however, it is very probable that the decrease of the values of the thermokinetic parameter is primarily due to the existence of much weaker sites in Z23M when compared to the Z23P. The largest change in the value of τ for Z23M starts at approximately 400 $\mu\text{mol/g}$, which is also the coverage at which the large drop in the differential heats of ammonia adsorption occurs.

Fig. 6.

4. Conclusions

Mesopore formation by alkaline treatment was achieved for ZSM-5 zeolites with $\text{SiO}_2/\text{Al}_2\text{O}_3 = 23, 50$ and 80. The desilication process was shown to depend on the silica to alumina ratio in terms of efficiency, resulting pore size distribution and acidity. The zeolite with the largest content of Al, Z23, proved to be the least susceptible to mesopore creation. Furthermore, the hydroxyde treatment of Z23 led to formation of extraframework Al deposits and substantial reduction of acidity. Samples with lower Al content yielded significant mesopore surfaces and preserved their original micropore structure.

The analysis of the results obtained by microcalorimetric investigation of ammonia adsorption enabled recognition of the differences between desilicated (mesoporous) and parent microporous zeolites. The distribution of strength of the acid sites in ZSM-5 zeolites with $\text{SiO}_2/\text{Al}_2\text{O}_3 = 50$ and 80 remained mostly unchanged by desilication process, while at the same time, the surface diffusion was improved, as indicated by the values of the thermokinetic parameter. Although Si/Al range dependant, the desilication process proved to

be an efficient route which can be used for mesopore introduction in ZSM-5 zeolite with preservation of framework active sites.

Acknowledgments

Serbian Ministry of Education and Science (Project 172018) is greatly acknowledged for financial support.

References

- [1] W. Vermeiren, J.P. Gilson, *Top. Catal.* 52 (2009) 1131–1161.
- [2] M. Panagiotis, *Micropor. Mesopor. Mater.* 144 (2011) 15–18.
- [3] C. R. Marcilly, *Top. Catal.* 13 (2000) 357–366.
- [4] S. van Donk, A.H. Janssen, J.H. Bitter, K.P. de Jong, *Catal. Rev. Sci. Eng.* 45 (2003) 297–319.
- [5] K. Egeblad, C.H. Christensen, M. Kustova, C.H. Christensen, *Chem. Mater.* 20 (2008) 946–960.
- [6] A. Corma, *Chem. Rev.* 97 (1997) 2373–2419.
- [7] A. Corma, M.S. Grande, V. Gonzalez-Alfaro, A.V. Orchillesy, *J. Catal.* 159 (1996) 375–382.
- [8] J. Perez-Ramirez, C.H. Christensen, K. Egeblad, C.H. Christensen, J.C. Groenef, *Chem. Soc. Rev.* 37 (2008) 2530–2542.
- [9] F.S. Xiao, L. Wang, C. Yin, K. Lin, Y. Di, J. Li, R. Xu, D.S. Su, R. Schlogl, T. Yokoi, T. Tatsumi, *Angew. Chem. Int. Ed.* 45 (2006) 3090–3093.
- [10] J. Zhao, Z. Hua, Z. Liu, Y. Li, L. Guo, W. Bu, X. Cui, M. Ruan, H. Chen, J. Shi, *Chem. Commun.* 48 (2009) 7578–7580.
- [11] R. Chal, T. Cacciaguerra, S. van Donk, C. Gérardin, *Chem. Commun.* 46 (2010) 7840–7842.
- [12] J.C. Groen, S. Abello, L.A. Villaescusa, J. Perez-Ramirez, *Micropor. and Mesopor. Mater.* 114 (2008) 93–102.
- [13] J.C. Groen, T. Bach, U. Ziese, A.M. Paulaime-van Donk, K.P. de Jong, J.A. Moulijn, J. Perez-Ramirez, *J. Am. Chem. Soc.* 127 (2005) 10792–10793.
- [14] J.C. Groen, W. Zhu, S. Brouwer, S.J. Huynink, F. Kapteijn, J.A. Moulijn, J. Perez-Ramirez, *J. Am. Chem. Soc.* 129 (2007) 355–360.
- [15] S. Abello, A. Bonilla, J. Perez-Ramirez, *Appl. Catal. A* 364 (2009) 191–198.
- [16] J.C. Groen, L.A.A. Peffer, J.A. Moulijn, J. Pérez-Ramirez, *Colloids Surf. A* 241 (2004) 53–58.
- [17] D. Verboekend, G. Vilé, J. Pérez-Ramírez, *Cryst. Growth Des.* 12 (2012) 3123–3132.
- [18] Z. Qin, B. Shen, X. Gao, F. Lin, B. Wang, C. Xu, *J. Catal.* 278 (2011) 266–275.
- [19] X. Wei, P.G. Smirniotis, *Micropor. Mesopor. Mater.* 97 (2006) 97–106.
- [20] D. Verboekend, G. Vilé, J. Pérez-Ramírez, *Adv. Funct. Mater.* 22 (2012) 916–928.

- [21] D. Verboekend, S. Mitchell, M. Milina, J.C. Groen, J. Perez-Ramirez, *J. Phys. Chem. C* 115 (2011) 14193–14203.
- [22] S. Mitchell, J. Pérez-Ramírez, *Catal. Today* 168 (2011) 28-37.
- [23] C. Fernandez, I. Stan, J.-P. Gilson, K. Thomas, A. Vicente, A. Bonilla, J. Perez-Ramirez, *Chem. Eur. J.* 16 (2010) 6224 – 6233.
- [24] S. Narayanan, A. Sultana, Q. Thinh Le, A. Auroux, *Appl. Catal. A* 168 (1998) 373-384.
- [25] A. Auroux, M. Huang, S. Kaliaguine, *Langmuir* 12 (1996) 4803-4807.
- [26] F. Rouquerol, J. Rouquerol, K. Sing, Adsorption by powders and porous solids, in: *Principles, Methodology and Applications*, Academic Press, London, 1999.
- [27] K.S.W. Sing, D.H. Everett, R.A.W. Haul, L. Moscou, R.A. Pierotti, J.Rouquerol, T. Siemieniewska, *Pure Appl. Chem.* 57 (1985) 603-619,.
- [28] D. Verboekend, J. Perez-Ramirez, *Chem. Eur. J.* 17 (2011) 1137 – 1147.
- [29] I. Ferino, R. Monaci, E. Rombi, V. Solinas, *J. Chem. Soc. Faraday Trans.* 94 (1998) 2647-2652.
- [30] C. Delitala, E. Cadoni, D. Delpiano, D. Meloni, M.D. Alba, A.I. Becerro, I. Ferino, *Micropor. Mesopor. Mater.* 118 (2009) 11–20.

Figure captions:

Fig. 1. Isotherms of nitrogen adsorption of parent and modified Z23, Z50 and Z80 zeolites.

Fig. 2. Pore size distribution of parent and modified Z23, Z50 and Z80 zeolites.

Fig. 3. XRD patterns of parent and modified Z23, Z50 and Z80 zeolites.

Fig. 4. ^{27}Al MAS NMR spectra of parent and modified Z23, Z50 and Z80 zeolites.

Fig. 5. Distribution of strength of acid sites in parent and modified Z23, Z50 and Z80 zeolites.

Fig. 6. Thermokinetic parameter of parent and modified Z23, Z50 and Z80 zeolites.

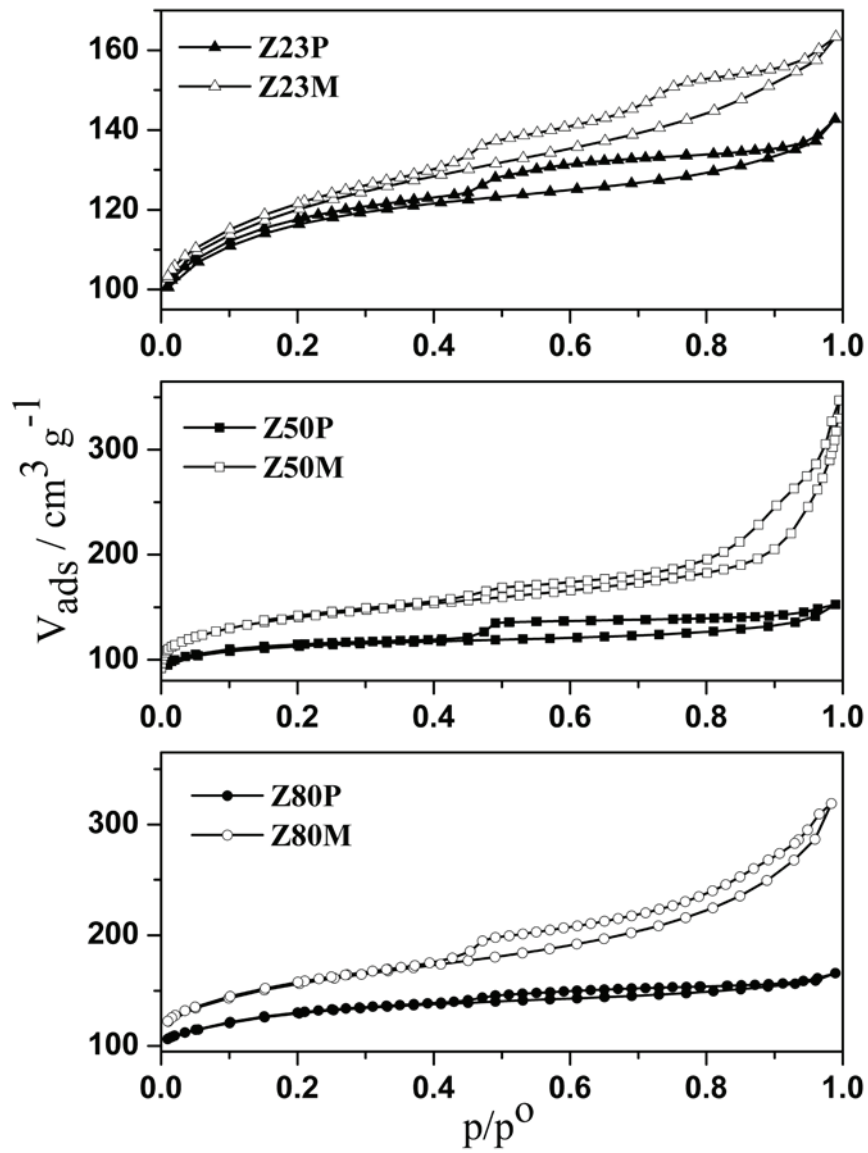


Fig. 1.

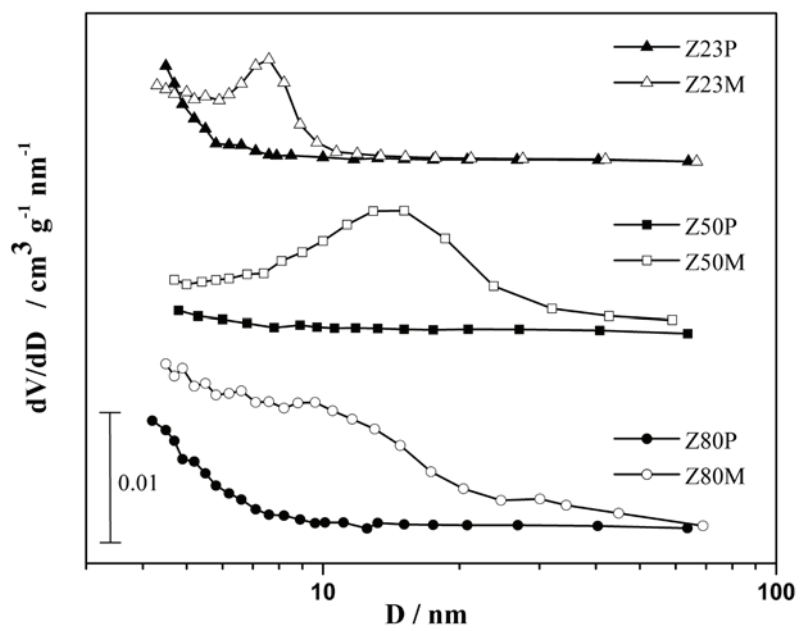


Fig. 2.

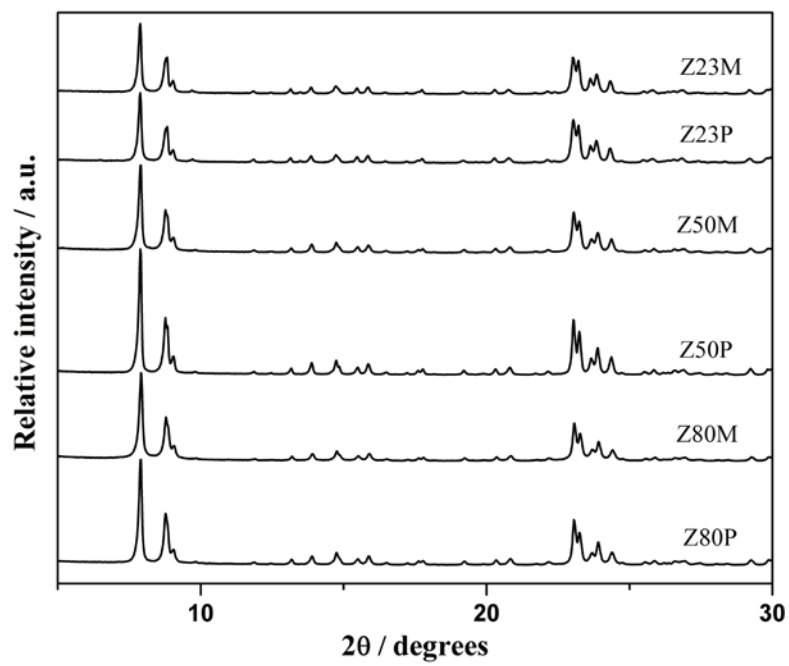


Fig. 3.

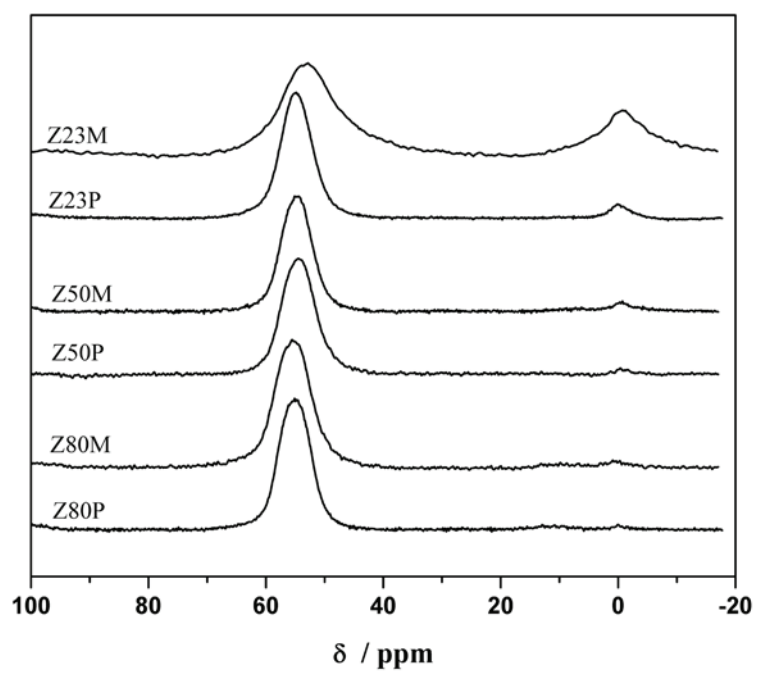


Fig. 4.

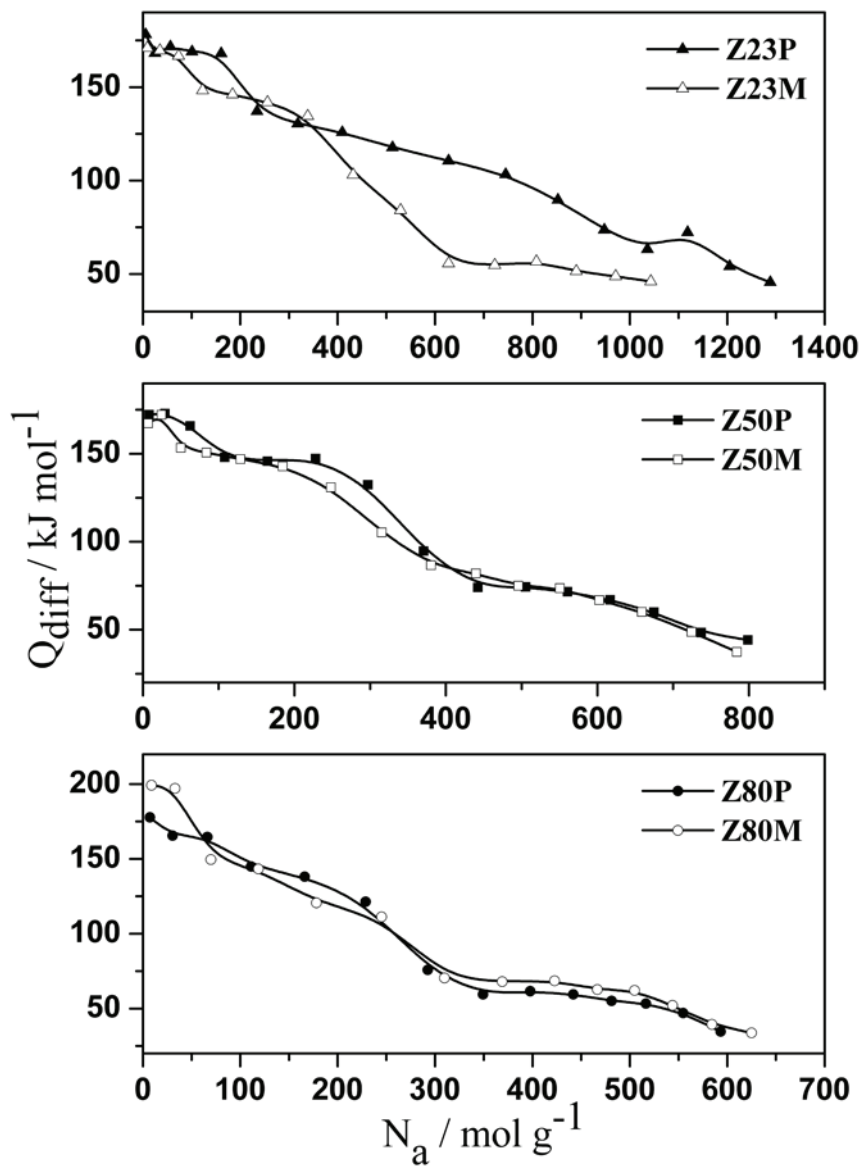


Fig. 5.

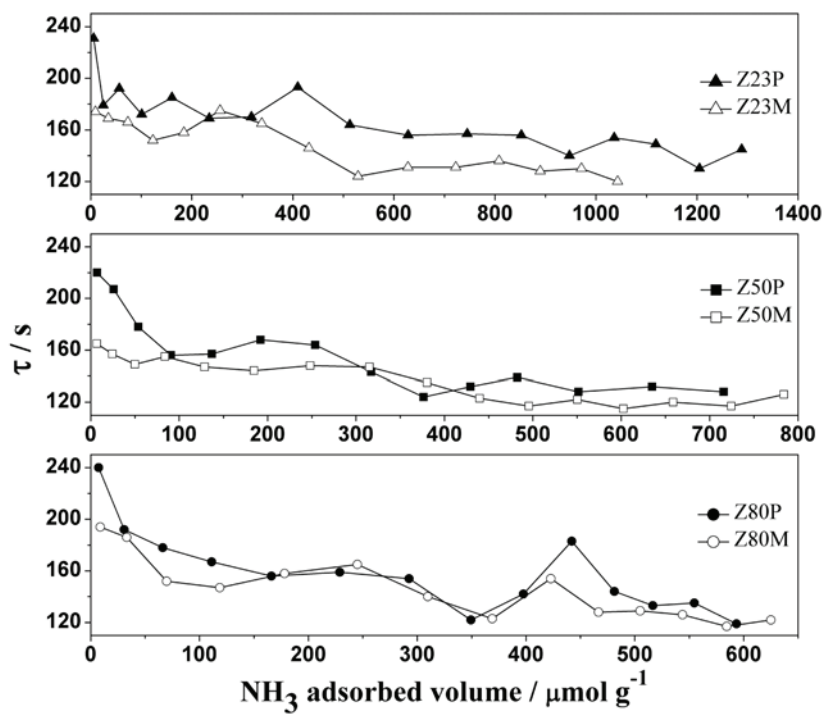


Fig. 6.

Table 1. Textural properties and crystallinity of parent and modified Z23, Z50 and Z80 zeolites

Sample	V_{pore} ($\text{cm}^3 \text{g}^{-1}$) ^a	V_{micro} ($\text{cm}^3 \text{g}^{-1}$) ^b	V_{meso} ($\text{cm}^3 \text{g}^{-1}$) ^c	S_{meso} ($\text{m}^2 \text{g}^{-1}$) ^b	S_{BET} ($\text{m}^2 \text{g}^{-1}$) ^d	Crystallinity (%)
Z23P	0.221	0.147	0.058	71	377	100
Z23M	0.253	0.139	0.095	103	392	91
Z50P	0.236	0.144	0.085	65	365	100
Z50M	0.449	0.138	0.380	173	470	76
Z80P	0.256	0.148	0.083	112	426	100
Z80M	0.493	0.145	0.324	214	521	84

^a Measured V_{ads} at $p/p^0=0.98$, ^b t-plot method, ^c BJH method, ^d BET method

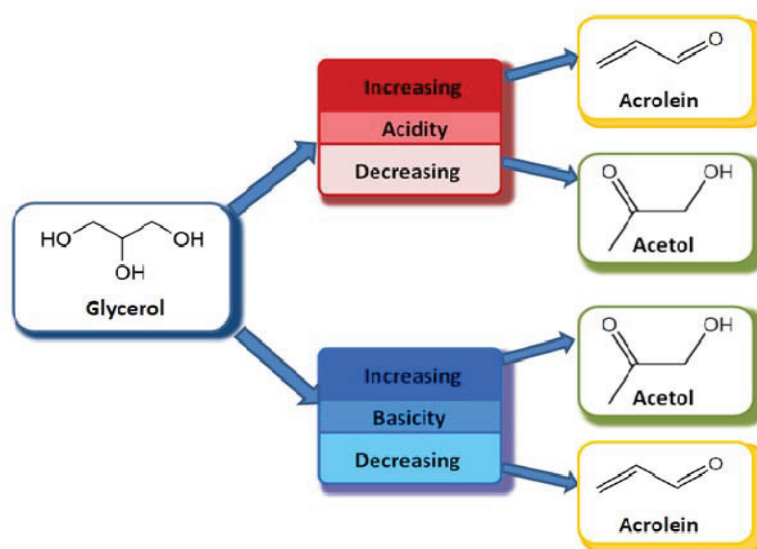
Table 2. Irreversibly adsorbed amounts of ammonia of parent and modified Z23, Z50 and Z80 zeolites

	Z23P	Z23M	Z50P	Z50M	Z80P	Z80M
V_{irr} ($\mu\text{mol g}^{-1}$)	644.1	535.8	411.3	351.9	345.6	341.8
ΔV_{irr} ($\mu\text{mol g}^{-1}$)	108.3		59.4		3.8	

5. Conclusions

The focus of this work was on the use of adsorption microcalorimetry technique for the characterization of solid catalysts. This technique provides information about acid-base properties of solid materials which can play a crucial role in determining their catalytic properties. Furthermore, this technique enables also to investigate the accessibility of active sites and diffusion phenomena; parameters which can be of great importance in heterogeneous catalysis.

General conclusions of this work are presented in the Schemes 5.1 and 5.2.



Scheme 5. 1. Influence of acid-base properties on the product distribution in glycerol dehydration in gas phase.

Scheme 5.1 shows that to get the targeted products in the glycerol dehydration in gas phase it is not only necessary to provide the active sites of desired strength and nature (acidic or basic), but it is also necessary to block the action of undesired sites. Therefore, with the purpose of producing acrolein in a high yield it is necessary to prepare materials with acid active centers present on the surface but also to decrease the number of basic ones. On the other hand, to produce acetol basicity is necessary, but also the reactions on the acidic sites should be prevented.

In the interest of getting high conversion of fructose and high yield of 5-HMF in fructose dehydration reaction it is crucial to provide catalyst with sufficient acidity (Scheme 5.2), but in order to prevent subsequent rehydration of 5-HMF, which leads to formation of levulinic and formic acid, it is also necessary to control this acidity. Having a certain amount of basic

5. Conclusions

sites will decrease the probability of wanted product to interact with acidic sites and therefore prevent production of unwanted ones.



Scheme 5. 2. Influence of the acid-base properties on the product distribution in fructose dehydration in water.

The design of solid materials with adequate acid-base features is important to get better performances in catalytic processes. Adsorption microcalorimetry gives opportunity to follow changes in these properties by different modifications of starting catalysts. Figure 5.1 classifies the investigated solids by their acid-base properties.

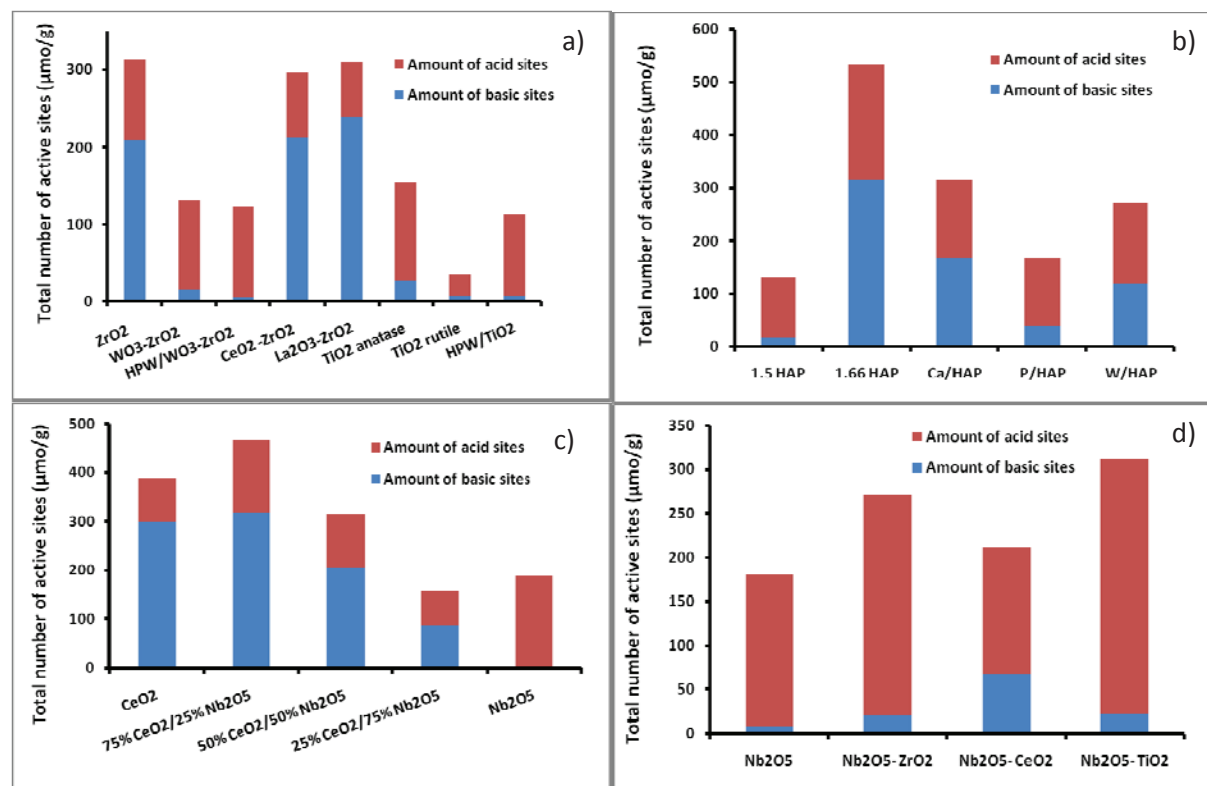


Figure 5.1. Histograms of amounts of acid and basic sites for each material investigated in this work.

5. Conclusions

From this figure it is easy to see how the acid-base properties of investigated solids are changing; with impregnation of another component oxide on the starting material (Figure 5.1 a), with mixing of oxides (Figure 5.1 a, d), with changing the relative amounts of two component oxides (Figure 5.1.c) or with changing the Ca/P ratio of calcium phosphate materials (Figure 5.1 b). Presented data gives opportunity to rationalize the amounts and nature of mixing oxides with the aim of getting the materials of desired features.

The acid-base properties, as determined by adsorption microcalorimetry, have been related to the catalytic activity in different reactions, such as glycerol dehydration in the gas phase and fructose dehydration in aqueous phase (Figure 5.2).

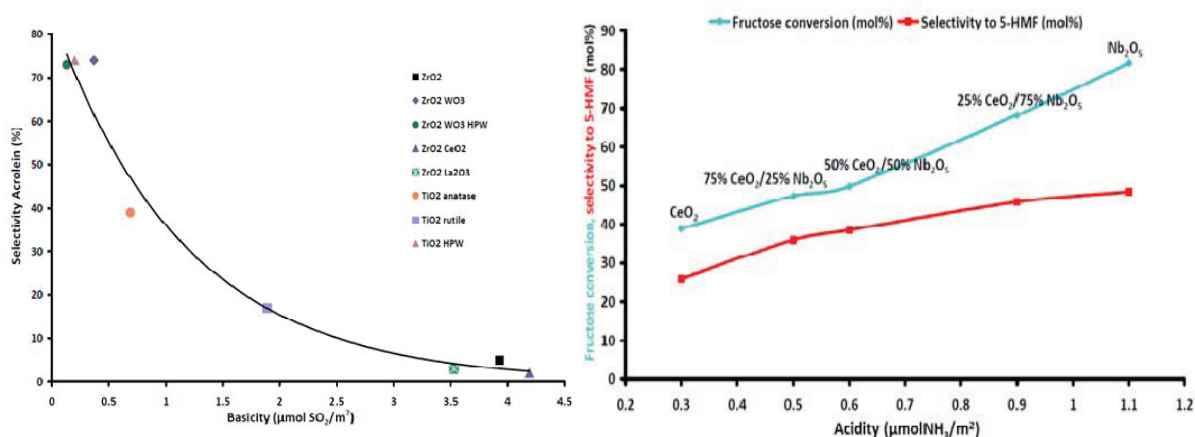


Figure 5.2. a) Selectivity to acrolein as a function of density of basic sites (see Publication I) and b) conversion of fructose and selectivity to 5-HMF as a function of density of acid sites (see Publication V).

The following is the short summary of the obtained results:

(1) Glycerol dehydration in the gas phase:

Two series of catalysts were prepared, characterized and tested in reaction of glycerol dehydration: a set of zirconia and titania based catalysts and a set of calcium phosphate catalysts.

Characterization of zirconia and titania based catalysts

Acid-base properties of zirconia and titania based catalysts were characterized by adsorption microcalorimetry of SO_2 and NH_3 molecules. Results show that all the investigated materials

5. Conclusions

express energetic heterogeneity of both acidic and basic active sites present on their surface. Surface acidic-basic features of these materials can be changed by making their mixtures with other oxides, which possess different acidic or basic character. Addition of tungstate species to the TiO₂ anatase or ZrO₂ does not bring significant change in the acidic properties, while it leads to suppression of their basic character. From calorimetric results it is also evident that mixing of lanthania and ceria with the starting material (ZrO₂) has as a consequence the decrease in acidic character, while the distribution of basic sites is only slightly affected. Furthermore, the acidity of titania is significantly decreased by phase transformation from anatase to rutile.

Characterization of calcium phosphate catalysts

Acidic/basic features of calcium phosphate materials were thoroughly explored here by microcalorimetry of ammonia and sulfur dioxide adsorption, as well as by FTIR (Fourier Transform Infrared Spectroscopy) of pyridine adsorption. Additionally, structural, textural, and surface properties of calcium phosphate materials have been fully characterized using appropriate techniques (low-temperature adsorption–desorption of nitrogen, thermogravimetric analysis, X-ray diffraction analysis (XRD), X-ray photoelectron spectroscopy (XPS), Raman spectroscopy and temperature-programmed reduction/oxidation (TPR/O)). Obtained results show that the addition of cations: Ca, P or W into the layered structure of hydroxyapatites enables the modification of their features important for catalytic behavior. Ca/P ratio is the directing parameter which crucially determines textural, acid–base and red-ox characteristics, thus giving the possibility to tune the properties of these materials and their modification. The modification of parent 1.66 HAP enabled creation of catalysts which are characterized by more prominent acidity. Beside already known importance of Ca/P ratio for acid–base features of these materials, it has been shown in this work that this value influences the red-ox properties, as well.

Catalytic activity of investigated materials

The results of catalytic test performed on both sets of catalytic materials showed that the activity in glycerol dehydration reaction is dependent not only on the total acidity of the catalysts, but also on the nature of acid sites present on their surface. Selectivity in the reaction is largely governed by the balance between acidic and basic active sites, but also by the ratio of Lewis to Brønsted acid sites. Results show that the number of basic sites directly

5. Conclusions

affects the selectivity in gas phase dehydration of glycerol to produce acrolein. Therefore, in order to get acrolein which is formed on acid sites, it is not only necessary to provide acidity, but also to hinder basic sites.

In the case of titania and zirconia based catalyst no correlation was found between acid-base properties and acetol yield, while for the calcium phosphate catalysts our results show that reducing of number and strength of acid centers increases the yield of acetol. The reason for finding the relationship between acid-base features and the yield of acetol for calcium phosphate catalysts, and absence of this correlation for the other set of catalysts may be in the different temperature at which reaction was performed. For zirconia and titania based catalysts temperature was 280 °C, whereas for calcium phosphates it was 350 °C, and it is known that temperature can influence significantly mechanism of glycerol dehydration and product distribution.

In general, it can be concluded that in order to realize the target reaction it is necessary to control not only the strength and the amount of the desired sites, but also to hinder as much as possible the number/strength/action of the undesired ones.

(2) Fructose dehydration in aqueous phase

Here, the results of characterization and catalytic activity of niobia-ceria mixed oxides and mesoporous Nb₂O₅-MeO₂ (M = Ce, Zr, Ti) mixed metal oxides will be discussed.

Characterization of ceria-niobia mixed oxides

Ceria–niobia mixed oxides have been prepared by coprecipitation method. The structural, textural, and surface properties of these materials have been fully characterized using appropriate techniques (low-temperature adsorption–desorption of nitrogen, thermogravimetric analysis, X-ray diffraction analysis (XRD), X-ray photoelectron spectroscopy (XPS), Raman spectroscopy and temperature-programmed reduction/oxidation (TPR/O)). The acid–base properties were estimated by the adsorption of appropriate probe molecules – NH₃ or SO₂ were used to estimate the population, strength and strength distribution of acid or basic sites, by means of adsorption microcalorimetry. The nature of acidic sites was determined through the adsorption/desorption of pyridine, studied by infrared spectroscopy.

5. Conclusions

Coprecipitation, the method applied for preparation of our samples allowed good homogeneity and dispersion of the two components in ceria–niobia mixed oxides formulations. Results obtained from XRD and Raman spectroscopy showed that there is no formation of any new phase between the two components of this mixed oxide system, while there are clear indications of their interaction. Furthermore, enrichment of the surface in niobia was observed by XPS technique, particularly, with increasing niobia content in the mixed oxide. Exposure of niobia on the surface can be of interest in applications where its unique properties, such as water insolubility, activity and stability in water phase are important. Amphoteric character and red-ox properties of ceria have been confirmed in this work. However, it is important to point out here that all mixed oxides investigated have also shown amphoteric behavior and red-ox features, depending on the relative amounts of ceria and niobia present in them.

Characterization of mesoporous Nb₂O₅-MeO₂ (M = Ce, Zr, Ti) mixed metal oxides

Mesoporous Nb₂O₅-MeO₂ (Me = Ti, Zr, Ce) mixed oxides were prepared using evaporation-induced self-assembly method. The structural and textural properties of these materials have been fully characterized using appropriate techniques (low-temperature adsorption–desorption of nitrogen, thermogravimetric analysis, X-ray diffraction analysis (XRD), scanning electron microscopy (SEM) and Raman spectroscopy). The acid–base properties were estimated by the adsorption of appropriate probe molecules – NH₃ or SO₂ were used to estimate the population, strength and strength distribution of acid or basic sites, by means of adsorption microcalorimetry.

Formation of mesoporous structure was confirmed by the results of XRD and BET techniques. Acidic-basic properties of synthesized materials proved to be dependent on the nature of the oxide that was mixed with niobia. Among the investigated mixed oxide formulations, only Nb₂O₅-CeO₂ was amphoteric, while the other samples showed prominent acidic character.

Catalytic activity of investigated materials

All investigated materials were active in fructose dehydration reaction. The activity and selectivity to 5-HMF were found to be dependent on the amount of strong acid sites present on the surface of the catalyst. In the series of niobia-ceria mixed oxides the activity and selectivity are also dependent on the niobia content, since the increase of relative amount of

5. Conclusions

Nb_2O_5 in the samples is followed by increase in acidity. Furthermore, it can also be inferred that presence of basic sites on the surface of the catalyst decreases the activity in the fructose dehydration reaction.

(3) Preparation and characterization of zeolites and hierarchical zeolites

In this work, the influence of the alkaline treatment on the acidity of zeolite ZSM-5 ($\text{SiO}_2/\text{Al}_2\text{O}_3 = 23, 50$ and 80) modified by desilication was investigated. A detailed microcalorimetric, volumetric and thermokinetic study was performed. The samples were characterized by X-ray diffraction, low temperature adsorption of nitrogen and solid-state ^{27}Al MAS NMR.

Mesopore formation by alkaline treatment was achieved for ZSM-5 zeolites with $\text{SiO}_2/\text{Al}_2\text{O}_3 = 23, 50$ and 80 . The desilication process was shown to depend on the silica to alumina ratio in terms of efficiency, resulting pore size distribution and acidity. The zeolite with the largest content of Al, Z23, proved to be the least susceptible to mesopore creation. Furthermore, the hydroxyde treatment of Z23 led to formation of extraframework Al deposits and substantial reduction of acidity. Samples with lower Al content yielded significant mesopore surfaces and preserved their original micropore structure.

The analysis of the results obtained by microcalorimetric investigation of ammonia adsorption enabled recognition of the differences between desilicated (mesoporous) and parent microporous zeolites. The distribution of strength of the acid sites in ZSM-5 zeolites with $\text{SiO}_2/\text{Al}_2\text{O}_3 = 50$ and 80 remained mostly unchanged by desilication process, while at the same time; the surface diffusion was improved, as indicated by the values of the thermokinetic parameter. Although Si/Al range dependant, the desilication process proved to be an efficient route which can be used for mesopore introduction in ZSM-5 zeolite with preservation of framework active sites.

The acidity of the active phase and textural properties can significantly influence the activity and selectivity of a tested catalyst in fructose dehydration in aqueous phase and glycerol dehydration in gas phase. Therefore, there is a need to test these materials, with high potential for use in heterogeneous catalysis and biomass conversion, in chemical processes investigated in this work.

Abstract (English, French)

Title

Acidic-basic properties of catalysts for the conversion of biomass

Abstract

Glycerol and fructose are molecules that are readily available in substantial quantities from the biomass. In this work dehydration routes for valorization of these compounds were investigated. Therefore, zirconia and titania based catalysts, and calcium phosphate materials were prepared and evaluated in the glycerol dehydration in gas phase. Niobia-ceria mixed oxides and mesoporous Nb₂O₅-MeO₂ (M = Ce, Zr, Ti) mixed oxides were prepared and tested in fructose dehydration reaction in aqueous phase. The surface acid-base properties of the studied catalysts were correlated to their catalytic performance.

Key words

adsorption microcalorimetry, acid-base properties, glycerol dehydration, fructose dehydration, acrolein, acetol, 5-hydroxymethylfurfural

Abstract (English, French)

Titre

Propriétés acido-basiques de catalyseurs pour la conversion de la biomasse

Résumé

Le glycérol et le fructose sont des molécules qui peuvent être extraites facilement de la biomasse et en des quantités substantielles. Ce travail de recherche porte sur la déshydratation comme moyen de valoriser ces composés. C'est dans ce but que des catalyseurs supportés sur oxydes de zirconium et de titane, ainsi que des matériaux de type phosphate de calcium, ont été préparés et testés pour la réaction de déshydratation du glycérol en phase gazeuse. Des oxydes mixtes de niobium et cerium ainsi que des oxydes mixtes mésoporeux de $\text{Nb}_2\text{O}_5\text{-MeO}_2$ ($M = \text{Ce, Zr, Ti}$) ont été également préparés et cette fois-ci testés pour la réaction de déshydratation du fructose en milieu aqueux. Dans les deux cas, les propriétés acido-basiques de surface des catalyseurs étudiés ont été corrélées à leur efficacité catalytique.

Mots-clés

microcalorimétrie d'adsorption, propriétés acido-basiques, déshydratation du glycérol, déshydratation du fructose, acroléine, acétole, 5-hydroxyméthylfurfural
